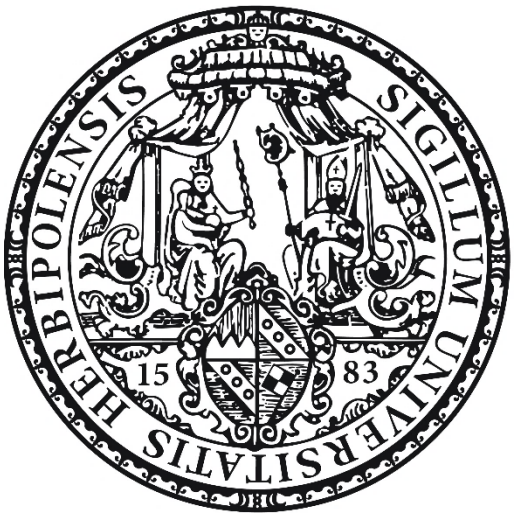

Relationship between wood properties, drought-induced embolism and environmental preferences across temperate diffuse-porous broadleaved trees

Beziehung zwischen Holzeigenschaften, trockenheitsbedingter Embolie und Umweltpräferenzen bei zerstreutporigen Laubbäumen der gemäßigten Breiten

Doctoral thesis for a doctoral degree
at the Graduate School of Life Sciences,
Julius-Maximilians-Universität Würzburg,
Section Integrative Biology

submitted by

Emilie Isasa

from

Cali, Colombia

Würzburg, 2022

Submitted on: ……..……...

Office stamp

Members of the Thesis Committee

Chairperson: Prof. Dr. Thomas Schmitt

Primary Supervisor: Prof. Dr. Bernhard Schuldt

Supervisor (Second): Prof. Dr. Juliano Sarmento Cabral

Supervisor (Third): Prof. Dr. Steven Jansen

Date of Public Defence: ……..……

Date of Receipt of Certificates: ……....

Table of contents

Table of contents ..... **I**

Summary ..... **V**

Zusammenfassung ..... **VII**

Publications presented in this work ..... **IX**

Abbreviations ..... **XI**

1. General introduction **3**

1.1. Impact of climate change on temperate forests 3
1.2. Tree strategies and processes during drought 4
1.3. How to predict drought induced tree mortality 5
1.3.1. Water transport and embolism resistance 5
1.3.2. Wood properties as a key functional trait to predict drought induced embolism 6
1.4. Evolutionary relationships between drought-related traits and climate variation 9
1.5. Thesis structure and project objectives 10
1.6. Project framework, methods and study area 13
1.6.1. Experimental design and study area 13
1.6.2. Species selection 14
1.6.3. Summary of the measured parameters 15

2. Chapter 1: Addressing controversies in embolism resistance – vessel diameter relationships **31**

2.1. Abstract 32
2.2. Introduction 33
2.3. Materials and Methods 35
2.3.1. Study site and plant material 35
2.3.2. Quantification of xylem hydraulic conductivity 36
2.3.3. Vulnerability curves with the flow-centrifuge method 37
2.3.4. Vessel anatomical traits from light microscopy 37
2.3.5. Pit anatomical traits from transmission electron microscopy 38
2.3.6. Statistical analyses 39
2.4. Results 41
2.4.1. Embolism resistance, hydraulic efficiency and wood anatomy across species 41
2.4.2. Determinants of embolism resistance 43
2.4.3. Importance of trait value range and the level of aggregation 44
2.5. Discussion 47
2.5.1. The role of pit membrane thickness for embolism resistance 47
2.5.2. How can we explain the $P_{50} – D_h$ relationship mechanistically 48
2.5.3. Reconciling discrepancies about the vessel diameter – embolism resistance relationship 49
2.6. Conclusions 51
Acknowledgements 52

3. Chapter 2: Accuracy of the pneumatic method for estimating xylem vulnerability to embolism in temperate diffuse-porous tree species 61

3.1. Abstract 62
3.2. Introduction 63
3.3. Materials and Methods 65
3.3.1. Plant material 65
3.3.2. Measurements of vulnerability curves with the pneumatic method 66
3.3.3. Xylem water potential measurement 68
3.3.4. Measurement of vulnerability curves with the flow-centrifuge method 68
3.3.5. Statistical analysis 69
3.4. Results 71
3.4.1. Estimated vulnerability curves 71
3.4.2. Overall agreement between methods 71
3.4.3. Influence of discharge time 73
3.5. Discussion 78
3.5.1. Agreement between flow-centrifuge and pneumatic vulnerability curves 78
3.5.2. Effect of the air discharge interval on measurement accuracy 79
3.5.3. Species-specific drying behaviour 80
3.5.4. Implications for future vulnerability curve method comparisons 81
3.6. Conclusion 82
Acknowledgements 83

4. Chapter 3: Relationships between drought-related traits and environmental preferences across four genera of temperate trees 91

4.1. Abstract 92
4.2. Introduction 93
4.3. Materials and Methods 95
4.3.1. Study site and plant material 95
4.3.2. Hydraulic measurements 97
4.3.3. Phylogeny 98
4.3.4. Occurrence data 99
4.3.5. Bioclimatic data and variable selection 100
4.3.6. Environmental preferences 100
4.3.7. Ecological and Macroevolutionary analyses 101
4.4. Results 102
4.4.1. Embolism resistance, wood density and wood anatomy across species 102
4.4.2. Macroevolution analyses 103
4.4.3. Macroecological analyses 105
4.5. Discussion 108
4.5.1. Functional traits related to embolism resistance 108
4.5.2. Evolutionary component in related drought tolerance traits 109
4.5.3. Trade-off between drought resistance traits and bioclimatic variables 109
4.6. Conclusion 110
Acknowledgements 111

5. Synthesis 123

5.1. Summary of present findings and discussion 123
5.2. Using diverse tree predictor traits to enhance drought-induced embolism research ... 124
5.2.1. Drought-induced embolism associated with leaf measurements 124
5.2.2. Tree architecture and seed dispersal mechanism as drought-related trait 127
5.3. Study of macroevolutionary processes and embolism resistance within 17 Sapindaceae species 132
5.4. Outlook 138
5.4.1. Implication on plant functional trait databases 138
5.4.2. Model optimisation to predict drought induced embolism 138
5.5. Final conclusion 140

6. Appendices 153

6.1. Chapter 1 153
6.2. Chapter 2 158
6.3. Chapter 3 164

Acknowledgments 177

Publication list 179

Curriculum Vitae 181

Affidavit 185

Eidesstattliche Erklärung 185

Summary

In the scope of climate warming and the increase in frequency and intensity of severe heat waves in Central Europe, identification of temperate tree species that are suited to cope with these environmental changes is gaining increasing importance. A number of tree physiological characteristics are associated with drought-stress resistance and survival following severe heat, but recent studies have shown the importance of plant hydraulic and anatomical traits for predicting drought-induced tree mortality, such as vessel diameter, and their potential to predict species distribution in a changing climate.

A compilation of large global datasets is required to determine traits related to drought-induced embolism and test whether embolism resistance can be determined solely by anatomical traits. However, most measurements of plant hydraulic traits are labour-intense and prone to measurement artefacts. A fast, accurate and widely applicable technique is necessary for estimating xylem embolism resistance (e.g., water potential at 50% loss of conductivity, P_{50}), in order to improve forecasts of future forest changes. These traits and their combination must have evolved following the selective pressure of the environmental conditions in which each species occurs. Describing these environmental-trait relationships can be useful to assess potential responses to environmental change and mitigation strategies for tree species, as future warmer temperatures may be compounded by drier conditions.

In Chapter 1, I discuss the findings of a field study based on the measurements of traits related to drought survival for 20 native and non-native temperate broad-leaved trees, including structural, hydraulic, anatomical, and foliar traits. These tree species are part of the initiative 'Stadtgrün 2021' by the Bavarian State Institute for Viticulture and Horticulture (LWG). We characterized the drought-stress resistance of the species sample and searched for trade-offs between vascular, hydraulic and foliar traits. Then, we focused on the inter- and intraspecific scaling of water potential at 50% loss of conductivity (P_{50}) with hydraulically-weighted vessel diameter (D_h). Therefore we measured the scaling of P_{50} and D_h and tested its link to pit membrane thickness (T_{PM}) and specific conductivity (K_s). There was an interspecific relationship between P_{50} and D_h, which was mirrored by P_{50} and K_s, but no intraspecific relationship between P_{50} and K_s was observed. We showed that species with thicker pits and narrower vessels were more embolism-resistant. Although D_h and T_{PM} were weakly associated, this did not explain the highly significant link between P_{50} and D_h after accounting for T_{PM}. In conclusion, we find robust evidence that P_{50} scales with D_h across species, suggesting previous controversies may be partially explained by differences in the range of traits covered and how data are gathered (species, tree, or sample level).

In Chapter 2, I present the results of a laboratory experiment based on 12 diffuse-porous temperate tree species covering a wide range of embolism resistance to compare the pneumatic method and flow-centrifuge method for constructing xylem vulnerability curves. Using both methods, we evaluated the agreement between the parameters estimated and the sensitivity of pneumatic measurements to measurement duration. The pneumatic method allows fast,

economical estimations of embolism resistance for a wide range of temperate, diffuse-porous species, which makes it an attractive method for predicting plant performance in climate change scenarios.

In Chapter 3, I first examined the results from a dataset of 24 species across four genera of Northern temperate diffuse-porous trees. I examined the relationship between key drought-related xylem functional traits ($P_{50,}$ D_h, and wood density (*WD*)). Then I used macroevolutionary models to study phylogenetic conservatism in key functional traits, reconstructing evolutionary pathways to identify which traits co-evolved with each other. Finally, I analyze the effects of temperature and precipitation variables on the key functional traits by using phylogenetic generalized least squares (PGLS) to control for phylogenetic constraints. We find that functional traits varied widely across species, but P_{50} and D_h displayed a strong correlation across genera, while P_{50} and *WD* showed no correlation. Our results shows that xylem vulnerability to embolism of Northern temperate tree species varies predictably with aridity and temperature. Natural selection has shown that some species are capable of adapting to rapid changes in climate conditions. Evolutionary processes play a limited role in preventing drought-induced tree mortality under changing environmental conditions

In summary, this study identifies a set of anatomical and functional traits that determine embolism resistance. Nevertheless, some of those relationships can be explained by differences in the range of traits covered and how data are collected. Additionally, the current work shows the results of a new faster and inexpensive method to measure embolism resistance on trees. Finally, we described physiological processes and trade-offs that act on the dynamics of tree structure and development. In this context, understanding trait evolution across species and identifying the climatic conditions that caused the development of a specific trait syndrome is of fundamental importance.

Zusammenfassung

Im Rahmen der Klimaerwärmung und der Zunahme der Häufigkeit und Intensität schwerer Hitzewellen in Mitteleuropa gewinnt die Identifizierung von Baumarten der gemäßigten Zonen, die mit diesen Umweltveränderungen zurechtkommen, zunehmend an Bedeutung. Eine Reihe von physiologischen Merkmalen von Bäumen wird mit der Trockenstressresistenz und dem Überleben nach schweren Hitzewellen in Verbindung gebracht. Jüngste Studien haben jedoch gezeigt, wie wichtig pflanzenhydraulische und anatomische Merkmale für die Vorhersage der trockenheitsbedingten Baumsterblichkeit sind, z. B. der Gefäßdurchmesser, und wie wichtig diese wiederum für die Vorhersage der Artenverteilung in einem sich verändernden Klima sind.

Eine Zusammenstellung großer globaler Datensätze ist erforderlich, um die Merkmale zu bestimmen, die mit trockenheitsbedingter Embolie zusammenhängen, und um zu prüfen, ob die Embolieresistenz allein durch anatomische Merkmale bestimmt werden kann. Die meisten Messungen der hydraulischen Eigenschaften von Pflanzen sind jedoch sehr arbeitsintensiv und anfällig für Messartefakte. Es wird ein schnelles, genaues und breit anwendbares Verfahren zur Schätzung der Xylem-Embolie-Resistenz (z. B. Wasserpotenzial bei 50 % Leitfähigkeitsverlust, P_{50}) benötigt, um die Vorhersage künftiger Waldveränderungen zu verbessern. Diese Merkmale und ihre Kombination müssen sich unter dem Selektionsdruck der Umweltbedingungen, in denen die einzelnen Arten vorkommen, entwickelt haben. Die Beschreibung dieser Beziehungen zwischen Umwelt und Merkmalen kann nützlich sein, um potenzielle Reaktionen auf Umweltveränderungen und Schutzstrategien für Baumarten zu bewerten, da künftige wärmere Temperaturen mit trockeneren Bedingungen einhergehen könnten.

In Kapitel 1 erörtere ich die Ergebnisse einer Feldstudie, die auf der Messung von Merkmalen basiert, die mit dem Überleben bei Trockenheit für 20 einheimische und nicht einheimische Laubbäume der gemäßigten Breiten zusammenhängen. Für diese Studie wurden strukturelle, hydraulische, anatomische und blatttechnische Merkmale aufgenommen. Diese Baumarten sind Teil der Initiative "Stadtgrün 2021" der Bayerischen Landesanstalt für Weinbau und Gartenbau (LWG). Wir charakterisierten die Trockenstress-Resistenz der untersuchten Arten und suchten nach Kompromissen zwischen vaskulären, hydraulischen und Blattmerkmalen. Anschließend konzentrierten wir uns auf die inter- und intraspezifische Skalierung des Wasserpotenzials bei 50 % Leitfähigkeitsverlust (P_{50}) mit dem hydraulisch gewichteten Gefäßdurchmesser (D_h). Dafür haben wir die Skalierung von P_{50} und D_h gemessen und prüften ihren Zusammenhang mit der Grubenmembrandicke (T_{PM}) und der spezifischen Leitfähigkeit (K_s). Es bestand eine interspezifische Beziehung zwischen P_{50} und D_h, die sich in P_{50} und K_s widerspiegelte, aber es wurde keine intraspezifische Beziehung zwischen P_{50} und K_s beobachtet. Wir konnten zeigen, dass Arten mit dickeren Tüpfeln und engeren Gefäßen embolieresistenter waren. Obwohl D_h und T_{PM} schwach assoziiert waren, erklärte dies nicht den hoch signifikanten Zusammenhang zwischen P_{50} und D_h nach Berücksichtigung der T_{PM}. Zusammenfassend lässt sich sagen, dass wir robuste Belege dafür gefunden haben, dass P_{50} über die Arten hinweg mit D_h skaliert, was darauf hindeutet, dass frühere Kontroversen teilweise durch Unterschiede in der Bandbreite der

erfassten Merkmale und der Art der Datenerfassung (Arten-, Baum- oder Stichprobenebene) erklärt werden können.

In Kapitel 2 stelle ich die Ergebnisse eines Laborexperiments vor, das auf 12 zerstreutporigen Baumarten der gemäßigten Zonen basiert, die einen breiten Bereich der Embolieresistenz abdecken, um die pneumatische Methode und die Durchfluss-Zentrifugen-Methode zur Erstellung von Xylem-Verletzlichkeitskurven zu vergleichen. Mit beiden Methoden haben wir die Übereinstimmung zwischen den geschätzten Parametern und die Empfindlichkeit der pneumatischen Messungen gegenüber der Messdauer bewertet. Die pneumatische Methode ermöglicht eine schnelle und kostengünstige Schätzung der Embolieresistenz für eine breite Palette von diffus-porösen Arten der gemäßigten Zonen, was sie zu einer attraktiven Methode für die Vorhersage der Pflanzenleistung in Klimawandelszenarien macht.

In Kapitel 3 Zunächst untersuchte ich die Ergebnisse eines Datensatzes von 24 Arten aus vier Gattungen zerstreutporiger Bäume der nördlichen gemäßigten Zonen. Ich untersuchte dabei die Beziehung zwischen den wichtigsten funktionellen dürrebezogenen Xylem-Merkmalen (P_{50}, D_h und Holzdichte (*WD*)). Dann habe ich makroevolutionäre Modelle verwendet, um den phylogenetischen Konservatismus der wichtigsten funktionellen Xylem-Merkmale zu untersuchen. Über evolutionäre Pfade rekonstruierte ich dann, welche Merkmale sich gemeinsam entwickelt haben. Schließlich analysierte ich die Auswirkungen von Temperatur- und Niederschlagsvariablen auf die wichtigsten funktionellen Merkmale mit Hilfe phylogenetischer verallgemeinerter kleinster Quadrate (PGLS), um phylogenetische Beschränkungen zu kontrollieren. Wir stellen fest, dass die funktionellen Merkmale zwischen den Arten stark variieren, aber der P_{50} und der D_h zeigten eine starke Korrelation zwischen den Gattungen, während der P_{50} und die *WD* keine Korrelation aufwiesen. Unsere Ergebnisse zeigen, dass die Anfälligkeit des Xylems für Embolien bei Baumarten der nördlichen gemäßigten Zonen vorhersehbar mit der Trockenheit und Temperatur variiert. Die natürliche Auslese hat gezeigt, dass einige Arten in der Lage sind, sich an schnelle Veränderungen der klimatischen Bedingungen anzupassen. Evolutionäre Prozesse spielen eine begrenzte Rolle bei der Verhinderung von trockenheitsbedingtem Baumsterben unter den sich ändernden Umweltbedingungen.

Zusammenfassend lässt sich sagen, dass diese Studie eine Reihe von anatomischen und funktionellen Merkmalen identifiziert, die die Embolieresistenz bestimmen. Einige dieser Zusammenhänge lassen sich jedoch durch Unterschiede in der Bandbreite der erfassten Merkmale und der Art der Datenerhebung erklären. Darüber hinaus zeigt die aktuelle Arbeit die Ergebnisse einer neuen, schnelleren und kostengünstigen Methode zur Messung der Embolieresistenz von Bäumen. Zuletzt haben wir physiologische Prozesse und Abwägungen beschrieben, die sich auf die Dynamik der Baumstruktur und -entwicklung auswirken. In diesem Zusammenhang ist es von grundlegender Bedeutung, die Entwicklung von Merkmalen über verschiedene Arten hinweg zu verstehen und die klimatischen Bedingungen zu ermitteln, die die Entwicklung eines bestimmten Merkmals verursacht haben.

Publications presented in this work

Chapter 1: **Emilie Isasa**, Roman Link, Steven Jansen, Fon Robinson Tezeh, Lucian Kaack, Juliano Sarmento Cabral, Bernhard, Schuldt. "Addressing controversies in the xylem embolism resistance – vessel diameter relationship"

Chapter 2: Sharath S. Paligi, Roman M. Link, **Emilie Isasa**, Paulo Bittencourt, Juliano Sarmento Cabral, Steven Jansen, Rafael S. Oliveira, Luciano Pereira, Bernhard Schuldt "Accuracy of the pneumatic method for estimating xylem vulnerability to embolism in temperate diffuse-porous tree species"

Chapter 3: **Emilie Isasa,** Ana Paula Moraes, Bernhard Schuldt, Juliano Sarmento Cabral. "Relationships between drought induced traits and environmental preferences across four genera of temperate trees"

Additional work published during my doctorate

Lucian Kaack, Matthias Weber, **Emilie Isasa**, Zohreh Karimi, Shan Li, Luciano Pereira, Christophe L. Trabi, Ya Zhang, H.Jochen Schen, Bernhard Schuldt, Volker Schmidt, Steven Jansen (2021). "Pore constrictions in intervessel pit membranes provide a mechanistic explanation for xylem embolism resistance in angiosperms". New Phytologist 230: 1829–1843. doi: 10.1111/nph.17282

Yonten Dorji, Bernhard Schuldt, Liane Neudam, Rinzin Dorji, Kali Middleby, **Emilie Isasa**, Klaus Körber, Christian Ammer, Peter Annighöfer, Dominik Seidel, 2021. " Three-dimensional quantification of tree architecture from mobile laser scanning and geometry analysis". Trees 35, 1385–1398. doi: 10.1007/s00468-021-02124-9

Yonten Dorji, **Emilie Isasa**, Juliano Sarmento Cabral, Bernhard Schuldt, Peter Annighöfer, Dominik Seidel (2022). " Insights into the relationship between xylem safety and tree structural complexity from Terrestrial Laser Scanning and fractal analysis" (Submitted, Tree physiology)

Additional work in preparation during my doctorate

Emilie Isasa, Alina Maxi Lea Wagner, Juliano Sarmento Cabral, Bernhard Schuldt. "Relationships between hydraulic traits and habitat preference across 20 worldwide *Acer* species" (2023, in preparation)

Abbreviations

ASI	annual stem increment
Crown	crown volume
DBH	diameter at breast height of trees (at ~ 1.3 m)
D_h	hydraulic vessel diameter
H	tree height
HV	Huber Value
HSM	hydraulic safety margin
K_s	stem hydraulic specific conductivity
LA	leaf area
PLC	percentage loss of hydraulic conductivity
P_{12}	water potential at 12% of hydraulic conductivity
P_{50}	water potential at 50% of hydraulic conductivity
P_{88}	water potential at 88% of hydraulic conductivity
Ψ_{min}	minimum xylem water potential
Ψ_p	xylem water potential
Ψ_{tlp}	water potential at turgor loss point
SWC	stem saturated water content
SLA	specific leaf area
T_{PM}	intervessel pit membrane thickness
VC	vulnerability curve
V_D	vessel density
V_G	vessel grouping index
VI	vulnerability index
V_S	solitary vessel index
WD	stem wood density

Part 1

General introduction

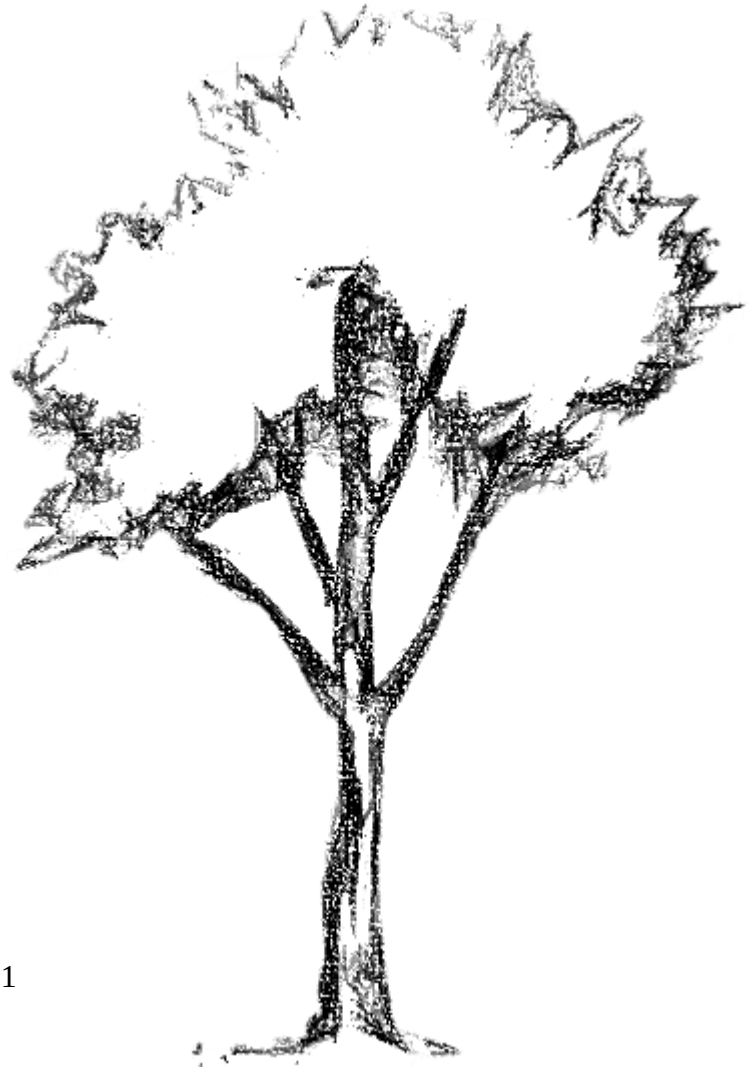

1. General introduction

1.1. Impact of climate change on temperate forests

Forests provide critical refuges for terrestrial biodiversity and play a central role in the earth's biogeochemical system. As major part in terrestrial ecosystems forests affect water and energy fluxes at the earth's surface through biogeophysical processes including changes in evapotranspiration, albedo and surface roughness. Forested ecosystems are expected to contribute in climate change mitigation as they can generally isolate more carbon than non-forested ecosystems, consequently, in accelerating or decelerating global climate change ((Grassi et al. 2017, IPCC (Intergovernmental Panel on Climate Change) 2022).

About 8,000 years ago, forest covered an estimated 6.2 billion hectares of the planet, about 47% of Earth's land surface (Billington et al. 1996). Unfortunately, over the last few centuries, their condition and area declined to a cover of 40% of the terrestrial area. In recent years, over 10 million hectares of natural forests have been deforested every year, most of it during the industrial age. In consequence 25 countries have no forest anymore and in 29 other countries 90% of the forest has disappeared (Meyfroidt and Lambin 2011).

Climate disturbances is a long-term challenge, there is no doubt that urgent action is required now. The need to improve ecological knowledge and restore affected systems is as relevant as ever since we entered a new era, the Anthropocene. Humans are increasingly influencing the biogeosphere, particularly through climate change that has been anthropogenically disturbed (Steffen et al. 2011, Hobbs et al. 2014, IPCC 2014, Ellis et al. 2015, Lewis and Maslin 2015). Forests provide wood and numerous other products that contribute significantly to human wellbeing and economic activity from local to global level (Shvidenko et al. 2005, Eggers et al. 2008). The increased frequency and intensity of extreme events, caused by human-induced climate change, made forest management progressively complex and more difficult. Extreme events, such as flooding, storms, severe drought compounded by unusually warm temperatures, increasingly are recognized as key drivers of vegetation change (Jentsch et al. 2007, Millán 2014, IPCC 2012), including climate impacts on the world's forests and induced tree mortality. The scientific community recognized that greenhouse gas emissions are major contributors to recent increases in global mean temperatures (about 0.5°C since 1970) as well as changes in the world's hydrological cycle (IPCC 2007a). It is likely that future climate change will result in further increases in mean temperatures (about 2 to 4 °C globally) along with significant drying in some regions (Seager et al. 2007), as well as an increase in droughts, extreme heat waves and extreme hot summer (IPCC. 2007a, Sterl et al. 2008). These scenarios would be critically harmful to trees and forests which have a long generations and low generational changes (Allen et al. 2010, Hartmann et al. 2018, Dauphin et al. 2020, Schuldt et al. 2020).

Drought directly triggers stress and mortality risk for trees (McDowell et al. 2008). Through physiological impacts, function and survival (Adams et al. 2009, Allen et al. 2010, 2015, Vanoni et al. 2016) or indirectly through effects on pests and pathogens (Weed et al. 2013) drought is a major danger for trees. It affects woody plants by reducing leaf area and causing 'dieback', also known as 'defoliation' in Europe (Carnicer et al. 2011). In addition, background

tree mortality rates have increased (van Mantgem et al. 2009, Senf et al. 2020) and large-scale forest die-offs have occurred (Breshears et al. 2005, Allen et al. 2010, Matusick et al. 2013, Worrall et al. 2013, Schuldt et al. 2020). Understanding the physiological mechanisms associated with tree death in response to drought is necessary to understand and predict tree responses to a rapidly changing environment (McDowell et al. 2020).

1.2. Tree strategies and processes during drought

As for every living being on this planet, water is essential for trees. Studying drought mortality in plants interrogates what are the different strategies adopted during drought or what are the processes responsible for a tree's death. There can be several mechanisms contributing to tree mortality during severe drought like carbon starvation (i.e. after stomatal closure, a successive deterioration in plant health occurs as carbohydrates are reduced from non-structural carbohydrate storage) , by hydraulic failure (i.e. uncontrolled embolism causes complete failure of the hydraulic pathway) or biotic agent demographics (i.e. damage to tissue caused by herbivore infestation facilitated by plants' weakened state) (McDowell et al. 2008, 2011). Under drought stress, tree species follow rather two contrary water regulation strategies. The anisohydric (waterspending) species and isohydric (water-saving) species (Martinez-Vilalta et al. 2014, Martınez-Vilalta and Garcia-Former 2017, Hochberg et al. 2018, Ratzmann et al. 2019). According to these studies, an isohydric species reacts to drought by closing early the stomata and maintaining a specific water potential. This leads to a tapping off to the environment to reduce the water loss and the spread of xylem embolism. In turn the early closing of the stomata means a less, or no, carbon uptake from the atmosphere which again leads to carbon starvation. Due to the low carbon uptake storage capacity would be decreased, so maintenance costs for metabolic processes, such as respiration, could be very high (Hartmann and Trumbore 2016). This fact makes the isohydric strategy vulnerable to prolonged droughts. In contrary more anisohydric plants keep their stomata open under drought conditions. Consequently, the carbon assimilation stays maximized. The cost of this strategy is a high-water loss. Plants with that strategy are more advantaged in long term droughts, which are not to serve, because carbon starvation is not occurring. In turn a very strong and short drought can lead to death for plants with an anisohydric behavior.

According to these two different strategies, different theories of tree survival and death have been developed in relation to water and carbon.

As a result, hydraulic failure and carbon starvation have been identified as the main causes of drought-related deaths (McDowell 2011, Anderegg et al. 2012, Sevanto et al. 2014). Nevertheless, the mechanisms of drought-induced mortality in trees from carbon starvation are also far from understood (Sala et al. 2010). There is, however, a delay in the onset of tree dieback for the majority of cases (Bigler et al. 2007, Phillips et al. 2010). Both processes are explicitly described as non-exclusive and as occurring simultaneously in many cases; furthermore, both are assumed to facilitate the spread of biotic agent’s outbreaks (McDowell et al. 2011).

Hydraulic failure caused by catastrophic xylem dysfunction is widely recognized as a major cause of tree death. There have been a number of studies that suggest hydraulic failure due to catastrophic xylem dysfunction is the more significant of the two processes under many circumstances (Sevanto et al. 2014, Hartmann et al. 2018). During hydraulic failure, the water conducting system would fail due to embolisms occurring under high pressure, such as very low xylem water potentials. (Choat et al. 2012, Urli et al. 2013).

1.3. How to predict drought induced tree mortality

It is important to consider the relationship between the functional characteristics of plants and the climate, since water plays such an essential role in several vital processes. The process of drought-induced tree mortality is complex and involves several interdependent tree key functional traits. To understand how plants function as organisms and determinants of ecosystems, we need a greater understanding of plant physiology and how it relates to the anatomy. Thus, a fundamental question in this study is whether key functional traits can be used to predict drought response in temperate trees by understanding the physiological basis for tree death.

1.3.1. Water transport and embolism resistance

In angiosperm trees, the water is transported through the xylem tissue, which is composed of water-conducting tracheary elements: tracheids and vessels. These cells are connected through large, circular bordered pits (Wilson and White 1986) concentrated in the radial walls including the tapered ends of the cells. Those pits developed from secondary cell walls and constituted by a pit membrane allow water to flow by the cell association (Choat et al. 2007). Trees require a long-distance water transport pathway to pull water from the soil via the roots through a specialized tissue (i.e., xylem) to the leaves, which is principally driven by transpiration (Nobel 1999).

Forming a continuous water column from soil to leaves (i.e., soil-plant-atmosphere continuum) and described by the widely accepted cohesion-tension theory (Dixon and Joly 1894, Tyree and Zimmermann 2002). This theory follows the thermodynamically thinking of a plant as a system, which is energised by the sun. With the process of transpiration and photosynthesis in the leaves a gradient of water potential occurs from the leaves through the xylem and roots to the soil. Water potential gradients ($\Delta\Psi x$; MPa) represent the negative pressure gradient along the hydraulic pathway; they are a measure of a liquid's potential energy compared to pure water. Water potential is a negative pressure (zero being pure water). In order to reach equilibrium, water moves passively from higher to lower water potential.

The water conducting system would suffer from embolisms when cavitation occurs due to high negative xylem tensions during droughts (very low xylem water potentials) (Choat et al. 2012, Urli et al. 2013). An important key process that leads to drought-induced tree mortality is the

development of xylem embolisms, which result in disruption of xylem conductive function (Anderegg et al. 2016, Hajek et al. 2022). Under conditions of negative pressure, a spontaneous transition from the liquid to the gas phase (cavitation) is theoretically possible, which may explain the formation of emboli. It is caused by the formation of gas bubbles that can spread and block the conduit.

As one of the most commonly reported metrics of xylem vulnerability to hydraulic failure, hydraulic safety is often quantified by the water potential at which 12, 50 and 88 percent loss of hydraulic conductivity (PLC) occurs (P_{12}, P_{50} and P_{88}, respectively) (Anderegg et al. 2016, Gleason et al. 2016a). Commonly, the relative (e.g., percent loss of maximum conductivity) is resulting from decreasing water potentials. Small decreases in water potential would result in a huge increase in xylem embolisms because of this sigmoidal shape. Species are typically compared by the Ψ_x value at which a 50% loss of hydraulic conductance occurs (Ψ_{50}, Davis et al. 1999), although other reference points may have more physiological importance, for example, Ψ_{88} (PLC) (Choat 2018). A critical point in angiosperms occurs when 88% of the conductive system is embolized, resulting in dieback of the crown or even tree death (Brodribb and Cochard 2009, Bouche et al. 2015). Under well-watered plants, the degree of xylem embolisms is nearly zero, but increases with a sigmoidal curve. Cai and Tyree (2010) and Cochard et al. (2013) describe vulnerability curves (VCs). In addition, P_{12}, the water potential at Ψ_{12}, is another common value extracted from VCs, giving an indication of the onset of embolism (Domec and Gartner 2001).

Cavitation resistance increases across species with decreasing mean annual precipitation (Maherali et al. 2004) and is related to the range of water potentials experienced in the field (Hacke et al. 2000), indicating that xylem embolism is correlated with drought tolerance (Pockmann and Sperry 2000) and species distribution. Drought-induced cavitation affects plants differently and their responses to drought depend on their hydraulic strategies (Breda et al. 2006). It has been consistently found that severe embolisms are the primary cause of death in drought-stressed temperate trees. A study by Tyree et al. (1998) found that each tree species was highly susceptible to drought-induced xylem embolisms. Those trees were more vulnerable to drought than trees located in sites with high drought frequencies, where the hydraulic system appears to be adjusted to the frequent occurrence of drought periods. The importance of determining key functional traits to predict drought induced embolism on temperate trees is essential.

1.3.2. Wood properties as a key functional trait to predict drought induced embolism

By exploring tree traits, we further examined a representative set of traits which have been recognized as determinants of drought resistance: anatomical traits: stem vessel diameter (Hacke et al. 2006), pit membrane properties (Jansen et al. 2009), vessel grouping/solitary grouping index (Martínez-Vilalta et al. 2012), tree structure, tree height (Domec et al. 2008), wood density (Hacke et al. 2001) and growth rate (Wheeler et al. 2005).

1.3.2.1. Vessel size and conductivity

The flow conductance in the vessels water conducting system is greatly influenced by the conduit diameter. This is particularly true in angiosperms, as demonstrated by the Hagen-Poiseuille equation, which raises the lumen conductivity with the fourth power (D^4, Calkin et al. 1986).
Having highly conductive sapwood is widely considered a prerequisite for high productivity (Tyree 2003). As a result, xylem hydraulic physiology has been referred as the "functional backbone of terrestrial plant productivity" (Brodribb 2009). Considering that productivity and xylem hydraulic efficiency are closely related, there may be a trade-off between hydraulic efficiency and stability against xylem failure that accounts for fast-growing tree species' higher susceptibility to drought.
It has long been known that vessel diameter directly influences water conduction, hence affecting xylem efficiency, i.e., xylem-specific hydraulic conductivity (K_s) (Sperry et al. 2008). Safety-efficiency trade-offs are necessary to compensate for the difference between xylem efficiency and embolism resistance. Otherwise, all woody plants would exhibit both high safety and high efficiency. As a result, plants with low safety do not always show high hydraulic efficiency at an interspecific level (Gleason et al. 2016).
Based on the vulnerability-diameter relationship individuals with relative wide conduits for a given hight may be more vulnerable to embolism, but also more conductive and efficient.
Thus, it would be relatively feasible to identify the most vulnerable individuals by evaluating populations based on their conduit width (Cai et al. 2010, Hargrave et al. 1994, Maherali et al. 2006, Hajek et al. 2014). Starting from this, conduit size can be viewed as a trade-off between xylem hydraulic conductance, which influences transpiration, carbon fixation, growth (Tyree 2003, Poorter et al. 2010) and drought-induced embolism (Tyree et al. 1994). However, a better understanding of the biophysical processes at the nanoscale will be necessary in order to establish the real diameter-vulnerability link. It can be misleading to link conduit diameter with embolism vulnerability based solely on comparative and ecological wood anatomy studies (Lens et al. 2022).
Nevertheless, a direct causal link between vessel size and drought vulnerability is still debated. According to Hacke and Jansen (2009), there should be no direct causal link between conduit diameter and the assumed cavitation mechanism due to water stress. There is rather an indirect link via a multitude of other quantities such as the number of intervessel pits per unit surface area, the average size and/or the thickness of the membrane (T_{PM}) of these pits xylem sap composition chemistry and thickness of conduit walls and finally and the concentration and vicinity of dissolved and undissolved gas (Choat et al. 2008, Lens et al. 2011, Tixier et al. 2014, Jansen et al. 2018, Lens et al. 2022), which puts the unconditional validity of the pit area hypothesis into question.

1.3.2.2. Pit properties

Bordered pit membrane structure which determines the entry of gas-water menisci from an embolised vessel into the adjacent water-filled vessel (air seeding hypothesis, Zimmermann 1983, Tyree and Sperry 1989, Choat et al. 2008, Mayr et al. 2014) and the vessel length distribution, tends to make up around 50% of the total flow resistance (Sperry et al. 2005, Wheeler et al. 2005). In particular, pit membrane thickness is likely to directly influence embolism resistance (Li et al. 2016). Consequently, air seeds more easily inside larger conduits because they have more bordered pits (Christman et al. 2009, Pittermann et al. 2010, Lens et al. 2011). Therefore, if the pit area per conduit remains constant, more conduits could increase conductivity without affecting safety. According to the 'rare pit hypothesis,' increasing the total area of the pit membrane should automatically result in a higher risk of at least one pit membrane pore allowing air to enter at a particular pressure potential gradient (Hacke et al. 2006, Choat and Pittermann 2009). In this way, the dimensions of pore size in pit membrane and vessels represent a compromise between maximizing hydraulic efficiency (hence potential carbon gain through photosynthesis) and minimizing the risk of hydraulic failure, which may explain the higher vulnerability of faster growing species which possess wider pores. In general, it appears that conduit size and total pit pore area may have a universal relationship, which would support the 'air seeding hypothesis' as well as the 'rare pit hypothesis'.

1.3.2.3. Vessel network

Another anatomical features which affect the hydraulic performance is the intervessel connectivity and compartmentalization of the “vessel network” vessel topology, grouping (Meyra et al. 2007, Jansen et al. 2018, Kaack et al. 2021). For the first time, Carlquist (1984) suggested that xeric species should have more grouped vessels than other species with vessels embedded in non-conductive tissues (parenchyma, fibers), regarded as a way of providing alternate routes in the event of embolism. According to Loepfe et al. (2007) and Martinez Vilalta et al. (2012), high vessel grouping is associated with low safety through increased chances of embolism spread. There are, however, few studies that test the vessel network hypothesis and no experiments have been conducted for a diverse set of phylogenetically diverse species.

1.3.2.4. Wood density and tree size

By extension, wood density (i.e., secondary vascular tissue commonly found in angiosperm dicots and gymnosperms) is identified as a mechanical support, water transport and storage capacity. It has been named “integrator of wood properties" (Chave et al. 2009) and have been closely associated with hydraulic characteristics such as embolism resistance (Bucci et al. 2013, Anderegg et al. 2016, Christoffersen et al. 2016). As a result of indirect relationships with water transport, wood density is a reliable indicator of stress resistance that correlates with growth

performance (King et al. 2006, Rüger et al. 2012, Gibert et al. 2016, Falster et al. 2018). Species with low wood density are less likely to be invested in construction because of their lower relative investment costs (Van Gelder et al. 2006). Moreover, wood density along with other variety of wood-anatomical traits, such as vessel density and vessel area fraction in xylem (Hoeber et al. 2014, Hietz et al. 2016), influence productivity and cope with water stress impacts (Anderegg and Meinzer 2015). Thus, it has been demonstrated repeatedly that trees with higher wood density are less vulnerable to embolisms (Hacke et al. 2001, Lens et al. 2011, Markesteijn et al. 2011, Christoffersen et al. 2016). By increasing xylem conduit wall mechanical strength via the relationship between wall thickness and conduit diameter, wood density reduces the risk of deficiency (Hacke et al. 2001, Lens et al. 2011). Besides, tree size has been correlated to vulnerability as well. Tall trees are more exposed to embolism because of their predictably wider conduit diameter, their long hydraulic path lengths, the higher canopy deficit of vapor pressure and the higher xylem demand for leaf-produced photosynthates (Lindenmayer and Laurance 2017, Olson et al. 2018, Stovall et al. 2019, Swemmer 2020).

1.4. Evolutionary relationships between drought-related traits and climate variation

In evolutionary ecology, a key challenge is to understand which factors promote and maintain biological diversity on both a taxonomic and functional level (Westoby and Wright 2006). Functional diversity is studied in plants through phenotypic traits called functional traits (Geber and Griffen 2003). As defined by Violle et al. (2007), a functional trait is a morpho-physio-phenological characteristic of plants that affects different fitness components (survival, growth, reproduction effort) throughout their life cycle. It is both environmental conditions and phenotypic characteristics that improve the fitness of individual species in specific environments (Ackerly 2003). Climate change and altered bioclimatic patterns, as previously mentioned, have been associated with large-scale species losses, shifts in vegetation communities and evolution of plants (Davis and Shaw 2001, Parmesan 2006, Franks et al. 2014). The ability of functional traits to respond to environmental stress has been largely used in plant ecology to explore functional strategies at different environments (Esperon-Rodriguez et al. 2020, Martinez-Vivalta et al. 2010, Nardini and Luglio al. 2013).

A key goal is to understand the impacts of global change on plants for determining the relative contributions to tree population persistence made by phenotypic plasticity, evolutionary change in phenology (Alberto et al. 2013), evolution of the plastic response in functional traits (Gienapp et al. 2008) and/or to species distributions (Blackman et al. 2012, Larter et al. 2017, Skelton et al. 2020). The response of organisms to changing environmental conditions is genetically mediated (Bradshaw 1965), so it may evolve as a result of the selection imposed by a changing environment (Alpert and Simms 2002, Hamann et al. 2020).

Adaptations to climatic conditions are believed to be key to this coordinated evolution of traits through natural selection. Edwards (2006) suggested that leaf and stem hydraulic traits in *Pereskia* may have evolved together as a result of adaptations to different precipitation regimes.

Field measurements are the most common method of studying trait-trait and trait-climate evolution. Thus, such associations could simply be the result of phenotypic plasticity, rather than evolution. Under common garden experiments, evolutionary divergence can only be distinguished from plastic effects (Ramirez-Valiente et al. 2010, Givnish and Montgomery 2014, Mason and Donovan 2015). The use of closely related species from well-resolved lineages in common gardens is the only way to detect true evolutionary coordination (Scoffoni et al. 2016)

1.5. Thesis structure and project objectives

In this thesis, I first present the impact of a changing climate on the temperate forest, then the different strategies and processes adopted by trees during drought events. I introduce our current knowledge of plant drought-related traits in order to better understand and predict the key mechanisms of drought-induced embolism, that leads to increased tree mortality. Finally, I will discuss the possible trait evolution and plasticity of trees throughout a changing environment on the base of the measured traits. (Fig. 1.2).

To avoid redundancy in this thesis, I will give a brief overview of the methods and measured parameters in Section 1.5. The main part of this cumulative thesis dissertation are manuscripts, which are addressing to the study question in the following paragraphs (Part II). A common format is used to present each chapter. It follows that Chapter 1 is currently under review at the journal New Phytologist, Chapter 2 is currently under review at the journal Plant Biology and Chapter 3 is being prepared for submission to the journal New Phytologist.
In Chapter 1, I aimed to build a compilation of large global datasets of traits related to drought-induced embolism and test whether embolism resistance can be determined solely by anatomical traits. In Chapter 2, I focused on using the knowledge from Chapter 1 to develop and improve an accurate and widely applicable technique for estimating xylem embolism resistance. To follow up, in Chapter 3 of this thesis I examined the evolutionary relationships between drought-related traits and environmental preferences. The focus was set on the precipitation and temperature preferences.

The main objectives of the present thesis are the following:

- **Chapter 1:** *Addressing controversies in embolism resistance – vessel diameter relationships*

    - to investigate easy measurable wood anatomical and hydraulic traits related to embolism resistance,
    - to study the inter- and intraspecific scaling of water potential at 50% loss of conductivity with the hydraulically weighted vessel diameter and to test its link to pit membrane thickness and specific conductivity related to drought-induced embolism;

- **Chapter 2**: *Accuracy of the pneumatic method for the construction of branch xylem vulnerability curves of temperate diffuse-porous trees*

    - to assess how well the parameters of the vulnerability curves obtained with the pneumatic method (Pneumatron) agree with estimates obtained from the flow-centrifuge method (Cavitron),
    - Identify the optimal duration for air discharge measurements;

- **Chapter 3:** *Relationships between drought induced traits and environmental preferences across four genera of temperate trees*

    - to determine the interspecific trait range capacity to prevent xylem embolism in six species from each plant family: Betulaceae, Rosaceae and Malvaceae Sapindaceae. Then examine the relationship between stem embolism resistance, vessel size and wood density among these 24 species,
    - to investigate how the drought-induced traits of those species are phylogenetically controlled and associated with ecological variables.

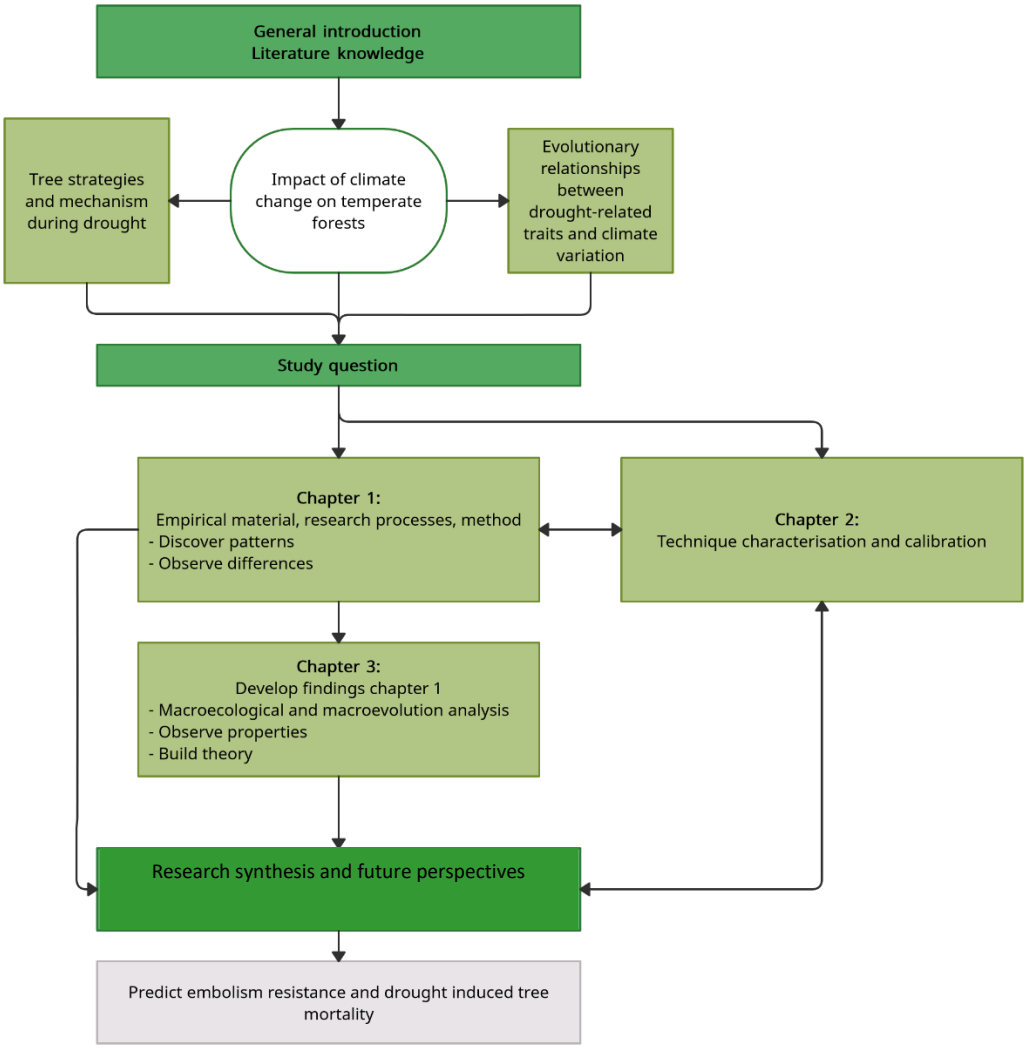

Figure 1.2: This diagram provides an overview of the thesis structure; arrows show how sections and chapters are connected to investigate the main thesis themes (grey box).

The overarching motivation for this work was to test the following hypotheses:

- ⇨ Chapter 1: Pit membrane thickness increases when the water potential at 50% loss of conductivity decreases and vessel diameter remains positively correlated with it;
- ⇨ Chapter 2: The estimated water potential at 50% of discharged air volume measured with the pneumatic method coincide with the measurements done with the flow-centrifuge method and 15 sec duration is the optimal discharge time used for measurements;
- ⇨ Chapter 3: Drought-induced traits show a strong phylogenetic signal across congeneric species and across families and there is a detectable trait-environment relationships across congeneric species and across families.

1.6. Project framework, methods and study area

In the following section, a brief overview of the measured parameters in this study are described. Furthermore, in the corresponding chapters, additional methodological information is provided.

1.6.1. Experimental design and study area

This study was conducted on three areas (Fig. 1.3): the Stutel-Arboretum at the Bavarian State Institute for Viticulture and Horticulture in Veitshöchheim, Germany (LWG) (49°51'49"N, 9°51'8"E), the Botanical Garden of the University in Würzburg (49°45'56.7"N, 9°55'58.1"E) and the University of Ulm in Germany (48°25'20.3"N, 9°57'20.2"E).
Located between latitudinal midpoints of approximately 25° and 75°, the arboretum is home to more than 400 different tree species. Originally raised in nurseries in Europe and Asia, the trees were brought to the arboretum as seedlings (maximum age of 2 years). As part of the extensive project called "Klimabäume Stutel" by the Bavarian State Institute for Viticulture and Horticulture (LWG), the trees have been planted in 42 rows with a spacing of at least 3 × 3 m and raised in the arboretum since 2010. Trees shared a common soil, geographical setting (south-west facing aspect and mild slope), climatic condition and were grown without interference from neighbouring trees, or any major disturbance to their growth form. The trees are monitored periodically by recording their growth but are maintained without disturbance to their growth form with the exception of some minor pruning in the first year after planting.
The long-term mean annual temperature and mean annual precipitation are 10.0 °C and 591 mm in Veitshöchheim, 9.6 °C and 560.4 mm in Würzburg and 9.1°C and 947mm, constituting a warm temperate continental climate according to the Köppen classification (Peel et al. 2007). The location of all study sites is provided in Fig. 1.3. We investigated in total 153 trees including 38 species.

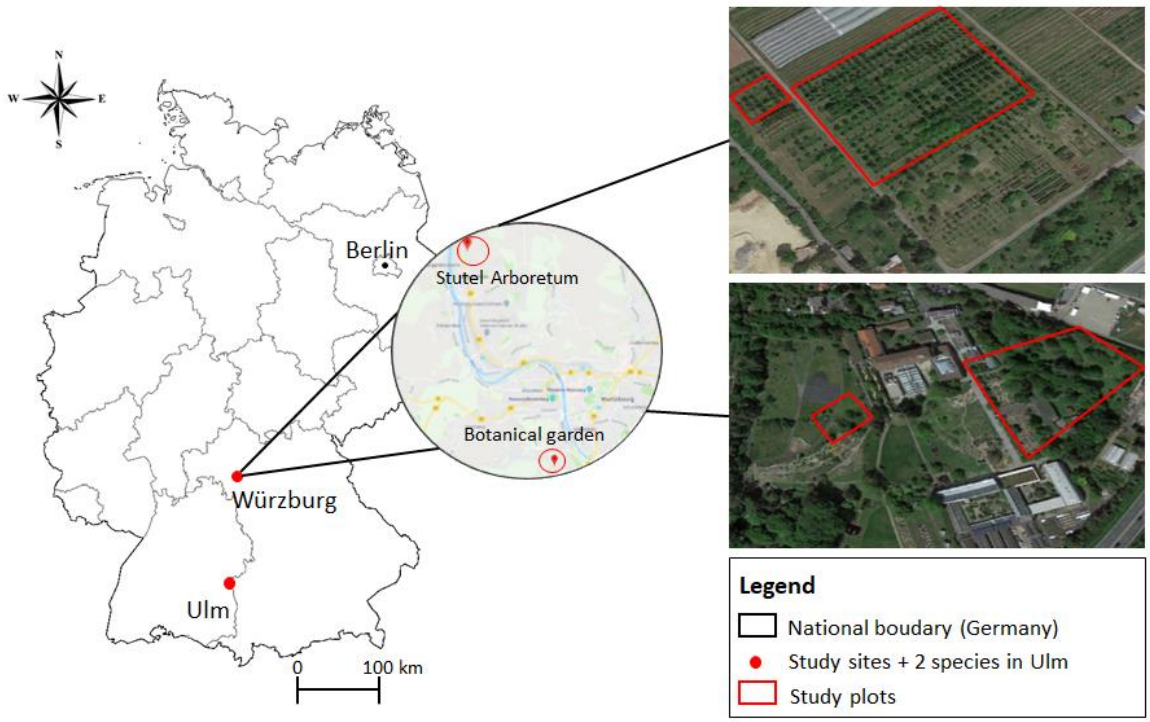

Figure 1.3: Map of Germany with the location of the research sites at Stutel-arboretum and at Würzburg, Germany. An aerial view of the arboretum and of the Botanical Garden of (Google Earth 2022) with the plots chosen for our experimental campaign.

1.6.2. Species selection

To answer our study questions (Section 2) 77 trees from 20 temperate angiosperm diffuse-porous tree species from 10 genera were chosen from the nursery in the Stutel-Arboretum. Additionally, 22 *Acer monspessulanum* trees were selected from the Botanical Garden of the University of Würzburg, Germany. Then to answer our study questions presented in Section 3, plant material from trees belonging to 12 temperate diffuse-porous tree species were collected in the Stutel-Arboretum and three extra trees were sampled at the University of Ulm and at the Botanical Garden of the Würzburg, Germany. Finally in order to answer our study questions presented in Section 4, plant material of 67 trees from 24 temperate angiosperm diffuse-porous tree species from four families (Betulaceae, Rosaceae, Malvaceae, Sapindaceae) were used. We selected the six species within each family based on their ability to withstand drought stress as well as their similar and/or parapatric geographical distribution (i.e., northern temperate climates). To capture trait differences based on the tree species evolutionary history rather than an ecological context of the tree individuals, it is essential that the individuals were grown under the same environmental conditions.

1.6.3. Summary of the measured parameters

The following parameters were measured in the context of the present PhD thesis. Several of them were not included in the different chapters of the study question but essential for the general discussion.

All samples for the hydraulic, wood and leaf anatomy measurements were freshly collected, and analysed between 2019 and 2021.

1.6.3.1. Tree structure measurements

To track changes in tree diameter, all trees studied (Part I, Chapter 1), were equipped with dendrometer bands (UMS GmbH, Munich, Germany) to measure the diameter at breast hight (*DBH*, cm) in September of each year 2019-2021. The annual stem increment (ASI) was estimated using the difference between the initial plantation radial value and the 2021 radius value.
The height (*H*, m) and crown volume (*Crown*, m^3) of the experimental trees was measured in February 2020 using a ground-based mobile laser scanning (MLS) (Geoslam ZEB-HORIZON, Geoslam Ltd., UK 2019). The raw data were processed using the 3D SLAM algorithm in the GeoSLAM Hub 6.0 processing software (Geoslam Ltd. UK). Open source CloudCompare software (CloudCompare v2.10.1, https://www.danielgm.net/cc/) was then used for post-processing the point clouds.

1.6.3.2. Hydraulic measurements

The vulnerability curves (VCs) where measured with the flow centrifuge (Cavitron) method (Cochard et al. 2013) and with the Pneumatic method (Pereira et al. 2016). Based on VCs the 12%, 50% and 88% loss of hydraulic conductivity, (respectively P_{12}, P_{50}, P_{88}) was calculated. All the xylem pressure (Ψp, MPa) were taken with a Scholander pressure chamber (PMS Instruments, Corvallis, Oregon, USA). Branch xylem hydraulic specific conductivity (K_s, Kg m^{-1} MPa^{-1} s^{-1}) was determined using the Xyl'em Plus embolism meter (Bronkhorst, Montigny-Les-Cormeilles, France).
Finally, the hydraulic safety margins (HSM, MPa) were calculated based on the difference of the minimum water potential, measured during midday (Ψ_{min}, MPa) and the P_{50}.

1.6.3.3. Wood anatomical traits

Wood anatomical trait were analysed following the hydraulic measurements. Stem wood density (*WD*, g cm^{-3}), saturated water content (SWC, %), vessel density (V_D, n mm^{-2}), hydraulically-weighted average vessel diameter (D_h, µm), solitary vessel index (V_S), grouping

vessel index (V_G) and Vulnerability index (VI, $\mu m^2\ mm^{-2}$) where determined using transverse sections of the wood anatomical samples which were made with a sliding microtome (G.S.L.1, Schenkung Dapples, Zürich, Switzerland). Finally, one sample per species was prepared for transmission electron microscope (TEM) analyses to measure pit membrane thickness (T_{PM}) following the protocol by Jansen et al. (2009).

1.6.3.4. Leaf anatomical and hydraulics trait

For all branch samples used for vulnerability curve measurements, all distal leaves were scanned and oven-dried at 70°C for at least 48h to determine the total leaf area (LA, cm^2), specific leaf area (SLA, $cm^2\ g^{-1}$) and the Huber Value (i.e., the ratio between sapwood area and leaf area, HV). The leaf turgor loss point (Ψ_{tlp}, Mpa) which is the leaf water potential at which turgor pressure is zero (i.e., of the tolerance of leaves to drought stress) was determined following the osmometer method of Bartlett et al. (2012) and the vapor pressure osmometer Wescor Vapro 5600 Vapor Pressure Osmometer.

References

Ackerly, D.D., 2003. Community Assembly, Niche Conservatism and Adaptive Evolution in Changing Environments. International Journal of Plant Sciences 164, S165–S184. https://doi.org/10.1086/368401

Adams, H.D., Guardiola-Claramonte, M., Barron-Gafford, G.A., Villegas, J.C., Breshears, D.D., Zou, C.B., Troch, P.A., Huxman, T.E., 2009. Temperature sensitivity of drought-induced tree mortality portends increased regional die-off under global-change-type drought. Proc. Natl. Acad. Sci. U.S.A. 106, 7063–7066. https://doi.org/10.1073/pnas.0901438106

Alberto, Florian J., Aitken, S.N., Alía, R., González-Martínez, S.C., Hänninen, H., Kremer, A., Lefèvre, F., Lenormand, T., Yeaman, S., Whetten, R., Savolainen, O., 2013. Potential for evolutionary responses to climate change – evidence from tree populations. Glob Change Biol 19, 1645–1661. https://doi.org/10.1111/gcb.12181

Alberto, Florian J, Derory, J., Boury, C., Frigerio, J.-M., Zimmermann, N.E., Kremer, A., 2013. Imprints of Natural Selection Along Environmental Gradients in Phenology-Related Genes of *Quercus petraea*. Genetics 195, 495–512. https://doi.org/10.1534/genetics.113.153783

Allen, C.D., Breshears, D.D., McDowell, N.G., 2015. On underestimation of global vulnerability to tree mortality and forest die-off from hotter drought in the Anthropocene. Ecosphere 6, art129. https://doi.org/10.1890/ES15-00203.1

Allen, C.D., Macalady, A.K., Chenchouni, H., Bachelet, D., McDowell, N., Vennetier, M., Kitzberger, T., Rigling, A., Breshears, D.D., Hogg, E.H. (Ted), Gonzalez, P., Fensham, R., Zhang, Z., Castro, J., Demidova, N., Lim, J.-H., Allard, G., Running, S.W., Semerci, A., Cobb, N., 2010. A global overview of drought and heat-induced tree mortality reveals emerging climate change risks for forests. Forest Ecology and Management 259, 660–684. https://doi.org/10.1016/j.foreco.2009.09.001

Alpert, P., Simms, E.L., 2002. The relative advantages of plasticity and fixity in different environments: when is it good for a plant to adjust? Evolutionary Ecology 16, 285–297. https://doi.org/10.1023/A:1019684612767

Anderegg, W.R.L., Berry, J.A., Smith, D.D., Sperry, J.S., Anderegg, L.D.L., Field, C.B., 2012. The roles of hydraulic and carbon stress in a widespread climate-induced forest die-off. Proc. Natl. Acad. Sci. U.S.A. 109, 233–237. https://doi.org/10.1073/pnas.1107891109

Anderegg, W.R.L., Klein, T., Bartlett, M., Sack, L., Pellegrini, A.F.A., Choat, B., Jansen, S., 2016a. Meta-analysis reveals that hydraulic traits explain cross-species patterns of drought-induced tree mortality across the globe. Proc. Natl. Acad. Sci. U.S.A. 113, 5024–5029. https://doi.org/10.1073/pnas.1525678113

Anderegg, W.R.L., Martinez-Vilalta, J., Cailleret, M., Camarero, J.J., Ewers, B.E., Galbraith, D., Gessler, A., Grote, R., Huang, C., Levick, S.R., Powell, T.L., Rowland, L., Sánchez-Salguero, R., Trotsiuk, V., 2016b. When a Tree Dies in the Forest: Scaling Climate-Driven Tree Mortality to Ecosystem Water and Carbon Fluxes. Ecosystems 19, 1133–1147. https://doi.org/10.1007/s10021-016-9982-1

Anderegg, W.R.L., Meinzer, F.C., 2015. Wood Anatomy and Plant Hydraulics in a Changing Climate, in: Hacke, U. (Ed.), Functional and Ecological Xylem Anatomy. Springer International Publishing, Cham, pp. 235–253. https://doi.org/10.1007/978-3-319-15783-2_9

Asadi Zarch, M.A., Sivakumar, B., Malekinezhad, H., Sharma, A., 2017. Future aridity under conditions of global climate change. Journal of Hydrology 554, 451–469. https://doi.org/10.1016/j.jhydrol.2017.08.043

Bartlett, M.K., Scoffoni, C., Ardy, R., Zhang, Y., Sun, S., Cao, K., Sack, L., 2012. Rapid determination of comparative drought tolerance traits: using an osmometer to predict turgor loss point: *Rapid assessment of leaf drought tolerance*. Methods in Ecology and Evolution 3, 880–888. https://doi.org/10.1111/j.2041-210X.2012.00230.x

Bigler, C., Gavin, D.G., Gunning, C., Veblen, T.T., 2007. Drought induces lagged tree mortality in a subalpine forest in the Rocky Mountains. Oikos 116, 1983–1994. https://doi.org/10.1111/j.2007.0030-1299.16034.x

Billington, C., Kapos, V., Edwards, M.E., Blyth, S., Iremonger, S., 1996. Estimated Original Forest Cover Map - A First Attempt.

Blackmann, C.J., Brodribb, T.J., Jordan, G.J., 2012. Leaf hydraulic vulnerability influences species' bioclimatic limits in a diverse group of woody angiosperme 11.

Bouche, P.S., Jansen, S., Cochard, H., Burlett, R., Capdeville, G., Delzon, S., 2015. Embolism resistance of conifer roots can be accurately measured with the flow-centrifuge method. JPH 2, e002. https://doi.org/10.20870/jph.2015.e002

Bradshaw, A.D., 1965. Evolutionary Significance of Phenotypic Plasticity in Plants, in: Advances in Genetics. Elsevier, pp. 115–155. https://doi.org/10.1016/S0065-2660(08)60048-6

Bréda, N., Huc, R., Granier, A., Dreyer, E., 2006a. Temperate Forest trees and stands under severe drought: a review of ecophysiological responses, adaptation processes and long-term consequences. Ann. For. Sci. 63, 625–644. https://doi.org/10.1051/forest:2006042

Bréda, N., Huc, R., Granier, A., Dreyer, E., 2006b. Temperate Forest trees and stands under severe drought: a review of ecophysiological responses, adaptation processes and long-term consequences. Ann. For. Sci. 63, 625–644. https://doi.org/10.1051/forest:2006042

Breshears, D.D., Cobb, N.S., Rich, P.M., Price, K.P., Allen, C.D., Balice, R.G., Romme, W.H., Kastens, J.H., Floyd, M.L., Belnap, J., Anderson, J.J., Myers, O.B., Meyer, C.W., 2005. Regional vegetation die-off in response to global-change-type drought. Proc. Natl. Acad. Sci. U.S.A. 102, 15144–15148. https://doi.org/10.1073/pnas.0505734102

Brodribb, T.J., 2009. Xylem hydraulic physiology: The functional backbone of terrestrial plant productivity. Plant Science 177, 245–251. https://doi.org/10.1016/j.plantsci.2009.06.001

Brodribb, T.J., Cochard, H., 2009. Hydraulic Failure Defines the Recovery and Point of Death in Water-Stressed Conifers. Plant Physiology 149, 575–584. https://doi.org/10.1104/pp.108.129783

Bucci, S.J., Scholz, F.G., Peschiutta, M.L., Arias, N.S., Meinzer, F.C., Goldstein, G., 2013. The stem xylem of Patagonian shrubs operates far from the point of catastrophic dysfunction and is additionally protected from drought-induced embolism by leaves and roots: Hydraulic segmentation in shrubs. Plant Cell Environ 36, 2163–2174. https://doi.org/10.1111/pce.12126

Cai, J., Tyree, M.T., 2010a. The Impact of Vessel Size on Vulnerability Curves: Data and Models for Within-Species Variability in Saplings of Aspen, *Populus tremuloides* Michx. Plant, Cell & Environment. https://doi.org/10.1111/j.1365-3040.2010.02127.x

Calkin, H.W., Gibson, A.C., Nobel, P.S., 1986. Biophysical Model of Xylem Conductance in Tracheids of the Fern *Pteris vittata*. J Exp Bot 37, 1054–1064. https://doi.org/10.1093/jxb/37.7.1054

Carlquist, S., n.d. Vessel grouping in dicotyledon wood significance and relationship to imperforate tracheary elements 10, 21.

Carnicer, J., Coll, M., Ninyerola, M., Pons, X., Sánchez, G., Peñuelas, J., 2011. Widespread crown condition decline, food web disruption and amplified tree mortality with increased climate change-type drought. Proc. Natl. Acad. Sci. U.S.A. 108, 1474–1478. https://doi.org/10.1073/pnas.1010070108

Chave, J., Coomes, D., Jansen, S., Lewis, S.L., Swenson, N.G., Zanne, A.E., 2009. Towards a worldwide wood economics spectrum. Ecology Letters 12, 351–366. https://doi.org/10.1111/j.1461-0248.2009.01285.x

Choat, B., Brodribb, T.J., Brodersen, C.R., Duursma, R.A., López, R., Medlyn, B.E., 2018. Triggers of tree mortality under drought. Nature 558, 531–539. https://doi.org/10.1038/s41586-018-0240-x

Choat, B., Cobb, A.R., Jansen, S., 2008. Structure and function of bordered pits: new discoveries and impacts on whole-plant hydraulic function. New Phytologist 177, 608–626. https://doi.org/10.1111/j.1469-8137.2007.02317.x

Choat, B., Jansen, S., Brodribb, T.J., Cochard, H., Delzon, S., Bhaskar, R., Bucci, S.J., Feild, T.S., Gleason, S.M., Hacke, U.G., Jacobsen, A.L., Lens, F., Maherali, H., Martínez-Vilalta, J., Mayr, S., Mencuccini, M., Mitchell, P.J., Nardini, A., Pittermann, J., Pratt, R.B., Sperry, J.S., Westoby, M., Wright, I.J., Zanne, A.E., 2012. Global convergence in the vulnerability of forests to drought. Nature 491, 752–755. https://doi.org/10.1038/nature11688

Choat, B., Pittermann, J., 2009. New insights into bordered pit structure and cavitation resistance in angiosperms and conifers. New Phytologist 182, 557–560. https://doi.org/10.1111/j.1469-8137.2009.02847.x

Christman, M.A., Sperry, J.S., Adler, F.R., 2009. Testing the 'rare pit' hypothesis for xylem cavitation resistance in three species of *Acer*. New Phytologist 182, 664–674. https://doi.org/10.1111/j.1469-8137.2009.02776.x

Christoffersen, B.O., Gloor, M., Fauset, S., Fyllas, N.M., Galbraith, D.R., Baker, T.R., Kruijt, B., Rowland, L., Fisher, R.A., Binks, O.J., Sevanto, S., Xu, C., Jansen, S., Choat, B., Mencuccini, M., McDowell, N.G., Meir, P., 2016. Linking hydraulic traits to tropical forest function in a size-structured and trait-driven model (TFS v.1-Hydro). Geosci. Model Dev. 9, 4227–4255. https://doi.org/10.5194/gmd-9-4227-2016

Cochard, H., Badel, E., Herbette, S., Delzon, S., Choat, B., Jansen, S., 2013. Methods for measuring plant vulnerability to cavitation: a critical review. Journal of Experimental Botany 64, 4779–4791. https://doi.org/10.1093/jxb/ert193

Dauphin, B., Rellstab, C., Schmid, M., Zoller, S., Karger, D.N., Brodbeck, S., Guillaume, F., Gugerli, F., 2021. Genomic vulnerability to rapid climate warming in a tree species with a long generation time. Glob. Change Biol. 27, 1181–1195. https://doi.org/10.1111/gcb.15469

Davis, M.B., Shaw, R.G., 2001. Range Shifts and Adaptive Responses to Quaternary Climate Change. Science 292, 673–679. https://doi.org/10.1126/science.292.5517.673

Davis, S.D., Sperry, J.S., Hacke, U.G., 1999. The relationship between xylem conduit diameter and cavitation caused by freezing. Am. J. Bot. 86, 1367–1372. https://doi.org/10.2307/2656919

Dixon, H., Joly, J., 1895. XII. On the ascent of sap. Phil. Trans. R. Soc. Lond. B 186, 563–576. https://doi.org/10.1098/rstb.1895.0012

Domec, J.-C., Gartner, B.L., 2001. Cavitation and water storage capacity in bole xylem segments of mature and young Douglas-fir trees. Trees 15, 204–214. https://doi.org/10.1007/s004680100095

Domec, J.-C., Lachenbruch, B., Meinzer, F.C., Woodruff, D.R., Warren, J.M., McCulloh, K.A., 2008. Maximum height in a conifer is associated with conflicting requirements for xylem design. Proc. Natl. Acad. Sci. U.S.A. 105, 12069–12074. https://doi.org/10.1073/pnas.0710418105

Edwards, E.J., 2006. Correlated evolution of stem and leaf hydraulic traits in *Pereskia* (Cactaceae). New Phytologist 172, 479–789. https://doi.org/10.1111/j.1469-8137.2006.01850.x

Eggers, J., Lindner, M., Zudin, S., Zaehle, S., Liski, J., 2008. Impact of changing wood demand, climate and land use on European forest resources and carbon stocks during the 21st century: Impact of changing wood demand climate and land use. Global Change Biology 14, 2288–2303. https://doi.org/10.1111/j.1365-2486.2008.01653.x

Ellis, E.C., 2015. Ecology in an anthropogenic biosphere. Ecological Monographs 85, 287–331. https://doi.org/10.1890/14-2274.1

Esperon-Rodriguez, M., Rymer, P.D., Power, S.A., Challis, A., Marchin, R.M., Tjoelker, M.G., 2020. Functional adaptations and trait plasticity of urban trees along a climatic gradient. Urban Forestry & Urban Greening 54, 126771. https://doi.org/10.1016/j.ufug.2020.126771

Falster, D.S., Duursma, R.A., FitzJohn, R.G., 2018. How functional traits influence plant growth and shade tolerance across the life cycle. Proc. Natl. Acad. Sci. U.S.A. 115. https://doi.org/10.1073/pnas.1714044115

Franks, S.J., Weber, J.J., Aitken, S.N., 2014. Evolutionary and plastic responses to climate change in terrestrial plant populations. Evol Appl 7, 123–139. https://doi.org/10.1111/eva.12112

Geber, M.A., Griffen, L.R., 2003. Inheritance and Natural Selection on Functional Traits. International Journal of Plant Sciences 164, S21–S42. https://doi.org/10.1086/368233

Gibert, A., Gray, E.F., Westoby, M., Wright, I.J., Falster, D.S., 2016. On the link between functional traits and growth rate: meta-analysis shows effects change with plant size, as predicted. J Ecol 104, 1488–1503. https://doi.org/10.1111/1365-2745.12594

Gienapp, P., Teplitsky, C., Alho, J.S., Mills, J.A., Merilä, J., 2008. Climate change and evolution: disentangling environmental and genetic responses. Molecular Ecology 17, 167–178. https://doi.org/10.1111/j.1365-294X.2007.03413.x

Givnish, T.J., Montgomery, R.A., 2014. Common-garden studies on adaptive radiation of photosynthetic physiology among Hawaiian lobeliads. Proc. R. Soc. B. 281, 20132944. https://doi.org/10.1098/rspb.2013.2944

Gleason, S.M., Westoby, M., Jansen, S., Choat, B., Hacke, U.G., Pratt, R.B., Bhaskar, R., Brodribb, T.J., Bucci, S.J., Cao, K., Cochard, H., Delzon, S., Domec, J., Fan, Z., Feild, T.S., Jacobsen, A.L., Johnson, D.M., Lens, F., Maherali, H., Martínez-Vilalta, J., Mayr, S., McCulloh, K.A., Mencuccini, M., Mitchell, P.J., Morris, H., Nardini, A., Pittermann, J., Plavcová, L., Schreiber, S.G., Sperry, J.S., Wright, I.J., Zanne, A.E., 2016. Weak trade-off between xylem safety and xylem-specific hydraulic efficiency across the world's woody plant species. New Phytol 209, 123–136. https://doi.org/10.1111/nph.13646

Grassi, G., House, J., Dentener, F., Federici, S., den Elzen, M., Penman, J., 2017. The key role of forests in meeting climate targets requires science for credible mitigation. Nature Clim Change 7, 220–226. https://doi.org/10.1038/nclimate3227

Hacke, U.G., Jansen, S., 2009. Embolism resistance of three boreal conifer species varies with pit structure. New Phytologist 182, 675–686. https://doi.org/10.1111/j.1469-8137.2009.02783.x

Hacke, U.G., Sperry, J.S., 2001. Functional and ecological xylem anatomy 19.

Hacke, U.G., Sperry, J.S., Ewers, B.E., Ellsworth, D.S., Schäfer, K.V.R., Oren, R., 2000. Influence of soil porosity on water use in Pinus taeda. Oecologia 124, 495–505. https://doi.org/10.1007/PL00008875

Hacke, U.G., Sperry, J.S., Wheeler, J.K., Castro, L., 2006. Scaling of angiosperm xylem structure with safety and efficiency. Tree Physiology 26, 689–701. https://doi.org/10.1093/treephys/26.6.689

Hajek, P., Leuschner, C., Hertel, D., Delzon, S., Schuldt, B., 2014. Trade-offs between xylem hydraulic properties, wood anatomy and yield in Populus. Tree Physiology 34, 744–756. https://doi.org/10.1093/treephys/tpu048

Hajek, P., Link, R.M., Nock, C.A., Bauhus, J., Gebauer, T., Gessler, A., Kovach, K., Messier, C., Paquette, A., Saurer, M., Scherer-Lorenzen, M., Rose, L., Schuldt, B., 2022. Mutually inclusive mechanisms of drought-induced tree mortality. Global Change Biology 28, 3365–3378. https://doi.org/10.1111/gcb.16146

Hamann, E., Pauli, C.S., Joly-Lopez, Z., Groen, S.C., Rest, J.S., Kane, N.C., Purugganan, M.D., Franks, S.J., 2021. Rapid evolutionary changes in gene expression in response to climate fluctuations. Mol Ecol 30, 193–206. https://doi.org/10.1111/mec.15583

Hargrave, K.R., Kolb, K.J., Ewers, F.W., Davis, S.D., 1994. Conduit diameter and drought-induced embolism in *Salvia mellifera* Greene (Labiatae). New Phytologist 126, 695–705. https://doi.org/10.1111/j.1469-8137.1994.tb02964.x

Hartmann, H., Schuldt, B., Sanders, T.G.M., Macinnis-Ng, C., Boehmer, H.J., Allen, C.D., Bolte, A., Crowther, T.W., Hansen, M.C., Medlyn, B.E., Ruehr, N.K., Anderegg, W.R.L., 2018. Monitoring global tree mortality patterns and trends. Report from the VW symposium 'Crossing scales and disciplines to identify global trends of tree mortality as indicators of forest health.' New Phytol 217, 984–987. https://doi.org/10.1111/nph.14988

Hartmann, H., Trumbore, S., 2016. Understanding the roles of nonstructural carbohydrates in forest trees – from what we can measure to what we want to know. New Phytol 211, 386–403. https://doi.org/10.1111/nph.13955

Hietz, P., Rosner, S., Hietz-Seifert, U., Wright, S.J., 2017. Wood traits related to size and life history of trees in a Panamanian rainforest. New Phytol 213, 170–180. https://doi.org/10.1111/nph.14123

Hobbs, R.J., Higgs, E., Hall, C.M., Bridgewater, P., Chapin, F.S., Ellis, E.C., Ewel, J.J., Hallett, L.M., Harris, J., Hulvey, K.B., Jackson, S.T., Kennedy, P.L., Kueffer, C., Lach, L., Lantz, T.C., Lugo, A.E., Mascaro, J., Murphy, S.D., Nelson, C.R., Perring, M.P., Richardson, D.M., Seastedt, T.R., Standish, R.J., Starzomski, B.M., Suding, K.N., Tognetti, P.M., Yakob, L., Yung, L., 2014. Managing the whole landscape: historical, hybrid and novel ecosystems. Frontiers in Ecology and the Environment 12, 557–564. https://doi.org/10.1890/130300

Hochberg, U., Rockwell, F.E., Holbrook, N.M., Cochard, H., 2018. Iso/Anisohydry: A Plant–Environment Interaction Rather Than a Simple Hydraulic Trait. Trends in Plant Science 23, 112–120. https://doi.org/10.1016/j.tplants.2017.11.002

Hoeber, S., Leuschner, C., Köhler, L., Arias-Aguilar, D., Schuldt, B., 2014. The importance of hydraulic conductivity and wood density to growth performance in eight tree species from a tropical semi-dry climate. Forest Ecology and Management 330, 126–136. https://doi.org/10.1016/j.foreco.2014.06.039

Jansen, S., Choat, B., Pletsers, A., 2009. Morphological variation of intervessel pit membranes and implications to xylem function in angiosperms. American Journal of Botany 96, 409–419. https://doi.org/10.3732/ajb.0800248

Jansen, S., Klepsch, M., Li, S., Kotowska, M.M., Schiele, S., Zhang, Y., Schenk, H.J., 2018. Challenges in understanding air-seeding in angiosperm xylem. Acta Hortic. 13–20. https://doi.org/10.17660/ActaHortic.2018.1222.3

Jentsch, A., Kreyling, J., Beierkuhnlein, C., 2007. A new generation of climate-change experiments: events, not trends. Frontiers in Ecology and the Environment 5, 365–374. https://doi.org/10.1890/1540-9295(2007)5[365:ANGOCE]2.0.CO;2

Kaack, L., Weber, M., Isasa, E., Karimi, Z., Li, S., Pereira, L., Trabi, C.L., Zhang, Y., Schenk, H.J., Schuldt, B., Schmidt, V., Jansen, S., 2020. Pore constrictions in intervessel pit membranes reduce the risk of embolism spreading in angiosperm xylem (preprint). Plant Biology. https://doi.org/10.1101/2020.10.19.345413

King, D.A., Davies, S.J., Tan, S., Noor, N.S.Md., 2006. The role of wood density and stem support costs in the growth and mortality of tropical trees: Tree demography and stem support costs. Journal of Ecology 94, 670–680. https://doi.org/10.1111/j.1365-2745.2006.01112.x

Larter, M., Pfautsch, S., Domec, J., Trueba, S., Nagalingum, N., Delzon, S., 2017. Aridity drove the evolution of extreme embolism resistance and the radiation of conifer genus *Callitris*. New Phytol 215, 97–112. https://doi.org/10.1111/nph.14545

Lens, F., Sperry, J.S., Christman, M.A., Choat, B., Rabaey, D., Jansen, S., 2011. Testing hypotheses that link wood anatomy to cavitation resistance and hydraulic conductivity in the genus *Acer*. New Phytologist 190, 709–723. https://doi.org/10.1111/j.1469-8137.2010.03518.x

Lens, F., Gleason, S.M., Bortolami, G., Brodersen, C., Delzon, S., Jansen, S., 2022. Functional xylem characteristics associated with drought-induced embolism in angiosperms. New Phytologist nph.18447. https://doi.org/10.1111/nph.18447

Lewis, S.L., Maslin, M.A., 2015. A transparent framework for defining the Anthropocene Epoch. The Anthropocene Review 2, 128–146. https://doi.org/10.1177/2053019615588792

Li, S., Lens, F., Espino, S., Karimi, Z., Klepsch, M., Schenk, H.J., Schmitt, M., Schuldt, B., Jansen, S., 2016. Intervessel pit membrane thickness as a key determinant of embolism resistance in angiosperm xylem: IAWA J 37, 152–171. https://doi.org/10.1163/22941932-20160128

Lindenmayer, D.B., Laurance, W.F., 2017. The ecology, distribution, conservation and management of large old trees: Ecology and management of large old trees. Biol Rev 92, 1434–1458. https://doi.org/10.1111/brv.12290

Loepfe, L., Martinez-Vilalta, J., Piñol, J., Mencuccini, M., 2007. The relevance of xylem network structure for plant hydraulic efficiency and safety. Journal of Theoretical Biology 247, 788–803. https://doi.org/10.1016/j.jtbi.2007.03.036

Maherali, H., Moura, C.F., Caldeira, M.C., Willson, C.J., Jackson, R.B., 2006. Functional coordination between leaf gas exchange and vulnerability to xylem cavitation in temperate forest trees. Plant Cell Environ 29, 571–583. https://doi.org/10.1111/j.1365-3040.2005.01433.x

Maherali, H., Pockman, W.T., Jackson, R.B., 2004. Adaptative variation in the vulnerability of wood plants to xylem cavitation. Ecology 85, 2184–2199. https://doi.org/10.1890/02-0538

Markesteijn, L., Poorter, L., Paz, H., Sack, L., Bongers, F., 2011. Ecological differentiation in xylem cavitation resistance is associated with stem and leaf structural traits: Vulnerability to cavitation of tropical dry forest tree species. Plant, Cell & Environment 34, 137–148. https://doi.org/10.1111/j.1365-3040.2010.02231.x

Martínez-Vilalta, J., Garcia-Forner, N., 2017. Water potential regulation, stomatal behaviour and hydraulic transport under drought: deconstructing the iso/anisohydric concept: Deconstructing the iso/anisohydric concept. Plant, Cell & Environment 40, 962–976. https://doi.org/10.1111/pce.12846

Martinez-Vilalta, J., Mencuccini, M., Alvarez, X., Camacho, J., Loepfe, L., Pinol, J., 2012. Spatial distribution and packing of xylem conduits. American Journal of Botany 99, 1189–1196. https://doi.org/10.3732/ajb.1100384

Martínez-Vilalta, J., Mencuccini, M., Vayreda, J., Retana, J., 2010. Interspecific variation in functional traits, not climatic differences among species ranges, determines demographic rates across 44 temperate and Mediterranean tree species: Determinants of demographic rates across species. Journal of Ecology 98, 1462–1475. https://doi.org/10.1111/j.1365-2745.2010.01718.x

Martínez-Vilalta, J., Poyatos, R., Aguadé, D., Retana, J., Mencuccini, M., 2014. A new look at water transport regulation in plants. New Phytol 204, 105–115. https://doi.org/10.1111/nph.12912

Mason, C.M., Donovan, L.A., 2015. Evolution of the leaf economics spectrum in herbs: Evidence from environmental divergences in leaf physiology across *Helianthus* (Asteraceae): EVOLUTION OF LEAF ECONOMICS IN DIVERSE SUNFLOWERS. Evolution 69, 2705–2720. https://doi.org/10.1111/evo.12768

Matusick, G., Ruthrof, K.X., Brouwers, N.C., Dell, B., Hardy, G.St.J., 2013. Sudden forest canopy collapse corresponding with extreme drought and heat in a mediterranean-type eucalypt forest in southwestern Australia. Eur J Forest Res 132, 497–510. https://doi.org/10.1007/s10342-013-0690-5

Mayr, S., Schmid, P., Laur, J., Rosner, S., Charra-Vaskou, K., Dämon, B., Hacke, U.G., 2014. Uptake of Water via Branches Helps Timberline Conifers Refill Embolized Xylem in Late Winter. Plant Physiology 164, 1731–1740. https://doi.org/10.1104/pp.114.236646

McDowell, N., Pockman, W.T., Allen, C.D., Breshears, D.D., Cobb, N., Kolb, T., Plaut, J., Sperry, J., West, A., Williams, D.G., Yepez, E.A., 2008. Mechanisms of plant survival and mortality during drought: why do some plants survive while others succumb to drought? New Phytologist 178, 719–739. https://doi.org/10.1111/j.1469-8137.2008.02436.x

McDowell, N.G., 2011. Mechanisms Linking Drought, Hydraulics, Carbon Metabolism and Vegetation Mortality. Plant Physiology 155, 1051–1059. https://doi.org/10.1104/pp.110.170704

McDowell, N.G., Allen, C.D., Anderson-Teixeira, K., Aukema, B.H., Bond-Lamberty, B., Chini, L., Clark, J.S., Dietze, M., Grossiord, C., Hanbury-Brown, A., Hurtt, G.C., Jackson, R.B., Johnson, D.J., Kueppers, L., Lichstein, J.W., Ogle, K., Poulter, B., Pugh, T.A.M., Seidl, R., Turner, M.G., Uriarte, M., Walker, A.P., Xu, C., 2020. Pervasive shifts in forest dynamics in a changing world. Science 368, eaaz9463. https://doi.org/10.1126/science.aaz9463

Meyer, L., Brinkman, S., van Kesteren, L., Leprince-Ringuet, N., van Boxmeer, F., n.d. Technical Support Unit for the Synthesis Report 169.

Meyfroidt, P., Lambin, E.F., 2011. Global Forest Transition: Prospects for an End to Deforestation. Annu. Rev. Environ. Resour. 36, 343–371. https://doi.org/10.1146/annurev-environ-090710-143732

Meyra, A.G., Kuz, V.A., Zarragoicoechea, G.J., 2007. Geometrical and physicochemical considerations of the pit membrane in relation to air seeding: the pit membrane as a capillary valve. Tree Physiology 27, 1401–1405. https://doi.org/10.1093/treephys/27.10.1401

Millán, M.M., 2014. Extreme hydrometeorological events and climate change predictions in Europe. Journal of Hydrology 518, 206–224. https://doi.org/10.1016/j.jhydrol.2013.12.041

Nardini, A., Luglio, J., 2014. Leaf hydraulic capacity and drought vulnerability: possible trade-offs and correlations with climate across three major biomes. Funct Ecol 28, 810–818. https://doi.org/10.1111/1365-2435.12246

Nobel, P.S., 2009. Physicochemical and environmental plant physiology, 4th ed. ed. Elsevier/Academic Press, Amsterdam Boston.

Olson, M.E., Soriano, D., Rosell, J.A., Anfodillo, T., Donoghue, M.J., Edwards, E.J., León-Gómez, C., Dawson, T., Camarero Martínez, J.J., Castorena, M., Echeverría, A., Espinosa, C.I., Fajardo, A., Gazol, A., Isnard, S., Lima, R.S., Marcati, C.R., Méndez-Alonzo, R., 2018. Plant height and hydraulic vulnerability to drought and cold. Proc. Natl. Acad. Sci. U.S.A. 115, 7551–7556. https://doi.org/10.1073/pnas.1721728115

Parmesan, C., 2006. Ecological and Evolutionary Responses to Recent Climate Change. Annu. Rev. Ecol. Evol. Syst. 37, 637–669. https://doi.org/10.1146/annurev.ecolsys.37.091305.110100

Pereira, L., Bittencourt, P.R.L., Rowland, L., Brum, M., Miranda, M.T., Pacheco, V.S., Oliveira, R.S., Machado, E.C., Jansen, S., Ribeiro, R.V., 2021. Using the Pneumatic method to estimate embolism resistance in species with long vessels: A commentary on the article "A comparison of five methods to assess embolism resistance in trees." Forest Ecology and Management 479, 118547. https://doi.org/10.1016/j.foreco.2020.118547

Phillips, O.L., van der Heijden, G., Lewis, S.L., López-González, G., Aragão, L.E.O.C., Lloyd, J., Malhi, Y., Monteagudo, A., Almeida, S., Dávila, E.A., Amaral, I., Andelman, S., Andrade, A., Arroyo, L., Aymard, G., Baker, T.R., Blanc, L., Bonal, D., de Oliveira, Á.C.A., Chao, K.-J., Cardozo, N.D., da Costa, L., Feldpausch, T.R., Fisher, J.B., Fyllas, N.M., Freitas, M.A., Galbraith, D., Gloor, E., Higuchi, N., Honorio, E., Jiménez, E., Keeling, H., Killeen, T.J., Lovett, J.C., Meir, P., Mendoza, C., Morel, A., Vargas, P.N., Patiño, S., Peh, K.S.-H., Cruz, A.P., Prieto, A., Quesada, C.A., Ramírez, F., Ramírez, H., Rudas, A., Salamão, R., Schwarz, M., Silva, J., Silveira, M., Ferry Slik, J.W., Sonké, B., Thomas, A.S., Stropp, J., Taplin, J.R.D., Vásquez, R., Vilanova, E., 2010. Drought-mortality relationships for tropical forests. New Phytologist 187, 631–646. https://doi.org/10.1111/j.1469-8137.2010.03359.x

Pittermann, J., Choat, B., Jansen, S., Stuart, S.A., Lynn, L., Dawson, T.E., 2010. The Relationships between Xylem Safety and Hydraulic Efficiency in the Cupressaceae: The Evolution of Pit Membrane Form and Function. Plant Physiology 153, 1919–1931. https://doi.org/10.1104/pp.110.158824

Pockman, W.T., Sperry, J.S., 2000. Vulnerability to xylem cavitation and the distribution of Sonoran Desert vegetation. Am. J. Bot. 87, 1287–1299. https://doi.org/10.2307/2656722

Poorter, L., McDonald, I., Alarcón, A., Fichtler, E., Licona, J., Peña-Claros, M., Sterck, F., Villegas, Z., Sass-Klaassen, U., 2010. The importance of wood traits and hydraulic conductance for the performance and life history strategies of 42 rainforest tree species. New Phytologist 185, 481–492. https://doi.org/10.1111/j.1469-8137.2009.03092.x

Ramirez-Valiente, J.A., Sanchez-Gomez, D., Aranda, I., Valladares, F., 2010. Phenotypic plasticity and local adaptation in leaf ecophysiological traits of 13 contrasting cork oak populations under different water availabilities. Tree Physiology 30, 618–627. https://doi.org/10.1093/treephys/tpq013

Ratzmann, G., Meinzer, F.C., Tietjen, B., 2019. Iso/Anisohydry: Still a Useful Concept. Trends in Plant Science 24, 191–194. https://doi.org/10.1016/j.tplants.2019.01.001

Rüger, N., Wirth, C., Wright, S.J., Condit, R., 2012. Functional traits explain light and size response of growth rates in tropical tree species. Ecology 93, 2626–2636. https://doi.org/10.1890/12-0622.1

Sala, A., Piper, F., Hoch, G., 2010. Physiological mechanisms of drought-induced tree mortality are far from being resolved. New Phytologist 186, 274–281. https://doi.org/10.1111/j.1469-8137.2009.03167.x

Schuldt, B., Buras, A., Arend, M., Vitasse, Y., Beierkuhnlein, C., Damm, A., Gharun, M., Grams, T.E.E., Hauck, M., Hajek, P., Hartmann, H., Hiltbrunner, E., Hoch, G., Holloway-Phillips, M., Körner, C., Larysch, E., Lübbe, T., Nelson, D.B., Rammig, A., Rigling, A., Rose, L., Ruehr, N.K., Schumann, K., Weiser, F., Werner, C., Wohlgemuth, T., Zang, C.S., Kahmen, A., 2020. A first assessment of the impact of the extreme 2018 summer drought on Central European forests. Basic and Applied Ecology 45, 86–103. https://doi.org/10.1016/j.baae.2020.04.003

Scoffoni, C., Chatelet, D.S., Pasquet-kok, J., Rawls, M., Donoghue, M.J., Edwards, E.J., Sack, L., 2016. Hydraulic basis for the evolution of photosynthetic productivity. Nature Plants 2, 16072. https://doi.org/10.1038/nplants.2016.72

Seager, R., Ting, M., Held, I., Kushnir, Y., Lu, J., Vecchi, G., Huang, H.-P., Harnik, N., Leetmaa, A., Lau, N.-C., Li, C., Velez, J., Naik, N., 2007. Model Projections of an Imminent Transition to a More Arid Climate in Southwestern North America. Science 316, 1181–1184. https://doi.org/10.1126/science.1139601

Senf, C., Buras, A., Zang, C.S., Rammig, A., Seidl, R., 2020. Excess forest mortality is consistently linked to drought across Europe. Nat Commun 11, 6200. https://doi.org/10.1038/s41467-020-19924-1

Sevanto, S., Mcdowell, N.G., Dickman, L.T., Pangle, R., Pockman, W.T., 2014. How do trees die? A test of the hydraulic failure and carbon starvation hypotheses. Plant Cell Environ 37, 153–161. https://doi.org/10.1111/pce.12141

Skelton, R.P., Anderegg, L.D.L., Diaz, J., Kling, M.M., Papper, P., Lamarque, L.J., Delzon, S., Dawson, T.E., Ackerly, D.D., 2021. Evolutionary relationships between drought-related traits and climate shape large hydraulic safety margins in western North American oaks. Proc. Natl. Acad. Sci. U.S.A. 118, e2008987118. https://doi.org/10.1073/pnas.2008987118

Sperry, J.S., Hacke, U.G., Wheeler, J.K., 2005. Comparative analysis of end wall resistivity in xylem conduits. Plant Cell Environ 28, 456–465. https://doi.org/10.1111/j.1365-3040.2005.01287.x

Sperry, J.S., Meinzer, F.C., McCULLOH, K.A., 2008. Safety and efficiency conflicts in hydraulic architecture: scaling from tissues to trees. Plant Cell Environ 31, 632–645. https://doi.org/10.1111/j.1365-3040.2007.01765.x

Steffen, W., Persson, Å., Deutsch, L., Zalasiewicz, J., Williams, M., Richardson, K., Crumley, C., Crutzen, P., Folke, C., Gordon, L., Molina, M., Ramanathan, V., Rockström, J., Scheffer, M., Schellnhuber, H.J., Svedin, U., 2011. The Anthropocene: From Global Change to Planetary Stewardship. AMBIO 40, 739–761. https://doi.org/10.1007/s13280-011-0185-x

Sterl, A., Severijns, C., Dijkstra, H., Hazeleger, W., Jan van Oldenborgh, G., van den Broeke, M., Burgers, G., van den Hurk, B., Jan van Leeuwen, P., van Velthoven, P., 2008. When can we expect extremely high surface temperatures? Geophys. Res. Lett. 35, L14703. https://doi.org/10.1029/2008GL034071

Stovall, A.E.L., Shugart, H., Yang, X., 2019. Tree height explains mortality risk during an intense drought. Nat Commun 10, 4385. https://doi.org/10.1038/s41467-019-12380-6

Swemmer, A., 2020. Locally high, but regionally low: the impact of the 2014–2016 drought on the trees of semi-arid savannas, South Africa. African Journal of Range & Forage Science 37, 31–42. https://doi.org/10.2989/10220119.2020.1723696

Tixier, A., Herbette, S., Jansen, S., Capron, M., Tordjeman, P., Cochard, H., Badel, E., 2014. Modelling the mechanical behaviour of pit membranes in bordered pits with respect to cavitation resistance in angiosperms. Annals of Botany 114, 325–334. https://doi.org/10.1093/aob/mcu109

Tyree, M.T., 2003. Plant hydraulics: The ascent of water. Nature 423, 923–923. https://doi.org/10.1038/423923a

Tyree, M.T., Davis, S.D., Cochard, H., 1994. Biophysical Perspectives of Xylem Evolution: is there a Trade-off of Hydraulic Efficiency for Vulnerability to Dysfunction? IAWA J 15, 335–360. https://doi.org/10.1163/22941932-90001369

Tyree, M.T., Sperry, J.S., 1989. Vulnerability of Xylem to Cavitation and Embolism. Annu. Rev. Plant. Physiol. Plant. Mol. Biol. 40, 19–36. https://doi.org/10.1146/annurev.pp.40.060189.000315

Tyree, M.T., Velez, V., Dalling, J.W., 1998. Growth dynamics of root and shoot hydraulic conductance in seedlings of five neotropical tree species: scaling to show possible adaptation to differing light regimes. Oecologia 114, 293. https://doi.org/10.1007/s004420050450

Tyree, M.T., Zimmermann, M.H., 2002a. Hydraulic Architecture of Whole Plants and Plant Performance, in: Xylem Structure and the Ascent of Sap, Springer Series in Wood Science. Springer Berlin Heidelberg, Berlin, Heidelberg, pp. 175–214. https://doi.org/10.1007/978-3-662-04931-0_6

Tyree, M.T., Zimmermann, M.H., 2002b. Xylem Structure and the Ascent of Sap, Springer Series in Wood Science. Springer Berlin Heidelberg, Berlin, Heidelberg. https://doi.org/10.1007/978-3-662-04931-0

Urli, M., Porte, A.J., Cochard, H., Guengant, Y., Burlett, R., Delzon, S., 2013. Xylem embolism threshold for catastrophic hydraulic failure in angiosperm trees. Tree Physiology 33, 672–683. https://doi.org/10.1093/treephys/tpt030

Van Gelder, H.A., Poorter, L., Sterck, F.J., 2006. Wood mechanics, allometry and life-history variation in a tropical rain forest tree community. New Phytologist 171, 367–378. https://doi.org/10.1111/j.1469-8137.2006.01757.x

van Mantgem, P.J., Stephenson, N.L., Byrne, J.C., Daniels, L.D., Franklin, J.F., Fulé, P.Z., Harmon, M.E., Larson, A.J., Smith, J.M., Taylor, A.H., Veblen, T.T., 2009. Widespread Increase of Tree Mortality Rates in the Western United States. Science 323, 521–524. https://doi.org/10.1126/science.1165000

Vanoni, M., Bugmann, H., Nötzli, M., Bigler, C., 2016. Quantifying the effects of drought on abrupt growth decreases of major tree species in Switzerland. Ecol Evol 6, 3555–3570. https://doi.org/10.1002/ece3.2146

Violle, C., Navas, M.-L., Vile, D., Kazakou, E., Fortunel, C., Hummel, I., Garnier, E., 2007. Let the concept of trait be functional! Oikos 116, 882–892. https://doi.org/10.1111/j.0030-1299.2007.15559.x

Weed, A.S., Ayres, M.P., Hicke, J.A., 2013. Consequences of climate change for biotic disturbances in North American forests. Ecological Monographs 83, 441–470. https://doi.org/10.1890/13-0160.1

Westoby, M., Wright, I.J., 2006. Land-plant ecology on the basis of functional traits. Trends in Ecology & Evolution 21, 261–268. https://doi.org/10.1016/j.tree.2006.02.004

Wheeler, J.K., Sperry, J.S., Hacke, U.G., Hoang, N., 2005a. Inter-vessel pitting and cavitation in woody Rosaceae and other vesselled plants: a basis for a safety versus efficiency trade-off in xylem transport. Plant Cell Environ 28, 800–812. https://doi.org/10.1111/j.1365-3040.2005.01330.x

Wheeler, J.K., Sperry, J.S., Hacke, U.G., Hoang, N., 2005b. Inter-vessel pitting and cavitation in woody Rosaceae and other vesselled plants: a basis for a safety versus efficiency trade-off in xylem transport. Plant Cell Environ 28, 800–812. https://doi.org/10.1111/j.1365-3040.2005.01330.x

Wilson, K., White, D.J.B., 1986. The anatomy of wood, its diversity and variability. Stobart, London.

Worrall, J.J., Rehfeldt, G.E., Hamann, A., Hogg, E.H., Marchetti, S.B., Michaelian, M., Gray, L.K., 2013. Recent declines of Populus tremuloides in North America linked to climate. Forest Ecology and Management 299, 35–51. https://doi.org/10.1016/j.foreco.2012.12.033

Zimmermann, M.H., 1983. Xylem Structure and the Ascent of Sap, Springer Series in Wood Science. Springer Berlin Heidelberg, Berlin, Heidelberg. https://doi.org/10.1007/978-3-662-22627-8

Part 2

Study questions of the thesis

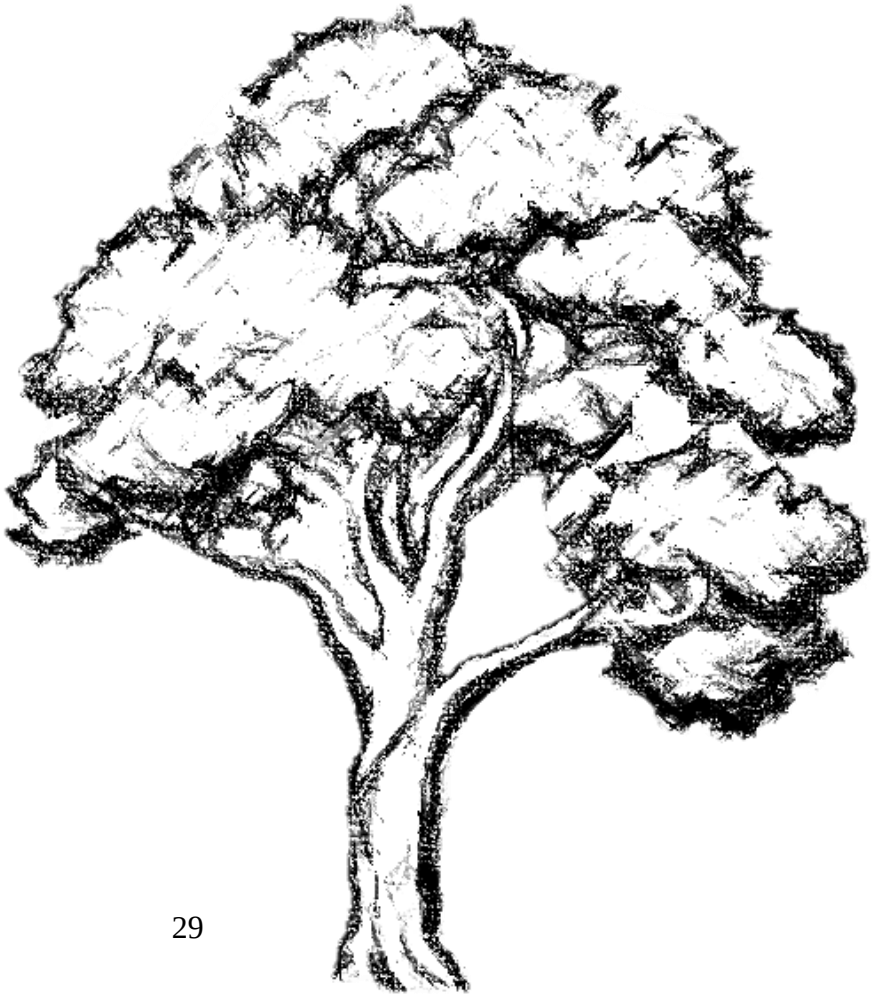

2. Chapter 1: Addressing controversies in embolism resistance – vessel diameter relationships

This chapter is based on the following publication.

Manuscript 1 (Revision in New Phytologist) Addressing controversies in embolism resistance – vessel diameter relationships.
Emilie Isasa, Roman Mathias Link Steven Jansen, Fon Robinson Tezeh, Lucian Kaack, Juliano Sarmento Cabral, Bernhard Schuldt.

Participated in	**Author Initials,** Responsibility decreasing from left to right					
Study Design Methods Development	B.S.	J.S.C	E.I.	R.M.L.		
Data Collection	E.I.	F.R.T.	L.K.			
Data Analysis and Interpretation	E.I.	R.M.L.	B.S.	J.S.C.		
Manuscript Writing	E.I.	R.M.L.	B.S.	J.S.C.	S.J.	
Writing of Introduction Writing of Materials & Methods Writing of Discussion Writing of First Draft	E.I.	R.M.L.	B.S.	J.S.C.	S.J.	
Figure	**Author Initials,** Responsibility decreasing from left to right					
1	E.I.	R.M.L.	F.R.T.	B.S.	J.S.C.	
2	R.M.L.	E.I.	B.S.	J.S.C.		
3	R.M.L.	E.I.	B.S.	J.S.C.		
4	R.M.L.	E.I.	F.R.T.	B.S.	J.S.C	
5	R.M.L.	E.I.	B.S.	J.S.C.		
Table	**Author Initials,** Responsibility decreasing from left to right					
1	E.I.	B.S..	J.S.C.			

Explanations:

The doctoral researcher confirms that she has obtained permission from the co-authors for legal second publication.
The doctoral researcher and the primary supervisor confirm the correctness of the above-mentioned assessment.

Emilie Isasa	25.11.2022	Würzburg	
Doctoral Researcher's Name	Date	Place	Signature
Prof. Dr. Bernhard Schuldt	25.11.2022	Dresden	
Primary Supervisor's Name	Date	Place	Signature

2.1. Abstract

Although xylem embolism is a key process during drought-induced tree mortality, its relationship to wood anatomy remains debated. While the functional link between bordered pits and embolism resistance is known, there is no direct, mechanistic explanation for the traditional assumption that wider vessels are more vulnerable than narrow ones.

We used data from 20 temperate broad-leaved tree species to study the inter- and intraspecific relationship of water potential at 50% loss of conductivity (P_{50}) with hydraulically-weighted vessel diameter (D_h), and tested its link to pit membrane thickness (T_{PM}) and specific conductivity (K_s) on species level.

Embolism-resistant species had thick pit membranes and narrow vessels. While D_h was weakly associated with T_{PM}, the $P_{50} – D_h$ relationship remained highly significant after accounting for T_{PM}. The interspecific pattern between P_{50} and D_h was mirrored by a link between P_{50} and K_s, but there was no evidence for an intraspecific relationship.

Our results provide robust evidence for an interspecific $P_{50} – D_h$ relationship across our species. As a potential cause for the inconsistencies in published $P_{50} – D_h$ relationships, our analysis suggests differences in the range of traits values covered, and the level of data aggregation (species, tree, or sample level) studied.

Keywords: angiosperm xylem, embolism resistance, hydraulic conductivity, vessel diameter, pit membrane, functional traits, data aggregation

2.2. Introduction

Xylem embolism formation, i.e., the disruption of water flow by the formation of large gas bubbles in xylem conduits, is a key process contributing to drought-induced tree mortality (Anderegg et al., 2016; Adams et al., 2017; Powers et al., 2020; Arend et al., 2021; Hajek et al., 2022). Therefore, recent work has been focused on analyzing the mechanisms that are at play during embolism formation, and on identifying xylem functional traits that are associated with embolism risk (Lens et al., 2022).

While the role of xylem embolism in mortality under drought is widely accepted, the exact mechanistic processes involved in embolism formation remain not well known. Along the hydraulic pathway from roots to leaves, the water column inside the xylem is under negative pressure and hence in a metastable state (Tyree and Zimmermann, 2002). As the water potentials necessary for a spontaneous transition from the liquid to the gas phase (i.e., homogeneous cavitation) exceed water potentials observed in living plants by orders of magnitude (Herbert and Caupin, 2005; Stroock et al., 2014; Kanduč et al., 2020), this process is unlikely to substantially contribute to embolism formation. The prevailing assumption is hence that embolism formation is triggered by 'air seeding', i.e., when gas bubbles enter functional conduits through the pores of pit membranes that are connected to adjacent, embolized conduits (Sperry & Tyree, 1988; Brodersen et al., 2013; Jansen et al., 2018; Roth-Nebelsick, 2019). Pit membranes hereby play the role of safety valves that prevent embolism from spreading to neighboring vessels (Meyra et al., 2007; Choat et al., 2008). Because pit membranes provide the largest pores and highest permeability between adjacent vessels, their structure is directly linked to embolism resistance (Wheeler et al., 2005; Jansen et al., 2009). More specifically, pit membrane thickness (T_{PM}) has been singled out as a key determinant of embolism resistance due to its direct relation to the size distribution of pore constrictions in pit membranes (Li et al., 2016; Bai et al., 2020; Kaack et al., 2021).

How embolism propagation at the pit membrane level translates to larger-scale wood anatomical features, particularly to vessel dimensions, is subject to current debate (Kaack et al., 2021; Levionnois et al., 2021; Lemaire et al., 2021). Here, a long-term assumption is that vessel diameter is negatively related to resistance against drought-induced embolism, which is thought to form the basis for an apparent trade-off between embolism safety and hydraulic efficiency (Tyree et al., 1994; Tyree & Zimmermann, 2002; Wheeler et al., 2005). However, there is no known mechanism that constitutes a direct link between vessel size and embolism resistance (Anfodillo and Olson, 2021), while the evidence for a stability-efficiency trade-off is frequently weak (Gleason et al., 2016), the existing evidence for a relationship is inconsistent (Anfodillo and Olson, 2021). In studies focusing on interspecific patterns, it is often found that vessel diameter is positively associated with the water potential at 50% loss of hydraulic conductivity (P_{50}) (Maherali et al., 2006; Hacke et al., 2006, 2017; Domec et al., 2010; Fu et al., 2012). However, it is not always clear whether embolism resistance measurements in some of these earlier studies were affected by vessel size-related measurement artefacts (cf. Wheeler et al., 2013; Lamarque et al., 2018). While vessel diameters tend to show a general pattern of widening from the leaves towards the roots

(Olson et al., 2014; Rosell et al., 2017), studies focusing on patterns in embolism resistance between plant organs within a single plant show less consistent results, indicating that diameter – P_{50} relationships within individual plants do not follow the interspecific trend. Some authors report leaves (Creek et al., 2018; Skelton et al., 2019) or roots (Maherali et al., 2006; Pratt et al., 2015) to be more vulnerable then stems, some found similar embolism resistance in roots, stems and leaves (Skelton et al., 2017; Wason et al., 2018, Lübbe et al., 2022), while others reported leaves to be more resistant than stems (Klepsch et al., 2018; Levionnois et al., 2020, Guan et al., 2022). Finally, microCT observations of intact plants tend to show no (cf. Choat et al., 2016) or inconsistent relationships between vessel diameter and embolism resistance (Losso et al., 2019).

Studies on relationships between wood traits tend to be based on aggregate variables. Prior to analysis, observations from single vessels or pit membranes are usually averaged across samples, individual trees, or species. These levels of aggregation correspond to different observational units that are influenced by mechanisms acting on different scales (Clark et al., 2011), which may partially explain aforementioned differences in outcomes between studies. The choice of the adequate level of aggregation to answer a research question can have profound consequences for the interpretation of a dataset and may result in very different interpretations of the same data (Pollet et al., 2015). The question whether individual trees of the same species with different average vessel diameters differ in embolism resistance, or whether species with different average vessel diameters differ in embolism resistance at the interspecific level, may have fundamentally different answers (cf. Poorter et al., 2018). So far, it is unknown to what extent the interpretation of embolism risk – vessel diameter relationships can be affected by these scale and aggregation issues.

Here, we investigate wood anatomical and hydraulic traits related to embolism resistance in a dataset of 77 tree individuals belonging to 20 temperate broadleaved tree species. Additionally, we focus on within-species patterns based on a dataset of 22 *Acer monspessulanum* trees. For both datasets, embolism resistance and wood anatomical traits were derived from the same upper canopy branches, and all trees were sampled at a consistent sampling height. Our design thus intended to minimize confounding effects of tree height- and flow path length-related patterns in vessel size. We use these datasets to address the questions whether embolism resistance (as measured by P_{50}) is related to hydraulically-weighted vessel diameter (D_h), how it relates to pit membrane thickness (T_{PM}), and how the answer to these questions is affected by choices during the data analysis. We hereby focus on a) whether or not an effect of D_h on P_{50} remains after accounting for the confounding effect of T_{PM}, b) to which extent the range of D_h covered by the species and samples studied may affect the outcome, and c) whether the observed relationship between P_{50} and D_h is consistent within and between species. To achieve the latter, we propose a simple statistical model to decompose trait relationships into intra- and interspecific components.

2.3. Materials and Methods

2.3.1. Study site and plant material

For this study, 77 trees from 20 temperate and diffuse-porous angiosperm tree species from 10 genera were chosen from the nursery in the Stutel-Arboretum from the Bavarian State Institute for Viticulture and Horticulture (LWG) at Veitshöchheim, Germany (49°51'49"N, 9°51'8"E). Additionally, 22 *Acer monspessulanum* trees were selected from the Botanical Garden of the University of Würzburg, Germany. The long-term mean annual temperature and mean annual precipitation are 10.0 °C and 591 mm in Veitshöchheim and 9.6 °C and 560 mm in Würzburg, respectively (Bavarian State Institute for Agriculture − LFL), constituting a continental climate according to the Köppen classification (Peel et al., 2007).

Plant material from the Stutel-Arboretum was collected June – September 2019 and 2020 (Table 2.1) from trees aged ca. 11 years. Two samples each were taken from two to four individuals per species, resulting in a total of 77 sampled trees (Table 2.1). Plant material from the 22 *Acer monspessulanum* trees was collected November – December 2020 before the onset of frost. Three replicate samples were taken per tree, resulting in a total of 66 samples, two of which had to be discarded due to measurement problems. At both sites, at least 60 cm long twigs were cut from the middle canopy at a height of ca. 4–5 m, wrapped in wet paper towels, bagged in dark, humidified plastic bags, transported to the laboratory, and processed on the same day. For the trees from Stutel, we measured vulnerability curves and wood anatomical traits on one sample, and hydraulic conductivity on the other. The age of the branches at the basal end (determined from microtome slides) was on average 3.7 yr (range: 2–7 yr) for the Stutel site, and on average 7.7 yr (range: 3–15 yr) for the botanical garden.

Table 2.1: Tree characteristics sorted by family. Given are the family, species name, sample code used in subsequent figures, number of sampled individuals (n_{tree}, with the number of trees for the individual level relationships in parentheses for *A. monspessulanum*) and the mean and standard deviation of diameter at breast height (DBH) and tree height (Height).

Family	Species	Code	n_{tree}	DBH (cm)	Height (m)
Aceraceae	*Acer campestre*	ACCA	4	10.8 ± 0.6	7.0 ± 0.2
	Acer monspessulanum	ACMO	2 (22)	12.6 ± 0.7	6.7 ± 0.1
	Acer platanoides	ACPL	4	12.3 ± 0.7	7.2 ± 0.2
	Acer rubrum	ACRU	4	8.7 ± 0.6	6.2 ± 0.2
Betulaceae	*Betula pendula*	BEPE	4	10.7 ± 1.2	8.4 ± 0.8
	Betula utilis	BEUT	4	8.6 ± 0.7	6.6 ± 0.3
	Carpinus betulus	CABE	4	10.9 ± 0.9	7.4 ± 0.3
	Crataegus persimilis	CRPE	4	7.2 ± 0.4	5.9 ± 0.1
	Ostrya carpinifolia	OSCA	4	8.9 ± 0.2	6.0 ± 0.2
Platanaceae	*Platanus orientalis*	PLOR	4	11.8 ± 0.9	7.7 ± 0.1
	Platanus x acerifolia	PLAC	4	9.6 ± 0.6	4.7 ± 0.4
Rosaceae	*Prunus padus*	PRPA	3	10.7 ± 0.8	6.4 ± 0.1
	Prunus serrulata	PRSE	4	11.7 ± 0.5	5.8 ± 0.4
	Pyrus calleryana	PYCA	4	11.2 ± 1.0	7.6 ± 0.8
	Sorbus latifolia	SOLA	4	9.2 ± 0.7	5.6 ± 0.3
	Sorbus x thuringiaca	SOTH	4	9.4 ± 0.6	5.9 ± 0.3
Malvaceae	*Tilia cordata*	TICO	4	11.4 ± 0.8	6.5 ± 0.4
	Tilia mongolica	TIMO	4	8.8 ± 0.3	5.1 ± 0.1
	Tilia platyphyllos	TIPL	4	12.2 ± 0.3	7.6 ± 0.2
	Tilia tomentosa	TITO	4	17.2 ± 1.0	7.5 ± 0.5

2.3.2. Quantification of xylem hydraulic conductivity

For measuring branch xylem hydraulic conductivity (K_h; kg m s^{-1} MPa^{-1}), fresh samples were allowed to rehydrate in water for at least 20 min, and then recut under water from both ends to a length of 35 cm, which exceeds the maximum vessel length for all species analyzed (Paligi et al., unpublished). Subsequently, lateral twigs were removed and the cuts immediately sealed using quick-drying adhesive (Loctite 431 with activator 7452; Henkel, Düsseldorf, Germany) to prevent leakage. Then, the samples were connected to a Xyl'em Plus embolism meter (Bronkhorst, Montigny-Les-Cormeilles, France) with silicone tubes to measure stem hydraulic conductivity using degassed, demineralized water containing 10 mM KCl and 1 mM $CaCl_2$. After measuring initial hydraulic conductivity at a low-pressure head of 6 kPa for 5 minutes, samples were repeatedly flushed at high pressure of 120 kPa for 10 minutes to remove emboli to measure

maximum hydraulic conductivity once the conductivity values were stable. Hydraulic conductivity was calculated as $K_h = f \cdot L / \Delta P$, where f (kg s^{-1}) is the flow rate, and ΔP (MPa) is the pressure drop along the length of the segment (L, m). The specific conductivity (K_s; Kg m^{-1} MPa^{-1} s^{-1}) was then computed by dividing K_h^{max} by the basal cross-sectional xylem area (A_{cross}, m^2), excluding bark.

2.3.3. Vulnerability curves with the flow-centrifuge method

Vulnerability curves based on the flow-centrifuge method were measured with a Cavitron device (Cochard et al., 2005) built from a Sorval RC 5 centrifuge with manual control of rotation speed, and using the Cavisoft software (Cavisoft v.5.2.1, University of Bordeaux, Bordeaux, France). A subset of the vulnerability curves in this paper were also used for a methodological comparison with the pneumatic method (Paligi et al., 2021).
In total, vulnerability curves were constructed for 77 branches from the Stutel arboretum (basal diameter: mean ± SD 8.87 ± 0.88 mm; Fig. S1) and 64 *Acer monspessulanum* branches from the botanical garden (diameter: 7.03 ± 0.82 mm). After sampling, the branches were submerged in demineralized water immediately upon arrival in the laboratory and recut several times using pruning shears to release the negative pressure in the xylem (Torres-Ruiz et al., 2015). Then, lateral twigs were removed and samples shortened to a final length of 27.5 cm. Subsequently, samples of 3–4 cm length were cut from the basal and apical sample end, and stored in 70% ethanol for anatomical observations. Before inserting the branch segments in a custom-made rotor, the bark was removed at both stem ends, and their diameters were measured. Conductance was measured using the solution mentioned above, starting at a water potential of −0.834 MPa (equivalent to 3000 rotations per minute) and reducing the water potential stepwise until at least 90% loss of initial conductance recorded with the Cavisoft software. For each increase in rotational velocity and hence in pressure, we waited for 2 minutes before conductance was measured.

2.3.4. Vessel anatomical traits from light microscopy

For all species, thin (20 µm) traverse sections of the wood anatomical samples were made with a sliding microtome (G.S.L.1, Schenkung Dapples, Zürich, Switzerland), stained with safranin-alcian blue, rinsed with distilled water and ethanol (95%), and permanently embedded on glass slides using Euparal (Carl Roth, Karlsruhe, Germany). Subsequently, the complete cross-section was digitalized at 100-times magnification using a light microscope equipped with an automated table and a digital camera (Observer.Z1, Carl Zeiss MicroImaging GmbH, Jena, Germany; Software: AxioVision c4.8.2, Carl Zeiss MicroImaging GmbH). Anatomical measurements were made by semi-automated image analysis using ImageJ version 1.52p (Schneider et al., 2012) and GIMP version 2.10.6 (GIMP Development Team, 2018). While the majority of vessels could be identified by applying this semi-automated approach, it was impossible to completely exclude

tracheids in our measurements of some species because narrow vessels cannot be easily distinguished from tracheids based on transverse sections. The equivalent vessel diameter according to White (1991) (d, µm), i.e., the diameter of a circular vessel with the same conductivity as an elliptical one with minor and major radius a and b, was calculated as:

$$\mathbf{d} = \left(\frac{\mathbf{32\ (ab)^3}}{\mathbf{a^2 + b^2}}\right)^{\mathbf{0.25}} \quad (1)$$

Based on d, the hydraulically-weighted average vessel diameter (D_h, µm) was calculated according to Sperry et al. (1994) as:

$$D_h = \frac{\sum d^5}{\sum d^4} \quad (2)$$

2.3.5. Pit anatomical traits from transmission electron microscopy

One sample per species was prepared for transmission electron microscope (TEM) analyses to measure pit membrane thickness (T_{PM}, nm) following the protocol by Jansen et al. (2009).
Small xylem slivers were cut with a fresh razor blade from the two outmost growth rings of the fresh and hydrated wood samples used for hydraulic measurements on the day of sample collection. The slivers were then cut to 1 mm^3 cubes in water and fixed in a standard fixative (5% glutaraldehyde in 0.1 mol cacodylate buffer). Then, the samples were washed in a 50 mmol cacodylate buffer and post-fixed in 2% buffered osmium tetroxide in 0.1 mol cacodylate buffer for 2 h in ice. They were then stained with 0.5% uranyl acetate, and dehydrated through a gradual ethanol series (30%, 50%, 70%, and 90%) for two to three minutes. Samples were embedded in Epon resin (Sigma-Aldrich, Steinheim, Germany) at 60 °C. Transverse, semi-thin (500 nm thick) sections were cut from the embedded samples with a glass knife, stained with 0.5% toluidine blue in 0.1 mol phosphate buffer, and mounted on slides with Eukitt (Plano GmbH, Berlin, Germany). Ultra-thin sections between 60 nm and 100 nm thick were cut with a diamond knife using an ultra-microtome (Leica Ultracut UCT, Leica Microsystems, Vienna, Austria) and deposited on a copper grid (Athena, Plano GmbH, Wetzlar, Germany). Several grids were prepared for each TEM sample. Intervessel pit membranes were observed under a JEOL 1210 TEM (Jeol Germany GmbH, Freising, Germany) at 120 kV accelerating voltage. TEM pictures were taken with a digital camera (Soft Imaging System, Münster, Germany). ImageJ version 1.52p was used to measure T_{PM} at least three times per pit membrane at opposite sides near the pit membrane annulus (i.e., close to the pit border) and in the center. Shrunken pit membranes were excluded because these were likely showing artefacts by deformation, aspiration, or aging, and thus may not represent functional pit membranes (Schmid & Machado, 1968; Sorek et al., 2021). Shrunken pit membranes were identified based on their electron dense appearance under TEM, while fresh pit membranes in

functional conduits generally have a low electron density, with a homogeneous, granular appearance of lipids on and/or in pit membranes (Zhang et al., 2017, 2020; Kotowska et al., 2020). While intervessel pit membranes were imaged as much as possible, it was not possible to distinguish narrow vessels from tracheids in some species based on a transverse TEM section. Therefore, both intervessel and vessel-tracheid pit membranes may be included in our analyses.

2.3.6. Statistical analyses

All statistical analyses were performed in R v. 4.2.2 (R Core Team, 2022) in the framework of the `tidyverse` v. 1.3.2 (Wickham et al., 2019).

Vulnerability curves were fitted with nonlinear least squares using the logistic model by Pammenter and Vander Willigen (1998) in the modified version based on hydraulic conductivity (Ogle et al. 2009):

$$K_{\mathrm{i}} \sim \mathrm{Normal}\left(K_{\mathrm{sat}} \cdot \left(1 - \frac{1}{1 + \exp\left(-\frac{S_{50}}{25}\left(P_{\mathrm{i}} - P_{50}\right)\right)}\right), \sigma\right), \quad (3)$$

where for each observation *i*, the conductivity K_{i} is assumed to be normally distributed with residual standard deviation σ around a logistic function of the water potential P_{i} with the parameters P_{50} (water potential at 50% loss of conductivity), S_{50} (corresponding slope on the percent loss of conductivity scale) and K_{sat} (conductivity at full saturation).

The significance of linear associations at the species level was tested with linear models of species averages fitted with ordinary least squares. To illustrate the effect of range restriction on regression results, we further fitted an analogous model of P_{50} vs. D_{h} with a subsample of species (arbitrarily restricted to a range of D_{h} of 35–45 µm for demonstrational purposes). After constructing a directed acyclic graph (cf. Shrier & Platt, 2008) to identify necessary covariate adjustments, we used multiple linear regression to test whether relationships between D_{h} and P_{50} resulted from a confounding effect of T_{PM}, or whether a diameter effect remained after accounting for T_{PM}.

To illustrate the importance of the level of aggregation for the interpretation of relationships between plant traits, we further fitted two models of P_{50} at the individual level. We hereby contrasted the classical linear mixed-effects model (LME) formulation with random intercepts and slopes with a modified LME that used *within-species centering* to separate within- and between-species effects of D_{h} analogous to the within-subject centering in Van de Pol and Wright (2009). In the classical formulation, the dependent variable y_{i} for each observation *i* in (1…N) is expressed as a linear function of the predictor variable x_{i} with intercept α and slope β, which are allowed to vary for each group *j* in (1…J):

$$y_i = (\alpha + u_j) + (\beta + v_j) \cdot x_i + \epsilon_i \quad (4)$$

Here, ϵ_i are the model residuals, while u_j and v_j are the species-wise random deviations from the overall average parameters, and usually modeled as realizations of a multivariate normal distribution with a covariance matrix estimated from the data. The slope β estimated by this model is only a valid estimate of the average intraspecific slope if there is no between-species variation in x (cf. Bafumi and Gelman, 2007; van de Pol and Wright, 2009), a condition that is likely not met by most studies of relationships between evolutionarily constrained traits. Moreover, this model provides no estimate of the interspecific slope, which often may be equally or more relevant than the intraspecific slope.

We contrasted the model in (4) with an LME with within-species centering, an alternative formulation that separates the effect of the predictor variable x_i into the species averages $\overline{x_j}$ and the deviations from these averages $(x_i - \overline{x_j})$. This allowed us to decompose the relationship studied into an across-species and a within-species component with separate parameters β_{across} and β_{within}.

$$y_i = (\alpha + u_j) + \beta_{across} \cdot \overline{x_j} + (\beta_{within} + v_j) \cdot (x_i - \overline{x_j}) + \epsilon_i \quad (5)$$

The models in Eqn. (4) and (5) were fitted in a Bayesian hierarchical modelling framework with moderately informative priors (cf. Lemoine, 2019) using the R package `brms` v.2.18.0 (Bürkner, 2017, 2018) (see Supplementary Material S1 for details).

2.4. Results

2.4.1. Embolism resistance, hydraulic efficiency and wood anatomy across species

Our results covered a wide interspecific range of xylem embolism resistance, i.e. xylem water potential at 50% loss of hydraulic conductivity (P_{50}), specific hydraulic conductivity (K_s) and hydraulically-weighted vessel diameter (D_h) in the branch xylem. In our study across 20 temperate, diffuse-porous, and broadleaved tree species (n = 77), P_{50} varied from −7.33 MPa to −1.70 MPa, K_s from 0.46 to 1.98 kg m^{-1} MPa^{-1} s^{-1}, and D_h from 25.25 µm to 45.17 µm (Fig. 2.1, Table S1, Fig. S2). Within *Acer monspessulanum* (n = 66), P_{50} ranged from −7.99 to −6.00 MPa and D_h from 25.9 to 35.4 µm.

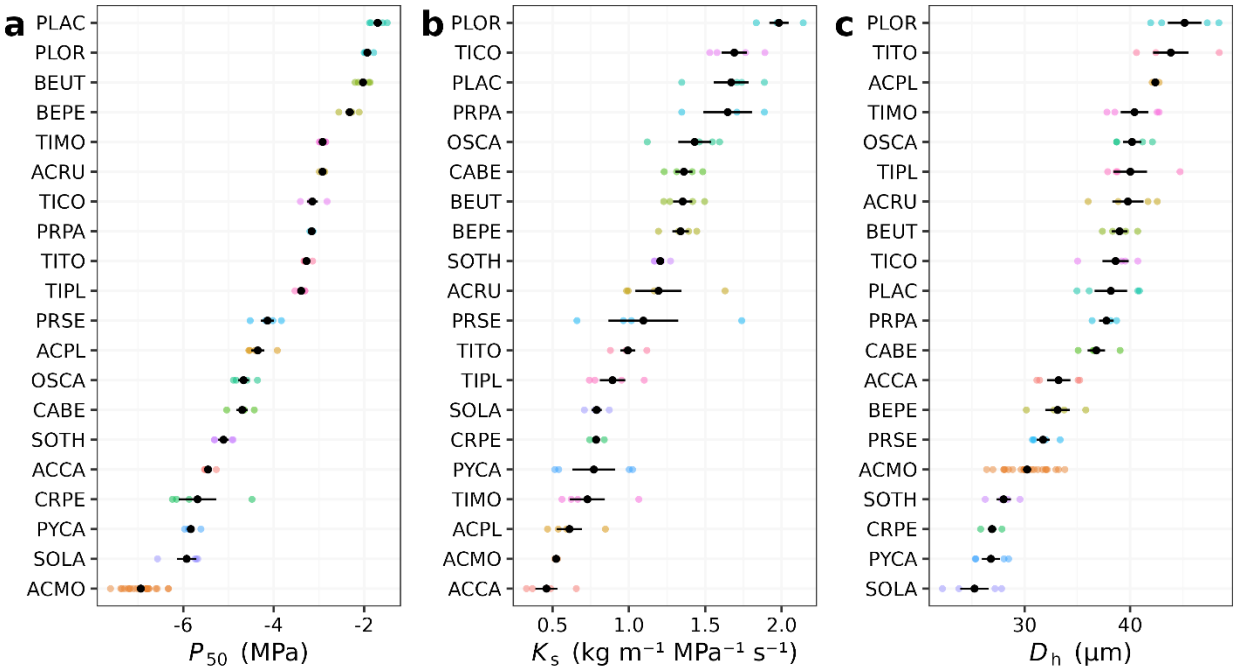

Figure 2.1: Observed ranges of a) the water potential at 50% loss of conductivity (P_{50}), b) the maximum specific conductivity (K_s), and c) the hydraulically-weighted vessel diameter (D_h) of 20 angiosperm tree species, with 3 to 4 (*A. monspessulanum*: 24) individuals per species. Shown are raw data from individual plants overlaid with mean ± standard errors, ordered by their mean values. For species codes, see Table 1.1.

In analyses of interspecific bivariate relationships (Fig. 2a–b, Table S2), species with a higher D_h had a less negative P_{50} and hence a lower embolism resistance (R^2 = 0.50, p < 0.001), while species with a higher pit membrane thickness (T_{PM}) were more embolism resistant (R^2 = 0.51, p = 0.001). P_{50} further increased significantly with K_s (R^2 = 0.47, p = 0.001), i.e., species with high xylem conductivity tended to have low embolism resistance (Fig. 2.2c, Table S2).

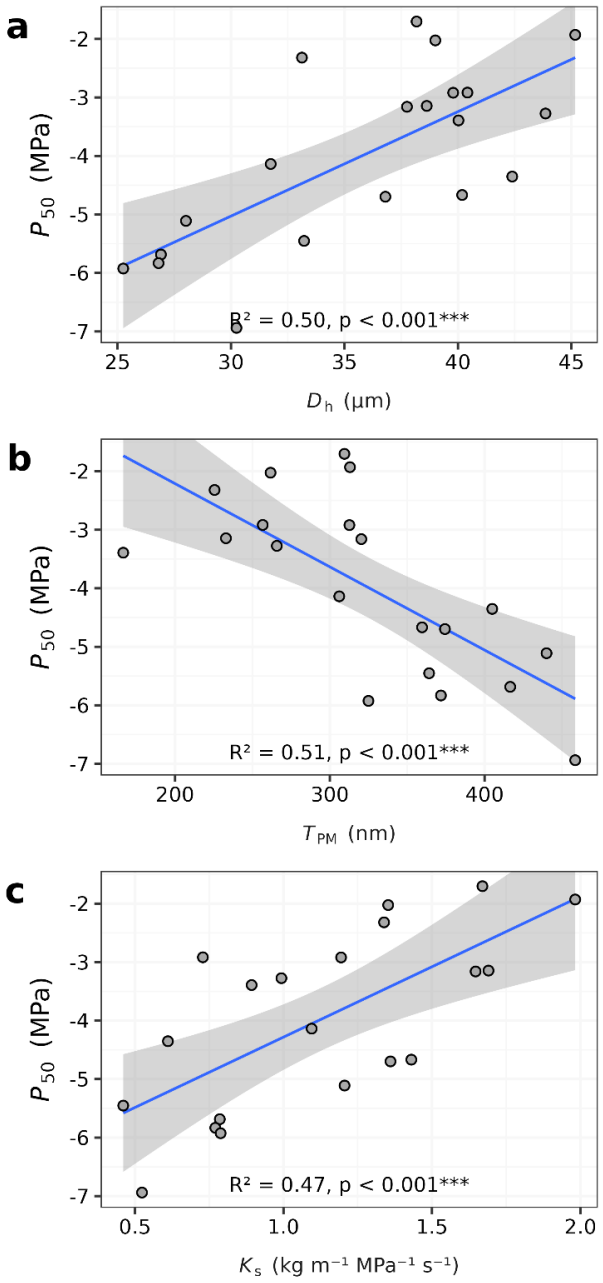

Figure 2.2: Results of simple species-level linear regressions of water potential at 50% loss of conductivity (P_{50}) vs. a) hydraulically-weighted vessel diameter (D_h), b) pit membrane thickness (T_{PM}) and c) maximum specific conductivity (K_s). Shown are the species level averages (blue) overlaid with the model predictions ± 95% confidence bands (grey). For regression, parameters see Table S2.

2.4.2. Determinants of embolism resistance

The hypothesized relationships between D_h, T_{PM} and P_{50} are reflected in the directed acyclic graph in Fig. 2.3 a, with the potential indirect path via intervessel pit area displayed as dashed arrows. While there was a significant negative correlation between D_h and T_{PM} ($r = -0.463$, $t = -2.215$, $df = 18$, $p = 0.039$), the direction and magnitude of this link were not nearly sufficient to explain the association observed between D_h and P_{50}. A key result is that a sizeable positive effect ($p = 0.006$) of D_h on P_{50} remained after accounting for the negative effect of T_{PM} ($p = 0.005$), i.e., species with the same value of T_{PM} were more embolism resistant when they had narrower vessels (Fig. 2.3 b-c, Table S2). Together, D_h and T_{PM} explained 68.9 % of the variance in species-level P_{50}. At the sample level, P_{50} was not significantly correlated with sample age, neither for the Stutel dataset ($r = -0.032$, $t = -0.277$, $df = 75$, $p = 0.782$), nor for the *Acer monspessulanum* dataset ($r = -0.126$, $t = -1.001$, $df = 62$, $p = 0.321$).

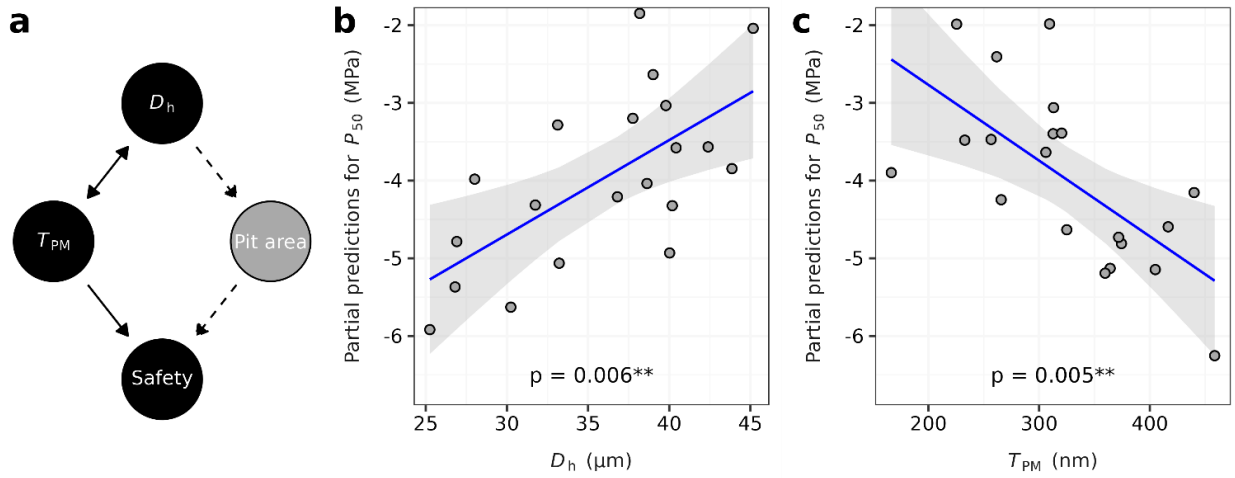

Figure 2.3: An alternative way of looking at the relationships between D_h, T_{PM} and embolism resistance. a) directed acyclic graph for the relationships between water potential at 50 % loss of conductivity (P_{50}), pit membrane thickness (T_{PM}), hydraulically-weighted vessel diameter (D_h) and total pit surface area (A_P). Unidirectional arrows: causal relationships, bidirectional arrows: correlative associations. The dashed arrows indicate the indirect effect of D_h on embolism safety via the unmeasured intervessel pit area per vessel (grey) hypothesized under H2. b) partial predictions from a multiple regression model of P_{50} vs. a) D_h and b) T_{PM}. Shown are counterfactual predictions for P_{50} (predictions for one variable when the other variable is held at its average value; blue lines) with 95% confidence bands (grey area), overlaid with partial residuals. For regression parameters, see Table S2.

2.4.3. Importance of trait value range and the level of aggregation

The range of trait values covered was found to strongly affect the results obtained (Fig. 2.4 a), with the slope of a linear regression explaining 50% of the variance in the full species level dataset ($p < 0.001$), and only 2% in a subset arbitrarily limited to a range of D_h between 35 and 45 µm ($p = 0.676$; Fig. 2.4 a, Table S2). Moreover, there was no evidence for a significant intraspecific association of P_{50} with D_h ($R^2 < 0.001$, $p = 0.961$; Fig. 2.4b, Table S2) for the 22 individual *Acer monspessulanum* trees.

The analyses of trait relationships on the individual level were strongly affected by model specification. Fig. 2.5 contrasts two alternative specifications for linear mixed-effects models of the association between P_{50} with D_h based on individual-level data. It is clear that the regular random intercept and slope formulation (Eqn. 4) was not able to recover the interspecific association observed (Fig. 2.5 a). The slope for the overall trend in this model was not credibly different from zero (slope 0.019, 95% CI: −0.015–0.053; Table S3). In the model formulation with within-species centering (Eqn. 5), we found evidence for a strong positive effect of D_h on species level (slope 0.177, 95% CI: 0.085–0.267), while the average within-species slope was not credibly different from zero (0.007, 95% CI: −0.029–0.042; Table S3, Fig. 2.5 b).

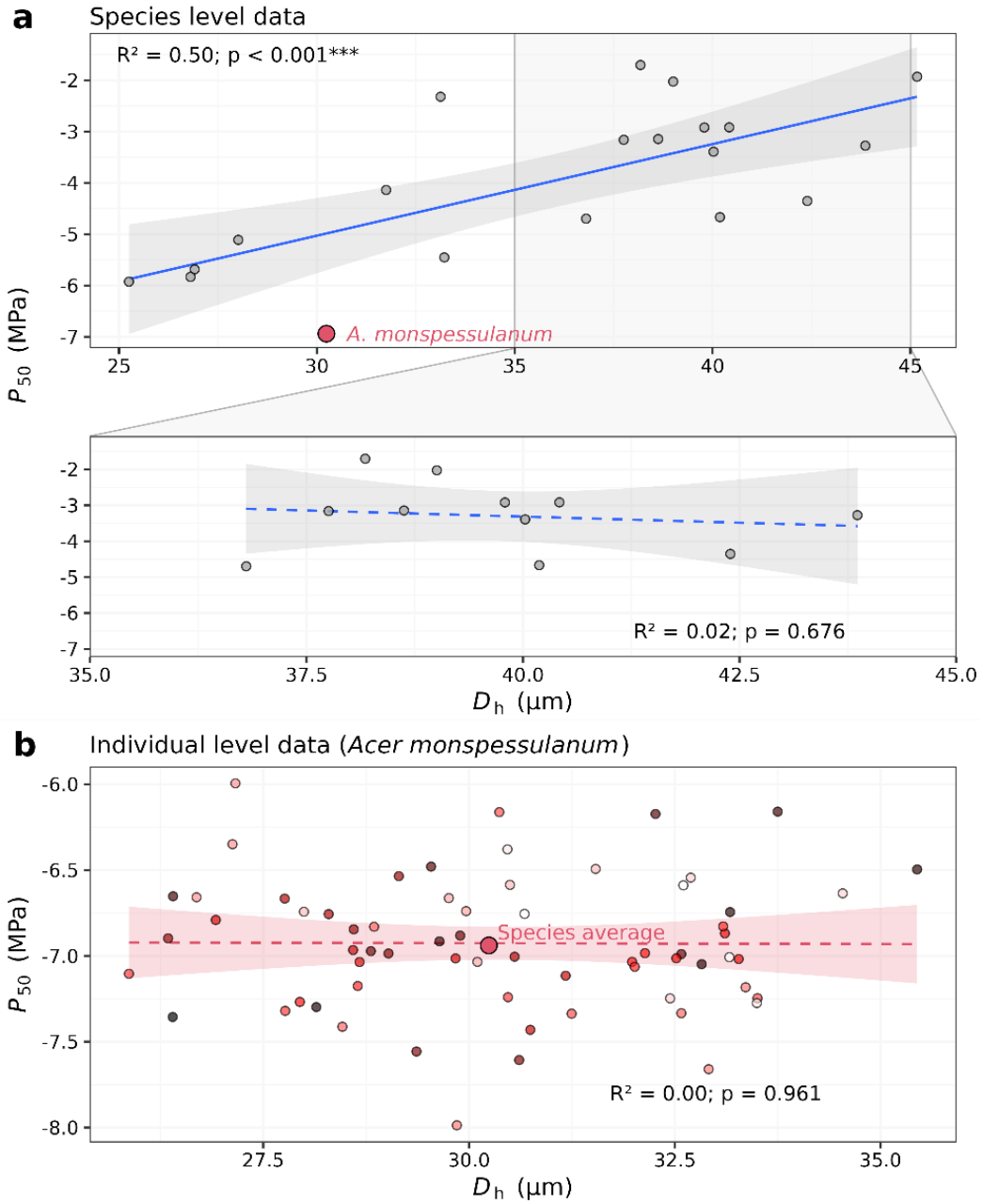

Figure 2.4: The range of observations and the observational scale can affect the observed P_{50}-D_h-relationships. a) Effect of range restriction on the outcome of a linear regression. The upper panel shows the full range of the data shown in the first panel of Fig. 2.2 with the explained variance and p-value in a linear regression, while the lower panel is based only on observations with a D_h between 35 and 45 µm. Shown are the species-level observations overlaid with the linear regression predictions (blue) and 95% confidence bands (grey). b) Within-species of *Acer monspessulanum* relationship of water potential at 50% loss of conductivity (P_{50}) vs. hydraulically-weighted vessel diameter (D_h). For regression parameters, see Table S2.

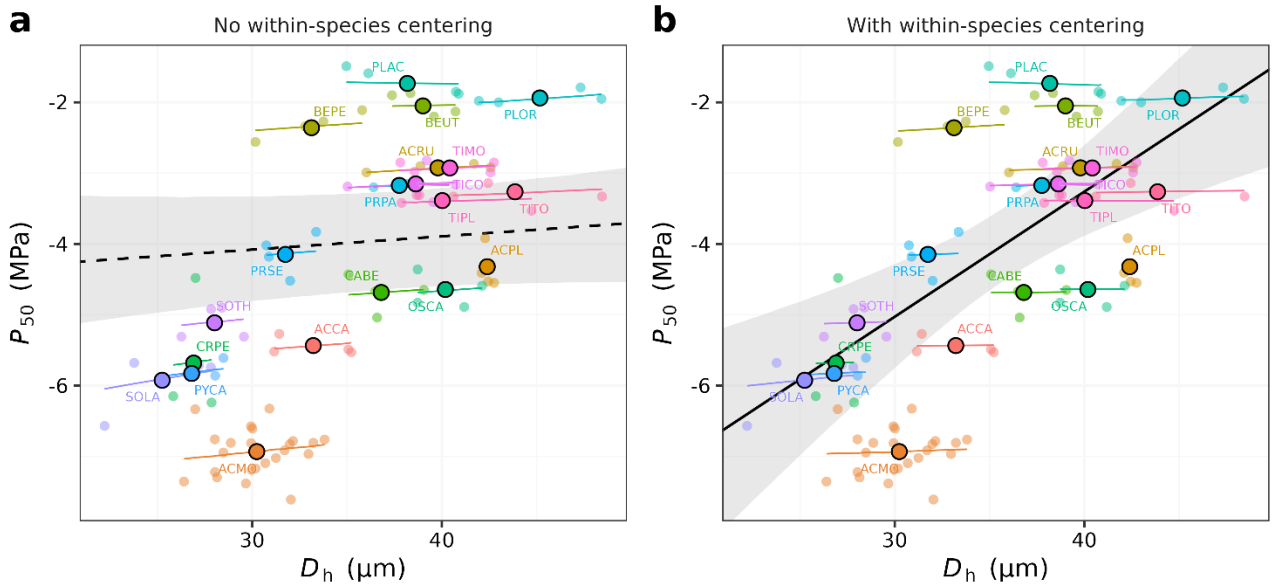

Figure 2.5: Dependence of trait relationships on the aggregational level and the implications of within-species centering for overall and species-specific predictions. a) Predictions from a mixed-effects model using a regular random slope and intercept formulation (Eq. 4). b) Within- and between-species predictions from a mixed model with random intercepts and slopes using within-species centering (Eq. 5). Shown are the raw data (small points) and species averages (big points with black contour) overlaid with marginal predictions (black) with 95% credible intervals (grey) as well as conditional within-species predictions (colored lines). For species codes, see Table 2.1; parameter estimates are provided in Table S3.

2.5. Discussion

Our results provide evidence for an interspecific relationship of xylem embolism resistance (as measured by the P_{50}-value) with both pit membrane thickness (T_{PM}) and hydraulically-weighted vessel diameter (D_h) in the branch xylem of temperate diffuse-porous angiosperm trees. They further demonstrate that a potential link between vessel diameter and pit membrane thickness cannot explain the lower embolism resistance of species with wider vessels. As such, our data provide clear evidence that in the species studied, vessel dimensions have an effect on embolism resistance, but that this relationship cannot be explained by pit membrane thickness only.

2.5.1. The role of pit membrane thickness for embolism resistance

The important role of pit membrane properties for embolism resistance has been demonstrated in various studies (Choat et al., 2003; Lens et al., 2011, 2013; Scholz et al., 2013; Li et al., 2016; Kaack et al., 2021). In our dataset, tree species with thicker intervessel pit membranes were more resistant to drought-induced embolism than species with thinner pit membranes (Fig. 2.2), which is in accordance with previous reports for angiosperm species both at the interspecific and intraspecific level (Lens et al., 2011; Scholz et al., 2013; Li et al., 2016; Schuldt et al., 2016).
A mechanistic explanation for the link between embolism resistance and T_{PM} is that due to the link between the thickness and pore size distribution of nonwoven fibrous media (cf. Bai et al., 2020), thicker pit membranes can be expected to have narrower maximum sizes of pore constrictions. If embolism formation is triggered by air passing through pore constrictions, thicker pit membranes should therefore result in reduced embolism risk (Jansen et al., 2018). The rare pit hypothesis assumes that a vessel's embolism risk depends on the size of its largest pore, which is predicted to be linked to its total pit area (A_P) and hence vessel dimensions (Hargrave et al, 1994; Wheeler et al., 2005). A corollary of this hypothesis is therefore that for given values of A_P, species with thicker pit membranes should have a higher embolism resistance (cf. Christman et al., 2009).
However, it has been pointed out that the rare pit hypothesis is based on a simplistic, two-dimensional view of pit membranes that does not capture the complexity of their spatial structure (Kaack et al., 2019). Models of air-seeding processes based on the Young-Laplace equation implicitly assume pit membranes to consist of a set of circular, parallel pores with constant diameter that connect both sides of the membrane. In reality, the pore space between cellulose microfibrils of pit membranes forms a large, highly interconnected pathway consisting of multiple pore spaces and narrow pore constrictions (Zhang et al., 2020). In agreement, mechanistic modelling and experimental data show that the minimum pore constrictions in pit membranes are smaller than expected, and leaky pit membranes are by far not common enough to support the rare pit hypothesis (Kaack et al., 2021). In addition, the presence of stable gas nanobubbles in the xylem sap (Schenk et al., 2015, 2017), dynamic changes in surface tension induced by local concentration

gradients of insoluble lipid-based surfactants (Yang et al., 2020), and uncertainties regarding the mechanisms that drive the spontaneous snap-off of gas bubbles at the air-water interface in membrane pore constrictions (Park et al., 2019) put into question whether direct bubble penetration as based on the air-seeding hypothesis represents the main mechanism behind embolism formation (Kaack et al., 2021). Indeed, pressure-driven gas diffusion across pit membranes may be as important for the spread of emboli as the bulk flow of gas implied by air-seeding (Guan et al., 2021). If the driving process for the formation of emboli is the spontaneous expansion of previously stable gas bubbles that either entered vessels as nanobubbles, or came out of solution, pit membrane thickness can be expected to have a strong effect on embolism resistance via its permeability. However, in this case it is less clear why P_{50} should be associated with vessel dimensions (Lens et al., 2022).

2.5.2. How can we explain the $P_{50} – D_h$ relationship mechanistically

One potential reason for the observed link between P_{50} and D_h is the dependence of embolism resistance on the connectivity of the conduit network, including vessels and tracheids (Loepfe et al., 2007; Mrad et al., 2018, 2019; Wason et al., 2021). If larger vessels have a higher connectivity, i.e., if each vessel shares bordered pits with a higher number of other vessels or tracheids as potential sources of embolism spread, this may constitute a link between embolism resistance and vessel dimensions, independent of the frequency of rare, leaky pits (cf. Levionnois et al., 2021).
The probabilistic argument that is at the core of the rare pit hypothesis (cf. Christman et al., 2009) can also be extended to processes other than bulk flow of bubbles through pit membranes. Embolism formation is a highly nonlinear process, where a slight state change can trigger the complete and largely irreversible loss of conductive function of a vessel once a certain tipping point has been crossed (cf. Arend et al., 2021; Johnson et al., 2022). If embolism formation depends on any stochastic process that can happen with a certain probability anywhere in a vessel, it is more likely to happen at least once in a vessel with a larger volume, which therefore will invariably possess a higher embolism risk. Importantly, this applies to all the drivers of embolism formation depending on gas dynamics discussed above. If embolism formation, for instance, was driven predominantly by the expansion of nanobubbles that exceed a critical size (Schenk et al., 2017; Park et al. 2019; Ingram et al., 2021), a single bubble exceeding this threshold size could cause the complete loss of functionality of the corresponding vessel. Similarly, if emboli spread predominantly via gas diffusion through pit membranes (Guan et al., 2021), it would only take one large enough bubble coming out of solution, e.g., after a temperature increase (see Fig. 1 in Schenk et al., 2016) to trigger a catastrophic state change. As both processes are more likely to happen at least once in larger xylem sap volumes, they are consistent with a link between embolism resistance and vessel dimensions that is independent of A_P. As all processes mentioned above depend on the occurrence of rare events that are hard to observe, the possibility for empirical testing is limited (Kaack et al., 2019). The most promising way of evaluating their importance is

therefore via mechanistic modelling approaches as in Kaack et al. (2021). If the processes of interest for embolism formation depend on the occurrence of rare events situated in the extreme tails of highly skewed probability distributions, a promising route to improve existing models may be to guide them by basic principles of extreme value theory (Coles et al., 2001; Reiss and Thomas, 2007). A recent application in an ecophysiological context is provided by Martínez-Vilalta et al. (2021), who proposed the use of methods from this field to improve estimates of minimum water potentials.

If embolism resistance indeed depended on vessel diameter, this relationship would establish a mechanistic link between plant drought responses and pervasive trends in wood anatomy. This provides a potential explanation for both large-scale patterns in the variation in vessel diameter along climate gradients (Pfautsch et al., 2016; Hacke et al., 2017) and patterns observed in growth rings of years differing in water availability (Zimmermann et al., 2021). Moreover, given the universal scaling of vessel diameter with path length within individuals (Olson et al., 2014), the existence of a xylem safety – vessel diameter relationship may help explain the higher embolism risk of taller plants (Anfodillo and Olson, 2021), and thus why water availability dictates global patterns in plant height (Moles et al., 2009). In addition, the link between D_h and P_{50} is at the basis of a potential hydraulic safety – efficiency tradeoff (Hacke et al., 2006). Indeed, our results showed a positive relationship between P_{50} and specific conductivity (K_s), with more embolism-resistant species having less efficient xylem (Fig. 2.2 c). Notably, the correlation between P_{50} and K_s observed here is strong compared to other values reported in literature (Gleason et al., 2016; Van der Sande et al., 2019; Lübbe et al., 2022). This strong link may result from using a sample of similarly sized trees from species with diffuse-porous wood covering a broad range of embolism resistance (Fig. 2.1), grown under identical conditions, and measured with consistent methods, which highlights the importance of controlled experimental conditions to minimize the influence of confounding covariates.

2.5.3. Reconciling discrepancies about the vessel diameter – embolism resistance relationship

One potential explanation for inconsistency in literature about the D_h – P_{50} relationship is bias induced by missing covariates (Shrier & Platt, 2010), most importantly pit membrane thickness. In our dataset, we observed a strong D_h – P_{50} relationship (Fig. 2.3-2.5). While a spurious association induced by a link between D_h and T_{PM} could be ruled out for our dataset, it is possible that an unaccounted positive D_h – T_{PM} relationship may mask an existing relationship in other datasets, especially when covering wider ranges of species with different pit morphologies. In either case, it is important to point out that tests of bivariate associations (cf. Fig. 2.2) and regression models with more than one predictor (cf. Fig. 2.3) answer fundamentally different questions. While the former is a sensible approach when the question is whether and how two traits are associated, the study of pairwise bivariate associations is generally not an adequate tool for inference about causal relationships between variables, e.g., whether or not one trait has an effect

on another trait (Pearl, 2000). If the latter is desired, it may be more adequate to use graphical approaches based on directed acyclic graphs (DAGs, cf. Fig. 2.3 a) (Greenland et al., 1999; Shrier & Platt, 2008) to identify the variables that have to be included in multiple regression models, or to employ formal causal inference frameworks such as structural equation modelling (Grace et al., 2012). One central takeaway from the DAG in Fig. 2.3 a is that if T_{PM} and D_h are correlated, it is impossible to obtain unbiased evidence about the existence of a D_h – P_{50} link without accounting for T_{PM}.

A second potential explanation why some studies report a link between D_h – P_{50}, while others do not, are differences in the range of trait values covered. As illustrated in Fig. 2.4 a, even if the D_h – P_{50} relationship remains identical, a restricted range in the traits sampled results in a lower power to detect an existing relationship (Bland & Altman, 2011). Hence, a weak correlation between two traits is insufficient to conclude that there is no relationship if the sampling covers only a small part of the potential variation of these traits. For instance, to identify a true relationship based on a Pearson correlation test with a nominal power of 0.8 and a significance level of 0.05 for an identical slope as in Fig. 2.4 a, one would need 12.4 observations, but 40.6 observations (i.e., over three times more) would be required for an equally strong relationship if D_h was constrained to values between 35 and 45 µm (calculated with R package `pwr` 1.3-0; Champely 2020). Accordingly, studies covering a restricted range of one or more traits are less likely to be able to identify an existing relationship. This is especially relevant for studies of intraspecific patterns, as hydraulic safety-related traits are evolutionarily conserved traits (Hajek et al., 2016; Fuchs et al., 2021; Weithmann et al., 2021).

A third – and perhaps the most relevant – factor contributing to disparate results in studies of xylem safety – vessel diameter relationships is the dependence of trait relationships on the level of data aggregation. Our dataset illustrates that trait relationships are not consistent across levels of aggregation, and that a strong interspecific pattern can be consistent with the complete absence of any intraspecific relationships between the same traits (Fig. 5b). While trait relationships are often analyzed at the species level, most processes that determine the fitness of plants, like competition and plant-environment interactions, act at the individual level (Clark et al., 2011). However, when focusing on the individual level, the trait relationships observed may be obscured or even reversed by ontogenetic trends, size-related constraints, or variation across organs (cf. Li et al., 2019; Zimmermann et al., 2021; Lübbe et al., 2022). For example, a major driver of intraspecific variability in D_h is the widening of vessels along the flow path, which tends to follow relatively static scaling relationships (Olson et al., 2014; Rosell et al., 2017). If not properly controlled or accounted for, these intra-individual patterns in D_h may mask existing relationships with P_{50} at the individual or species level. This would especially be the case if T_{PM} changed along the flow path (Kotowska et al., 2020; Guan et al., 2021). Accounting for size-effects that drive intratree and intraspecific variation is especially relevant when analyzing trait associations measured on different observational units, e.g., the relationship between branch P_{50} and stem D_h, or D_h and P_{50} measured on different trees with different sizes. The design of this study, which focused on traits

measured on the same branch samples and at similar positions along the flow path, permitted us to minimize the effect of these confounding size effects.

The complete absence of a credible intraspecific effect of D_h on P_{50} in the presence of a strong interspecific pattern (Fig. 2.5 b) illustrates that for analyses of trait relationships it is crucial to consider which level of aggregation inference is desired. Importantly, conflating inference on different levels of aggregation is not merely imprecise, but constitutes a logical fallacy (ecological/individualistic fallacy) that may lead to erroneous conclusions (cf., Robinson 1950; Subramanian et al., 2009; Pollet et al., 2015).

As illustrated in Fig. 2.5, the classical random slopes and intercepts LME only estimate the intraspecific slope, which may not always answer the biologically most meaningful questions. Moreover, its estimate of the intraspecific slope is biased when species are not independent of the predictor variable (Bafumi and Gelman, 2007). The within-species centering model we propose here (Eqn. 5, Supplementary Material S1) allows to separate trait relationships into within- and across-species components based on a standard LME syntax. As this model permits 'borrowing strength' (Tukey, 1972) across species via partial pooling (Gelman, 2006) to estimate an average within-species slope, it alleviates the issue of restricted trait ranges and small sample sizes within species, which can strongly affect the power of intraspecific analyses performed separately for each species (see above).

2.6. Conclusions

Our work provides clear evidence that across species, embolism resistance relates to both pit membrane thickness and vessel diameter, and that this diameter effect cannot be explained by an association of both diameter and embolism resistance with pit membrane thickness. Therefore, a D_h – P_{50} relationship could be explained by a functional link between D_h and A_P, or could be independent of A_P, driven for instance by multiphase processes at the gas-liquid-solid-surfactant interface in pit membranes, such as the dynamics of bubble behavior. Future work should hence be directed at identifying the mechanisms that drive the D_h – P_{50} relationship to reconcile recent models of embolism formation with anatomical evidence at the pit and vessel level, including vessel dimensions and connectivity. In this regard, both direct measurements of total intervessel pit area or number and mechanistic modelling of the processes behind embolism formation are crucial.

Further, our study illustrates those inconsistencies in the D_h – P_{50} relationship reported in literature may be reinforced by differences in the size range of variables studied, missing covariates, and most importantly, the conflation of different scales of aggregation. The latter is underlined by the total absence of an intraspecific P_{50} – D_h relationship, which contrasts with the pronounced interspecific trend in our dataset. The within-species centering model proposed expands the toolbox of trait-based ecology by a simple tool to separate cross-species and within-species patterns of trait associations.

Acknowledgements

We thank the Bavarian State Institute for Viticulture and Horticulture, Veitshochheim, Germany, for granting us access to the Stutel-Arboretum facility, as well as Klaus Körber and all others involved in the 'Klimabäume Stutel' project. We thank Christine Gernert and Yvonne Heppenstiel, as well as all members of the Imaging Core Facility, University of Würzburg, for technical support. The Transmission Electron Microscope has been funded by the German Research Foundation (Deutsche Forschungsgemeinschaft DFG), grant number 218894163.

References

Adams HD, Zeppel MJB, Anderegg WRL, Hartmann H, Landhäusser SM, Tissue DT, Huxman TE, Hudson PJ, Franz TE, Allen CD, et al. 2017. A multi-species synthesis of physiological mechanisms in drought-induced tree mortality. Nature Ecology & Evolution 1: 1285–1291.

Anderegg WRL, Klein T, Bartlett M, Sack L, Pellegrini AFA, Choat B, Jansen S. 2016. Meta-analysis reveals that hydraulic traits explain cross-species patterns of drought-induced tree mortality across the globe. Proceedings of the National Academy of Sciences 113: 5024–5029.

Anfodillo T, Olson ME. 2021. Tree Mortality: Testing the link between drought, embolism vulnerability, and xylem conduit diameter remains a priority. Frontiers in Forests and Global Change 4: 704670.

Arend M, Link RM, Patthey R, Hoch G, Schuldt B, Kahmen A. 2021. Rapid hydraulic collapse as cause of drought-induced mortality in conifers. Proceedings of the National Academy of Sciences 118: e2025251118.

Bafumi J, Gelman A. 2007. Fitting multilevel models when predictors and group effects correlate. SSRN Electronic Journal. URL: https://ssrn.com/abstract=1010095

Bai H, Qian X, Fan J, Qian Y, Duo Y, Liu Y, Wang X. 2020. Computing pore size distribution in non-woven fibrous filter media. Fibers and Polymers 21: 196–203.

Bland JM, Altman DG. 2011. Correlation in restricted ranges of data. BMJ 342: d556.

Brodersen CR, McElrone AJ, Choat B, Lee EF, Shackel KA, Matthews MA. 2013. In vivo visualizations of drought-induced embolism spread in *Vitis vinifera*. Plant Physiology 161: 1820–1829.

Bürkner P-C. 2017. brms: An R package for Bayesian multilevel models using Stan. Journal of Statistical Software 80: 1–28.

Bürkner P-C. 2018. Advanced Bayesian multilevel modeling with the R package brms. The R Journal 10: 395–411.

Champely S. 2020. pwr: Basic functions for power analysis. URL: https://CRAN.R-project.org/package=pwr

Choat B, Badel E, Burlett R, Delzon S, Cochard H, Jansen S. 2016. Noninvasive measurement of vulnerability to drought-induced embolism by X-ray microtomography. Plant Physiology 170: 273–282.

Choat B, Ball M, Luly J, Holtum J. 2003. Pit membrane porosity and water stress-induced cavitation in four co-existing dry rainforest tree species. Plant Physiology 131: 41–48.

Choat B, Cobb AR, Jansen S. 2008. Structure and function of bordered pits: new discoveries and impacts on whole-plant hydraulic function. New Phytologist 177: 608–626.

Christman MA, Sperry JS, Adler FR. 2009. Testing the 'rare pit' hypothesis for xylem cavitation resistance in three species of *Acer*. New Phytologist 182: 664–674.

Clark JS, Bell DM, Hersh MH, Kwit MC, Moran E, Salk C, Stine A, Valle D, Zhu K. 2011. Individual-scale variation, species-scale differences: inference needed to understand diversity. Ecology Letters 14: 1273–1287.

Coles S, Bawa J, Trenner L, Dorazio P. 2001. An introduction to statistical modeling of extreme values. Springer.

Creek D, Blackman CJ, Brodribb TJ, Choat B, Tissue DT. 2018. Coordination between leaf, stem, and root hydraulics and gas exchange in three arid-zone angiosperms during severe drought and recovery. Plant, Cell & Environment 41: 2869–2881.

Domec J-C, Schafer K, Oren R, Kim HS, McCarthy HR. 2010. Variable conductivity and embolism in roots and branches of four contrasting tree species and their impacts on whole-plant hydraulic performance under future atmospheric CO_2 concentration. Tree Physiology 30: 1001–1015.

Fu P-L, Jiang Y-J, Wang A-Y, Brodribb TJ, Zhang J-L, Zhu S-D, Cao K-F. 2012. Stem hydraulic traits and leaf water-stress tolerance are co-ordinated with the leaf phenology of angiosperm trees in an Asian tropical dry karst forest. Annals of Botany 110: 189–199.

Fuchs S, Leuschner C, Link RM, Schuldt B. 2021. Hydraulic variability of three temperate broadleaf tree species along a water availability gradient in central Europe. New Phytologist 231: 1387–1400.

Gelman A. 2006. Multilevel (hierarchical) modeling: What it can and cannot do. Technometrics 48: 432–435.

GIMP Development Team. 2018. GIMP v. 20.10.6. URL: https://www.gimp.org/

Gleason SM, Westoby M, Jansen S, Choat B, Hacke UG, Pratt RB, Bhaskar R, Brodribb TJ, Bucci SJ, Cao K-F, et al. 2016. Weak tradeoff between xylem safety and xylem-specific hydraulic efficiency across the world's woody plant species. New Phytologist 209: 123–136.

Grace JB, Schoolmaster DR, Guntenspergen GR, Little AM, Mitchell BR, Miller KM, Schweiger EW. 2012. Guidelines for a graph-theoretic implementation of structural equation modeling. Ecosphere 3: 1–44.

Greenland S, Pearl J, Robins JM. 1999. Causal diagrams for epidemiologic research. Epidemiology 10: 37–48.

Guan X, Pereira L, McAdam SAM, Cao K-F, Jansen S. 2021. No gas source, no problem: Proximity to pre-existing embolism and segmentation affect embolism spreading in angiosperm xylem by gas diffusion. Plant, Cell & Environment 44: 1329–1345.

Guan X, Werner J, Cao K-F, Pereira L, Kaack L, McAdam S a. M, Jansen S. 2022. Stem and leaf xylem of angiosperm trees experiences minimal embolism in temperate forests during two consecutive summers with moderate drought. Plant Biology n/a.

Hacke UG, Sperry JS, Wheeler JK, Castro L. 2006. Scaling of angiosperm xylem structure with safety and efficiency. Tree Physiology 26: 689–701.

Hacke UG, Spicer R, Schreiber SG, Plavcová L. 2017. An ecophysiological and developmental perspective on variation in vessel diameter. Plant, Cell & Environment 40: 831–845.

Hajek P, Kurjak D, von Wühlisch G, Delzon S, Schuldt B. 2016. Intraspecific variation in wood anatomical, hydraulic, and foliar traits in ten European beech provenances differing in Growth yield. Frontiers in Plant Science 7.

Hajek P, Link RM, Nock CA, Bauhus J, Gebauer T, Gessler A, Kovach K, Messier C, Paquette A, Saurer M, et al. 2022. Mutually inclusive mechanisms of drought-induced tree mortality. Global Change Biology 28: 3365–3378.

Hargrave KR, Kolb KJ, Ewers FW, Davis SD. 1994. Conduit diameter and drought-induced embolism in *Salvia mellifera* Greene (Labiatae). New Phytologist 126: 695–705.

Herbert E, Caupin F. 2005. The limit of metastability of water under tension: theories and experiments. Journal of Physics: Condensed Matter 17: S3597–S3602.

Ingram S, Salmon Y, Lintunen A, Hölttä T, Vesala T, Vehkamäki H. 2021. Dynamic Surface tension enhances the stability of nanobubbles in xylem sap. Frontiers in Plant Science 12.

Jansen S, Choat B, Pletsers A. 2009. Morphological variation of intervessel pit membranes and implications to xylem function in angiosperms. American Journal of Botany 96: 409–419.

Jansen S, Klepsch M, Li S, Kotowska MM, Schiele S, Zhang Y, Schenk HJ. 2018. Challenges in understanding air-seeding in angiosperm xylem. Acta Horticulturae: 13–20.

Johnson DM, Katul G, Domec J-C. 2022. Catastrophic hydraulic failure and tipping points in plants. Plant, Cell & Environment n/a.

Kaack L, Altaner CM, Carmesin C, Diaz A, Holler M, Kranz C, Neusser G, Odstrcil M, Schenk HJ, Schmidt V, et al. 2019. Function and three-dimensional structure of intervessel pit membranes in angiosperms: a review. IAWA Journal 40: 673–702.

Kaack L, Weber M, Isasa E, Karimi Z, Li S, Pereira L, Trabi CL, Zhang Y, Schenk HJ, Schuldt B, et al. 2021. Pore constrictions in intervessel pit membranes provide a mechanistic explanation for xylem embolism resistance in angiosperms. New Phytologist 230: 1829–1843.

Kanduč M, Schneck E, Loche P, Jansen S, Schenk HJ, Netz RR. 2020. Cavitation in lipid bilayers poses strict negative pressure stability limit in biological liquids. Proceedings of the National Academy of Sciences 117: 10733–10739.

Klepsch M, Zhang Y, Kotowska MM, Lamarque LJ, Nolf M, Schuldt B, Torres-Ruiz JM, Qin D-W, Choat B, Delzon S, et al. 2018. Is xylem of angiosperm leaves less resistant to embolism than branches? Insights from microCT, hydraulics, and anatomy. Journal of Experimental Botany 69: 5611–5623.

Kotowska MM, Thom R, Zhang Y, Schenk HJ, Jansen S. 2020. Within-tree variability and sample storage effects of bordered pit membranes in xylem of *Acer pseudoplatanus*. Trees 34: 61–71.

Lamarque LJ, Corso D, Torres-Ruiz JM, Badel E, Brodribb TJ, Burlett R, Charrier G, Choat B, Cochard H, Gambetta GA, et al. 2018. An inconvenient truth about xylem resistance to embolism in the model species for refilling *Laurus nobilis* L. Annals of Forest Science 75: 1–15.

Lemaire C, Quilichini Y, Brunel-Michac N, Santini J, Berti L, Cartailler J, Conchon P, Badel É, Herbette S. 2021. Plasticity of the xylem vulnerability to embolism in *Populus tremula x alba* relies on pit quantity properties rather than on pit structure. Tree Physiology: tpab018.

Lemoine NP. 2019. Moving beyond noninformative priors: why and how to choose weakly informative priors in Bayesian analyses. Oikos 128: 912–928.

Lens F, Sperry JS, Christman MA, Choat B, Rabaey D, Jansen S. 2011. Testing hypotheses that link wood anatomy to cavitation resistance and hydraulic conductivity in the genus *Acer*. New Phytologist 190: 709–723.

Lens F, Tixier A, Cochard H, Sperry JS, Jansen S, Herbette S. 2013. Embolism resistance as a key mechanism to understand adaptive plant strategies. Current Opinion in Plant Biology 16: 287–292.

Lens F, Gleason SM, Bortolami G, Brodersen C, Delzon S, Jansen S. 2022. Functional xylem characteristics associated with drought-induced embolism in angiosperms. New Phytologist n/a.

Levionnois S, Jansen S, Wandji RT, Beauchêne J, Ziegler C, Coste S, Stahl C, Delzon S, Authier L, Heuret P. 2021. Linking drought-induced xylem embolism resistance to wood anatomical traits in Neotropical trees. New Phytologist 229: 1453–1466.

Levionnois S, Ziegler C, Jansen S, Calvet E, Coste S, Stahl C, Salmon C, Delzon S, Guichard C, Heuret P. 2020. Vulnerability and hydraulic segmentations at the stem–leaf transition: coordination across Neotropical trees. New Phytologist 228: 512–524.

Li S, Lens F, Espino S, Karimi Z, Klepsch M, Schenk HJ, Schmitt M, Schuldt B, Jansen S. 2016. Intervessel pit membrane thickness as a key determinant of embolism resistance in angiosperm xylem. IAWA Journal 37: 152–171.

Li S, Li X, Link RM, Li R, Deng L, Schuldt B, Jiang X, Zhao R, Zheng J, Li S, et al. 2019. Influence of Cambial Age and Axial Height on the Spatial Patterns of Xylem Traits in *Catalpa bungei*, a Ring-Porous Tree Species Native to China. Forests 10: 662.

Loepfe L, Martinez-Vilalta J, Piñol J, Mencuccini M. 2007. The relevance of xylem network structure for plant hydraulic efficiency and safety. Journal of Theoretical Biology 247: 788–803.

Losso A, Bär A, Dämon B, Dullin C, Ganthaler A, Petruzzellis F, Savi T, Tromba G, Nardini A, Mayr S, et al. 2019. Insights from in vivo micro-CT analysis: testing the hydraulic vulnerability segmentation in *Acer pseudoplatanus* and *Fagus sylvatica* seedlings. New Phytologist 221: 1831–1842.

Lübbe T, Lamarque LJ, Delzon S, Torres Ruiz JM, Burlett R, Leuschner C, Schuldt B. 2022. High variation in hydraulic efficiency but not xylem safety between roots and branches in four temperate broad-leaved tree species. Functional Ecology 36: 699–712.

Maherali H, Moura CF, Caldeira MC, Willson CJ, Jackson RB. 2006. Functional coordination between leaf gas exchange and vulnerability to xylem cavitation in temperate forest trees. Plant, Cell and Environment 29: 571–583.

Martínez-Vilalta J, Santiago LS, Poyatos R, Badiella L, Cáceres M, Aranda I, Delzon S, Vilagrosa A, Mencuccini M. 2021. Towards a statistically robust determination of minimum water potential and hydraulic risk in plants. New Phytologist 232: 404–417.

Meyra AG, Kuz VA, Zarragoicoechea GJ. 2007. Geometrical and physicochemical considerations of the pit membrane in relation to air seeding: the pit membrane as a capillary valve. Tree Physiology 27: 1401–1405.

Moles AT, Warton DI, Warman L, Swenson NG, Laffan SW, Zanne AE, Pitman A, Hemmings FA, Leishman MR. 2009. Global patterns in plant height. Journal of Ecology 97: 923–932.

Mrad A, Domec J-C, Huang C-W, Lens F, Katul G. 2018. A network model links wood anatomy to xylem tissue hydraulic behaviour and vulnerability to cavitation: Model links wood anatomy to plant hydraulics. Plant, Cell & Environment 41: 2718–2730.

Mrad A, Sevanto S, Domec J-C, Liu Y, Nakad M, Katul G. 2019. A Dynamic Optimality Principle for Water Use Strategies Explains Isohydric to Anisohydric Plant Responses to Drought. Frontiers in Forests and Global Change 2: 49.

Ogle K, Barber JJ, Willson C, Thompson B. 2009. Hierarchical statistical modeling of xylem vulnerability to cavitation. New Phytologist 182: 541–554.

Olson ME, Anfodillo T, Rosell JA, Petit G, Crivellaro A, Isnard S, León-Gómez C, Alvarado-Cárdenas LO, Castorena M. 2014. Universal hydraulics of the flowering plants: vessel diameter scales with stem length across angiosperm lineages, habits and climates. Ecology Letters 17: 988–997.

Paligi SS, Link RM, Isasa E, Bittencourt P, Cabral JS, Jansen S, Oliveira RS, Pereira L, Schuldt B. 2021. Accuracy of the pneumatic method for estimating xylem vulnerability to embolism in temperate diffuse-porous tree species (preprint). biorXiv. doi: 10.1101/2021.02.15.431295

Pammenter NW, Vander Willigen C. 1998. A mathematical and statistical analysis of the curves illustrating vulnerability of xylem to cavitation. Tree Physiology 18: 589–593.

Park J, Go T, Ryu J, Lee SJ. 2019. Air spreading through wetted cellulose membranes: Implications for the safety function of hydraulic valves in plants. Physical Review E 100: 032409.

Pearl J. 2000. Causality: Models, reasoning, and inference. Cambridge: Cambridge University Press.

Peel MC, Finlayson BL, McMahon TA. 2007. Updated world map of the Köppen-Geiger climate classification. Hydrology and Earth System Sciences 11: 1633–1644.

Pfautsch S. 2016. Hydraulic anatomy and function of trees—basics and critical developments. Current Forestry Reports 2: 236–248.

van de Pol M, Wright J. 2009. A simple method for distinguishing within- versus between-subject effects using mixed models. Animal Behaviour 77: 753–758.

Pollet TV, Stulp G, Henzi SP, Barrett L. 2015. Taking the aggravation out of data aggregation: A conceptual guide to dealing with statistical issues related to the pooling of individual-level observational data: Data Aggregation and the Ecological Fallacy. American Journal of Primatology 77: 727–740.

Powers JS, Vargas G. G, Brodribb TJ, Schwartz NB, Pérez-Aviles D, Smith-Martin CM, Becknell JM, Aureli F, Blanco R, Calderón-Morales E, et al. 2020. A catastrophic tropical drought kills hydraulically vulnerable tree species. Global Change Biology 26: 3122–3133.

Pratt RB, MacKinnon ED, Venturas MD, Crous CJ, Jacobsen AL. 2015. Root resistance to cavitation is accurately measured using a centrifuge technique. Tree Physiology 35: 185–196.

R Core Team. 2022. R: A language and environment for statistical computing. Vienna, Austria. URL: https://www.R-project.org/

Reiss R-D, Thomas M. 2007. Statistical analysis of extreme values: with applications to insurance, finance, hydrology and other fields. Basel: Birkhäuser.

Robinson WS. 1950. Ecological correlations and the behavior of individuals. American Sociological Review 15: 351–357.

Rosell JA, Olson ME, Anfodillo T. 2017. Scaling of xylem vessel diameter with plant size: Causes, predictions, and outstanding questions. Current Forestry Reports 3: 46–59.

Roth-Nebelsick A. 2019. It's contagious: calculation and analysis of xylem vulnerability to embolism by a mechanistic approach based on epidemic modeling. Trees 33: 1519–1533.

van der Sande MT, Poorter L, Schnitzer SA, Engelbrecht BMJ, Markesteijn L. 2019. The hydraulic efficiency–safety trade-off differs between lianas and trees. Ecology 100: e02666.

Schenk HJ, Espino S, Romo DM, Nima N, Do AYT, Michaud JM, Papahadjopoulos-Sternberg B, Yang J, Zuo YY, Steppe K, et al. 2017. Xylem surfactants introduce a new element to the cohesion-tension theory. Plant Physiology 173: 1177–1196.

Schenk HJ, Espino S, Visser A, Esser BK. 2016. Dissolved atmospheric gas in xylem sap measured with membrane inlet mass spectrometry. Plant, Cell & Environment 39: 944–950.

Schenk HJ, Steppe K, Jansen S. 2015. Nanobubbles: a new paradigm for air-seeding in xylem. Trends in Plant Science 20: 199–205.

Schmid R, Machado RD. 1968. Pit membranes in hardwoods—Fine structure and development. Protoplasma 66: 185–204.

Schneider CA, Rasband WS, Eliceiri KW. 2012. NIH Image to ImageJ: 25 years of image analysis. Nature Methods 9: 671–675.

Scholz A, Rabaey D, Stein A, Cochard H, Smets E, Jansen S. 2013. The evolution and function of vessel and pit characters with respect to cavitation resistance across 10 *Prunus* species. Tree Physiology 33: 684–694.

Schuldt B, Knutzen F, Delzon S, Jansen S, Müller-Haubold H, Burlett R, Clough Y, Leuschner C. 2016. How adaptable is the hydraulic system of European beech in the face of climate change-related precipitation reduction? New Phytologist 210: 443–458.

Shrier I, Platt RW. 2008. Reducing bias through directed acyclic graphs. BMC Medical Research Methodology 8: 70.

Skelton RP, Anderegg LDL, Papper P, Reich E, Dawson TE, Kling M, Thompson SE, Diaz J, Ackerly DD. 2019. No local adaptation in leaf or stem xylem vulnerability to embolism, but consistent vulnerability segmentation in a North American oak. New Phytologist 223: 1296–1306.

Skelton RP, Brodribb TJ, Choat B. 2017. Casting light on xylem vulnerability in an herbaceous species reveals a lack of segmentation. New Phytologist 214: 561–569.

Sorek Y, Greenstein S, Netzer Y, Shtein I, Jansen S, Hochberg U. 2021. An increase in xylem embolism resistance of grapevine leaves during the growing season is coordinated with stomatal regulation, turgor loss point and intervessel pit membranes. New Phytologist 229: 1955–1969.

Sperry JS, Nichols KL, Sullivan JEM, Eastlack SE. 1994. Xylem embolism in ring-porous, diffuse-porous, and coniferous trees of Northern Utah and Interior Alaska. Ecology 75: 1736–1752.

Sperry JS, Tyree MT. 1988. Mechanism of water stress-induced xylem embolism. Plant Physiology 88: 581–587.

Stroock AD, Pagay VV, Zwieniecki MA, Michele Holbrook N. 2014. The physicochemical hydrodynamics of vascular plants. Annual Review of Fluid Mechanics 46: 615–642.

Subramanian SV, Jones K, Kaddour A, Krieger N. 2009. Revisiting Robinson: The perils of individualistic and ecologic fallacy. International Journal of Epidemiology 38: 342–360.

Torres-Ruiz JM, Jansen S, Choat B, McElrone AJ, Cochard H, Brodribb TJ, Badel E, Burlett R, Bouche PS, Brodersen CR, et al. 2015. Direct X-ray microtomography observation confirms the induction of embolism upon xylem cutting under tension. Plant Physiology 167: 40–43.

Tukey JW. 1972. Data analysis, computation and mathematics. Quarterly of Applied Mathematics 30: 51–65.

Tyree MT, Davis SD, Cochard H. 1994. Biophysical perspectives of xylem evolution: Is there a tradeoff of hydraulic efficiency for vulnerability to dysfunction? IAWA Journal 15: 335–360.

Tyree MT, Zimmermann MH. 2002. Xylem structure and the ascent of sap. Berlin, Heidelberg: Springer Verlag.

Wason JW, Anstreicher KS, Stephansky N, Huggett BA, Brodersen CR. 2018. Hydraulic safety margins and air-seeding thresholds in roots, trunks, branches and petioles of four northern hardwood trees. New Phytologist 219: 77–88.

Wason J, Bouda M, Lee EF, McElrone AJ, Phillips RJ, Shackel KA, Matthews MA, Brodersen C. 2021. Xylem network connectivity and embolism spread in grapevine (*Vitis vinifera* L.). Plant Physiology 186: 373–387.

Weithmann G, Schuldt B, Link RM, Heil D, Hoeber S, John H, Müller-Haubold H, Schüller L-M, Schumann K, Leuschner C. 2021. Leaf trait modification in European beech trees in response to climatic and edaphic drought. Plant Biology n/a.

Wheeler JK, Huggett BA, Tofte AN, Rockwell FE, Holbrook NM. 2013. Cutting xylem under tension or supersaturated with gas can generate PLC and the appearance of rapid recovery from embolism: Sampling induced embolism. Plant, Cell & Environment 36: 1938–1949.

Wheeler JK, Sperry JS, Hacke UG, Hoang N. 2005. Inter-vessel pitting and cavitation in woody Rosaceae and other vesselled plants: a basis for a safety versus efficiency trade-off in xylem transport. Plant, Cell and Environment 28: 800–812.

White FM. 1991. Viscous fluid flow. New York: McGraw-Hill.

Wickham H, Averick M, Bryan J, Chang W, McGowan LD, François R, Grolemund G, Hayes A, Henry L, Hester J, et al. 2019. Welcome to the tidyverse. Journal of Open Source Software 4: 1686.

Yang J, M Michaud J, Jansen S, Schenk HJ, Zuo YY. 2020. Dynamic surface tension of xylem sap lipids. Tree Physiology 40: 433–444.

Zhang Y, Carmesin C, Kaack L, Klepsch MM, Kotowska M, Matei T, Schenk HJ, Weber M, Walther P, Schmidt V, et al. 2020. High porosity with tiny pore constrictions and unbending pathways characterize the 3D structure of intervessel pit membranes in angiosperm xylem. Plant, Cell & Environment 43: 116–130.

Zhang Y, Klepsch M, Jansen S. 2017. Bordered pits in xylem of vesselless angiosperms and their possible misinterpretation as perforation plates. Plant, Cell & Environment 40: 2133–2146.

Zimmermann J, Link RM, Hauck M, Leuschner C, Schuldt B. 2021. 60-year record of stem xylem anatomy and related hydraulic modification under increased summer drought in ring- and diffuse-porous temperate broad-leaved tree species. Trees 35: 919–937

3. Chapter 2: Accuracy of the pneumatic method for estimating xylem vulnerability to embolism in temperate diffuse-porous tree species

This chapter is based on the following publication.

Manuscript 2 (Preprint in Plant Biology) Accuracy of the pneumatic method for estimating xylem vulnerability to embolism in temperate diffuse-porous tree species. biorXiv. doi: 10.1101/2021.02.15.431295

Sharath S. Paligi, Roman M. Link, **Emilie Isasa**, Paulo Bittencourt, Juliano Sarmento Cabral, Steven Jansen, Rafael S. Oliveira, Luciano Pereira and Bernhard Schuldt

Participated in	**Author Initials,** Responsibility decreasing from left to right				
Study Design Methods Development	B.S.	R.M.L.	S.S.P.	E.I.	
Data Collection	S.S.P.	E.I.	P.B.	L.P.	
Data Analysis and Interpretation	S.S.P.	R.M.L.	E.I.	B.S.	S.J.
Manuscript Writing Writing of Introduction	R.M.L.	B.S.	S.S.P.	E.I.	
Writing of Materials & Methods	S.S.P.	E.I.	R.M.L.		
Writing of Discussion Writing of First Draft	R.M.L.	B.S.	S.S.P.	E.I.	

Figure	**Author Initials,** Responsibility decreasing from left to right				
1	S.P. / R.M.L.	E.I.	B.S.	J.S.C.	
2	S.P. / R.M.L.	E.I.	B.S.	J.S.C.	
3	S.P. / R.M.L.	B.S.	J.S.C.		
4	S.P. / R.M.L.	B.S.	J.S.C.		
5	S.P. / R.M.L.	B.S.	J.S.C.		

Table	**Author Initials,** Responsibility decreasing from left to right				
1	S.P.	R.M.L.			
2	S.P.	R.M.L.			

Explanations:

The doctoral researcher confirms that she has obtained permission from the co-authors for legal second publication.

The doctoral researcher and the primary supervisor confirm the correctness of the above-mentioned assessment.

Emilie Isasa	25.11.2022	Würzburg	
Doctoral Researcher's Name	Date	Place	Signature

Prof. Dr. Bernhard Schuldt	25.11.2022	Dresden	
Primary Supervisor's Name	Date	Place	Signature

3.1. Abstract

The increasing frequency of global change-type droughts has created a need for fast, accurate and widely applicable techniques for estimating xylem embolism resistance to improve forecasts of future forest changes.

We used data from 12 diffuse-porous temperate tree species covering a wide range of xylem safety to compare the pneumatic and flow-centrifuge method for constructing xylem vulnerability curves. We evaluated the agreement between parameters estimated with both methods and the sensitivity of pneumatic measurements to the measurement duration.

The agreement between xylem water potentials at 50% air discharged (PAD) estimated with the Pneumatron and 50% loss of hydraulic conductivity (PLC) estimated with the flow-centrifuge method was high (mean signed deviation: 0.12 MPa, Pearson correlation: 0.96 after 15 sec of gas extraction). However, the relation between the estimated slopes was more variables, resulting in lower agreement in xylem water potential at 12% and 88% PAD/PLC. All parameters were sensitive to the duration of the pneumatic measurement, with highest overall agreement between methods after 16 sec.

We conclude that, if applied correctly, the pneumatic method enables fast and inexpensive estimations of embolism resistance for a wide range of temperate, diffuse-porous species, which makes it attractive for predicting plant performance under climate change.

Keywords: Cavitron, drought tolerance traits, xylem embolism resistance, vulnerability curve, methods comparison, Pneumatron, plant hydraulics.

3.2. Introduction

In the last decades, unprecedented climate fluctuations and the resulting extreme drought events have led to large-scale tree dieback events worldwide (Allen et al., 2010, 2015; Brando et al., 2019). With the global rise in frequency, intensity and duration of drought spells predicted by current climate projections (cf. Field et al., 2012; Trenberth et al., 2014), large-scale drought-induced tree mortality events become increasingly likely (Brodribb et al., 2020).

To improve the prediction of demographic and compositional changes in forest ecosystems, a better understanding of physiological mechanisms associated with the death of trees in response 26 to drought is necessary (Allen et al., 2010; McDowell et al., 2013a, 2013b). In this context, traits that quantify the vulnerability of a tree's xylem to drought-induced embolism have received particular attention (Choat et al., 2018; Brodribb et al., 2020). Vulnerability to embolism is usually expressed by the parameters of xylem vulnerability curves (VCs), i.e., curves describing the consecutive loss of hydraulic conductance (percent loss of conductivity, PLC) as a function of increasingly negative xylem pressures (cf. Sperry et al., 1988; Cochard et al., 2013). Most commonly, VCs are described by the water potential at 12, 50 or 88% loss of hydraulic conductance (P_{12}, P_{50} and P_{88}, respectively) and the slope of the curve at one of the respective locations. The parameters of VCs have been linked to mechanistic thresholds for xylem functioning (cf. Brodribb & Cochard, 2009; Urli et al., 2013; Delzon & Cochard, 2014) and are closely coordinated with stomatal regulation (Martin-StPaul et al., 2017). Across biomes, xylem embolism resistance has been associated with the susceptibility of a species to drought-induced mortality (Anderegg et al., 2016; Adams et al., 2017; Correia et al., 2019; Powers et al., 2020) and thus mirrors the distribution of species along aridity gradients (Blackman et al., 2014; Trueba et al., 2017; Oliveira et al., 2019). Due to their immediate mechanistic interpretation, VC parameters and derived quantities such as hydraulic safety margins (Meinzer et al., 2009) are increasingly incorporated in process-based vegetation models to describe plant drought responses and associated drought-induced tree mortality (McDowell et al., 2013a, 2013b; Christoffersen et al., 2016; Xu et al., 2016; Davi & Cailleret 2017; Eller et al., 2020).

Xylem VCs can be established through a large number of different techniques, such as the bench dehydration (Sperry et al., 1988), air injection (Cochard et al., 1992), flow-centrifuge (Cochard et al., 2005), micro-CT (Brodersen et al., 2010), pneumatic (Pereira et al., 2016), optical (Brodribb et al., 2016) and relative water loss method (Rosner et al., 2019). However, none of these methods is unequivocally reliable for angiosperm and gymnosperm species, either due to measurement artefacts associated with vessel length and porosity (Cochard et al., 2013; Jansen et al., 2015) or because they are not suitable for rapid measurements of large number of samples (Cochard et al., 2013; Nolf et al., 2017). Given their usefulness to predictive models, methods for the measurement of xylem embolism that are simple, accessible, reliable and applicable for a wide range of taxonomic groups and xylem types are needed.

A novel, promising route for fast indirect VC measurements is the pneumatic method (Pereira et al., 2016; Jansen et al., 2020), which estimates the amount of xylem embolism by measuring the increase of air volume in the xylem in bench-dried plant samples with increasingly negative xylem pressure. Recently, Pereira et al. (2020) proposed an automated device, the Pneumatron, which automatically measures air discharge from a plant sample at a high temporal resolution and permits a high sample throughput. As the measurement principle of the Pneumatron does not directly depend on the measurement of xylem water transport and embolism is induced by bench dehydration, it is assumed to be relatively robust against measurement artefacts related to sample excision and preparation as well as vessel length related artefacts (Pereira et al., 2016, 2020), which are known to affect several hydraulic VCs methods (cf. Choat et al., 2010; Wheeler et al., 2013; Martin-St Paul et al., 2014; Torres-Ruiz et al., 2014, 2015).

The pneumatic method has already been applied to construct VCs for branches, leaves and roots of tropical, subtropical and temperate species, covering diffuse-porous, ring-porous and coniferous species (Pereira et al., 2016, 2020; Zhang et al., 2018; Wu et al., 2020; Sergent et al., 2020). The results from these studies indicate the suitability of the method for diffuse-porous (Pereira et al., 2016; Zhang et al., 2018; Sergent et al., 2020) and for ring-porous species (though the latter only after gluing growth rings other than the current year rings; cf. Zhang et al., 2018). However, Zhang et al. (2018) reported that the pneumatic method resulted in lower estimates of embolism resistance of two conifer species compared to the flow-centrifuge method. Similarly, in a recent methodological comparison of VC techniques, Sergent et al. (2020) found the pneumatic method to result in lower embolism resistance estimates compared to other methods in further two conifer species and reported inconsistent estimates for long-vesseled species.

Several sources of uncertainty have been identified for the pneumatic method that leave room for potential methodological improvements. Notably, its estimates are known to be sensitive to the choice of the reservoir volume and the duration of the air discharge measurement (Pereira et al., 2016, 2020). Prior studies have used vastly different time intervals to measure air discharge (AD) from the xylem segment, ranging from 150 sec (Pereira et al., 2016; Chen et al., 2021), over 120 sec (Zhang et al., 2018; Sergent et al., 2020; Wu et al., 2020), to only 30 sec (Pereira et al., 2020). Since a 15 sec duration was predicted as optimal discharge time based on the Unit Pipe Pneumatic model (Yang et al., 2021), there is a need to test this hypothesis experimentally. Moreover, despite considerable attention to measuring artefacts and methodological concerns, we currently lack a rigorous statistical framework to compare embolism resistance methods.

This study uses a dataset of vulnerability curve measurements from 36 trees belonging to 12 temperate, diffuse-porous tree species to i) assess how well the parameters of the vulnerability curves obtained with the pneumatic method (Pneumatron) agree with estimates obtained from the flow-centrifuge method (Cavitron) in terms of systematic deviations, random deviations and overall agreement and to ii) identify the optimal duration for air discharge measurements.

3.3. Materials and Methods

3.3.1. Plant material

Plant material from trees belonging to 12 temperate diffuse-porous tree species (Table 3.1) was collected between mid-July and mid-September 2019 from a nursery in Veitshöchheim (49°50'24.3"N, 9°52'38.4"E) near Würzburg, Germany. These trees were planted in the year 2011 in the framework of a long-term comparative experiment designed to identify appropriate tree species for urban planting. The plant material cultivated in Veitshöchheim was obtained from selected nurseries across Central Europe. Due to anomalies in the data for some of the species (see below), additional branch samples were obtained from adult *Tilia cordata* and *Tilia platyphyllos* trees growing at Ulm University, Germany (48°25'20.3"N, 9°57'20.2"E) and of *Tilia japonica* from the Würzburg botanical garden (49°45'56.7"N 9°55'58.1"E) in September 2020.
The samples were collected before 9:30 a.m. to assure sample excision took place in a relaxed state, thus avoiding measurement artefacts associated with cutting under tension (Wheeler et al., 2013). From each of the experimental trees, one sun-exposed branch - 120 cm in length or any kind of damage to avoid leaks and consequent embolism overestimation. All suspicious leakage points were sealed using a fast-drying contact adhesive (Loctite 431 with Loctite activator SF 7452, Henkel, Düsseldorf, Germany). Fruits present on the branches were removed and sealed with the same glue, as they easily detach with progressing dehydration and are hence a potential site of air-entry. Similarly, in the case of *Crataegus persimilis*, thorns were removed and sealed in the same manner to ease the handling of the branches.

Table 3.1: List of the 12 diffuse-porous tree species used in the present study, average midday leaf water potential (Ψ_{midday}) measured in August 2020 and the average diameter at breast height (DBH) of the selected trees per species (mean ± SE); *n*P and *n*H indicate the number of xylem vulnerability curves measured for the pneumatic and the flow-centrifuge method, respectively (values in brackets indicate when branch samples were collected from a single tree). Asterisks (*) indicate xylem pressures measured with stem psychrometers; hashes (#) indicate individuals from the same species measured with the pressure bomb.

Species	Family	n_P	n_H	Ψ_{midday} (MPa)	DBH (cm)
Betula pendula	Betulaceae	3	3	-1.60 ± 0.04	10.93 ± 0.64
Betula utilis	Betulaceae	3	3	-1.54 ± 0.06	08.88 ± 0.42
Carpinus betulus	Betulaceae	3	3	-2.47 ± 0.06	10.75 ± 0.44
Crataegus persimilis	Rosaceae	3	3	-3.42 ± 0.18	07.55 ± 0.16
Ostrya carpinifolia	Betulaceae	3	3	-2.97 ± 0.11	09.18 ± 0.11
Platanus x acerifolia	Platanaceae	3	3	-1.74 ± 0.03	10.00 ± 0.24
Platanus orientalis	Platanaceae	3	3	-1.51 ± 0.04	12.07 ± 0.35
Pyrus calleryana	Rosaceae	2	3	-3.52 ± 0.30	11.88 ± 0.32
Sorbus latifolia	Rosaceae	3	3	-3.64 ± 0.19	09.30 ± 0.39
*Tilia cordata**	Malvaceae	5(1)	5(1)	NA	28.00 ± 0.00
Tilia cordata#	Malvaceae	3	3	-1.90 ± 0.04	11.40 ± 0.46
Tilia japonica	Malvaceae	3(1)	4(1)	NA	30.40 ± 0.00
*Tilia platyphyllos**	Malvaceae	4(1)	7(1)	NA	70.00 ± 0.21
Tilia platyphyllos#	Malvaceae	3	3	-1.80 ± 0.08	12.38 ± 0.21

3.3.2. Measurements of vulnerability curves with the pneumatic method

Branch xylem vulnerability curves based on the pneumatic method (Pereira et al., 2016) were obtained for 44 samples from 35 experimental trees (Table 3.1) using the Pneumatron, a device that combines a microcontroller-activated vacuum pump and a pressure transducer to allow for automated measurements of air discharge (Pereira et al., 2020; Jansen et al., 2020). The reservoir pressure was tracked with the Pneumatron in 0.5 sec intervals over a span of two minutes per measurement (including a pump time of approximately 2 sec in semi-automated mode and few milliseconds in automated mode).

The amount of air discharged (AD) into the reservoir was calculated based on the ideal gas law (Pereira et al., 2016). The semi-automated mode of the Pneumatron was used to measure AD for the samples obtained from Veitshöchheim and Würzburg, whereas the additional branch samples

of *T. cordata* and *T. platyphyllos* processed in Ulm were measured in automated mode. After each AD measurement, the xylem water potential was measured (see below). The maximum detectable amount of AD is associated with a change of pressure in the system by ~50 kPa (Pereira et al., 2020). As the time necessary for a pressure change of 50 kPa depends on the ratio between the reservoir volume (including the cut-open conduit volume) and the volume of gas extracted from intact, embolised conduits, the choice of the optimal reservoir volume is crucial (cf. Pereira et al., 2020).

For this study, reservoir volumes of 1.7 – 3.3 ml were selected based on the available information about the species' embolism resistance from the xylem functional traits database (Choat et al., 2012), assuming that higher embolism resistance corresponds to a lower volume of gas extracted from intact, embolised conduits and hence a lower optimal reservoir volume and vice-versa. Meanwhile, however, Pereira et al. (2020), recommend determining the maximum reservoir volume from a completely dried branch per species. Throughout the measurements, the volume of the vacuum reservoir was kept constant for each branch. Once the branch was fully hydrated, a clean cut was made in air at the basipetal end using a sharp razor blade to clear obstructions for air flow (Pereira et al., 2016; Jansen et al., 2020). Although this seems counterintuitive at first glance, cutting in air was done intentionally because the cut-open conduits need to be embolised when starting pneumatic measurements.

The branch was then connected to the pneumatic apparatus using rigid and elastic tubing, plastic clamps and three-way stopcocks (Fig. S1, S2). The volume of the elastic tube was kept as small as possible to minimize pressure-dependent changes in reservoir volume. The elastic tubing was tightened with a plastic clamp to ensure no leakage occurred during the measurement (Bittencourt et al., 2018). Before each series of measurements and in case of suspicious increases in the amount of AD, the connections and the plant material were thoroughly inspected to identify and seal potential air-entry points.

Before AD measurements were taken, the branch samples were bagged in dark plastic bags to equilibrate water potential. During AD measurement, the branches were kept bagged to minimize transpiration. Between measurements, the branches were dehydrated at room temperature on a laboratory bench to induce embolism (Sperry et al., 1988). The branches were initially dried for intervals of about 15 – 30 min, which were subsequently increased to 1 – 4 h depending on how quickly the sample dried. To allow xylem water potential to equilibrate after each drying interval, the samples were bagged for about 30 min in the initial steps of dehydration and for at least one hour in the later stages to account for the decrease in the leaf- stem conductance (cf. Pereira et al., 2016). The AD measurements were made on multiple branches on the same day (see Fig. S1 – S3). The elastic tubing was always kept connected to the branch samples when switching branches to keep the reservoir volume constant throughout all measurements. The AD measurements were taken until the branches were completely dehydrated and no considerable variation was observed in the amount of AD in consecutive measurements over at least 24 h, or until the maximum absolute xylem water potential measurable with the Scholander pressure chamber (10 MPa) was reached. This resulted in measurement durations of 3 – 7 days as well as in 10 – 20 AD and leaf

water potential measurements per branch when following the semi-automated mode of the Pneumatron. The percentage of air discharged (PAD) was calculated as described by Pereira et al. (2016):

$$\boldsymbol{PAD_i = 100 * (AD_i - AD_{min}) / (AD_{max} - AD_{min})} \quad (1)$$

where AD_i is the amount of air discharged for measurement i, AD_{min} is the minimum amount of air discharged from the fully hydrated branch and AD_{max} is the maximum amount of air discharged from the branch when completely desiccated.

3.3.3. Xylem water potential measurement

For the 35 branch samples measured in semi-automated mode, the xylem pressure was measured with a Scholander pressure chamber (PMS Instruments, Corvallis, Oregon, USA) after every AD measurement. At each pressure step, two leaves were cut-off from the branch and xylem water potential was averaged over two pressure chamber measurements. When the petiole was too small for measurement in the pressure chamber, small terminal twigs were used. The cut was immediately sealed using an instant adhesive (Loctite 431) to prevent leakage during the subsequent AD measurements. For the nine branches of *T. cordata* and *T. platyphyllos* measured using the automated mode of a Pneumatron, a stem psychrometer (ICT International, Armidale NSW Australia) was installed at a distal part of the branch to record xylem pressures for every 15 min. To obtain pressure estimates for each point in time and to reduce the impact of measurement uncertainty in the psychrometric water potentials, the psychrometer measurements for each sample were smoothed with shape-constrained additive models using monotone decreasing P-splines based on R package `scam` v. 1.2-8 (Pya, 2020).

3.3.4. Measurement of vulnerability curves with the flow-centrifuge method

The flow-centrifuge technique (Cavitron; Cochard et al., 2005) was used as a reference method for comparing the agreement of xylem vulnerability curves based on hydraulic measurement methods with curves based on the Pneumatron. Flow-centrifuge measurements were performed for 49 samples from 36 trees with a Cavitron device built from a Sorval RC 5 series centrifuge with manual control of rotation speed and using the `Cavisoft` software (`Cavisoft` version 5.2.1, University of Bordeaux, Bordeaux, France). Samples were recut several times under water to a final length of 27.5 cm to release the tension in the xylem (Torres-Ruiz et al., 2015).
Subsequently, the non-flushed branch segments were inserted in a custom-made rotor after removing the bark at both ends. They were then spun using the principle of centrifugal force to

generate a negative pressure in the xylem segment while simultaneously measuring hydraulic conductance. Flow centrifuge measurements were performed with filtered (0.2 µm) and degassed demineralized water that was enriched with 10 mM KCl and 1 mM $CaCl_2$. Measurements began at xylem water potentials of around -0.8 MPa and were continued under increasingly negative xylem pressures until the percentage loss of hydraulic conductivity (PLC) reached at least 90%.

3.3.5. Statistical analysis

All data handling and statistical analyses were performed in `R` version 4.0.2 (`R` Core Team, 2020) in the framework of the `tidyverse` (Wickham et al., 2019). Both the vulnerability curves based on pneumatic and flow-centrifuge measurements were described with tree-level nonlinear regression models using the logistic function by Pammenter & Van der Willigen (1998). For the flow-centrifuge method, vulnerability curves were based on the raw conductivity measured by the Cavitron (cf. Ogle et al., 2009):

$$\boldsymbol{K_i = \text{Normal}\left(k_{sat}\left(1 - \frac{1}{1 + \exp\left(\frac{S_{50H}}{25}\,(\mathrm{P_i} - \mathrm{P_{50H}})\right)}\right), \sigma\right)} \quad (2)$$

where K_i and P_i are the measured hydraulic conductivity and xylem pressure for observation i, respectively, k_{sat} is the hydraulic conductivity under fully saturated conditions and S_{50H} is the slope at 50% loss of conductivity (P_{50H}). For the pneumatic measurements, analogous models were constructed based on PAD for estimating P_{50P} (Eq. 1):

$$\boldsymbol{PAD_i = \text{Normal}\left(\frac{100}{1 + \exp\left(\frac{S_{50P}}{25}\,(\mathrm{P_i} - \mathrm{P_{50P}})\right)}, \sigma\right)} \quad (3)$$

To evaluate the effect of the air-discharge time on the accuracy of the estimates of vulnerability curve parameters, separate pneumatic vulnerability curves were fit on PAD calculated for all measurement durations between the initial pressure immediately after pumping and variable final pressures in 0.5 sec intervals, from 4.5 to 115 sec. The P_{12} and P_{88} (xylem pressure at 12% and 88% loss of conductivity, respectively) were calculated from the estimated model parameters (P_{50} and the corresponding slope at this pressure) by rearranging the model equation (Eqs. 2 & 3) and with confidence intervals based on parametric bootstrap (n = 10,000). The uncertainty in VC parameters was taken into account for the calculation of species averages of VC parameters and

their standard errors by using inverse-variance weighting analogous to a fixed-effects meta-analytical model (cf. Rosenberg et al., 2013).

We subsequently calculated a set of statistics that describe the degree of agreement of the Pneumatron parameter estimates with the flow-centrifuge based values in terms of systematic deviations, random deviations and overall agreement. For the Pneumatron measurements from *Tilia japonica*, *T. cordata* and *T. platyphyllos*, these calculations were based on tree averages of the flow-centrifuge parameters when replicate measurements were performed per tree (Tab. 1).

Systematic deviations between Pneumatron and flow-centrifuge based VC parameter estimates were quantified by the mean signed deviation (MSD). The MSD only measures additive bias between the parameter estimates obtained by the pneumatic and flow-centrifuge methods (θP and θH, respectively) and does not penalize scatter in the relationship.

$$\mathbf{MSD} = \frac{\mathbf{1}}{\boldsymbol{n}}\sum(\boldsymbol{\theta_P} - \boldsymbol{\theta_H}) \tag{5}$$

Random deviations between the estimates of both methods were evaluated by the Pearson correlation ρ between θP and θH. The correlation coefficient only penalizes the degree of scatter around a hypothetical line through θP and θH and does not include information about systematic differences.

$$\boldsymbol{\rho} = \frac{\mathbf{cov}(\boldsymbol{\theta_P}, \boldsymbol{\theta_H})}{\mathbf{SD}(\boldsymbol{\theta_p})\,\mathbf{SD}(\boldsymbol{\theta_H})} \tag{4}$$

The overall agreement of the parameter estimates was evaluated by the root mean square deviation (RMSD). Unlike the aforementioned metrics, the RMSD penalizes both systematic and random deviations between θP and θH.

$$\mathbf{RMSD} = \sqrt{\frac{\mathbf{1}}{\boldsymbol{n}}\sum(\boldsymbol{\theta_P} - \boldsymbol{\theta_H})^{\mathbf{2}}} \tag{6}$$

In addition, as a pragmatic measure to quantify the overall match of the flow-centrifuge and pneumatic vulnerability curves over their entire range, we calculated the L_2 distance (cf. Cramér, 1928) between each pair of flow-centrifuge and pneumatic vulnerability curves

$$\boldsymbol{L_2} = \left(\int_{-\infty}^{\infty} \left(\boldsymbol{PLC_H(P)} - \boldsymbol{PLC_P(P)}\right)^{\mathbf{2}}\,\mathbf{dP}\right)^{\mathbf{1/2}} \tag{7}$$

This quantity describes the degree of similarity of the two vulnerability curves and approaches zero for identical curves.

In addition to the comparison of metrics describing the agreement between estimates, we used linear mixed effects models based on R package `lme4` version 1.1-23 (Bates et al., 2015) to test for statistically significant differences between the Cavitron-based estimates of P_{12}, P_{50}, P_{88} and (natural log-transformed) S_{50} and their Pneumatron-based equivalents for AD intervals of 15, 30, 60, 90 and 115 sec from the initial pressure at 4 sec. Each model was fit to each parameter using restricted maximum likelihood with "method" as a fixed effect and random intercepts for species and individual trees nested in species. The flow-centrifuge was considered as baseline and contrasted with each one term for the Pneumatron estimates in five different intervals. Model assumptions were checked by residual diagnostic plots. Inference was based on Wald *t*-tests with Sattherthwaite's approximation to the degrees of freedom using R package `lmerTest` version 3.1-2 (Kuznetsova et al., 2017).

3.4. Results

3.4.1. Estimated vulnerability curves

The average P_{50H} estimates obtained from the flow-centrifuge method covered a wide range of embolism resistance from -1.85 MPa to -6.02 MPa for *Platanus* × *acerifolia* and *Crataegus persimilis*, respectively. Parameters estimated with the pneumatic method largely fell into the same range (cf. Table S1). In general, there was a good agreement in overall shape between the flow-centrifuge and pneumatic vulnerability curves (VCs) for most of the species studied.

However, the estimates in P_{12P}, P_{50P} and P_{88P} for *T. cordata* and *T. platyphyllos* based on the pneumatic method were on average at least 0.5 MPa higher than the corresponding estimates of the flow-centrifuge method when their xylem pressure was measured using a pressure chamber (Table S1). Additional measurements performed to explain this discrepancy showed that embolism resistance was largely within a comparable range when xylem pressure was determined by stem psychrometers (with the exception of P_{88P} for *T. cordata*; Table S1; Fig. S4). As there were reasons to assume that the differences observed were caused by inaccurate xylem water potential measurements with the pressure chamber, results for the best AD measurement intervals are based only on the observations with xylem pressure measurements based on stem psychrometers.

3.4.2. Overall agreement between methods

The parameters of the vulnerability curves estimated with the two methods were generally highly correlated, with Pearson correlations above 0.54 for all parameters and over 0.74 for P_{12}, P_{50} and P_{88} for all AD times considered in Table S2 and all 12 tree species (Table S2). In particular, this

was true for the P_{50} estimates, where correlations exceeded 0.95 in all cases. Moreover, the P_{50} estimates of the two methods were very close to the 1:1 line (cf. Fig. 3.2 b, Table S2). The Pneumatron-based estimates of the slope of the vulnerability curve, however, on average showed a negative systematic deviation that ranged from −25.5% (retransformed from log scale, 15 sec AD time) to −28.1% (115 sec AD time; cf. Fig. 3.1, 2d; Table S2). The deviation was notably larger in samples with lower slopes and was not observed for the samples measured with stem psychrometers (Fig. 3.2). Due to the direct relationship between slope and P_{50}, the systematically lower slope estimates translated to a higher P_{12P} (by up to 0.77 MPa on average at 115 sec AD time) and, in some cases, a lower P_{88P} (by up to −0.26 MPa on average at 15 sec AD time; Fig. 3.2, Table S2).

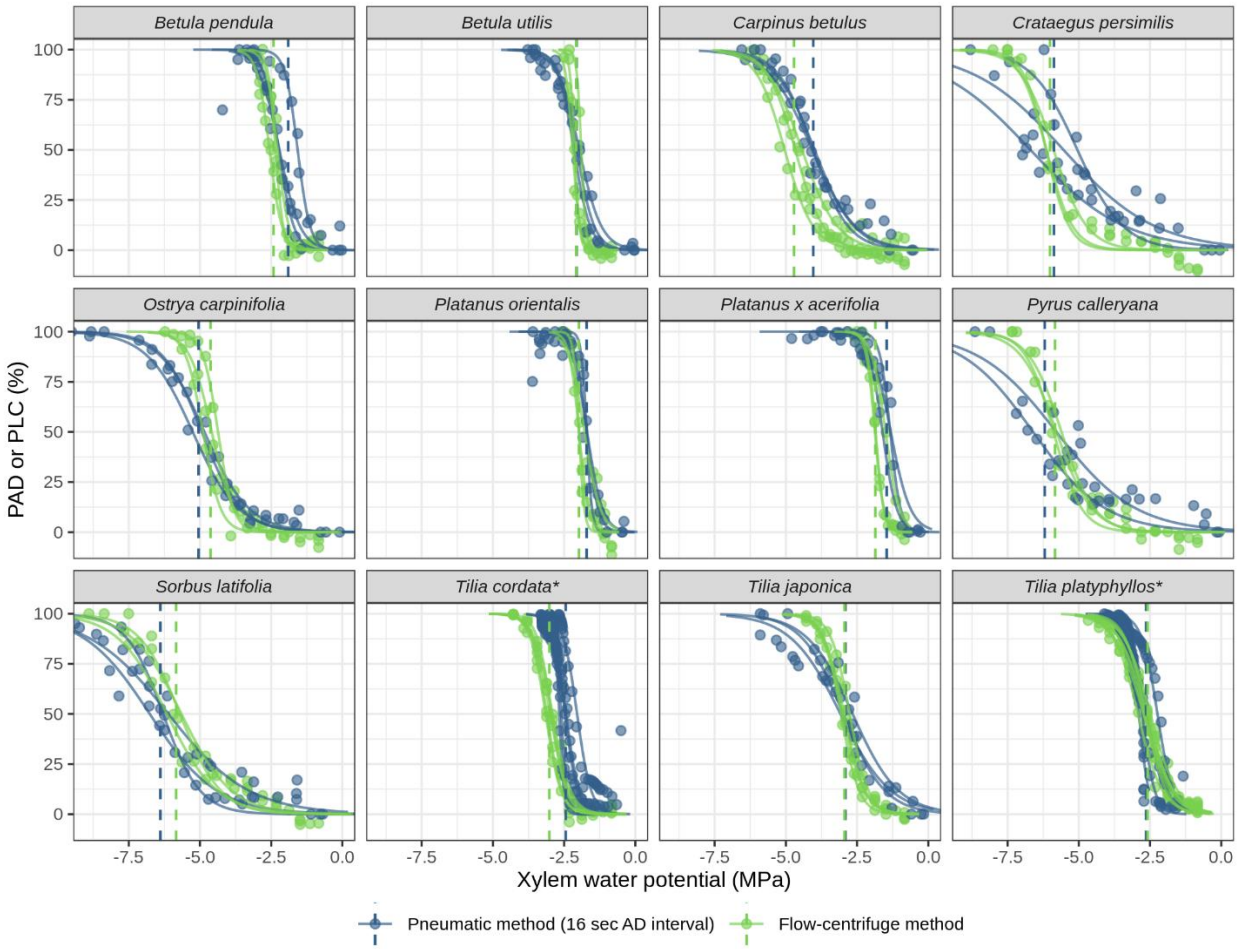

Figure 3.1: Xylem vulnerability curves obtained with the pneumatic method after a measurement duration of 15 sec (green) and the flow-centrifuge method (blue) for 12 diffuse-porous tree species. Circles: observed values (for the centrifuge data, rescaled from conductance to PLC using the estimated k_{sat}); solid lines: predicted PLC/PAD; dashed lines: estimated P_{50}. Asterisks (*) at the end of species names indicate xylem pressure measurements with stem psychrometers.

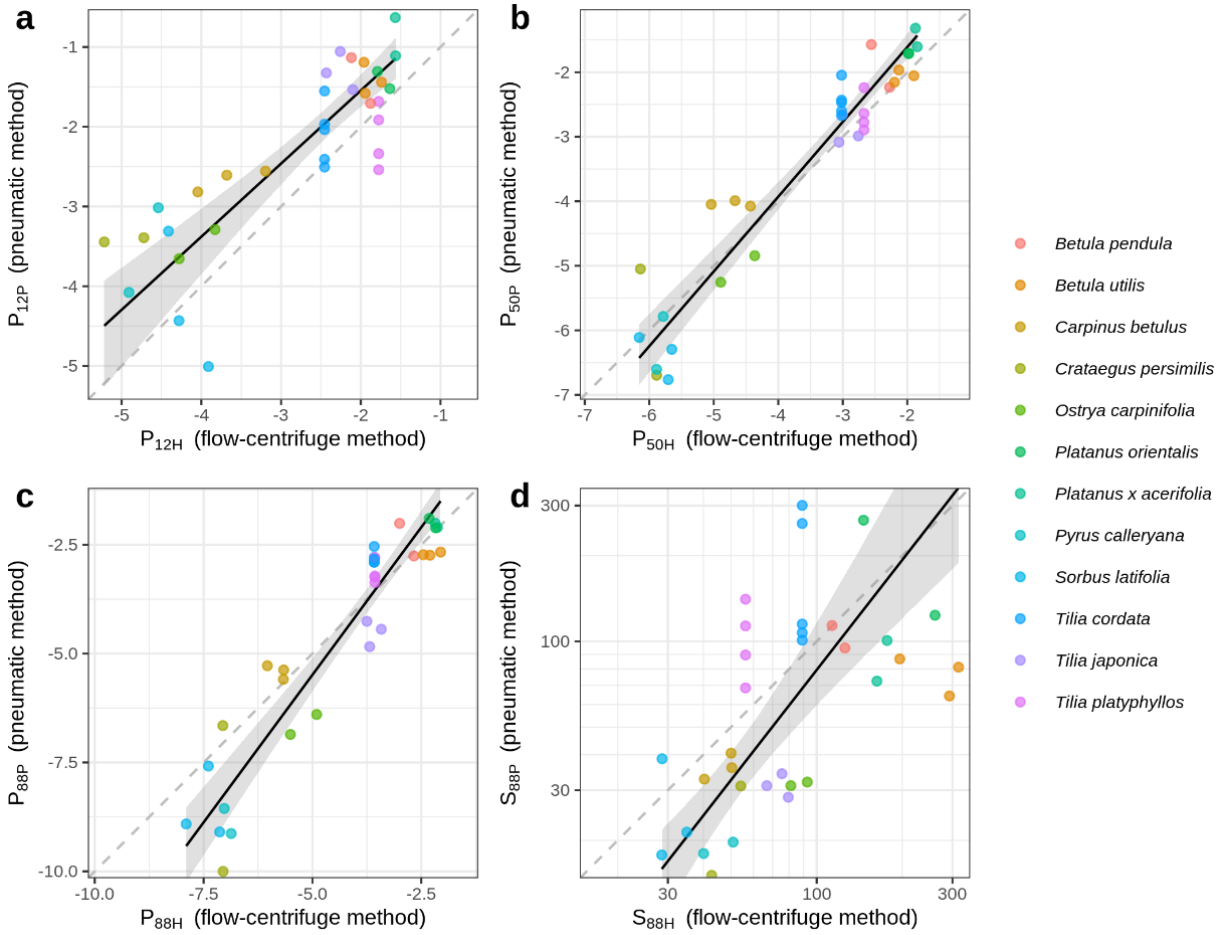

Figure 3.2: Relationship between estimates from the flow-centrifuge method (x-axis) and the pneumatic method with 15 sec air discharge interval (y-axis). a) P_{12}, b) P_{50}, c) P_{88} (xylem water potentials at 12%, 50% and 88%, respectively) and d) slope at 50% loss of conductivity (displayed on a log scale). Colours – species identity (empty circles indicate pressure chamber-based *Tilia* measurements); solid black line – standardized major axis (SMA) regression fit through all points ± 95% bootstrap confidence interval; grey dashed line: 1:1 line.

3.4.3. Influence of discharge time

The pneumatic estimates of all VC parameters were sensitive to the chosen discharge time (Table 3.2, S2, Fig. 3.3, 3.4, 3.5). However, the change in agreement with air discharge time was neither consistent between parameters nor between species (Table S2, Fig. 3.4, 3.5). Consequently, the discharge interval associated with the lowest deviation between flow-centrifuge and pneumatic estimates of P_{50} (Fig. 3.3) and other parameters differed largely between species, with an increasing deviation with discharge time for some species (*Betula, Carpinus, Crataegus* and *Tilia*) and a decreasing deviation for others (*Ostrya, Platanus, Pyrus* and *Sorbus*). After accounting for random variation between species and

trees, significant systematic differences between the reference value based on the flow-centrifuge method and the pneumatic method at all analysed AD times remained for all parameters, with the exception of P_{88} (Table 2).

Table 3.2: Parameter estimates of the linear mixed effect models for the xylem water potential at 12%, 50% and 88% loss of conductivity (P_{12}, P_{50} and P_{88}, respectively) and the natural log-transformed slope at 50% loss of conductivity (S_{50}). Given are estimates for the intercept (average for flow-centrifuge based reference value) as well as the differences from the reference for different AD times, with the corresponding standard errors, *t*-statistics, approximate degrees of freedom based on the Satterthwaite approximation and corresponding *P*-values.

Parameter	Treatment	Estimate	Std.error	*t*-statistic	edf	*P*-value
P_{12}	(Intercept)	-2.802	0.308	-9.104	11.3320	< 0.001
	Δ 16 s	0.498	0.077	6.435	189.23	< 0.001
	Δ 30 s	0.564	0.077	7.279	189.23	< 0.001
	Δ 60 s	0.663	0.077	8.559	189.23	< 0.001
	Δ 90 s	0.734	0.077	9.472	189.23	< 0.001
	Δ 115 s	0.790	0.077	10.20	189.23	< 0.001
P_{50}	(Intercept)	-3.648	0.492	-7.411	11.0660	< 0.001
	Δ 16 s	0.125	0.050	2.504	195.53	0.013
	Δ 30 s	0.183	0.050	3.647	195.53	< 0.001
	Δ 60 s	0.258	0.050	5.152	195.53	< 0.001
	Δ 90 s	0.304	0.050	6.069	195.53	< 0.001
	Δ 115 s	0.331	0.050	6.608	195.53	< 0.001
P_{88}	(Intercept)	-4.486	0.694	-6.465	11.1020	< 0.001
	Δ 16 s	-0.247	0.09	-2.736	193.5	0.007
	Δ 30 s	-0.198	0.09	-2.192	193.5	0.030
	Δ 60 s	-0.146	0.09	-1.619	193.5	0.107
	Δ 90 s	-0.125	0.09	-1.386	193.5	0.167
	Δ 115 s	-0.127	0.09	-1.41	193.5	0.160
S_{50}	(Intercept)	4.278	0.193	22.20	11.9130	< 0.001
	Δ 16 s	-0.277	0.068	-4.08	194.68	< 0.001
	Δ 30 s	-0.287	0.068	-4.228	194.68	< 0.001
	Δ 60 s	-0.307	0.068	-4.528	194.68	< 0.001
	Δ 90 s	-0.324	0.068	-4.775	194.68	< 0.001
	Δ 115 s	-0.347	0.068	-5.11	194.68	< 0.001

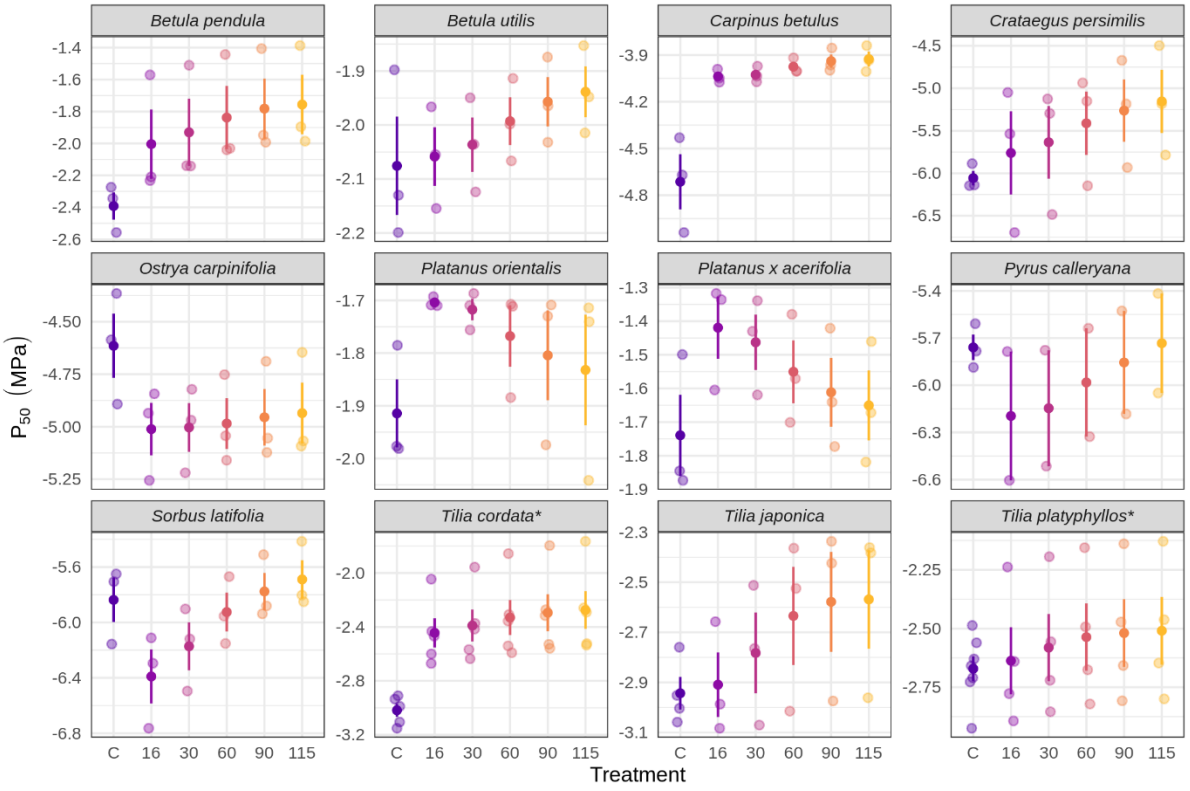

Figure 3.3: Comparison of P_{50} values between the flow-centrifuge and different air discharge intervals for the pneumatic method (compared on the same branch). C indicates the P_{50} values from the flow-centrifuge method, 15, 30, 60, 90 and 115 indicate AD measurement intervals (in seconds) evaluated from the pneumatic method. Shown are the raw estimates overlaid with their mean ± SE. Asterisks (*) at the end of species name indicate xylem pressure was determined using stem psychrometer.

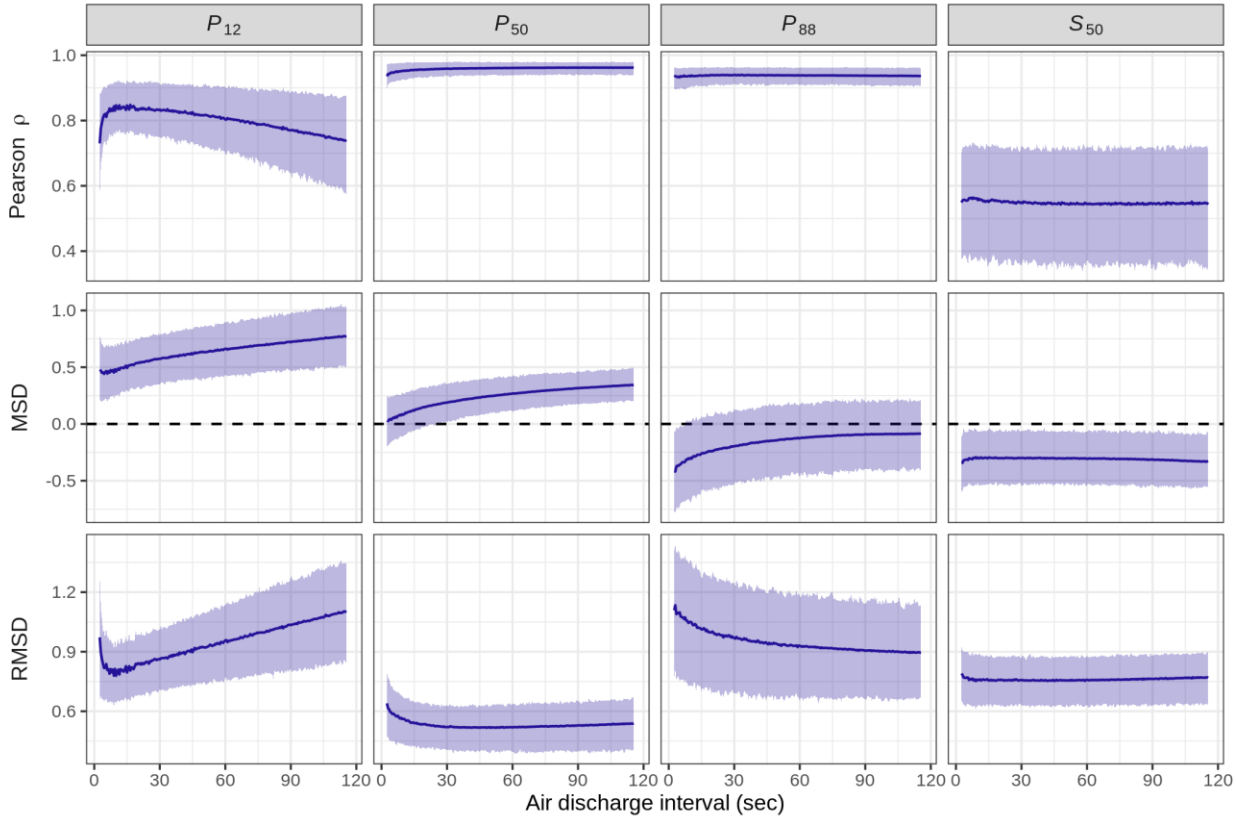

Figure 3.4: Statistics describing the agreement between the estimated vulnerability curve parameters from the pneumatic method and the flow-centrifuge method vs. the duration of air discharge measurement (estimates ± 95% bootstrap confidence intervals based on 1,000 bootstrap draws). The metrics shown are the Pearson correlation (Pearson ρ) as a measure of random deviation between the two methods (values close to one indicate a perfect linear relationship), mean signed deviation (MSD) as a measure of systematic deviations (values close to zero indicate a low bias) and root mean square deviation (RMSD) as a measure of overall agreement (low values indicate a high agreement between methods).

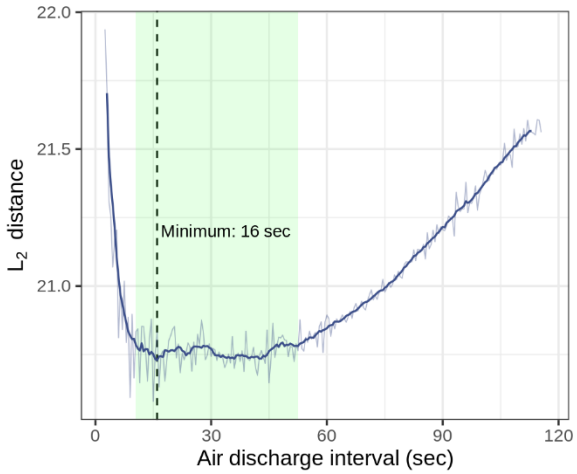

Figure 3.5: Average L_2 distance between the pneumatic and flow-centrifuge vulnerability curves vs. air discharge time as a measure of overall accuracy (raw averages and ±5 s running average). Vertical lines indicate the minimum of the running average at 16 sec; the shaded area indicates the range with a running average differing from the minimum by less than 1% (10.5 – 44.5 sec).

The response of the pneumatic estimates of the vulnerability curve parameters to AD time was not consistent between parameters (Fig. 3.4). Depending on the parameter, the overall agreement with the flow-centrifuge method was either highest at low AD times (P_{12}), remained relatively stable over a wide range of AD times (P_{50}, S_{50}) or increased continuously with increasing AD time (P_{88}; cf. Fig. 3.4). In any case, the L_2 distance (which describes the overall match of the curves over their entire range instead of focusing on a point estimate) was lowest at relatively low AD times with a minimum at 16 sec and a relatively broad range of equivalent values from 10.5 to 44.5 sec (Fig. 5). This indicates that the lowest degree of dissimilarity between the curves corresponded to AD times in this range, which moreover was associated with the lowest systematic differences in P_{50}estimates (Table 3.2, S2; Fig. 3.4).

3.5. Discussion

In agreement with previous assessments of the pneumatic method for vulnerability curve(VC) measurements (Pereira et al., 2016, 2020; Zhang et al., 2018; Sergent et al., 2020), we find that the estimated water potential at 50% of discharged air volume (P_{50P}) coincide well with the water potential at 50% loss of conductance (P_{50H}) measured with the flow-centrifuge method for the 12 diffuse-porous temperate tree species studied, with low systematic and random deviations and a high overall agreement (MSD = +0.117 MPa, $\rho\rho$= 0.956, RMSD = ±0.538MPa, respectively for 15 sec AD time, TableS2). However, we find evidence for a high variance and systematic differences in the estimates of the slope of the VC(Fig. 3.1), that were on average at least 25.5% (15 sec air discharge time, cf. Table S2) lower for the pneumatic method, which also resulted in a lower agreement in the estimates of P_{12P} and P_{88P}. Similar conclusions were found based on a pneumatic modelling approach (Yang et al., 2021) and based on experimental evidence by comparing the pneumatic and the optical method(Pereira et al., 2020; Guan et al.,2021). A mechanistic explanation for the difference in P_{12} and P_{88} values is provided by the open-xylem artefact, which suggests that embolism spreading could be enhanced by the proximity to gas under atmospheric pressure in the open-cut conduits (Guan et al., 2021). Moreover, our results demonstrate that the estimates obtained with the pneumatic method are sensitive to the choice of air discharge time (cf. Pereira et al., 2016, 2020), to which they respond in a nonlinear and species-specific manner. For the analysed set of species, the best overall match between the flow-centrifuge and pneumatic VCs could be achieved for air discharge times of around 15 sec (cf. Fig. 3.4), which experimentally confirms the ideal AD time identified by a modelling approach (Yang et al., 2021).

Moreover, our results demonstrate that the estimates obtained with the pneumatic method are sensitive to the choice of air discharge time (cf. Pereira et al., 2016, 2020), to which they respond in a nonlinear and species-specific manner. For the analysed set of species, the best overall match between the flow-centrifuge and pneumatic VCs could be achieved for air discharge times of around 15 sec (cf. Fig. 3.4), which experimentally confirms the ideal AD time identified by a modelling approach (Yang et al., 2021).

3.5.1. Agreement between flow-centrifuge and pneumatic vulnerability curves

The gradual loss of conductance and the increasing amount of gas extracted, which are quantified by the PLC and PAD, are necessarily positively associated as they share a common cause, namely embolism spreading under progressing dehydration. However, PAD quantifies the air volume inside embolised vessels, while PLC measures their contribution to the conductance of the branch. Thus, both arise from vessel properties that scale with different powers of their length and diameter (Pereira et al., 2016). While the volume of a vessel scales with the second power of diameter and is proportional to its length, its flow resistance (i.e., the inverse of its conductance) can be approximated by the sum of the resistance posed by its lumen and the resistance posed by the transition through pit membranes (Sperry et al., 2005; Wheeler et al., 2005). According to the

Hagen-Poseuille-equation, the flow resistance of the lumen scales with the inverse of the fourth power of its diameter and is proportional to its length. The flow resistance posed by the transition through pit membranes can be assumed to scale with the inverse of expected vessel length (Sperry et al., 2005). Due to these different scaling relationships, the association between PAD and PLC does not necessarily have to be linear. Observed systematic differences between the parameters of curves obtained with different methods (cf. Table 3.2) might therefore not be surprising and deserve further testing.

It should also be noted that an additional downward bias in the slope might be introduced by treating the unknown true minimum and maximum amount of air discharged (AD_{min} and AD_{max}, cf. Eq. 1) as fixed quantities measured without error. For hydraulic vulnerability curves, problems induced by treating maximum conductivity as fixed can be circumvented by treating the saturated hydraulic conductivity as a model parameter (k_{sat} in Eq. 2; Ogle et al., 2009; Duursma & Choat, 2017). Implementing a similar solution for the pneumatic method is not straightforward due to the common identifiability issues in sigmoidal models where the lower and upper bound are both treated as model parameters.

Given the direct mathematical relation between the model parameters, a bias in slope can be expected to result in a bias in P_{12} and/or P_{88}, which may be problematic in process-based vegetation modelling that use these VC parameters to describe drought resistance. Our results indicate that while the pneumatic method produces reliable estimates of the P_{50} for diffuse-porous tree species, the curves obtained might not always be interchangeable with curves constructed with the flow-centrifuge method.

3.5.2. Effect of the air discharge interval on measurement accuracy

The observed sensitivity of the pneumatic method to the AD interval provides experimental evidence that is in line with predictions by the Unit Pipe Pneumatic model (Yang et al., 2021). To understand the relationship between the AD interval and the amount of air discharged in that interval, it is necessary to focus on the underlying assumptions about the gas flow between sample and reservoir. One central assumption of the pneumatic method is that the amount of air discharged into the vacuum reservoir over a given time span is a function of the amount of air N inside embolised conduits at different points during the dehydration process (Jansen et al., 2020; Yang et al.,2021).

This assumption is necessary to be able to use PAD measurements to infer the degree of embolization. Further, if the PAD calculated over different AD times t is to result in identical vulnerability curves, the change in AD with time must have the same shape at different dehydration steps and only differ by a multiplicative constant proportional to the amount of air N in the xylem, i.e., $AD(t, N1) / N1 = AD(t, N2) / N2$ must hold. This assumption is likely only approximately met under typical measurement conditions. During the drying process, the xylem undergoes

substantial changes that may affect the shape of AD (*t*, *N*), such as an increase in gas conductivity with progressing embolism.

Moreover, it is possible that embolised conduits that were not disconnected from to the cut surface at earlier drying steps subsequently become connected to the network of open vessels connecting to the vacuum reservoir (Pereira et al. 2016). In such cases, the amount of air in these spaces would not be included in the earlier estimates. For these reasons, the relationship between the AD measured in different desiccation steps after a certain discharge interval and the total amount of air within the xylem at those points in time is likely empirical. This may explain the pronounced species differences in the response to AD time (Table S2, 4, Fig. 3.3) and contribute to the previously reported differences in accuracy for species with different types of wood anatomy (e.g., Zhang et al., 2018).

While the effect of AD time depended on species identity and was different for different parameters, Fig. 3.4 indicates that overall mismatch between flow-centrifuge and pneumatic VCs could be minimized by choosing low AD times of ca.16 sec. In our setting, this might be a consequence of small amounts of air-entry into the xylem where the branch is damaged, which– unlike the other discussed factors influencing AD – will have an effect that accumulates with discharge time. Thus, the net gains in accuracy due to integrating over a larger time interval are overcompensated by the increasing contribution of potential leakage to the total AD. Interestingly, the higher agreement with hydraulic reference values at lower AD times contrasts with the higher accuracy for longer AD times reported in earlier works using the manual pneumatic method (cf. Fig. S3 in Pereira et al. 2016). Most likely, this difference results from the higher temporal resolution and more accurate AD time measurement enabled by the automated Pneumatron device (Pereira et al. 2020). When using a Pneumatron, the choice of short AD times therefore is a pragmatic way to improve the accuracy of the pneumatic method.

3.5.3. Species-specific drying behaviour

As noted previously (Zhang et al., 2018; Sergent et al., 2020), the degree of similarity between VCs measured with the pneumatic method and hydraulic reference methods differs between species. In this study, we observed a mismatch for *T. cordata* and *T. platyphyllos* when xylem pressure was expressed based on leaf water potentials measured with a pressure chamber However, the difference largely disappeared when a stem psychrometer was used to determine xylem pressure (Fig. 3.1, S4).

Possible explanations for the observed differences are the presence of abundant mucilage in the xylem tissues of *Tilia* species (Franz & Kram, 1985; Pigott et al., 2012), which has been reported to affect xylem pressures measured with the pressure chamber technique (Zimmermann et al., 2002). Furthermore, it could be speculated that the truncated shape of the pressure-chamber based Pneumatron VCs for the *Tilia* species (especially *T. cordata*, cf. Fig. S4) and the fact they never reached water potentials substantially more negative than -3 MPa, indicates that the measurements

were terminated before the stems of the specimens were fully dehydrated. This results in underestimated values for *AD*max, thus shifting the curve towards less negative water potentials. As detailed before, the desiccation was continued until a near constancy in the measured *AD* values over at least 24 h was reached. This criterion to finish *AD* measurements may not be ideal, as the drying process may slow down notably after full stomatal closure, which especially for isohydric species may happen in a relatively well-hydrated state.

Notably, while *Tilia* species have often been considered to be relatively anisohydric (cf. Leuzinger et al., 2005; Galiano et al., 2017; Kiorapostolou et al., 2018; but see Niinemets et al., 1999), recent work by Leuschner et al. (2019) indicates that at least *T. cordata* has a fairly stringent, more isohydric stomatal control mechanism. Due to the anticipated hydraulic segmentation between leaf petioles and stem xylem in drought-avoiding and more isohydric species (Hartmann et al., 2021), this may have contributed to the mismatch between flow-centrifuge and pneumatic VCs. It is well documented that certain species rely on early drought-induced leaf shedding (Wolfe et al., 2016; Hochberg et al., 2017), most likely caused by a pronounced hydraulic segmentation (cf. Pivovaroff et al., 2016; Zhu et al., 2016; Klepsch et al., 2018). As these processes decouple leaf and branch water potentials, measuring leaf water potential with a Scholander pressure chamber may result in extreme water potential readings that do not reflect the actual status in the xylem. Conversely, the slowdown of dehydration induced by leaf shedding may result in prematurely terminated measurements when measuring

branch water potentials with e.g., a stem psychrometer, or when determining the end of the dehydration process based on the state of the leaves. As a cautionary example, the leaves of *C. persimilis* were almost fully dehydrated on the third day of measurements, while the branch water potential values continued to decline for seven days. Similar behaviour was reported by Wolfe et al. (2016) for the tropical species *Genipa americana*.

Due to these species-specific differences in drying behaviour, the stability of *AD*max can have a strong influence on the shape of the vulnerability curves because all pneumatic *PAD* values are normalized against *AD*min and *AD*max. It may therefore be advantageous to continue the drying process until the constancy of *AD*max has been confirmed based on several measurements to avoid bias resulting from underestimating *AD*max. An important corollary of the observed problems associated with water potential measurements is that the same kind of bias in water potential may also affect hydraulic VC measurements in other methods that rely on bench dehydration.

3.5.4. Implications for future vulnerability curve method comparisons

An important limitation that affects all evaluation studies of VC methods – as well as most other measurement methods in biology – is the lack of true reference values for VC parameters. While in this study, we used measurements with the flow-centrifuge method as a reference, there are many indications that this method may be affected by measurement artefacts that arise during sample excision (Wheeler et al., 2013) and preparation (Torres-Ruiz et al., 2015) or as a result

from vessel lengths exceeding the sample dimensions (Choat et al., 2010; Martin-StPaul et al., 2014; Torres-Ruiz et al., 2014). A mismatch between curves obtained with the pneumatic method and the flow-centrifuge method may thus in part also be attributed to the imperfections of the latter. While there is hardly a way to overcome the limitation of imperfect reference values, we argue that methodological comparisons of VC methods may benefit from adopting a more principled approach of quantifying the agreement between different methods in terms of different components of accuracy (cf. Fuchs et al., 2017; Flo et al., 2019). To our knowledge, none of the previously published methodological comparisons (see e.g., Li et al., 2008; Choat et al., 2010; Hacke et al., 2015; Brodribb et al., 2017; López et al., 2019; Venturas et al., 2019; Chen et al., 2021; Pratt et al., 2020; Sergent et al., 2020; Zhao et al., 2020) formally differentiate between systematic and random differences in parameter estimates and none provide metrics that quantify the similarity over the entire curves. While our choice of the L2-distance as a measure of overall agreement between curves is relatively arbitrary and there are many equally appropriate distance metrics, it is most definitely an improvement compared to the common practice of comparing methods by the Pearson correlation between parameter estimates, as the latter only penalizes deviations from a bivariate linear relationship while being insensitive to systematic deviations. We hope that our framework can serve as a starting point for more formal VC method comparisons based on rigorous metrological principles and theory.

3.6. Conclusion

Our data indicate a high degree of agreement between the P_{50P} estimated with the pneumatic method and the P_{50H} estimated with the flow-centrifuge method for the analysed diffuse-porous temperate tree species, especially when using short air discharge times of around 15 sec. The relatively low effort required to construct a curve with this method and its high degree of automation when using a Pneumatron device in conjunction with a stem psychrometer allow for a high throughput. The method is therefore attractive in descriptive or predictive contexts where the main purpose is to generate a good proxy for plant drought resistance. However, the observed systematic deviation in slope estimates as well as potential artefacts associated with xylem water potential determination and species-specific drying behaviour deserve further attention.

Acknowledgements

We thank Klaus Körber and Andreas Lösch from the Bavarian state institute for viticulture and horticulture (Bayerische Landesanstalt für Wein- und Gartenbau, LWG) for granting access to their research facility at Stutel and Xinyi Guan for her support with the automated pneumatic measurements. P.R.L.B. acknowledges Royal Society's Newton International for its Fellowship (NF170370). S.J. acknowledges funding from the German Research Foundation (Deutsche Forschungsgemeinschaft, DFG, project nr. 410768178).

References

Adams HD, Zeppel MJB, Anderegg WRL, Hartmann H, Landhäusser SM, Tissue DT, Huxman TE, Hudson PJ, Franz TE, Allen CD, et al. 2017. A multi-species synthesis of physiological mechanisms in drought-induced tree mortality. Nature Ecology & Evolution 1: 1285–1291.

Allen CD, Breshears DD, McDowell NG. 2015. On underestimation of global vulnerability to tree mortality and forest die-off from hotter drought in the Anthropocene. Ecosphere 6: art129.

Allen CD, Macalady AK, Chenchouni H, Bachelet D, McDowell N, Vennetier M, Kitzberger T, Rigling A, Breshears DD, Hogg EH (Ted), et al. 2010. A global overview of drought and heat-induced tree mortality reveals emerging climate change risks for forests. Forest Ecology and Management 259: 660–684.

Anderegg WRL, Klein T, Bartlett M, Sack L, Pellegrini AFA, Choat B, Jansen S. 2016. Meta-analysis reveals that hydraulic traits explain cross-species patterns of drought-induced tree mortality across the globe. Proceedings of the National Academy of Sciences 113: 5024–5029.

Bates D, Mächler M, Bolker B, Walker S. 2015a. Fitting linear mixed-effects models using lme4. Journal of Statistical Software 67: 1–48.

Bittencourt PRL, Pereira L, Oliveira RS. 2018. Pneumatic Method to Measure Plant Xylem Embolism. Bio-Protocol 8.

Blackman CJ, Gleason SM, Chang Y, Cook AM, Laws C, Westoby M. 2014. Leaf hydraulic vulnerability to drought is linked to site water availability across a broad range of species and climates. Annals of Botany 114: 435–440.

Brando PM, Paolucci L, Ummenhofer CC, Ordway EM, Hartmann H, Cattau ME, Rattis L, Medjibe V, Coe MT, Balch J. 2019. Droughts, Wildfires and Forest Carbon Cycling: A Pantropical Synthesis. Annual Review of Earth and Planetary Sciences 47: 555–581.

Brodersen CR, McElrone AJ, Choat B, Matthews MA, Shackel KA. 2010. The Dynamics of Embolism Repair in Xylem: In Vivo Visualizations Using High-Resolution Computed Tomography. Plant Physiology 154: 1088–1095.

Brodribb TJ, Skelton RP, McAdam SA, Bienaimé D, Lucani CJ, Marmottant P. 2016. Visual quantification of embolism reveals leaf vulnerability to hydraulic failure. New Phytologist 209: 1403–1409.

Brodribb TJ, Carriqui M, Delzon S, Lucani C. 2017. Optical Measurement of Stem Xylem Vulnerability. Plant Physiology 174: 2054–2061.

Brodribb TJ, Cochard H. 2009. Hydraulic Failure Defines the Recovery and Point of Death in Water-Stressed Conifers. Plant Physiology 149: 575–584.

Brodribb TJ, Powers J, Cochard H, Choat B. 2020. Hanging by a thread? Forests and drought. Science 368: 261–266.

Cai J, Tyree MT. 2010. The Impact of Vessel Size on Vulnerability Curves: Data and Models for Within-Species Variability in Saplings of Aspen, Populus tremuloides Michx. Plant, Cell & Environment.

Chen Y, Maenpuen P, Zhang Y, Barai K, Katabuchi M, Gao H, Kaewkamol S, Tao L, Zhang J. 2020. Quantifying vulnerability to embolism in tropical trees and lianas using five methods: can discrepancies be explained by xylem structural traits? New Phytologist: nph.16927.

Choat B, Brodribb TJ, Brodersen CR, Duursma RA, López R, Medlyn BE. 2018. Triggers of tree mortality under drought. Nature 558: 531–539.

Choat B, Drayton WM, Brodersen C, Matthews MA, Shackel KA, Wada H, Mcelrone AJ. 2010. Measurement of vulnerability to water stress-induced cavitation in grapevine: a comparison of four techniques applied to a long-vesseled species: Comparison of vulnerability curve technique in grapevine. Plant, Cell & Environment.

Choat B, Jansen S, Brodribb TJ, Cochard H, Delzon S, Bhaskar R, Bucci SJ, Feild TS, Gleason SM, Hacke UG, et al. 2012. Global convergence in the vulnerability of forests to drought. Nature 491: 752–755.

Christoffersen BO, Gloor M, Fauset S, Fyllas NM, Galbraith DR, Baker R, Kruijt B, Rowland L, Fisher RA, Binks OJ, et al. 2016. Linking hydraulic traits to tropical forest function in a size-structured and trait-driven model (TFS v.1-Hydro). Geosci. Model Dev.: 30.

Cochard H, Cruiziat P, Tyree MT. 1992. Use of Positive Pressures to Establish Vulnerability Curves 1. Plant Physiology 100: 205–209.

Cochard H, Badel E, Herbette S, Delzon S, Choat B, Jansen S. 2013. Methods for measuring plant vulnerability to cavitation: a critical review. Journal of Experimental Botany 64: 4779–4791.

Cochard H, Damour G, Bodet C, Tharwat I, Poirier M, Améglio T. 2005. Evaluation of a new centrifuge technique for rapid generation of xylem vulnerability curves. Physiologia Plantarum 124: 410–418.

Correia DLP, Bouchard M, Filotas É, Raulier F. 2019. Disentangling the effect of drought on stand mortality and productivity in northern temperate and boreal forests. Journal of Applied Ecology 56: 758–768.

Cramér H. 1928. On the composition of elementary errors. II Statistical applications. Skandinavisk Aktuarietidskrift 11: 141–180.

Davi H, Cailleret M. 2017. Assessing drought-driven mortality trees with physiological process-based models. Agricultural and Forest Meteorology 232: 279–290.

Delzon S, Cochard H. 2014. Recent advances in tree hydraulics highlight the ecological significance of the hydraulic safety margin. New Phytologist 203: 355–358.

Domec J-C, Schafer K, Oren R, Kim HS, McCarthy HR. 2010. Variable conductivity and embolism in roots and branches of four contrasting tree species and their impacts on whole-plant hydraulic performance under future atmospheric CO2 concentration. Tree Physiology 30: 1001–1015.

Duursma RA, Choat B. 2017. fitplc : an R package to fit hydraulic vulnerability curves. Journal of Plant Hydraulics.

Field CB, Barros V, Stocker TF, Dahe Q (Eds.). 2012. Managing the Risks of Extreme Events and Disasters to Advance Climate Change Adaptation: Special Report of the Intergovernmental Panel on Climate Change. Cambridge: Cambridge University Press.

Flo V, Martinez-Vilalta J, Steppe K, Schuldt B, Poyatos R. 2019. A synthesis of bias and uncertainty in sap flow methods. Agricultural and Forest Meteorology 271: 362–374.

Franz G, Kram G. 1985. Structural investigations on the watersoluble polysaccharides of lime tree flowers. Die Pharmazie 41: 501.

Fuchs S, Leuschner C, Link R, Coners H, Schuldt B. 2017. Calibration and comparison of thermal dissipation, heat ratio and heat field deformation sap flow probes for diffuse-porous trees. *Agricultural and Forest Meteorology* 244–245: 151–161.

Galiano L, Timofeeva G, Saurer M, Siegwolf R, Martínez-Vilalta J, Hommel R, Gessler A. 2017. The fate of recently fixed carbon after drought release: towards unravelling C storage regulation in Tilia platyphyllos and Pinus sylvestris. Plant, Cell & Environment 40: 1711–1724.

Hacke UG, Venturas MD, MacKinnon ED, Jacobsen AL, Sperry JS, Pratt RB. 2015. The standard centrifuge method accurately measures vulnerability curves of long-vesselled olive stems. New Phytologist 205: 116–127.

Hajek P, Leuschner C, Hertel D, Delzon S, Schuldt B. 2014. Trade-offs between xylem hydraulic properties, wood anatomy and yield in Populus. Tree Physiology 34: 744–756.

Hartmann H, Link RM, Schuldt B. 2021. A whole-plant perspective of isohydry: stem-level support for leaf-level plant water regulation. *Tree Physiology*, accepted.

Hochberg U, Windt CW, Ponomarenko A, Zhang Y-J, Gersony J, Rockwell FE, Holbrook NM. 2017. Stomatal Closure, Basal Leaf Embolism and Shedding Protect the Hydraulic Integrity of Grape Stems. Plant Physiology 174: 764–775.

Jansen S, Guan X, Kaack L, Trabi C, Miranda MT, Ribeiro RV, Pereira L. 2020. The Pneumatron estimates xylem embolism resistance in angiosperms based on gas diffusion kinetics: a mini-review. Preprint: 8.

Jansen S, Schuldt B, Choat B. 2015. Current controversies and challenges in applying plant hydraulic techniques. New Phytologist 205: 961–964.

Kiorapostolou N, Galiano-Pérez L, von Arx G, Gessler A, Petit G. 2018. Structural and anatomical responses of Pinus sylvestris and Tilia platyphyllos seedlings exposed to water shortage. Trees 32: 1211–1218.

Klepsch M, Zhang Y, Kotowska MM, Lamarque LJ, Nolf M, Schuldt B, Torres-Ruiz JM, Qin D-W, Choat B, Delzon S, et al. 2018. Is xylem of angiosperm leaves less resistant to embolism than branches? Insights from microCT, hydraulics and anatomy. Journal of Experimental Botany 69: 5611–5623.

Kuznetsova A, Brockhoff PB, Christensen RHB. 2017. lmerTest Package: Tests in Linear Mixed Effects Models. Journal of Statistical Software 82: 1–26.

Leuschner C, Wedde P, Lübbe T. 2019. The relation between pressure–volume curve traits and stomatal regulation of water potential in five temperate broadleaf tree species. Annals of Forest Science 76: 60.

Leuzinger S, Zotz G, Asshoff R, Korner C. 2005. Responses of deciduous forest trees to severe drought in Central Europe. Tree Physiology 25: 641–650.

Li Y, Sperry JS, Taneda H, Bush SE, Hacke UG. 2008. Evaluation of centrifugal methods for measuring xylem cavitation in conifers, diffuse- and ring-porous angiosperms. New Phytologist 177: 558–568.

López R, Nolf M, Duursma RA, Badel E, Flavel RJ, Cochard H, Choat B. 2019. Mitigating the open vessel artefact in centrifuge-based measurement of embolism resistance (R Tognetti, Ed.). Tree Physiology 39: 143–155.

Martin-StPaul N, Delzon S, Cochard H. 2017. Plant resistance to drought depends on timely stomatal closure. Ecology Letters 20: 1437–1447.

Martin-StPaul NK, Longepierre D, Huc R, Delzon S, Burlett R, Joffre R, Rambal S, Cochard H. 2014. How reliable are methods to assess xylem vulnerability to cavitation? The issue of 'open vessel' artifact in oaks. Tree Physiology 34: 894–905.

McDowell NG, Fisher RA, Xu C, Domec JC, Hölttä T, Mackay DS, Sperry JS, Boutz A, Dickman L, Gehres N, et al. 2013a. Evaluating theories of drought-induced vegetation mortality using a multimodel-experiment framework. New Phytologist 200: 304–321.

McDowell NG, Ryan MG, Zeppel MJB, Tissue DT. 2013b. Feature: Improving our knowledge of drought-induced forest mortality through experiments, observations and modeling. New Phytologist 200: 289–293.

Meinzer FC, Johnson DM, Lachenbruch B, McCulloh KA, Woodruff DR. 2009. Xylem hydraulic safety margins in woody plants: coordination of stomatal control of xylem tension with hydraulic capacitance. Functional Ecology 23: 922–930.

Niinemets Ü, Sõber A, Kull O, Hartung W, Tenhunen JD. 1999. Apparent Controls on Leaf Conductance by Soil Water Availability and via Light-Acclimation of Foliage Structural and Physiological

Properties in a Mixed Deciduous, Temperate Forest. *International Journal of Plant Sciences* **160**: 707–721.

Nolf M, López R, Peters J, Flavel R, Koloadin L, Young I, Choat B. 2017. Visualization of xylem embolism by X-ray microtomography: A direct test against hydraulic measurements. New Phytologist 214.

Oliveira RS, Costa FRC, Baalen E van, Jonge A de, Bittencourt PR, Almanza Y, Barros F de V, Cordoba EC, Fagundes MV, Garcia S, et al. 2019. Embolism resistance drives the distribution of Amazonian rainforest tree species along hydro-topographic gradients. New Phytologist 221: 1457–1465.

Ogle K, Barber JJ, Willson C, Thompson B. 2009. Hierarchical statistical modeling of xylem vulnerability to cavitation. New Phytologist 182: 541–554.

Pammenter NW, Vander Willigen C. 1998. A mathematical and statistical analysis of the curves illustrating vulnerability of xylem to cavitation. Tree Physiology 18: 589–593.

Pereira L, Bittencourt PRL, Oliveira RS, Junior MBM, Barros FV, Ribeiro RV, Mazzafera P. 2016. Plant pneumatics: stem air flow is related to embolism - new perspectives on methods in plant hydraulics. New Phytologist 211: 357–370.

Pereira L, Bittencourt PRL, Pacheco VS, Miranda MT, Zhang Y, Oliveira RS, Groenendijk P, Machado EC, Tyree MT, Jansen S, et al. 2020. The Pneumatron: An automated pneumatic apparatus for estimating xylem vulnerability to embolism at high temporal resolution. Plant, Cell & Environment 43: 131–142.

Pigott D. 2012. Lime-trees and Basswoods: A Biological Monograph of the Genus *Tilia*. Cambridge University Press.

Pivovaroff AL, Burlett R, Lavigne B, Cochard H, Santiago LS, Delzon S. 2016. Testing the 'microbubble effect' using the Cavitron technique to measure xylem water extraction curves. AoB Plants 8.

Powers JS, Vargas-G G, Brodribb TJ, Schwartz NB, Perez-Aviles D, Smith-Martin CM, Becknell JM, Aureli F, Blanco R, Calderón-Morales E, et al. 2020. A catastrophic tropical drought kills hydraulically vulnerable tree species. Global Change Biology n/a.

Pratt RB, Castro V, Fickle JC, Jacobsen AL. 2020. Embolism resistance of different aged stems of a California oak species (*Quercus douglasii*): optical and microCT methods differ from the benchtop-dehydration standard (M Ball, Ed.). Tree Physiology 40: 5–18.

Pya N. 2020. scam: Shape Constrained Additive Models. R package version 1.2-8. URL: https://CRAN.R-project.org/package=scam

R Core Team. 2020. R: A language and environment for statistical computing. Vienna, Austria.

Rosenberg MS, Koricheva J, Gurevitch J, Mengersen K. 2013. Moment and least-squares based approaches to meta-analytic inference. In: Handbook of meta-analysis in ecology and evolution. Princeton and Oxford: Princeton University Press, 108–124.

Rosner S, Heinze B, Savi T, Dalla-Salda G. 2019. Prediction of hydraulic conductivity loss from relative water loss: new insights into water storage of tree stems and branches. Physiologia Plantarum 165: 843–854.

Sergent AS, Varela SA, Barigah TS, Badel E, Cochard H, Dalla-Salda G, Delzon S, Fernández ME, Guillemot J, Gyenge J, et al. 2020. A comparison of five methods to assess embolism resistance in trees. Forest Ecology and Management 468: 118175.

Sperry JS, Donnelly JR, Tyree MT. 1988. A method for measuring hydraulic conductivity and embolism in xylem. Plant, Cell and Environment 11: 35–40.

Sperry JS, Hacke UG, Wheeler JK. 2005. Comparative analysis of end wall resistivity in xylem conduits. Plant, Cell and Environment 28: 456–465.

Sperry JS, Tyree MT. 1988. Mechanism of Water Stress-Induced Xylem Embolism. Plant Physiology 88: 581–587.

Torres-Ruiz JM, Cochard H, Mayr S, Beikircher B, Diaz-Espejo A, Rodriguez-Dominguez CM, Badel E, Fernández JE. 2014. Vulnerability to cavitation in Olea europaea current-year shoots: further evidence of an open-vessel artifact associated with centrifuge and air-injection techniques. Physiologia Plantarum 152: 465–474.

Torres-Ruiz JM, Jansen S, Choat B, McElrone AJ, Cochard H, Brodribb TJ, Badel E, Burlett R, Bouche PS, Brodersen CR, et al. 2015. Direct X-Ray Microtomography Observation Confirms the Induction of Embolism upon Xylem Cutting under Tension. Plant Physiology 167: 40–43.

Trenberth KE, Dai A, van der Schrier G, Jones PD, Barichivich J, Briffa KR, Sheffield J. 2014. Global warming and changes in drought. Nature Climate Change 4: 17–22.

Trueba S, Pouteau R, Lens F, Feild TS, Isnard S, Olson ME, Delzon S. 2017. Vulnerability to xylem embolism as a major correlate of the environmental distribution of rain forest species on a tropical island. Plant, Cell & Environment 40: 277–289.

Urli M, Porte AJ, Cochard H, Guengant Y, Burlett R, Delzon S. 2013. Xylem embolism threshold for catastrophic hydraulic failure in angiosperm trees. Tree Physiology 33: 672–683.

Venturas MD, Pratt RB, Jacobsen AL, Castro V, Fickle JC, Hacke UG. 2019. Direct comparison of four methods to construct xylem vulnerability curves: Differences among techniques are linked to vessel network characteristics. Plant, Cell & Environment 42: 2422–2436.

Wheeler JK, Huggett BA, Tofte AN, Rockwell FE, Holbrook NM. 2013. Cutting xylem under tension or supersaturated with gas can generate PLC and the appearance of rapid recovery from embolism: Sampling induced embolism. Plant, Cell & Environment 36: 1938–1949.

Wheeler JK, Sperry JS, Hacke UG, Hoang N. 2005. Inter-vessel pitting and cavitation in woody Rosaceae and other vesselled plants: a basis for a safety versus efficiency trade-off in xylem transport. Plant, Cell and Environment 28: 800–812.

Wickham H, Averick M, Bryan J, Chang W, McGowan LD, François R, Grolemund G, Hayes A, Henry L, Hester J, et al. 2019. Welcome to the Tidyverse. Journal of Open Source Software 4: 1686.

Wolfe BT, Sperry JS, Kursar TA. 2016. Does leaf shedding protect stems from cavitation during seasonal droughts? A test of the hydraulic fuse hypothesis. New Phytologist 212: 1007–1018.

Wu M, Zhang Y, Oya T, Marcati CR, Pereira L, Jansen S. 2020. Root xylem in three woody angiosperm species is not more vulnerable to embolism than stem xylem. Plant and Soil 450: 479–495.

Xu X, Medvigy D, Powers JS, Becknell JM, Guan K. 2016. Diversity in plant hydraulic traits explains seasonal and inter-annual variations of vegetation dynamics in seasonally dry tropical forests. New Phytologist 212: 80–95.

Zhang Y, Lamarque LJ, Torres-Ruiz JM, Schuldt B, Karimi Z, Li S, Qin D-W, Bittencourt P, Burlett R, Cao K-F, et al. 2018. Testing the plant pneumatic method to estimate xylem embolism resistance in stems of temperate trees. Tree Physiology 38: 1016–1025.

Zhao H, Jiang Z, Ma J, Cai J. 2020. What causes the differences in cavitation resistance of two shrubs? Wood anatomical explanations and reliability testing of vulnerability curves. Physiologia Plantarum 169: 156–168.

Zhu S-D, Liu H, Xu Q-Y, Cao K-F, Ye Q. 2016. Are leaves more vulnerable to cavitation than branches? Functional Ecology 30: 1740–1744.

Zimmermann U, Wagner H-J, Heidecker M, Mimietz S, Schneider H, Szimtenings M, Haase A, Mitlöhner R, Kruck W, Hoffmann R, et al. 2002. Implications of mucilage on pressure bomb measurements and water lifting in trees rooting in high-salinity water. Trees 16: 100–111.

4. Chapter 3: Relationships between drought-related traits and environmental preferences across four genera of temperate trees

This chapter is based on the following publication.

Manuscript 3 (Final draft) Relationships between drought-related traits and environmental preferences across four genera of temperate trees.

Emilie Isasa, Ana Paula Moraes, Bernhard Schuldt, Juliano Sarmento Cabral

Participated in	**Author Initials,** Responsibility decreasing from left to right				
Study Design Methods Development	J.S.C.	B.S.	E.I.		
Data Collection	E.I.				
Data Analysis and Interpretation	E.I.	J.S.C.	A.P.M.	B.S.	
Manuscript Writing	E.I.	J.S.C.	B.S.	A.P.M.	
Figure	**Author Initials,** Responsibility decreasing from left to right				
1	E.I.	A.P.M.	J.S.C.	B.S.	
2	E.I.	B.S.	J.S.C.	A.P.M.	
3	E.I.	A.P.M.	J.S.C.	B.S.	
4	E.I.	J.S.C.	B.S.	A.P.M.	
Table	**Author Initials,** Responsibility decreasing from left to right				
1	E.I.	J.S.C.	B.S.	A.P.M.	
2	E.I.	J.S.C.	A.P.M.	B.S.	
3	E.I.	J.S.C.	A.P.M.	B.S.	

Explanations:

The doctoral researcher confirms that she has obtained permission from the co-authors for legal second publication.

The doctoral researcher and the primary supervisor confirm the correctness of the above-mentioned assessment.

Emilie Isasa	25.11.2022	Würzburg	
Doctoral Researcher's Name	Date	Place	Signature
Prof. Dr. Bernhard Schuldt	25.11.2022	Dresden	
Primary Supervisor's Name	Date	Place	Signature

4.1. Abstract

Drought-induced tree mortality is primarily influenced by tree hydraulic mechanisms and anatomical characteristics. These traits and their combination might be under selective pressure and thus assessing the environmental-trait relationships should provide insights on potential responses to environmental change.

The study examined the relationship between water potential at 50% loss of conductivity (P_{50}), hydraulically-weighted vessel diameter (D_h) and wood density (*WD*) of 24 species of four diffuse-porous tree Holarctic genera and families. Phylogenetic generalized least squares were used to control for phylogenetic constraints when examining preferences in six temperature and precipitation-related climate variables.

Our results provide a strong correlation between P_{50} and D_h across families, but no correlation between P_{50} and *WD*. The *WD* varies independently of the other two traits, providing a physiological flexibility. We observed phylogenetic conservatism in P_{50} and *WD* across families but not for D_h.

There was a significant correlation between drought-related traits and the precipitation preferences for the Sapindaceae as well as with the temperature preferences for the Rosaceae, Malvaceae and Sapindaceae families. According to this study, trees are relatively flexible within their functional trait space to cope with climatic conditions: by decreasing P_{50}, D_h in drier conditions (e.g., Sapindaceae) or by increasing P_{50} and decreasing *WD* with higher temperature (e.g., Rosaceae).

Keyword: climate change, drought, plant hydraulic traits, evolution, phylogeny, species distribution, angiosperms.

4.2. Introduction

A central target in plant ecology and evolutionary ecology is to understand fitness and its components (survival, growth, reproductive effort). Fitness is linked to environmental conditions as well as to phenotypic characteristics that improve the performance of individual species in specific environments (Ackerly 2003).

It is essential to understand why some plant lineages shift among different climatic regions whereas others maintain their ancestral climatic niche (Wiens et al., 2010; Edwards and Donoghue, 2013). Being long-lived, sessile organisms with slow vegetative and population dynamics, tree individuals and species can react to changing climate. They can change by genetically or phenotypically adapting to the new environmental conditions or by shifting the occurrence range to stay at their environmental requirements. They can combine these responses, or, in the worst scenario, they can go extinct by failing to adapt or to migrate (Aitken et al., 2008). Indeed, they are already experiencing increasingly warmer and more frequent extreme climate events that cause heat and drought stress, both of which are associated directly with recent widespread forest dieback (Allen et al., 2010, Matusik et al., 2013; McDowell et al., 2020, Yi et al 2022). Hence, improving our understanding on tree responses to drought stress is urgent because the high pace of impending climate change will catch up with the evolutionary changes of tree populations (Davis and Shaw, 2001).

Functional traits are often associated with environmental stress and have been largely used in plant ecology to explore functional strategies at different environments (Esperon-Rodriguez et al., 2020; Martinez-Vivalta et al., 2010; Nardini et al., 2013). In this sense, the tree's preferences in water availability (Pockman and Sperry, 2000; Choat et al., 2007; Nardini et al., 2012) and temperature (Blackman et al., 2017; Cochard et al., 2000) can be related to the plant vascular function, also called plant hydraulic system (e.g., resistance to dehydration), to anatomy (e.g., xylem vessel size, wood density), to phenology (Alberto et al., 2013) or to species distributions (Blackman et al., 2012; Larter et al., 2017; Skelton et al., 2020). It is thus paramount to understand how the plant vascular function and the various related traits evolved under environmental selection.

Water movement in terrestrial vascular plants is driven by the process of transpiration at the leaf–atmosphere level. A large number of traits (e.g., vessel diameter, pit membrane thickness, wood density) has been associated with the research on the drought resistance of plants (Hacke et al., 2001, 2006; 2017; Isasa et al., 2022; Maherali et al., 2006; Markesteijn et al., 2011). All those studied traits characterize the physical tolerance to dehydration, which has a main vulnerable point: the risk of xylem embolism. In fact, xylem vulnerability to cavitation and, more precisely, the risk of hydraulic failure, has been described as the main cause of the dieback and death of tree individuals (Brodribb and Cochard, 2009; Venturas et al., 2017).

To quantify this risk, species are commonly compared by the water potential at 50% loss of hydraulic conductivity (P_{50}) (Gleason et al., 2016a). This happens when water potential in conduits decline to levels that provoke embolism formation (Tyree and Zimmermann, 2002). This

phenomenon is provoked by the direct entry of gas nanobubbles between an embolised and a functional conduit, which blocks the water flow in more xylem conduits (Cochard et al., 2009; Guan et al., 2021; Jansen et al., 2018). Besides P_{50}, xylem vulnerability to cavitation results from the interactions between several physiological and anatomical traits (e.g., leaf habit, stomatal closure, minimum cuticular conductance, vessel size - D_h, wood density - *WD*) related to the mechanical properties of wood (Brodribb et al., 2014; Chave et al., 2009; Choat et al., 2018; Martínez-Vilalta et al., 2010; Martin-StPaul et al., 2017; Poorter 2008). To unravel the causes of the diversity of physiological functions found in woody species, we need to identify evolutionary convergence between drought tolerance and eventual trade-offs with other traits (Skelton et al., 2020).

We have selected 24 species of four Holoarctic Angiosperm genera and families to compare drought-related traits (P_{50}, D_h and *WD*), for which we have chosen congeneric parapatric species with different environmental preferences, as well as allopatric species that may also occur in the same environment. Because of their geographic distribution within each family, both latitude and longitude, they represent an ideal group for studying plant ecophysiology and drought tolerance from both evolutionary and ecological perspective. Still, to understand the relationship among the traits and between them and the environment, it is essential to control for phylogenetic constraints to detect the selective pressure imposed by the environment on the species.

Here, we address the following questions: (1.1) What is the interspecific trait range capacity to prevent xylem embolism in six species from each plant family: Betulaceae, Rosaceae, Malvaceae and Sapindaceae? (1.2) What is the relationship between stem embolism resistance (P_{50}), vessel size (D_h) and wood density (*WD*) among these 24 species? (2) To what extent are the drought-related traits of those species phylogenetically controlled? (3) Are drought-related traits associated with ecological variables (i.e., preferences to bioclimatic environmental variables)?

We expect that drought-related traits show a strong phylogenetic signal across congeneric species and across families (Larter et al., 2017). Nevertheless, we assume that there are detectable trait-environment relationships across congeneric species and across families as drier and warmer conditions should exert directional selective pressure towards lower P_{50}, lower D_h and higher wood density *WD*.

4.3. Materials and Methods

4.3.1. Study site and plant material

Six temperate Angiosperm diffuse-porous tree species from each of four families (Betulaceae, Rosaceae, Malvaceae, Sapindaceae) were used (Table 4.1). We selected such species based on their ability to withstand drought stress as well as their similar and/or parapatric geographical distribution (i.e., northern temperate climates).

To capture trait differences based on the tree species' evolutionary history rather than an ecological context of the tree individuals, it is essential that the individuals were grown under the same environmental conditions. To control this, all samples were obtained from the nursery in the Stutel-Arboretum from the Bavarian State Institute for viticulture and horticulture in Veitshöchheim, Germany (LWG) (49°51’49’’N, 9°51’8’’E) and from the Botanical Garden of the University of Würzburg, Germany. The long-term mean annual temperature and mean annual precipitation are 10.0 °C and 591 mm in Veitshöchheim and 9.6 °C and 560.4 mm in Würzburg, respectively (Bavarian State Institute for agriculture,−LFL), constituting a warm temperate continental climate according to the Köppen classification (Peel et al., 2007).

The samples were collected between June and September for three consecutive years (2019, 2020 and 2021; Table 4.1). Samples were taken from two to four individuals per species, resulting in a total of 67 sampled trees. At both sites, 60 cm long twigs were cut and wrapped in wet paper towels, bagged in dark humidified plastic bags and transported to the laboratory where they were analysed on the same day. For each sample, we measured the vulnerability curves, as well as pit and xylem properties and wood density.

Table 4.1: Summary of the analysed functional traits. The number of trees for the wood anatomical and hydraulic measurements (n_{tree}), the mean ± standard deviation of the water potential at 50% loss of hydraulic conductivity (P_{50}), hydraulically-weighted vessel diameter (D_h), wood density (*WD*).

Family	Specie	Code	n_{tree}	P_{50} (MPa)	D_h (µm)	*WD* (g cm^{-3})
Betulaceae	*Betula alleghaniensis*	BEAL	4	-1.86 ± 0.06	37.76 ± 2.84	0.60 ± 0.02
	Betula lenta	BELE	4	-1.78 ± 0.34	43.83 ± 2.39	0.63 ± 0.03
	Betula maximowicziana	BEMA	4	-1.77 ± 0.04	43.83 ± 6.45	0.51 ± 0.04
	Betula pendula	BEPE	4	-2.32 ± 0.19	33.13 ± 2.34	0.72 ± 0.13
	Betula pubescens	BEPU	4	-1.87 ± 0.07	30.84 ± 1.75	0.59 ± 0.02
	Betula utilis	BEUT	4	-2.02 ± 0.16	39.01 ± 1.46	0.62 ± 0.05
Rosaceae	*Prunus avium*	PRAV	3	-4.45 ± 0.10	26.33 ± 1.02	0.66 ± 0.06
	Prunus mahaleb	PRMA	4	-4.10 ± 0.51	41.95 ± 2.28	0.73 ± 0.07
	Prunus padus	PRPA	3	-3.16 ± 0.04	37.76 ± 1.21	0.58 ± 0.03
	Prunus pensylvanica	PRPE	4	-2.86 ± 0.12	34.19 ± 2.09	0.61 ± 0.03
	Prunus sargentii	PRSA	4	-3.40 ± 0.12	33.33 ± 7.12	0.68 ± 0.05
	Prunus serrulata	PRSE	4	-4.13 ± 0.29	31.75 ± 1.22	0.74 ± 0.14
Malvaceae	*Tilia americana*	TIAM	4	-2.30 ± 0.08	34.27 ± 3.96	0.34 ± 0.02
	Tilia cordata	TICO	4	-3.14 ± 0.24	38.63 ± 2.49	0.44 ± 0.16
	Tilia japonica	TIJA	4	-2.66 ± 0.13	37.64 ± 4.02	0.36 ± 0.03
	Tilia mongolica	TIMO	4	-2.91 ± 0.08	40.42 ± 2.61	0.39 ± 0.08
	Tilia platyphyllos	TIPL	4	-3.39 ± 0.11	40.02 ± 3.17	0.49 ± 0.05
	Tilia tomentosa	TITO	4	-3.27 ± 0.09	43.86 ± 3.35	0.38 ± 0.06
Sapindaceae	*Acer campestre*	ACCA	4	-5.45 ± 0.12	33.22 ± 2.23	0.62 ± 0.08
	Acer monspessulanum	ACMO	2	-7.32 ± 0.04	27.27 ± 1.23	0.75 ± 0.12
	Acer platanoides	ACPL	4	-4.35 ± 0.29	42.39 ± 0.28	0.50 ± 0.09
	Acer rubrum	ACRU	4	-2.92 ± 0.05	39.79 ± 2.97	0.64 ± 0.04
	Acer saccharinum	ACSA	3	-2.94 ± 1.06	30.57 ± 3.27	0.50 ± 0.04
	Acer tataricum	ACTA	3	-5.01 ± 1.52	27.06 ± 7.12	0.48 ± 0.08

4.3.2. Hydraulic measurements

4.3.2.1. Vulnerability curves with the flow-centrifuge method

All hydraulic measurements were done with the Cavitron device (Cochard et al., 2005), built from a Sorval RC 5 series centrifuge with manual control of rotation speed and using the Cavisoft software (Cavisoft v.5.2.1, University of Bordeaux, Bordeaux, France). The principle of the flow centrifuge method is to use centrifugal force to induce a negative pressure in the xylem to provoke drought-induced embolism. A subset of the vulnerability curve measurements discussed in this paper were used for addressing controversies in safety-vessel diameter relationships (Isasa et al., unpublished; Paligi et al., 2021).

In total, 67 branches were measured (mean diameter at basipetal end ± SD: 7.18 ± 0.85 mm), immediately submerged in demineralized water and recut several times using pruning shears to a final length of 27.5 cm to release the tension in the xylem (Torres-Ruiz et al., 2015). Thereafter, lateral twigs were removed. Lateral branches were evened with a razor blade and shortened to a final length of 27.5 cm. Subsequently, samples of 3–4 cm length were cut from the basipetal and acropetal sample ends and stored in 70% ethanol for anatomical analyses.

Branch segments were removed from the bark and measured at both ends before being inserted into a custom-made rotor. Cavisoft software was used to measure conductance using degassed, demineralized water containing 10 mM KCl and 1 mM $CaCl_2$ and starting at a water potential of -0.834 MPa (equivalent to 3,000 rotations per minute) and progressively reducing the water potential until 90% of the initial conductance had been lost. To ensure stable conductance values, a two minutes waiting period was maintained before each pressure step.

Vulnerability curves were fitted in R v. 4.1.0 (R Core Team 2021) with nonlinear least squares using the logistic model by Pammenter and Vander Willigen (1998) in the modified version based on hydraulic conductivity (Ogle et al., 2009):

$$K_{\mathrm{i}} \sim \mathrm{Normal}\left(K_{\mathrm{sat}} \cdot \left(1 - \frac{1}{1 + \exp\left(-\frac{S_{50}}{25}\left(P_{\mathrm{i}} - P_{50}\right)\right)}\right), \sigma\right), \qquad (1)$$

where for each observation *i*, the conductivity K_{i} is assumed to be normally distributed with residual standard deviation σ around a logistic function of the water potential P_{i} with the parameters P_{50} (water potential at 50% loss of conductivity), S_{50} (corresponding slope on the percent loss of conductivity scale) and K_{sat} (conductivity at full saturation).

4.3.2.2. Xylem anatomy measurements

For all species, semi-thin (20 µm) transverse sections of the wood anatomical samples were made with a sliding microtome (G.S.L.1, Schenkung Dapples, Zürich, Switzerland), stained with safranin-alcian blue, rinsed with distilled water and ethanol (95%) and permanently embedded on glass slides using Euparal (Carl Roth, Karlsruhe, Germany). Subsequently, the complete cross-section was digitalized at 100-times magnification using a light microscope equipped with an automated table and a digital camera (Observer.Z1, Carl Zeiss MicroImaging GmbH, Jena, Germany; Software: AxioVision c4.8.2, Carl Zeiss MicroImaging GmbH). Anatomical measurements were made by semi-automated image analysis using ImageJ version 1.52p (Schneider et al., 2012) and GIMP v. 2.10.6 (GIMP Development Team, 2018). The equivalent vessel diameter was calculated according to White (1991) (*d, µm*), i.e., the diameter of a circular vessel with the same conductivity as an elliptical one with minor and major radius *a* and *b*:

$$d = \left(\frac{32\,(ab)^3}{a^2 + b^2}\right)^{0.25} \quad (2)$$

Based on *d*, the hydraulically-weighted average vessel diameter (D_h, µm) was calculated according to Sperry et al., (1994) as following:

$$D_h = \frac{\sum d^5}{\sum d^4} \quad (3)$$

4.3.3. Phylogeny

The DNA sequences for the 24 species studies here along with two species used as outgroup (*Ceratophyllum demersum* L., *Ceratophyllum submersum* L.) were obtained from the GenBank database (Table S1; Benson et al., 2013). The phylogeny was built using four markers, three plastid genome regions (*mat*K-*trn*K, *atp*B-*rbc*L and *ycf*1) and one nuclear region, the internal transcribed spacer (ITS). For each marker, the sequences from all species were aligned by MAFFT v.7.453 software using its progressive alignment and iterative refinement methods (Katoh and Standley 2014; Katoh et al., 2019). The aligned sequences were trimmed manually optimized on UNIgene software (Okonechnikov et al., 2012) and the final concatenated matrix was analysed under Maximum Likelihood (ML).

The ML analysis was performed using IQ-TREE2 (Minh et al., 2020). The nucleotide substitution models were chosen by ModelFinder applying the Bayesian Information Criterion (BIC; Kalyaanamoorthy et al., 2017): K3Pu+F+G4 to *mat*K-*trn*K, K3Pu+F+G4 to *atp*B-*rbc*L, TVM+F+G4 to *ycf*1 and K2P+G4 to ITS, with each model being applied to its partition on the

concatenated matrix (Chernomor et al., 2016). We used 100 bootstrapping to assess branch supports. The phylogenetic tree was edited with FigTree v.1.4.4 (http://tree.bio.ed.ac.uk/software/figtree/) and GIMP v. 2.10.6 (GIMP Development Team, 2018) (Fig. 4.1) The matrix is available under request. For macroevolutionary analysis, the outgroup was removed using the function drop.tip from the 'ape' package in the R v. 4.1.0 (R Core Team, 2021). To ensure that the differences between plant families would not overshadow the differences among congeneric species, one phylogeny per plant family was also constructed by removing the tips of remainder plant families using the same function.

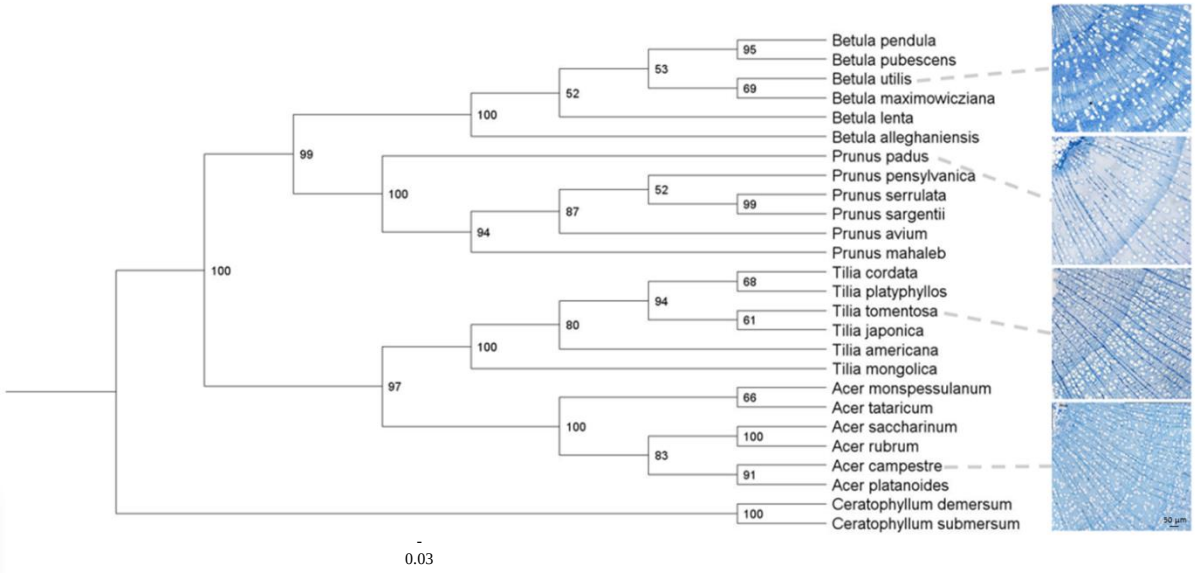

Figure 4.1: Maximum likelihood phylogenetic tree based on matK–trnK, atpB-rbcL, ycf1 and ITS markers. Insets of the phylogenetic tree show stem anatomical cuts representative of all families: Betulaceae, Rosaceae, Malvaceae, Sapindaceae and the outgroup Ceratophyllum. Photos credits: E. Isasa

4.3.4. Occurrence data

For all 24 species, we extracted occurrence points from two online databases: GBIF (Holstein 2001; https://www.gbif.org) and BIEN (Enquist et al., 2016; Maitner et al., 2018; http://bien.nceas.ucsb.edu). We excluded duplicate occurrence entries, flawed geographic coordinates and dubious entries, retaining a total of 94572 occurrence points. *Betula maximowicziana* showed the fewest points with 148 occurrences.

4.3.5. Bioclimatic data and variable selection

From each occurrence point, we extracted information on 19 bioclimatic variables provided by WorldClim 2.0 (https://www.worldclim.org; Fick and Hijmans 2017) at a spatial resolution of 30 arc seconds (approx. 1 km^2) based on historical values of the climate variables (1970-2000).

For the subsequent analysis, species climatic range was characterized by the key environmental variables, based on their relevance to the characterization related to water availability and temperature stress, both of which are related to drought-related traits and for a given species distribution (Blackman et al., 2014, 2017; Larter et al., 2017; Martinez-Vilalta et al., 2010; Skelton et al., 2020). In this sense, we focused on the following six environmental variables: isothermality (Bio3), mean temperature of the warmest quarter (Bio10), mean temperature of the coldest quarter (Bio11), mean annual precipitation (Bio12), mean precipitation of the driest quarter (Bio17), mean precipitation of the warmest quarter (Bio18) (Table S2).

The environmental preferences were obtained for each species by averaging each of the six chosen variables across all the occurrences where the species was natively present. We assumed the non-independence of different variables. Subsequently, a multiple comparison tests based on Tukey contrasts were performed on the environmental preferences (i.e., the mean environmental variable values across occurrence points) across families, which represents a robust non-parametric procedure for comparing multiple means under heteroscedasticity (Herberich et al. 2010) (Fig. S1, Table S2).

4.3.6. Environmental preferences

We found that across the geographical range of the different families, average realized isothermality varied from 23.98 °C (Table S2) for *Acer platanoides* in central Europe to over 35.89 °C for *Betula utilis* in Southern Asia. Variation was found also for the mean temperature of the warmest quarter, ranging from 13.97 °C for *Betula pubescens* in Northern Europe to 21.23°C for *Prunus sargentii* in Eastern Asia. The mean temperature of the coldest quarter varied from -9.16°C for *Prunus pensylvanica* in East America to 4.03 for *Acer monspessulanum* in Western Europe. Concerning the mean annual precipitation, a variation was observed from 657.33 mm $year^{-1}$ for *Acer tataricum* in Asia from 1624.43 mm $year^{-1}$ for *Tilia japonica* in Eastern Asia. Regarding the precipitation in the driest quarter, variations were observed from 825.78 mm for *Betula utilis* in Southern Asia to 241.60 mm for *Betula lenta* in Eastern America. Finally, the mean precipitation of the warmest quarter variations changes from 152.34 mm for *Acer monspessulanum* in Western Europe to 605.38 mm for *Prunus sargentii* in East Asia.

4.3.7. Ecological and Macroevolutionary analyses

To answer question (1.1), we determined the range of variation in key hydraulic traits by comparing the minimum and maximum trait values among the angiosperms tree species. Vulnerability curves were fitted in R v. 4.1.0 (R Core Team, 2021) with nonlinear least squares using the logistic model. For our question (1.2), the significance of linear associations between drought-related traits on the species level was tested with regular linear models of species averages fitted with ordinary least squares.

Regarding our question (2), macroevolutionary analyses were performed using the constructed phylogenies. We used a time-resolved phylogeny for the four families to assess phylogenetic relatedness of our 24 sample species and two as the outgroup. Phylogenetically independent contrasts for all trait data were calculated using the trait correlation function in the ape package in R v. 4.1.0 (R Core Team, 2021).

We verified the mode of evolution of P_{50}, D_h and *WD* and checked whether they show phylogenetic signals within and across family. Using the 'geiger' package (Pennell et al., 2014), we tested three evolution models across all families to confirm the best macroevolutionary model for our hydraulic traits: Brownian motion (Felsenstein, 1973), Ornstein–Uhlenbeck (Butler and King, 2004; Cressler et al., 2015) and Early Burst (Felsenstein, 1973; Harmon et al., 2010). Given the overall effect of phylogeny on variation in drought-related traits, we estimated the phylogenetic signal using Pagel's λ (Pagel, 1999) under maximum likelihood (ML). According to their Akaike Information Criterion corrected for small sample sizes (AICc), the best models (BMs) were identified, considering that $\Delta AICc < 2$ are putative most parsimonious models (Burnham and Anderson, 2002, 2004) (see Supplementary Material S5, S6). The macroevolutionary models were separately repeated for each family.

To answer question (3), a principal component analysis (PCA Biplot) (PCA1) was performed using species-mean trait values per compartment type (i.e., P_{50}, D_h and *WD*) as data points to evaluate how the traits were associated. The second PCA (PCA2) assessed relationships among the environmental preferences of the species across the six chosen bioclimatic variables. We ran the PCAs using the 'factoextra' package in R v. 4.1.0 (R Core Team, 2021). Following Villeger et al., (2012), we standardized all traits to make them dimensionally homogeneous and put equal weight on each trait in the calculations of functional diversity. The first and second axes of both PCAs (PCA1.1, PCA1.2, PCA2.1 and PCA2.2) were kept, consistently containing over 70% of the variation (see Supplementary Material S7, S8). Each axis separately from the PCA2 was further used for the macroecological analyses with the six environmental variables together.

To determine whether drought-related traits are influenced by environmental PCA, we used phylogenetic generalized least squares regression (PGLS, Freckleton, Harvey & Pagel 2002) accounting for phylogenetic relationships. We considered both PCA2.1 plus PCA2.2 as independent variables in the maximum model (MM). We fitted each PGLS model assuming a Brownian model of character evolution (Martins and Hansen, 1997). The PGLS models were run using the CAPER package v.0.5.2 (Orme, 2013) in R v. 4.1.0 (R Core Team, 2021).

4.4. Results

4.4.1. Embolism resistance, wood density and wood anatomy across species

Our results revealed a wide interspecific range of P_{50}, D_h and *WD*. Across the studied 24 temperate broadleaved tree species (n = 67), P_{50} varied from -1.77 ± 0.04 MPa in *Betula maximowicziana* to -7.32 ± 0.04 MPa in *Acer monspessulanum* (mean ± SD; Table 4.1). The D_h values varied from 26.33 ± 1.02 in *Prunus avium* and to 43.86 ± 3.35 in *Tilia tomentosa*. The *WD* values varied from 0.34 ± 0.02 in *Tilia americana* to 0.75 ± 0.12 in *Acer monspessulanum*. In the cross-species bivariate relationships, we observed hydraulic and structural trade-offs with embolism resistance. The P_{50} values were significantly correlated with D_h (r = 0.48, p = 0.018) while not showing correlation with *WD*. No relationship for P_{50} vs. *WD* and D_h vs. *WD* (Fig. 4.2 A-B-C, Table 4.1). In summary, higher embolism resistance was associated with reduced conduit diameter.

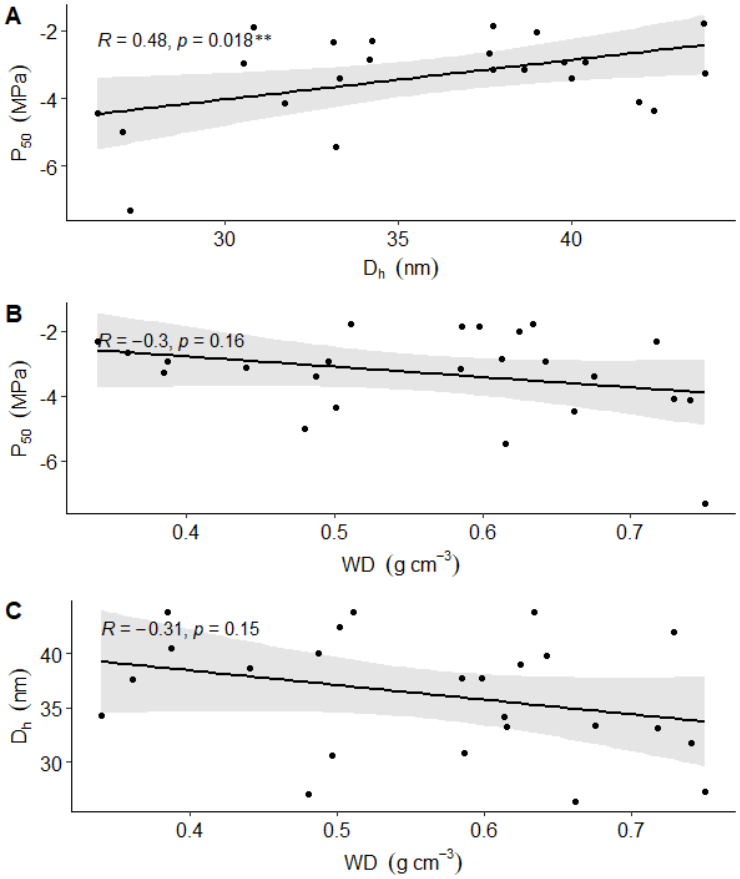

Figure 4.2: Results of simple species-level linear regressions of water potential at 50% loss of conductivity (P_{50}) vs. A) hydraulically-weighted vessel diameter (D_h), B) Wood density (*WD*). C) hydraulically-weighted vessel diameter (D_h) vs. Wood density (*WD*). Shown are the species level averages (black) overlaid with the model predictions ±95% confidence bands (grey). For regression parameters see Table 4.1.

4.4.2. Macroevolution analyses

We mapped the evolution of xylem vulnerability to embolism, vessel diameter and wood density onto the phylogeny across all the four families. Each trait was indicated to evolve under BM and Pagel´s λ for P_{50} and *WD* reveal a significant phylogenetic signal (λ = 0.99 and λ = 0.61, respectively; Fig. 4.3 A-B-C, Table S3) but no phylogenetic signal was found for D_h.
When assessing trait evolution separately per family, the results showed some variation among families (Fig. S3, S4, S5, S6, Table S3). For Betulaceae, all traits were indicated to evolve under EB, but Pagel´s λ revealed no phylogenetic signal (λ = 0) for all P_{50}, D_h and *WD*. For Malvaceae, all traits were indicated to evolve under BM and Pagel´s λ for P_{50} revealed a strong phylogenetic signal (λ = 1.000) while D_h and *WD* did not show a phylogenetic signal (λ = 0). For Rosaceae, all traits were indicated to evolve under BM, but Pagel´s λ revealed no phylogenetic signal (λ = 0) for all P_{50}, D_h and *WD*. Finally, for Sapindaceae we were unable to choose among the three macroevolutionary models for P_{50} as their BIC values differed by less than two units. This is not surprising, since a large amount of variation in trait distributions and phylogenetic signal can be generated under BM and both the EB and the OU models represent deviations from BM. However, both D_h and *WD* followed BM for Sapindaceae. Pagel´s λ for P_{50} revealed a strong phylogenetic signal (λ = 1.000), while D_h and *WD* did not show a phylogenetic signal (λ = 0).

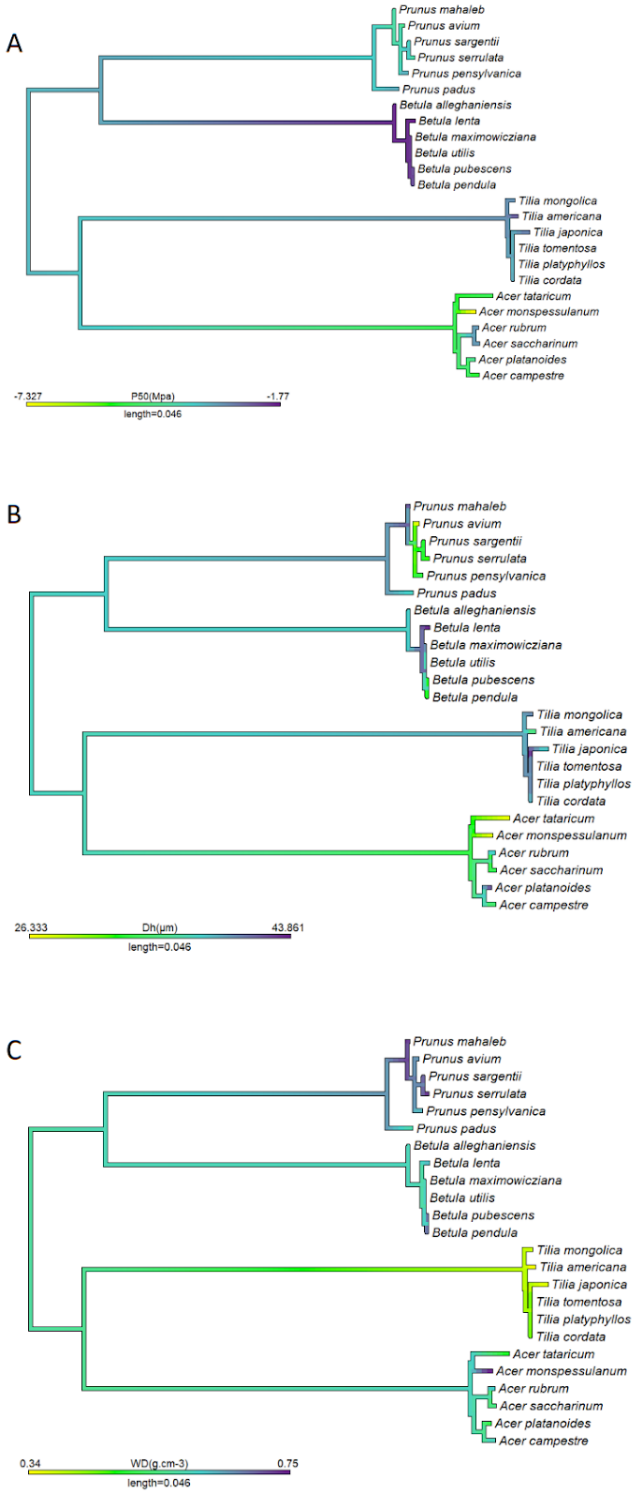

Figure 4.3: The spectrum of traits evolution variation in six Betulaceae, six Rosaceae, six Malvaceae and six Sapindaceae species. A) 50% loss of conductivity (P_{50}), B) hydraulically-weighted vessel diameter (D_h), C) wood density (*WD*). Branch colors reflect changes in traits evolution through time (reconstructed using maximum likelihood).

4.4.3. Macroecological analyses

4.4.3.1. Plant architecture and environmental preferences

The first principal component analysis (PCA1) showed that there is a high degree of coordination among the three drought-related traits (P_{50}, D_h and *WD*). The first axis of this first PCA (PCA1.1 with 51.1% of explained variability) was coherent with all three traits variable across the 24 species (loadings >0.4). The second axis of this PCA (29.7% of explained variability) was coherent with only *WD* (loadings >0.4). Species with more negative P_{50} values tended to have smaller D_h and higher *WD*. The PCA1 also showed that the *Tilia* species clustered together, contrary to the other families which showed a spread of values within the trait space (Fig. 4.4 A).
The second PCA (PCA2) showed that there is a high degree of coordination of the chosen bioclimatic variables. The mean temperature of warmest quarter, mean annual precipitation, mean precipitation of driest quarter and mean precipitation of warmest quarter are negatively correlated to isothermality and mean temperature of the coldest quarter. The first axis of this second PCA (PCA2.1) explained 51.1% of the variability and was coherent with the mean annual precipitation, mean precipitation of the driest quarter, mean precipitation of the warmest quarter (loadings >0.4). This axis can be called precipitation preference axis. The second axis (PCA2.2) explained 29.7% of the variability and was coherent with mean temperature of the coldest quarter and isothermality (loadings >0.4). This axis can be called temperature preference axis (Fig. 4.4 B).

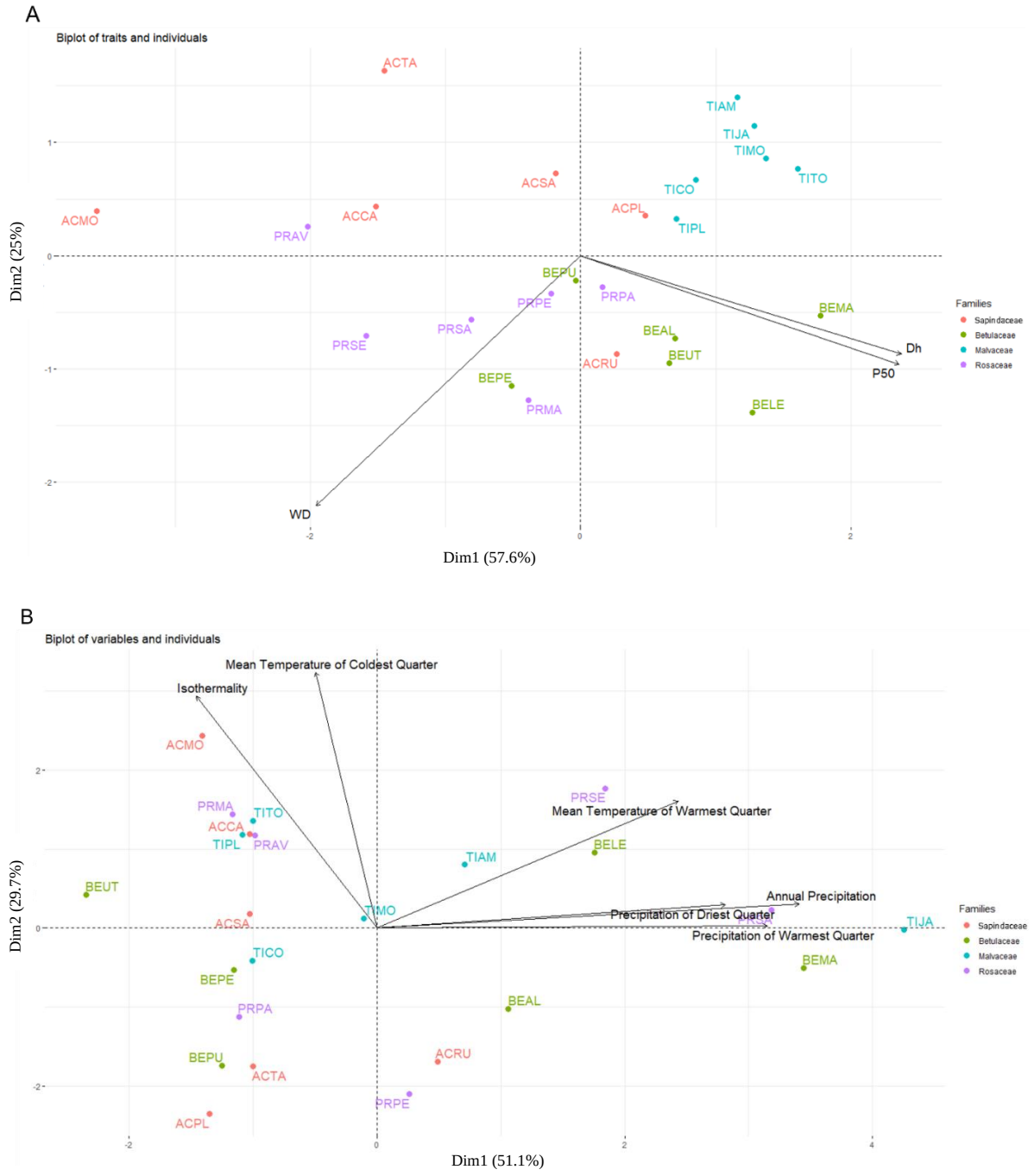

Figure 4.4: A) Principal-component analysis based on drought-related traits variation in 24 angiosperm tree species. The first two axes of the PCA (PCA1.1, PCA1.2) (accounting for 82.6% of the variance) show the coordination of stem P_{50}, D_h and *WD*. B) Principal-component analysis based on six bioclimatic preferences (isothermality, mean temperature of the warmest quarter, mean temperature of the coldest quarter, mean annual precipitation, mean precipitation of the driest quarter, mean precipitation of the warmest quarter) variation in 24 angiosperm tree species (Table 4.1). The first two axes of the PCA (PCA2.1, PCA2.2) (accounting for 80.8% of the variance) show the coordination of the six bioclimatic preferences.

4.4.3.2. Correlation between drought-related traits and environmental preferences

We detected significant correlations between drought-related traits and bioclimatic preferences for the Betulaceae, Rosaceae and Sapindaceae families (Table 4.2; Table 4.3).

Table 4.2: Summary of phylogeny-corrected regressions aiming to explain variation in drought-resistance traits four Angiosperm families using the PCA2.1 (precipitation axis) loadings of environmental preferences (six bioclimatic variables) associated with species distribution.

Family	Traits	Intercept	PCA2.1	λ [maximum likelihood]	Residual standard error	Adjusted R-squared	Degree of freedom	F-statistic	P-value
	P_{50}	-1.92	-0.07	0.00	3.10	0.38	4	4.18 on 1	0.11
Betulaceae	D_h	36.61	-1.40	0.00	88.57	0.14	4	1.81 on 1	0.24
	WD	0.61	0.02	0.00	1.07	0.26	4	2.77 on 1	0.17
	P_{50}	-2.85	-0.20	0.96	9.40	0.65	4	10.21 on 1	**0.03**
Malvaceae	D_h	39.05	1.18	0.00	80.18	0.12	4	1.67 on 1	0.25
	WD	0.39	0.02	0.00	1.36	0.17	4	2.03 on 1	0.23
	P_{50}	-3.69	-0.02	0.00	9.75	-0.24	4	0.01 on 1	0.92
Rosaceae	D_h	34.69	1.11	0.00	83.19	-0.10	4	0.55 on 1	0.50
	WD	-0.67	-0.01	0.00	0.93	-0.09	4	0.57 on 1	0.49
	P_{50}	-4.66	0.81	0.00	15.18	0.68	4	11.92 on 1	**0.02**
Sapindaceae	D_h	34.31	3.67	1.00	81.72	0.74	4	15.71on 1	**0.01**
	WD	0.58	-0.03	0.00	1.47	0.25	4	2.69 on 1	0.17

Table 4.3: Summary of phylogeny-corrected regressions aiming to explain variation in drought-resistance traits in four Angiosperm families (six species from each plant family) using the PCA2.2 (temperature axis) loadings of environmental preferences (six bioclimatic variables) associated with species distribution.

Family	Traits	Intercept	PCA2.2	λ [maximum likelihood]	Residual standard error	Adjusted R-squared	Degree of freedom	F-statistic	P-value
	P_{50}	-1.91	-0.03	0.00	4.20	-0.11	4	0.46 on 1	0.53
Betulaceae	D_h	39.49	1.17	0.00	95.29	0.004	4	1.02 on 1	0.37
	WD	0.61	0.006	0.00	1.37	-0.21	4	0.14 on 1	0.72
	P_{50}	-3.05	-0.18	1.00	16.18	0.91	4	52.79 on 1	$\mathbf{1.9*10^{-3}}$
Malvaceae	D_h	39.78	0.75	0.00	91.36	-0.14	4	0.37 on 1	0.58
	WD	0.41	0.02	0.00	1.51	-0.03	4	0.84 on 1	0.41
	P_{50}	-3.67	0.44	0.00	2.69	0.91	4	48.96 on 1	$\mathbf{2.1*10^{-3}}$
Rosaceae	D_h	35.05	-0.03	0.00	88.77	-0.29	4	0.0002 on 1	0.99
	WD	0.66	-0.04	0.00	0.55	0.50	4	8.68 on 1	**0.04**
	P_{50}	-5.12	-0.05	1.00	27.82	-0.24	4	0.03 on 1	0.86
Sapindaceae	D_h	34.01	-0.16	0.00	114.6	-0.25	4	0.005 on 1	0.94
	WD	0.61	0.05	1.00	0.64	0.65	4	10.63 on 1	**0.03**

For Sapindaceae, the PGLS analysis revealed a significant positive effect of PCA2.1 on P_{50} (F = 11.92, p = 0.02, λ = 0.00) and on D_h (F = 15.171, p = 0.01, λ = 1.000), whereas it showed no relationship with *WD* (Table 4.2). For Malvaceae, only a significant negative effect of PCA2.1 on P_{50} was found (F = 10.21, p = 0.03, λ = 0.96; Table 4.2). For the Betulaceae and Rosaceae, no significant effect of PCA2.1 on the traits was found (Table 4.2).
A significant positive effect of PCA2.2 was revealed in *WD* for the Sapindaceae (F =10.63, p = 0.03, λ = 1.000; Table 4.3). Whereas it showed no relationship with P_{50} and D_h. A significant negative effect was found in P_{50} for the Malvaceae (F = 52.79, p = 0.0019, λ = 1.000; Table 4.2) whereas it showed no relationship with D_h and *WD*. A significant positive effect of PCA2.2 was revealed in P_{50} for the Rosaceae (F = 48.96, p = 0.0021, λ = 0.000; Table 4.2) and a negative effect on *WD* (F = 8.68, p = 0.04, λ = 0.000; Table 4.2), whereas it showed no relationship with D_h. No significant effect was found of PCA2.2 on the traits of the Betulaceae species (Table 4.3).

4.5. Discussion

4.5.1. Functional traits related to embolism resistance

In terms of the coordination among functional traits, our results are generally consistent with the relationships reported previously across species. Furthermore, our results focused on stems since stem xylem vulnerability to embolism is more commonly reported than leaf xylem vulnerability. In particular, we provide evidence for an interspecific scaling of xylem embolism resistance (P_{50}) and hydraulically-weighted vessel diameter (D_h) in the branch xylem of temperate diffuse-porous angiosperm trees. Species with larger vessel diameters have a higher embolism risk (Fig. 4.1). Nevertheless, embolism spread depends on multiple anatomical features which play a role such as pit membrane pore constrictions and intervessel connectivity (Schenk et al., 2015; Jansen et al., 2018; Kaack et al., 2021). The existence of a vessel diameter-xylem safety relationship has been shown in previous studies (Hacke et al., 2006, 2017; Lobo et al., 2018; Maherali et al., 2006; Sperry et al., 2006). However, it is also important to point out that this vessel diameter hypothesis can differ from one study to another depending on the datasets used, on how measurements were made and on how analyses were run (Isasa et al., unpublished). The relationship between xylem-safety and vessel diameter aligns our understanding of plant drought responses with the widespread findings inferred from wood anatomy who varies along climate gradients, since large vessels increase with increasing precipitation (Nola et al., 2020; Zimmermann et al., 2021).
Wood density has a correlated component with the other traits (Fig. 4.3 A), but an independent component as well. There was no significant correlation between *WD* and P_{50} in this study. This could be explained by the insufficient range of traits covered in the studied species (Isasa et al., unpublished). The *WD* can vary independently from the other traits, which provides some physiological flexibility to cope with environmental conditions. Two key factors affect *WD*: the climatic conditions (e.g., temperature) and the soil nutrient concentrations (Chave et al., 2006;

Swenson & Enquist 2007; Heineman et al., 2016). Considering the combination between climatic responses with wood anatomy, we can gain a better perception of how plants react to weather patterns along climate gradients as well as large-scale variations in vessel diameter (Pfautsch et al., 2016; Hacke et al., 2017).
As a result, anatomical traits implied with embolism resistance can adaptively change from species to species to cope with the environment (Sperry et al., 2006) and climate preferences are likely to independently influence trait values (Chave et al., 2009). However, the adaptive ability might vary from lineage to lineage, as trait-environment relationships depended on the studied family.

4.5.2. Evolutionary component in related drought tolerance traits

In contrast to D_h, which showed a random variation and evolutionary flexibility inside each plant familie, we found phylogenetic conservatism for P_{50} and *WD* (Ackerly et al., 2003; Baas et al., 2004; Cavender-Bares et al., 2004; Oliveira et al., 2019; Preston et al., 2006; Skelton et al., 2020). The phylogenetic conservatism assumes that close relatives tend to be more similar than to distant related taxa (Davies et al., 2013) and suggests (Hietz et al., 2016) that such traits are under strong selection in the evolutionary short term due to a limited capacity for adaptations (Lamy et al., 2014). Concerning our data, probably the evolutionary trajectory-maintained xylem embolism resistance and wood density constant while vessel diameter changes in both directions across families.
However, similarity in a trait among species cannot be explained by phylogeny alone, but instead must be explained by eco-evolutionary processes. For example, a trait strongly associated with fitness could present lower heritability than those less strongly associated with fitness (Gustafsson, 1986; Mousseau and Roff, 1987) when the environmental variance is high (Houle, 1992). Besides, there is a combination of ecological processes influencing biogeographical change (e.g., species travel along aridity gradients based on their physiological tolerances) and deeper evolutionary processes of biogeography influencing traits (e.g., evolution toward greater capacity to avoid embolism in arid or drying regions) (Ackerly, 2009). As a result, some lineages have followed similar environments to those their ancestors were already adapted to, preserving ancestral traits over time, such as the Sapindaceae. It is therefore essential to conduct large-scale studies to identify phylogenetic signals indicative of evolutionary trends (Coelho de Souza et al., 2016).

4.5.3. Trade-off between drought resistance traits and bioclimatic variables

The analysed bioclimatic variables across families are comparable and a distinct scheme between environmental correlations with drought-related traits was observed across families. We would have expected a more significant relationship between drought-related traits and the bioclimatic preferences across families. According to our results, drought-related traits are described by

specific ecological axes depending on the family, but on a global scale, more traits and families are affected by temperature than precipitation, indicating that temperature plays a key role in understanding drought vulnerability (Table 4.2; Table 4.3).

Sapindaceae species showed a strong relationship between xylem embolism resistance and precipitation (Larter et al., 2017) as well as vessel diameter besides wood density showed relationships only with temperature. Some species may adopt strategies that do not need to amplify resistance to embolism, decrease vessel diameter or increase wood density, especially where water is not a limiting resource (Reich, 2014). We found that our studied drought resistance traits cannot be explained by responses to environmental conditions in the Betula. The absence of relationships among functional traits and climate of origin at occurrence points among Betulaceae may be because mean or median climate parameters do not represent the range of climatic conditions experienced by the plants, particularly where habitats can have large interannual or seasonal variation in rainfall or aridity. Alternatively, those species could exhibit plasticity in how they express traits based on environmental conditions and may not be strongly genetically controlled (Guerin et al., 2012; Stotz et al., 2021).

Plant traits collected in habitats with vastly different environmental conditions, but from species with a narrow geographical range, tended to correlate with the environment, but not if collected in offspring grown in gardens (Baruch et al., 2018). Therefore, if trait expression is highly plastic and the adaptive potential of a species is realized by functional acclimation, it is unlikely that trait differences among subspecies will be conserved genetically. Hence, rapid and plastic trait response, not long-term evolutionary processes, may be more important in responding to changes in environmental conditions and climate (Xu et al., 2021). Due to high genetic variation the Betulaceae are an excellent model system for adapting northern trees to climate change (Oksanen et al., 2021). In addition, high plasticity and genotypic variation lead to an excellent adaptation to rapidly changing environments.

4.6. Conclusion

Drought-related traits associated with the capacity to withstand xylem embolism have a strong relationship with both evolutionary histories and bioclimatic variables, while showing different functional strategies. We found evidence that some families could expand ligneously under increasing drought conditions due to their long-term adaptation to drought and different environmental conditions (e.g., *Acer*), whereas other families may favour trait plasticity to drought response (e.g., *Betula*). This plasticity should further be studied, especially with other drought-related traits such as rooting depth and leaf area adjustments.

A physiological explanation for the current drought-induced shift toward embolism resistance, smaller xylem vessels and denser wooded trees in temperate regions can be derived from the coordination between drought tolerance and ecological strategies. Identifying and predicting plant responses to environmental change will be greatly enhanced if we can unravel the internal

mechanisms of plant tolerance to water deficits while developing useful plant functional types for modelling and predicting plant responses to future environmental changes.

Acknowledgements

We thank the Bavarian State Institute for Viticulture and Horticulture, Veitshochheim, Germany, for granting us access to the Stutel-Arboretum facility, as well as Klaus Körber and all others involved in the 'Klimabäume Stutel' project. We thank the Botanical from the University of Würzburg for granting us access to the garden.

References

Ackerly, D., 2009. Conservatism and diversification of plant functional traits: Evolutionary rates versus phylogenetic signal. Proc. Natl. Acad. Sci. U.S.A. 106, 19699–19706. https://doi.org/10.1073/pnas.0901635106

Ackerly, D.D., 2009. Evolution, origin and age of lineages in the Californian and Mediterranean floras. Journal of Biogeography 36, 1221–1233. https://doi.org/10.1111/j.1365-2699.2009.02097.x

Ackerly, D.D., 2003. Community Assembly, Niche Conservatism and Adaptive Evolution in Changing Environments. International Journal of Plant Sciences 164, S165–S184. https://doi.org/10.1086/368401

Aitken, S.N., Yeaman, S., Holliday, J.A., Wang, T., Curtis-McLane, S., 2008. Adaptation, migration or extirpation: climate change outcomes for tree populations: Climate change outcomes for tree populations. Evolutionary Applications 1, 95–111. https://doi.org/10.1111/j.1752-4571.2007.00013.x

Alberto, F.J., Derory, J., Boury, C., Frigerio, J.-M., Zimmermann, N.E., Kremer, A., 2013. Imprints of Natural Selection Along Environmental Gradients in Phenology-Related Genes of *Quercus petraea*. Genetics 195, 495–512. https://doi.org/10.1534/genetics.113.153783

Allen, C.D., Macalady, A.K., Chenchouni, H., Bachelet, D., McDowell, N., Vennetier, M., Kitzberger, T., Rigling, A., Breshears, D.D., Hogg, E.H. (Ted), Gonzalez, P., Fensham, R., Zhang, Z., Castro, J., Demidova, N., Lim, J.-H., Allard, G., Running, S.W., Semerci, A., Cobb, N., 2010. A global overview of drought and heat-induced tree mortality reveals emerging climate change risks for forests. Forest Ecology and Management 259, 660–684. https://doi.org/10.1016/j.foreco.2009.09.001

Baas, P., Ewers, F.W., Davis, S.D., Wheeler, E.A., 2004. Evolution of xylem physiology, in: The Evolution of Plant Physiology. Elsevier, pp. 273–295. https://doi.org/10.1016/B978-012339552-8/50016-0

Baruch, Z., Jones, A.R., Hill, K.E., McInerney, F.A., Blyth, C., Caddy-Retalic, S., Christmas, M.J., Gellie, N.J.C., Lowe, A.J., Martin-Fores, I., Nielson, K.E., Breed, M.F., 2018. Functional acclimation across microgeographic scales in Dodonaea viscosa. AoB PLANTS 10. https://doi.org/10.1093/aobpla/ply029

Blackman, C.J., Aspinwall, M.J., Tissue, D.T., Rymer, P.D., 2017. Genetic adaptation and phenotypic plasticity contribute to greater leaf hydraulic tolerance in response to drought in warmer climates. Tree Physiology 37, 583–592. https://doi.org/10.1093/treephys/tpx005

Blackman, C.J., Brodribb, T.J., Jordan, G.J., 2012. Leaf hydraulic vulnerability influences species' bioclimatic limits in a diverse group of woody angiosperms. Oecologia 168, 1–10. https://doi.org/10.1007/s00442-011-2064-3

Blackman, C.J., Gleason, S.M., Chang, Y., Cook, A.M., Laws, C., Westoby, M., 2014. Leaf hydraulic vulnerability to drought is linked to site water availability across a broad range of species and climates. Annals of Botany 114, 435–440. https://doi.org/10.1093/aob/mcu131

Brodribb, T.J., Cochard, H., 2009. Hydraulic Failure Defines the Recovery and Point of Death in Water-Stressed Conifers. Plant Physiology 149, 575–584. https://doi.org/10.1104/pp.108.129783

Brodribb, T.J., McAdam, S.A.M., Jordan, G.J., Martins, S.C.V., 2014. Conifer species adapt to low-rainfall climates by following one of two divergent pathways. Proc. Natl. Acad. Sci. U.S.A. 111, 14489–14493. https://doi.org/10.1073/pnas.1407930111

Burnham, K.P., Anderson, D.R. (Eds.), 2004a. Model Selection and Multimodel Inference. Springer New York, New York, NY. https://doi.org/10.1007/b97636

Burnham, K.P., Anderson, D.R., 2004b. Multimodel Inference: Understanding AIC and BIC in Model Selection. Sociological Methods & Research 33, 261–304. https://doi.org/10.1177/0049124104268644

Butler, M.A., King, A.A., 2004. Phylogenetic Comparative Analysis: A Modeling Approach for Adaptive Evolution. The American Naturalist 164, 683–695. https://doi.org/10.1086/426002

Cavender-Bares, J., Ackerly, D.D., Baum, D.A., Bazzaz, F.A., 2004. Phylogenetic Overdispersion in Floridian Oak Communities. The American Naturalist 163, 823–843. https://doi.org/10.1086/386375

Chacón-Madrigal, E., Wanek, W., Hietz, P., Dullinger, S., 2018. Traits indicating a conservative resource strategy are weakly related to narrow range size in a group of neotropical trees. Perspectives in Plant Ecology, Evolution and Systematics 32, 30–37. https://doi.org/10.1016/j.ppees.2018.01.003

Chave, J., Coomes, D., Jansen, S., Lewis, S.L., Swenson, N.G., Zanne, A.E., 2009. Towards a worldwide wood economics spectrum. Ecology Letters 12, 351–366. https://doi.org/10.1111/j.1461-0248.2009.01285.x

Chave, J., Muller-Landau, H.C., Baker, T.R., Easdale, T.A., Steege, H. ter, Webb, C.O., 2006. Regional and phylogenetic variation of wood density across 2456 neotropical tree species. Ecological Applications 16, 2356–2367. https://doi.org/10.1890/1051-0761(2006)016[2356:RAPVOW]2.0.CO;2

Chernomor, O., von Haeseler, A., Minh, B.Q., 2016. Terrace Aware Data Structure for Phylogenomic Inference from Supermatrices. Syst Biol 65, 997–1008. https://doi.org/10.1093/sysbio/syw037

Choat, B., Brodribb, T.J., Brodersen, C.R., Duursma, R.A., López, R., Medlyn, B.E., 2018. Triggers of tree mortality under drought. Nature 558, 531–539. https://doi.org/10.1038/s41586-018-0240-x

Choat, B., Sack, L., Holbrook, N.M., 2007. Diversity of hydraulic traits in nine *Cordia* species growing in tropical forests with contrasting precipitation. New Phytologist 175, 686–698. https://doi.org/10.1111/j.1469-8137.2007.02137.x

Cochard, H., Damour, G., Bodet, C., Tharwat, I., Poirier, M., Améglio, T., 2005. Evaluation of a new centrifuge technique for rapid generation of xylem vulnerability curves. Physiologia Plantarum 124, 410–418. https://doi.org/10.1111/j.1399-3054.2005.00526.x

Cochard, H., Hölttä, T., Herbette, S., Delzon, S., Mencuccini, M., 2009. New Insights into the Mechanisms of Water-Stress-Induced Cavitation in Conifers. Plant Physiol. 151, 949–954. https://doi.org/10.1104/pp.109.138305

Cochard, H., Martin, R., Gross, P., Bogeat-Triboulot, M.B., 2000. Temperature effects on hydraulic conductance and water relations of Quercus robur L. Journal of Experimental Botany 51, 1255–1259. https://doi.org/10.1093/jexbot/51.348.1255

Coelho de Souza, F., Dexter, K.G., Phillips, O.L., Brienen, R.J.W., Chave, J., Galbraith, D.R., Lopez Gonzalez, G., Monteagudo Mendoza, A., Pennington, R.T., Poorter, L., Alexiades, M., Álvarez-Dávila, E., Andrade, A., Aragão, L.E.O.C., Araujo-Murakami, A., Arets, E.J.M.M., Aymard C, G.A., Baraloto, C., Barroso, J.G., Bonal, D., Boot, R.G.A., Camargo, J.L.C., Comiskey, J.A., Valverde, F.C., de Camargo, P.B., Di Fiore, A., Elias, F., Erwin, T.L., Feldpausch, T.R., Ferreira, L., Fyllas, N.M., Gloor, E., Herault, B., Herrera, R., Higuchi, N., Honorio Coronado, E.N., Killeen, T.J., Laurance, W.F., Laurance, S., Lloyd, J., Lovejoy, T.E., Malhi, Y., Maracahipes, L., Marimon, B.S., Marimon-Junior, B.H., Mendoza, C., Morandi, P., Neill, D.A., Vargas, P.N., Oliveira, E.A., Lenza, E., Palacios, W.A., Peñuela-Mora, M.C., Pipoly, J.J., Pitman, N.C.A., Prieto, A., Quesada, C.A., Ramirez-Angulo, H., Rudas, A., Ruokolainen, K., Salomão, R.P., Silveira, M., Stropp, J., ter Steege, H., Thomas-Caesar, R., van der Hout, P., van der Heijden, G.M.F., van der Meer, P.J., Vasquez, R.V., Vieira, S.A., Vilanova, E., Vos, V.A., Wang, O., Young, K.R., Zagt, R.J., Baker, T.R., 2016. Evolutionary heritage influences Amazon tree ecology. Proc. R. Soc. B. 283, 20161587. https://doi.org/10.1098/rspb.2016.1587

Cressler, C.E., Butler, M.A., King, A.A., 2015. Detecting Adaptive Evolution in Phylogenetic Comparative Analysis Using the Ornstein–Uhlenbeck Model. Syst Biol 64, 953–968. https://doi.org/10.1093/sysbio/syv043

Davies, T.J., Wolkovich, E.M., Kraft, N.J.B., Salamin, N., Allen, J.M., Ault, T.R., Betancourt, J.L., Bolmgren, K., Cleland, E.E., Cook, B.I., Crimmins, T.M., Mazer, S.J., McCabe, G.J., Pau, S., Regetz, J., Schwartz, M.D., Travers, S.E., 2013. Phylogenetic conservatism in plant phenology. J Ecol 101, 1520–1530. https://doi.org/10.1111/1365-2745.12154

De Oliveira, G.L., de Oliveira, M.E., de Oliveira Macêdo, E., Andrade, A.C., Edvan, R.L., 2020. Effect of shading and canopy height on pasture of Andropogon gayanus in silvopastoral system. Agroforest Syst 94, 953–962. https://doi.org/10.1007/s10457-019-00458-5

Díaz, S., Kattge, J., Cornelissen, J.H.C., Wright, I.J., Lavorel, S., Dray, S., Reu, B., Kleyer, M., Wirth, C., Colin Prentice, I., Garnier, E., Bönisch, G., Westoby, M., Poorter, H., Reich, P.B., Moles, A.T., Dickie, J., Gillison, A.N., Zanne, A.E., Chave, J., Joseph Wright, S., Sheremet'ev, S.N., Jactel, H., Baraloto, C., Cerabolini, B., Pierce, S., Shipley, B., Kirkup, D., Casanoves, F., Joswig, J.S., Günther,

A., Falczuk, V., Rüger, N., Mahecha, M.D., Gorné, L.D., 2016. The global spectrum of plant form and function. Nature 529, 167–171. https://doi.org/10.1038/nature16489

Edwards, E.J., Donoghue, M.J., 2013. Is it easy to move and easy to evolve? Evolutionary accessibility and adaptation. Journal of Experimental Botany 64, 4047–4052. https://doi.org/10.1093/jxb/ert220

Enquist, B.J., Condit, R., Peet, R.K., Schildhauer, M., Thiers, B.M., 2016. Cyberinfrastructure for an integrated botanical information network to investigate the ecological impacts of global climate change on plant biodiversity (preprint). PeerJ Preprints. https://doi.org/10.7287/peerj.preprints.2615v2

Esperon-Rodriguez, M., Rymer, P.D., Power, S.A., Challis, A., Marchin, R.M., Tjoelker, M.G., 2020. Functional adaptations and trait plasticity of urban trees along a climatic gradient. Urban Forestry & Urban Greening 54, 126771. https://doi.org/10.1016/j.ufug.2020.126771

Felsenstein, J., 1973. Maximum-likelihood estimation of evolutionary trees from continuous characters. Am J Hum Genet 25, 471–492.

Fick, S.E., Hijmans, R.J., 2017. WorldClim 2: new 1-km spatial resolution climate surfaces for global land areas. Int. J. Climatol 37, 4302–4315. https://doi.org/10.1002/joc.5086

Freckleton, R.P., Harvey, P.H., Pagel, M., 2002. Phylogenetic Analysis and Comparative Data: A Test and Review of Evidence. The American Naturalist 160, 712–726. https://doi.org/10.1086/343873

Gleason, S.M., Blackman, C.J., Chang, Y., Cook, A.M., Laws, C.A., Westoby, M., 2016. Weak coordination among petiole, leaf, vein and gas-exchange traits across Australian angiosperm species and its possible implications. Ecol Evol 6, 267–278. https://doi.org/10.1002/ece3.1860

Guan, X., Pereira, L., McAdam, S.A.M., Cao, K., Jansen, S., 2021. No gas source, no problem: Proximity to pre-existing embolism and segmentation affect embolism spreading in angiosperm xylem by gas diffusion. Plant Cell Environ 44, 1329–1345. https://doi.org/10.1111/pce.14016

Guerin, G.R., Wen, H., Lowe, A.J., 2012. Leaf morphology shift linked to climate change. Biol. Lett. 8, 882–886. https://doi.org/10.1098/rsbl.2012.0458

Gustafsson, L., 1986. Lifetime Reproductive Success and Heritability: Empirical Support for Fisher's Fundamental Theorem. The American Naturalist 128, 761–764. https://doi.org/10.1086/284601

Hacke, U.G., Sperry, J.S., n.d. Functional and ecological xylem anatomy 19.

Hacke, U.G., Sperry, J.S., Wheeler, J.K., Castro, L., 2006. Scaling of angiosperm xylem structure with safety and efficiency. Tree Physiology 26, 689–701. https://doi.org/10.1093/treephys/26.6.689

Hacke, U.G., Spicer, R., Schreiber, S.G., Plavcová, L., 2017. An ecophysiological and developmental perspective on variation in vessel diameter: Variation in xylem vessel diameter. Plant, Cell & Environment 40, 831–845. https://doi.org/10.1111/pce.12777

Harmon, L.J., Losos, J.B., Jonathan Davies, T., Gillespie, R.G., Gittleman, J.L., Bryan Jennings, W., Kozak, K.H., McPeek, M.A., Moreno-Roark, F., Near, T.J., Purvis, A., Ricklefs, R.E., Schluter, D., Schulte II, J.A., Seehausen, O., Sidlauskas, B.L., Torres-Carvajal, O., Weir, J.T., Mooers, A.Ø., 2010. Early bursts of body size and shape evolution are rare in comparative data. Evolution no-no. https://doi.org/10.1111/j.1558-5646.2010.01025.x

Heineman, K.D., Turner, B.L., Dalling, J.W., 2016. Variation in wood nutrients along a tropical soil fertility gradient. New Phytol 211, 440–454. https://doi.org/10.1111/nph.13904

Herberich, E., Sikorski, J., Hothorn, T., 2010. A Robust Procedure for Comparing Multiple Means under Heteroscedasticity in Unbalanced Designs. PLoS ONE 5, e9788. https://doi.org/10.1371/journal.pone.0009788

Holstein, J., Häuser, C.L., 2005. Die Global Biodiversity Information Facility (GBIF) - Struktur, Aufgaben und Ziele. contrib.entomol. 55, 421–431. https://doi.org/10.21248/contrib.entomol.55.2.421-431

Houle, D., 1992. Comparing evolvability and variability of quantitative traits. Genetics 130, 195–204. https://doi.org/10.1093/genetics/130.1.195

Jansen, S., Klepsch, M., Li, S., Kotowska, M.M., Schiele, S., Zhang, Y., Schenk, H.J., 2018. Challenges in understanding air-seeding in angiosperm xylem. Acta Hortic. 13–20. https://doi.org/10.17660/ActaHortic.2018.1222.3

Kaack, L., Weber, M., Isasa, E., Karimi, Z., Li, S., Pereira, L., Trabi, C.L., Zhang, Y., Schenk, H.J., Schuldt, B., Schmidt, V., Jansen, S., 2021. Pore constrictions in intervessel pit membranes provide a mechanistic explanation for xylem embolism resistance in angiosperms. New Phytol 230, 1829–1843. https://doi.org/10.1111/nph.17282

Kaack, L., Weber, M., Isasa, E., Karimi, Z., Li, S., Pereira, L., Trabi, C.L., Zhang, Y., Schenk, H.J., Schuldt, B., Schmidt, V., Jansen, S., 2020. Pore constrictions in intervessel pit membranes reduce the risk of embolism spreading in angiosperm xylem (preprint). Plant Biology. https://doi.org/10.1101/2020.10.19.345413

Kalyaanamoorthy, S., Minh, B.Q., Wong, T.K.F., von Haeseler, A., Jermiin, L.S., 2017. ModelFinder: fast model selection for accurate phylogenetic estimates. Nat Methods 14, 587–589. https://doi.org/10.1038/nmeth.4285

Katoh, K., Rozewicki, J., Yamada, K.D., 2019. MAFFT online service: multiple sequence alignment, interactive sequence choice and visualization. Briefings in Bioinformatics 20, 1160–1166. https://doi.org/10.1093/bib/bbx108

Katoh, K., Standley, D.M., 2014. MAFFT: Iterative Refinement and Additional Methods, in: Russell, D.J. (Ed.), Multiple Sequence Alignment Methods, Methods in Molecular Biology. Humana Press, Totowa, NJ, pp. 131–146. https://doi.org/10.1007/978-1-62703-646-7_8

Lamy, J., Delzon, S., Bouche, P.S., Alia, R., Vendramin, G.G., Cochard, H., Plomion, C., 2014. Limited genetic variability and phenotypic plasticity detected for cavitation resistance in a M editerranean pine. New Phytol 201, 874–886. https://doi.org/10.1111/nph.12556

Larter, M., Pfautsch, S., Domec, J., Trueba, S., Nagalingum, N., Delzon, S., 2017. Aridity drove the evolution of extreme embolism resistance and the radiation of conifer genus *Callitris*. New Phytol 215, 97–112. https://doi.org/10.1111/nph.14545

Levionnois, S., Jansen, S., Wandji, R.T., Beauchêne, J., Ziegler, C., Coste, S., Stahl, C., Delzon, S., Authier, L., Heuret, P., 2021. Linking drought-induced xylem embolism resistance to wood anatomical traits in Neotropical trees. New Phytol 229, 1453–1466. https://doi.org/10.1111/nph.16942

Lobo, A., Torres-Ruiz, J.M., Burlett, R., Lemaire, C., Parise, C., Francioni, C., Truffaut, L., Tomášková, I., Hansen, J.K., Kjær, E.D., Kremer, A., Delzon, S., 2018. Assessing inter- and intraspecific variability of xylem vulnerability to embolism in oaks. Forest Ecology and Management 424, 53–61. https://doi.org/10.1016/j.foreco.2018.04.031

Maherali, H., Moura, C.F., Caldeira, M.C., Willson, C.J., Jackson, R.B., 2006. Functional coordination between leaf gas exchange and vulnerability to xylem cavitation in temperate forest trees. Plant Cell Environ 29, 571–583. https://doi.org/10.1111/j.1365-3040.2005.01433.x

Maherali, H., Pockman, W.T., Jackson, R.B., 2004. Adaptative variation in the vulnerability of woody plants to xylem cavitation. Ecology 85, 2184–2199. https://doi.org/10.1890/02-0538

Markesteijn, L., Poorter, L., Paz, H., Sack, L., Bongers, F., 2011. Ecological differentiation in xylem cavitation resistance is associated with stem and leaf structural traits: Vulnerability to cavitation of tropical dry forest tree species. Plant, Cell & Environment 34, 137–148. https://doi.org/10.1111/j.1365-3040.2010.02231.x

Martínez-Vilalta, J., Mencuccini, M., Vayreda, J., Retana, J., 2010. Interspecific variation in functional traits, not climatic differences among species ranges, determines demographic rates across 44 temperate and Mediterranean tree species: Determinants of demographic rates across species. Journal of Ecology 98, 1462–1475. https://doi.org/10.1111/j.1365-2745.2010.01718.x

Martins, E.P., Hansen, T.F., 1997. Phylogenies and the Comparative Method: A General Approach to Incorporating Phylogenetic Information into the Analysis of Interspecific Data. The American Naturalist 149, 646–667. https://doi.org/10.1086/286013

Martin-StPaul, N., Delzon, S., Cochard, H., 2017. Plant resistance to drought depends on timely stomatal closure. Ecol Lett 20, 1437–1447. https://doi.org/10.1111/ele.12851

Matusick, G., Ruthrof, K.X., Brouwers, N.C., Dell, B., Hardy, G.St.J., 2013. Sudden forest canopy collapse corresponding with extreme drought and heat in a mediterranean-type eucalypt forest in southwestern Australia. Eur J Forest Res 132, 497–510. https://doi.org/10.1007/s10342-013-0690-5

McDowell, N.G., Allen, C.D., Anderson-Teixeira, K., Aukema, B.H., Bond-Lamberty, B., Chini, L., Clark, J.S., Dietze, M., Grossiord, C., Hanbury-Brown, A., Hurtt, G.C., Jackson, R.B., Johnson, D.J., Kueppers, L., Lichstein, J.W., Ogle, K., Poulter, B., Pugh, T.A.M., Seidl, R., Turner, M.G., Uriarte, M., Walker, A.P., Xu, C., 2020. Pervasive shifts in forest dynamics in a changing world. Science 368, eaaz9463. https://doi.org/10.1126/science.aaz9463

Méndez-Alonzo, R., Paz, H., Zuluaga, R.C., Rosell, J.A., Olson, M.E., 2012. Coordinated evolution of leaf and stem economics in tropical dry forest trees. Ecology 93, 2397–2406. https://doi.org/10.1890/11-1213.1

Minh, B.Q., Schmidt, H.A., Chernomor, O., Schrempf, D., Woodhams, M.D., von Haeseler, A., Lanfear, R., 2020. IQ-TREE 2: New Models and Efficient Methods for Phylogenetic Inference in the Genomic Era. Molecular Biology and Evolution 37, 1530–1534. https://doi.org/10.1093/molbev/msaa015

Mousseau, T.A., Roff, D.A., 1987. Natural selection and the heritability of fitness components. Heredity 59, 181–197. https://doi.org/10.1038/hdy.1987.113

Nardini, A., Battistuzzo, M., Savi, T., 2013. Shoot desiccation and hydraulic failure in temperate woody angiosperms during an extreme summer drought. New Phytol 200, 322–329. https://doi.org/10.1111/nph.12288

Nardini, A., Pedà, G., Rocca, N.L., 2012. Trade-offs between leaf hydraulic capacity and drought vulnerability: morpho-anatomical bases, carbon costs and ecological consequences. New Phytol 196, 788–798. https://doi.org/10.1111/j.1469-8137.2012.04294.x

Nola, P., Bracco, F., Assini, S., von Arx, G., Castagneri, D., 2020. Xylem anatomy of Robinia pseudoacacia L. and Quercus robur L. is differently affected by climate in a temperate alluvial forest. Annals of Forest Science 77, 8. https://doi.org/10.1007/s13595-019-0906-z

Ogle, K., Barber, J.J., Willson, C., Thompson, B., 2009. Hierarchical statistical modeling of xylem vulnerability to cavitation. New Phytologist 182, 541–554. https://doi.org/10.1111/j.1469-8137.2008.02760.x

Oksanen, E., 2021. Birch as a Model Species for the Acclimation and Adaptation of Northern Forest Ecosystem to Changing Environment. Front. For. Glob. Change 4, 682512. https://doi.org/10.3389/ffgc.2021.682512

Okonechnikov, K., Golosova, O., Fursov, M., 2012. Unipro UGENE: a unified bioinformatics toolkit. Bioinformatics 28, 1166–1167. https://doi.org/10.1093/bioinformatics/bts091

Pagel, M., 1999. Inferring the historical patterns of biological evolution. Nature 401, 877–884. https://doi.org/10.1038/44766

Paligi, S.S., Link, R.M., Isasa, E., Bittencourt, P., Cabral, J.S., Jansen, S., Oliveira, R.S., Pereira, L., Schuldt, B., 2021. Accuracy of the pneumatic method for estimating xylem vulnerability to embolism in temperate diffuse-porous tree species (preprint). Plant Biology. https://doi.org/10.1101/2021.02.15.431295

Pammenter, N.W., Van der Willigen, C., 1998. A mathematical and statistical analysis of the curves illustrating vulnerability of xylem to cavitation. Tree Physiology 18, 589–593. https://doi.org/10.1093/treephys/18.8-9.589

Peel, M.C., Finlayson, B.L., McMahon, T.A., 2007. Updated world map of the Ko¨ppen-Geiger climate classification. Hydrol. Earth Syst. Sci. 12.

Pennell, M.W., Eastman, J.M., Slater, G.J., Brown, J.W., Uyeda, J.C., FitzJohn, R.G., Alfaro, M.E., Harmon, L.J., 2014. geiger v2.0: an expanded suite of methods for fitting macroevolutionary models to phylogenetic trees. Bioinformatics 30, 2216–2218. https://doi.org/10.1093/bioinformatics/btu181

Pfautsch, S., Harbusch, M., Wesolowski, A., Smith, R., Macfarlane, C., Tjoelker, M.G., Reich, P.B., Adams, M.A., 2016. Climate determines vascular traits in the ecologically diverse genus *Eucalyptus*. Ecol Lett 19, 240–248. https://doi.org/10.1111/ele.12559

Pockman, W.T., Sperry, J.S., 2000. Vulnerability to xylem cavitation and the distribution of Sonoran Desert vegetation. Am. J. Bot. 87, 1287–1299. https://doi.org/10.2307/2656722

Preston, K.A., Cornwell, W.K., DeNoyer, J.L., 2006. Wood density and vessel traits as distinct correlates of ecological strategy in 51 California coast range angiosperms. New Phytologist 170, 807–818. https://doi.org/10.1111/j.1469-8137.2006.01712.x

Reich, P.B., 2014. The world-wide 'fast-slow' plant economics spectrum: a traits manifesto. J Ecol 102, 275–301. https://doi.org/10.1111/1365-2745.12211

Schenk, H.J., Steppe, K., Jansen, S., 2015. Nanobubbles: a new paradigm for air-seeding in xylem. Trends in Plant Science 20, 199–205. https://doi.org/10.1016/j.tplants.2015.01.008

Schneider, C.A., Rasband, W.S., Eliceiri, K.W., 2012. NIH Image to ImageJ: 25 years of image analysis. Nature Methods 9, 671–675. https://doi.org/10.1038/nmeth.2089

Skelton, R.P., West, A.G., Dawson, T.E., 2015. Predicting plant vulnerability to drought in biodiverse regions using functional traits. Proc. Natl. Acad. Sci. U.S.A. 112, 5744–5749. https://doi.org/10.1073/pnas.1503376112

Sperry, J.S., Hacke, U.G., Pittermann, J., 2006. Size and function in conifer tracheids and angiosperm vessels. American Journal of Botany 93, 1490–1500. https://doi.org/10.3732/ajb.93.10.1490

Sperry, J.S., Nichols, K.L., Sullivan, J.E.M., Eastlack, S.E., 1994. Xylem Embolism in Ring-Porous, Diffuse-Porous and Coniferous Trees of Northern Utah and Interior Alaska. Ecology 75, 1736–1752. https://doi.org/10.2307/1939633

Stotz, G.C., Salgado-Luarte, C., Escobedo, V.M., Valladares, F., Gianoli, E., 2021. Global trends in phenotypic plasticity of plants. Ecology Letters 24, 2267–2281. https://doi.org/10.1111/ele.13827

Swenson, N.G., Enquist, B.J., 2007. Ecological and evolutionary determinants of a key plant functional trait: wood density and its community-wide variation across latitude and elevation. American Journal of Botany 94, 451–459. https://doi.org/10.3732/ajb.94.3.451

The GIMP Development Team, 2019. *GIMP*, Available at: https://www.gimp.org.

Torres-Ruiz, J.M., Jansen, S., Choat, B., McElrone, A.J., Cochard, H., Brodribb, T.J., Badel, E., Burlett, R., Bouche, P.S., Brodersen, C.R., Li, S., Morris, H., Delzon, S., 2015. Direct X-Ray Microtomography Observation Confirms the Induction of Embolism upon Xylem Cutting under Tension. Plant Physiol. 167, 40–43. https://doi.org/10.1104/pp.114.249706

Tyree, M.T., Zimmermann, M.H., 2002. Hydraulic Architecture of Whole Plants and Plant Performance, in: Xylem Structure and the Ascent of Sap, Springer Series in Wood Science. Springer Berlin Heidelberg, Berlin, Heidelberg, pp. 175–214. https://doi.org/10.1007/978-3-662-04931-0_6

Venturas, M.D., Sperry, J.S., Hacke, U.G., 2017. Plant xylem hydraulics: What we understand, current research and future challenges. J. Integr. Plant Biol. 59, 356–389. https://doi.org/10.1111/jipb.12534

Villéger, S., Grenouillet, G., Suc, V., Brosse, S., 2012. Intra- and interspecific differences in nutrient recycling by European freshwater fish: *Nutrient recycling by European fish*. Freshwater Biology 57, 2330–2341. https://doi.org/10.1111/fwb.12009

Wiens, J.J., Ackerly, D.D., Allen, A.P., Anacker, B.L., Buckley, L.B., Cornell, H.V., Damschen, E.I., Jonathan Davies, T., Grytnes, J.-A., Harrison, S.P., Hawkins, B.A., Holt, R.D., McCain, C.M., Stephens, P.R., 2010. Niche conservatism as an emerging principle in ecology and conservation biology: Niche conservatism, ecology and conservation. Ecology Letters 13, 1310–1324. https://doi.org/10.1111/j.1461-0248.2010.01515.x

Xu, G.-Q., Farrell, C., Arndt, S.K., 2022. Climate of origin has no influence on drought adaptive traits and the drought responses of a widely distributed polymorphic shrub. Tree Physiology 42, 86–98. https://doi.org/10.1093/treephys/tpab085

Yi, C., Hendrey, G., Niu, S., McDowell, N., Allen, C.D., 2022. Tree mortality in a warming world: causes, patterns and implications. Environ. Res. Lett. 17, 030201. https://doi.org/10.1088/1748-9326/ac507b

Zenni, R.D., Lamy, J.-B., Lamarque, L.J., Porté, A.J., 2014. Adaptive evolution and phenotypic plasticity during naturalization and spread of invasive species: implications for tree invasion biology. Biol Invasions 16, 635–644. https://doi.org/10.1007/s10530-013-0607-8

Zimmermann, J., Link, R.M., Hauck, M., Leuschner, C., Schuldt, B., 2021. 60-year record of stem xylem anatomy and related hydraulic modification under increased summer drought in ring- and diffuse-porous temperate broad-leaved tree species. Trees 35, 919–937. https://doi.org/10.1007/s00468-021-02090-2

Part 3

General discussion

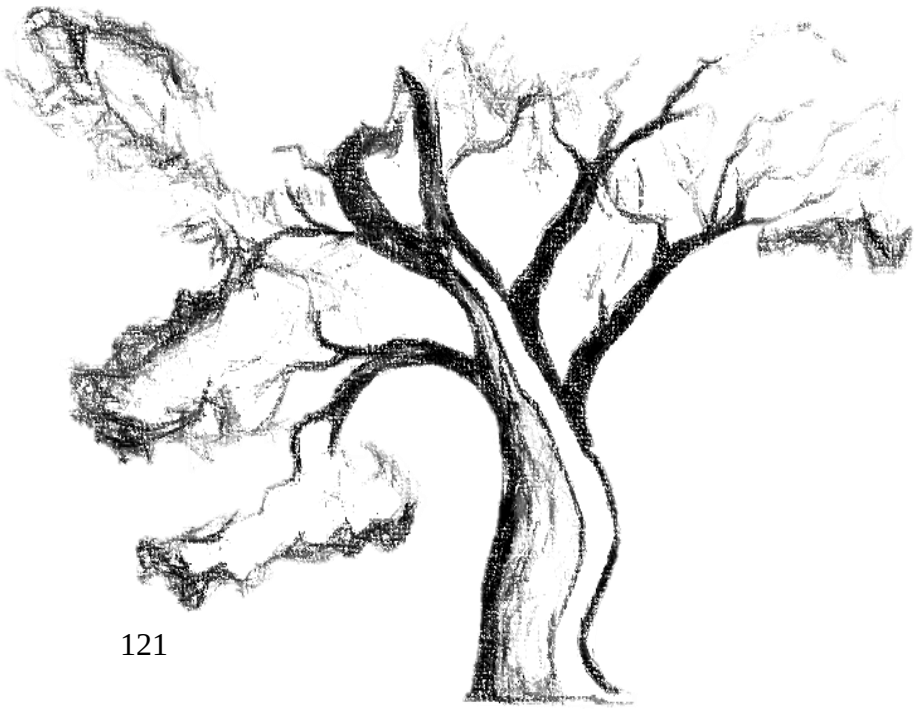

5. Synthesis

In the following, I will start with a general discussion, where I summarize the main findings from the three manuscripts presented in this dissertation. Thereafter, I discuss the outcome of my work based on the current state of knowledge regarding plant ecophysiology related to drought-induced tree embolism. As a final note, I provide an overview of the research and provide my overall conclusions.

The present work was motivated by the following research objectives (Section 1.5):

- plant drought-induced tree embolism trait relationships (Chapter 1)
- calibration of widely applicable methods by estimating xylem embolism resistance traits using a fast accurate technique (Chapter 2)
- evolution and adaptation of drought-related traits due to climate variation (Chapter 3)

5.1. Summary of present findings and discussion

In the previous chapters, I examined traits associated with drought-induced embolism in temperate species. At first, I started by exploring whether wood anatomical attributes correlated with embolism resistance. Then I showed that vessel dimensions and embolism resistance are related. However, this cannot be explained by a common scaling of both traits' values, but rather by many structural parameters of the pits. I also showed that differences in the studied ranges of trait variables, missing covariates and conflation of different scales of aggregation may reinforce existing controversies about vessel diameter and embolism resistance relationships.
In a following step, I explored the possibility of the fast, precise and unexpansive method, the pneumatic method. I verified that the xylem embolism resistance measured by the pneumatic method and the flow centrifuge method is comparable. Furthermore, I found that, in some instances, there is an existing potential artefact associated with xylem water potential determination and species-specific drying behavior that requires further study.
Lastly, to determine how drought-related traits are phylogenetically controlled and their associations with ecological variables, I conducted time-resolved phylogenies and generalized least squares regressions. According to my analyses, traits which are associated with xylem embolism resistance have a strong relationship with both evolutionary histories and bioclimatic factors, depending on the studied families. In that sense, it supports our knowledge of how distinct families adopt different strategies.
Finally, I discuss my overall conclusions and an overview of the research. Hence, in the following sections, I will discuss the implications of leaf traits and tree architecture traits in diffuse-porous angiosperm trees that are associated with embolism. In the conclusion of my thesis, I will give a

short overview of all my fundings, how they can be improved by further work and how to contribute to develop mechanistic models for prediction of xylem safety.

5.2. Using diverse tree predictor traits to enhance drought-induced embolism research

In Chapter 1, I showed that, vulnerability to drought-induced embolism is a major trait for assessment of species' drought resistance since it is linked to major hydraulic failure (Brodribb and Cochard 2009, Brodribb et al. 2009). In this study, we therefore provided unique reliable data for xylem embolism resistance in a selection of diffuse-porous angiosperm tree species.
As hypothesized, our analysis showed that easy measurable wood anatomical traits are related to embolism resistance. Nevertheless, there is a wide range of traits linked to drought induced-embolism, such as leaf trait and structural features. A combination of trait measurements concerning the fields of wood anatomy, tree structure, hydraulics, leaf physiology and anatomy, would further contribute to a better understanding of the strategies of trees with respect to drought-tolerance.

5.2.1. Drought-induced embolism associated with leaf measurements

It has been particularly difficult to model and predict drought-induced embolism due to uncertainty regarding traits and mechanisms underlying tree death (Powell 2013, McDowell 2011). It is also possible to determine an individual species' embolism level based on the hydraulic, leaf and stomatal characteristics of the plant (Anderegg et al. 2016, Rosas et al. 2021). As the organs at the interface with the atmosphere, leaves have evolved multiple properties to mitigate evaporative demand (Sack et al. 2015).
A leaf's hydraulic resistance can account for 30% or more of the whole-plant hydraulic resistance (Sack and Holbrook 2006). Through transpiration, leaves lose water as their stomata open to capture CO_2 for photosynthesis, which needs to be replaced by flow through the hydraulic system. The turgor of guard- and adjacent-cells play a crucial role in regulating water flow within the cells, determines stomatal aperture and play a role in cellular structural integrity, metabolism and whole-plant performance (Kramer and Boyer 1995). These water relations are important and measured as water potential, which consists of two components: pressure (turgor) and osmotic potential. Turgor loss point defines the leaf water potential below which the plant cannot take up sufficient water to recover from wilting and it has been described as a functional trait clarifying the species-level drought responses and biogeographic trends (Barlett et al. 2012). It also has been proposed that this trait quantifies plants' and leaves' drought tolerance (Sack et al. 2003).
In addition, leaf turgor loss and stomatal closure thresholds were observed at leaf water potentials just above P_{50} stem water potential, suggesting that stomatal closure plays a protective role in

preventing extensive embolisms from occurring in the stem (Jones & Sutherland 1991, Sparks & Black 1999).

A trade-off between xylem cavitation risk and leaf gas exchange is thought to be responsible for the tight coordination of leaf gas exchange and stem hydraulics (Tyree & Sperry 1988, Sperry et al. 2002). Therefore, another relevant parameter is the pressure safety margins within the xylem, which is identified as the difference between Ψ_{50}/ Ψ_{88} and the minimum water potential trees experienced and between single tree compartments (e.g., leaf – twig) are imperative for tree survival (Johnson et al. 2012).

To sum up, stomatal closure before embolism formation is another fundamental component of drought tolerance in plants (Delzon and Cochard 2014, Martin-StPaul et al. 2017). With early stomatal closure, plants are able to reduce water loss and maintain a positive safety margin between water potential and water potential-inducing embolism, which prevents water deficit-induced damage (Hochberg et al. 2017, Skelton et al. 2017). Nevertheless, long droughts associated with high temperatures may ultimately lead to complete stomatal closure and even tightly closed stomata can leak water if evaporative demand is too high (e.g., through cuticular conductance; Duursma et al. 2019).

These different hypotheses, linking to different potential mechanisms. Our finding in Chapter 1 and Fig. 5.1 suggested the existing link between multiple traits determinants and embolism resistance. In this view, embolism resistance results from the association of several anatomical and physiologic traits inter-related together. Finally Studying at different organ level such as at the roots level and integrating it into our findings is important, as well as understanding the interactions with the environment (e.g., soil-plant interactions).

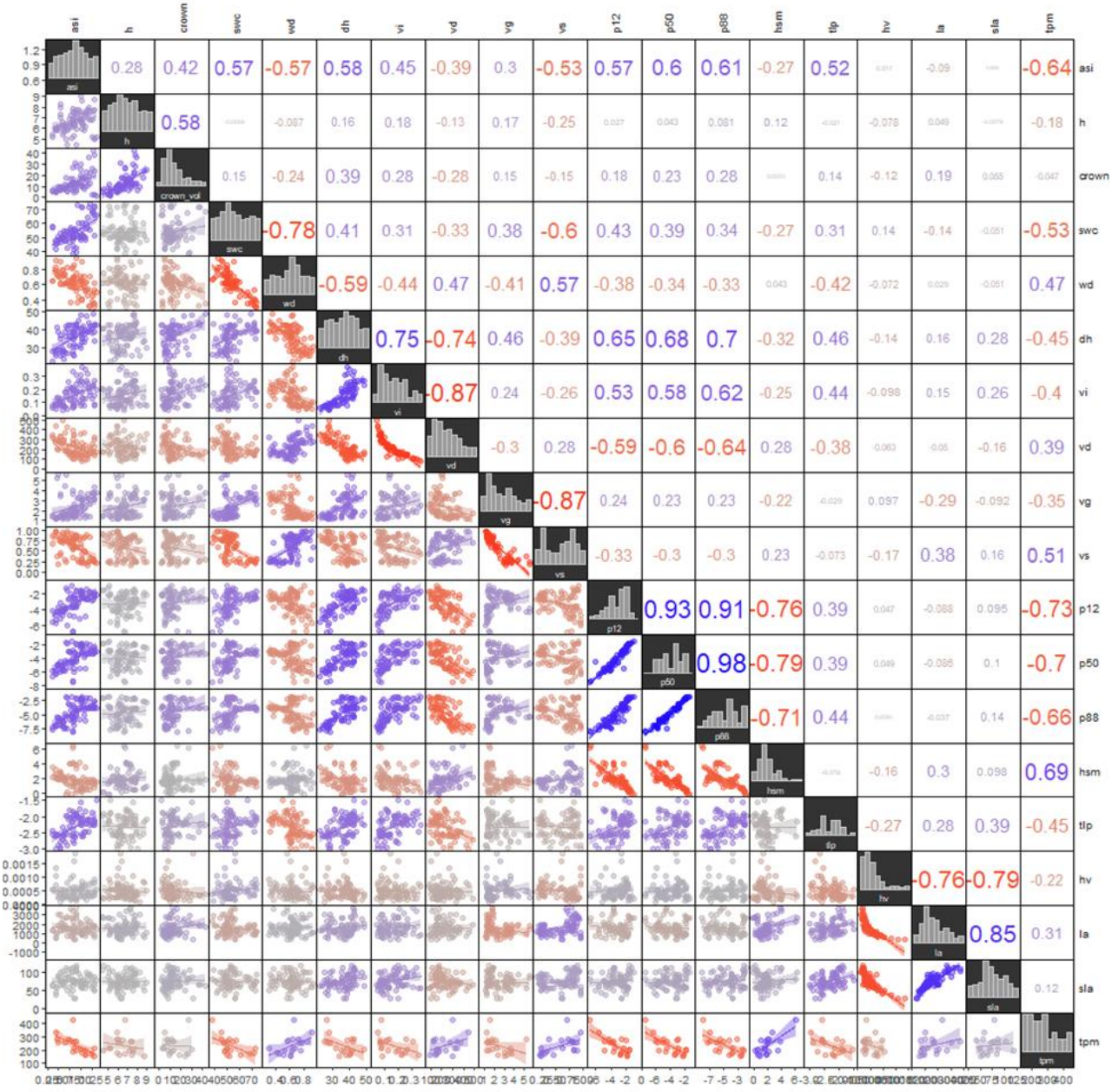

Figure 5.1: Correlation matrix of the species level averages of the analysed variables. Shown are the annual stem increment (*ASI*, cm yr^{-1}), height (*H*, m), Crown volume (*Crown*, m^3), stem water content (*SWC*, %), wood density (*WD*, g cm^{-3}) , hydraulically-weighted vessel diameter (D_h, µm), vulnerability index (*VI*, $µm^2$ mm^{-2}) vessel density (V_D, n mm^{-2}), vessel grouping index (V_G), vessel solitary index (V_S), water potential at 12% loss of conductance (P_{12}, MPa), water potential at 50% loss of conductance (P_{50}, MPa), water potential at 88% loss of conductance (P_{88}, MPa), hydraulic safety margin (*HSM*, MPa), leaf turgor loss point (Ψ_{tlp}, MPa), Huber Value (*HV*), leaf area (*LA*, cm^2), leaf specific area (*SLA*; cm^2 g^{-1}), pit membrane thickness (T_{PM}, nm). The upper panel shows the Pearson correlations, the lower panel observed values overlaid with linear regression fits with 95% confidence intervals and the plot diagonal histograms for the corresponding variables. Figure created with R package corrmorant v. 0.0.0.9007 (https://github.com/r-link/corrmorant).

5.2.2. Tree architecture and seed dispersal mechanism as drought-related trait

5.2.2.1. Tree architecture study

The purpose of this section is to present the preliminary results of a study carried out at the Stutel-Arboretum which quantified relationship between xylem safety and tree structural complexity from Terrestrial Laser Scanning. The results are part of a manuscript, Dorji et al*. (in preparation) that is intended for publication in 2023. A brief discussion of theory and results is presented below.*

The results presented in Chapter 2 clearly demonstrate a relationship between embolism resistance and vessel size across species. An explanation of this link cannot be found by comparing the characteristics of pit membranes to both traits. The study of embolism resistance involves a complex relationship between several drought-related traits (Fig. 5.1).
Water relations, gas exchanges throughout the crown of trees, distribution of trees in different habitats and perhaps even the maximum height a particular species can reach can all be influenced by the hydraulic architecture of trees. It is for this reason that tree architecture should be studied.
In the general introduction (Section 1.1) it is pointed out that the structure and function of a forest ecosystem is ultimately determined by the composition and structure of its trees (West et al. 2009, Seidel et al. 2019). Furthermore, the diversity of tree species in forest stands affects the growth pace and health of forest ecosystems by varying crown sizes and light gradients (Sterck et al. 2001, Poorter et al. 2006).
The stochastic growth of a tree is the outcome of the interaction between the genetic growth plan and both the biotic and abiotic environment (Busov et al. 2008). In fact, various environmental factors influence tree shape and form, including wind (Watt et al. 2005), sunlight angle (Kuuluvainen 1992), seed distribution strategy (Dorji et al. 2021), water availability (Niinemets and Kull 1995), elevation (Barij et al. 2007) and competition (Castagneri et al. 2022).
The plasticity of tree architecture in response to environmental variables (Borchert and Slade, 1981) was described to be the outcome of an individual's drive to maximize certain ecophysiological or life-history functions, such as reproductive potential and sunlight absorption (Valladares and Niinemets 2007, Hollender and Dardick 2015).
Due to the development in light detection and ranging (LiDAR), in modelling of tree architecture and in the use of fractal analysis, tree architecture can be analysed accurately in three-dimensions (3D) (Fig. 5.2). A variety of studies have found that the study of tree structure and their form in 3D is of great importance, including functional ecology of tree drought-related traits (Section II, Chapter 1), phylogenetics (Section II, Chapter 3), ecosystem modelling (Section III, 5.3), remote sensing of forest landscapes, carbon stock computation and the suitability of urban trees for climate change (Chave et al. 2005, Arseniou et al. 2021).
While tree architecture is of great importance, 3D quantification has been a challenging task (destructive, laborious and time-consuming). Besides, there have only been studied of small trees (Bentley et al. 2013). Due to insufficient data, it has been difficult to develop and test theories linking tree structures to their physiological function and mechanism (Malhi et al. 2018). Tree

architecture, like geometry, is a direct result of both inborn and variable morphological traits that determine the tree's growth and survival. Furthermore, fractal approaches are increasingly used to model and analyse ecosystems at landscape scales, including ecological phenomena that are non-linear and unevenly structured (Halley et al. 2004). Trees' structural complexity can be quantified by the box-dimension (D_b) using fractal analysis (Seidel 2018, Saarinen et al. 2021).

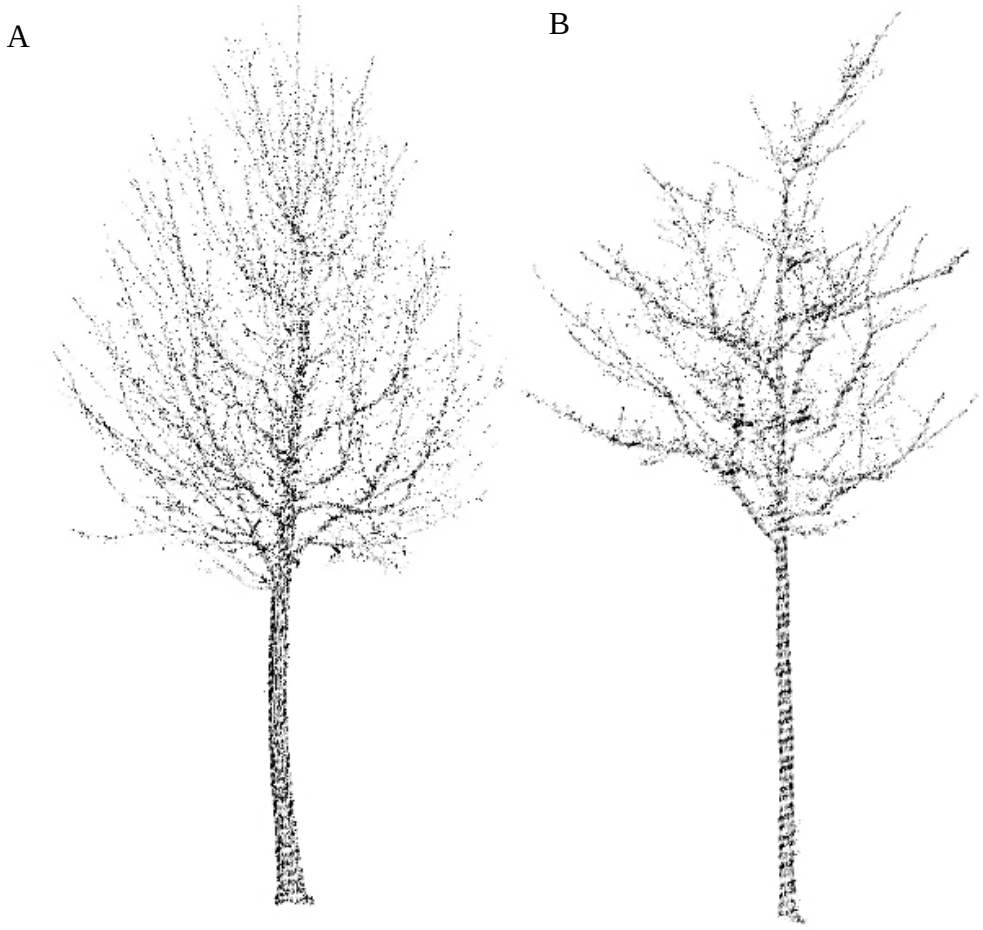

Figure 5.2: Two examples of 3D tree point clouds with the highest and lowest box-dimension (D_b) values observed in our research study. A) *Tilia cordata* (D_b = 2.04) and B) *Crataegus persimilis* (D_b = 1.55). (Edited from Dorji et al. Unpublished).

Our preliminary findings revealed that the tree's structural complexity (D_b), at species-level, is significatively related to xylem safety (P_{50}) measure ($p < 0.001$) (Fig. 5.3). Also, we found that the D_b of trees in our study had a greater effect on hydraulic vulnerability than their height or DBH. Additionally, we found that that the tree's structural complexity (D_b), at species-level had a clear tendency to significance related to xylem safety (D_h) (p = 0.057; Fig. 5.4 A) and a positive significative correlation with the branch xylem hydraulic specific conductivity (K_s) (p = 0.02; Fig. 5.4 B).

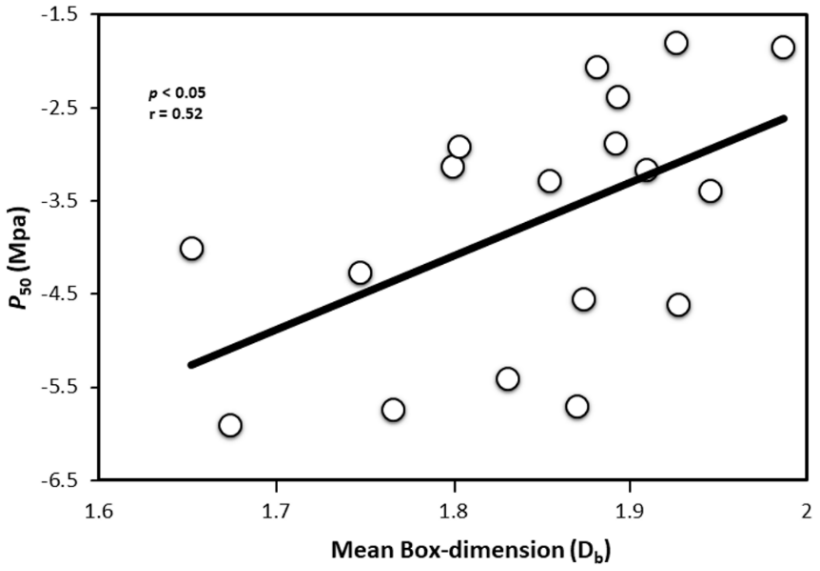

Figure 5.3: Results of simple species-level linear regressions of water potential at 50% loss of conductivity (P_{50}) vs D_b (box-dimension). (Edited from Dorji et al. Unpublished).

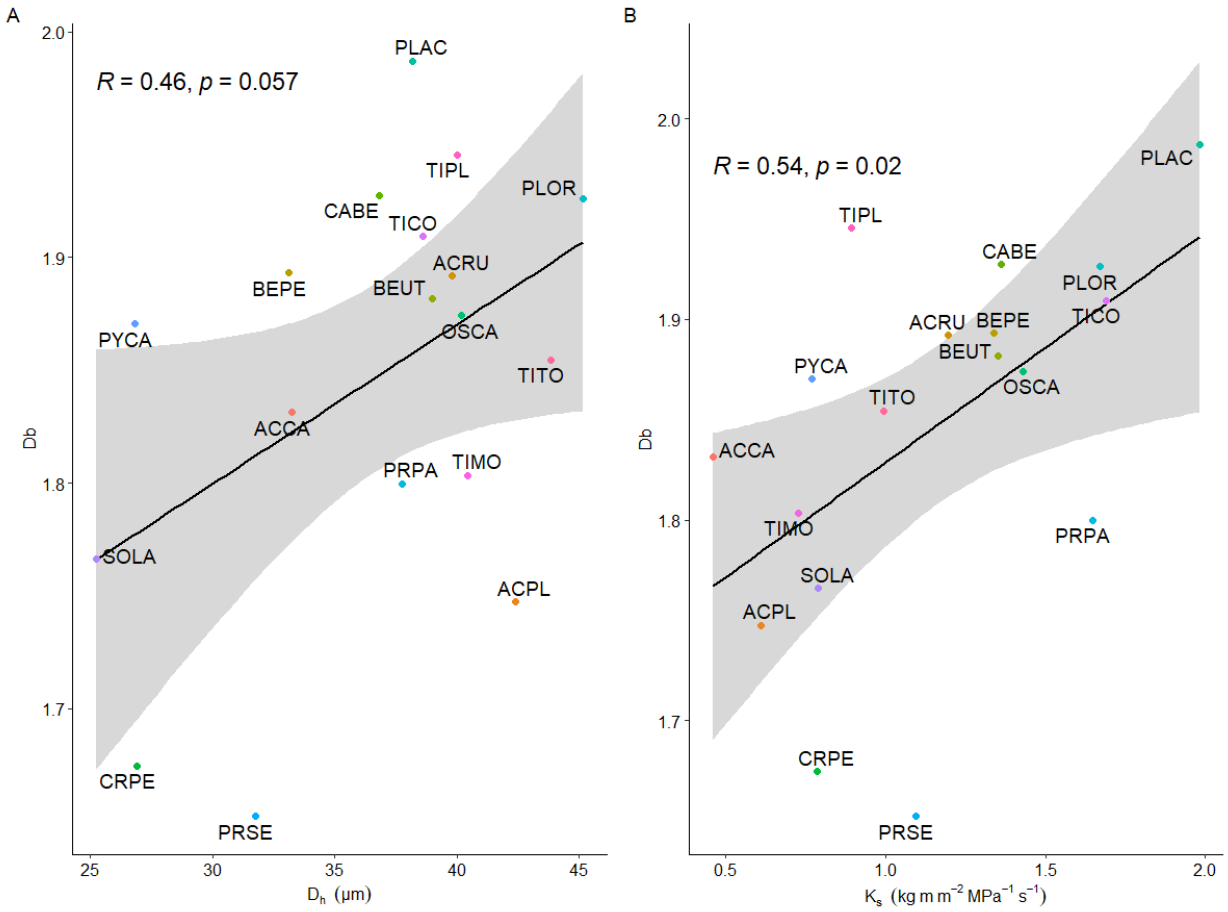

Figure 5.4: Results of simple species-level linear regressions of D_b (box-dimension) vs. A) hydraulically-weighted average vessel diameter (D_h), B) branch xylem hydraulic specific conductivity (K_s).

To conclude, there is a possibility that a more complex crown could be associated with a greater total leaf area, which would result in increased water demand and hydraulic conductivity, resulting in larger xylem vessels that are more susceptible to drought-related dysfunction (Tyree and Ewers, 1991). Consequently, more complex trees are more susceptible to drought.

5.2.2.2. Tree architecture and seed dispersal strategies

The purpose of this section is to present the results of a study carried out at the Stutel-Arboretum which quantified the tree architecture using three-dimensional and geometry analyses conducted with mobile laser scanning. A brief discussion of the theory and the results is presented in this passage. The final publication is available on Tree journal (Dorji et al. *2021).*

As environmental factors influence the tree shape (Section 5.2.2) it is likely that trees adaptive geometry is a result of an individuals need to optimize fitness in a given location, including structural stability, light intercept and reproductive success (Valladares and Niinemets 2007, Hollender and Dardick 2015, Horn 1971).
There has been an increase in studies that investigate genetic predispositions that can influence tree growth and branching patterns (Scotti-Saintagne et al. 2004, Kenis and Keulemans 2007). Many trees are distinguished by their particular form according to their environment at the growing site (Lindh et al. 2018). Few studies have examined the relationship between seed dispersal strategy and tree architecture (Malhi et al. 2018), despite extensive research only based on seed dispersal strategies (Tiebel et al. 2020).
Our results showed that tree structural complexity was positively correlated with tree growth. In addition, there was a difference in tree architectural complexity as a result of different seed dispersal strategies. Additionally, we found that the tree geometry at our study site differed depending on the latitude of the species origin. Particularly, lower latitude trees had a wider horizontal crown area than those from higher latitudes.
We also found that wind-dispersed seeds were more structurally complex than those dispersed by animals ($p < 0.001$). Finally, tree architectural complexity was positively related to the growth performance (expressed as the annual radial increment) of the trees ($p < 0.001$).

From this and the previous subsection, we demonstrate that the growth patterns and architecture (e.g., box dimension, structural complexity) of individual tree species affect the structure and dynamics of a forest. A variety of physiological and functional motif in trees and forests can be correlated with this measure of complexity. We have demonstrated that laser scanning provides a unique way to examine the relationship between tree structure and function. Hence, it may be the most effective method for developing functional-structural plant models that are needed to better explain mixed stand growth. In order to get a deeper understanding of terrestrial ecosystems

5.3. Study of macroevolutionary processes and embolism resistance within 17 Sapindaceae species

The purpose of this section is to present the preliminary results of a study carried out at the Stutel-Arboretum and Botanical Garden of Würzburg which present the relationships between drought-related traits and environmental preferences across 17 Acer species. The results are part of a manuscript Isasa et al. *in preparation that is intended for publication in 2023. A brief discussion of the theory and the results is presented below.*

Presented and discussed in the previous section (Section II, Chapter 1 and Chapter 3), Xylem embolism resistance traits exhibit a strong relationship with evolutionary histories and bioclimatic variables, while exhibiting different functional strategies. Because some families, such as *Sapindaceae*, have adapted to drought and different environmental conditions over time, they can expand linearly under increasing drought conditions.
Temperate regions can benefit from drought tolerance and ecological strategies that are coordinated to reduce embolisms, decrease xylem vessel diameters and increase tree wood density. By unraveling the internal mechanisms of plant tolerance to water deficits and developing useful functional types for modelling and predicting plant responses to future environmental changes, we will greatly enhance our ability to identify and predict plant responses to environmental change.
A specific family, the *Sapindaceae*, is highlighted in this study. The *Acer* genus is one of the most important tree genera in the deciduous forests and is mainly native to temperate zones of the northern hemisphere (Grimm et al. 2007, Grossman 2021). About 152 species of deciduous and evergreen trees and shrubs can be found in eastern Asia and in Europe and North America (Gao et al. 2020). The most common maples in Central Europe are *Acer campestre*, *Acer pseudoplatanus* and *Acer platanoides* (Caudullo and Rigo, 2016, Röhrig et al. 2020). Acer plants are an interesting topic of research due to their diversity and extraordinary wide range of distribution, which is attributed to the availability of water, as well as the fact that little research is done on interspecific variability of hydraulic traits. Using anatomical and physiological measurements, this study aims to quantify maple species' drought resistance and establish evolutionary relationships with regards to their climatic preferences.

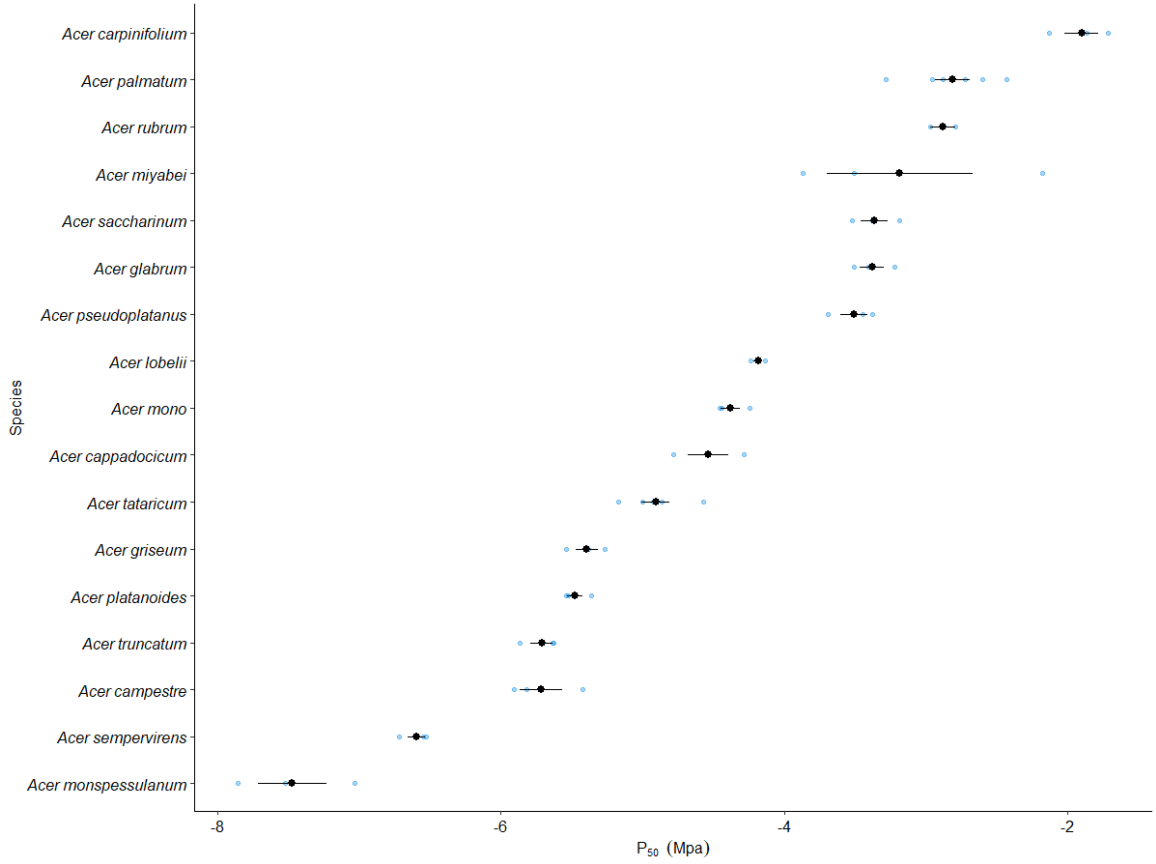

Figure 5.4: Observed ranges of the water potential at 50% loss of conductivity (P_{50}). Shown are raw data from individual plants overlaid with mean ± standard errors, ordered by their mean values.

The studied *Acer* species covered a wide range of P_{50} values (Fig. 5.4). Our drought-related trait analysis shows high pair-wise correlations between all the measured traits, particularly between 50% loss of hydraulic conductivity (P_{50}) and leaf thickness (L_t), between vessel density (V_D) and hydraulically-weighted vessel diameter (D_h) and between the surface leaf per area (*SLA*) and the Huber-Value (*HV*) (Fig. 5.5). A strong positive correlation was found between the lumen to sapwood area ratio ($\%_{Lumen}$) and the stem hydraulic conductivity (K_p), D_h with K_p and K_p and the turgor loss point (Ψ_{TLP}). A weak correlation was found between P_{50} and Ψ_{TLP}.

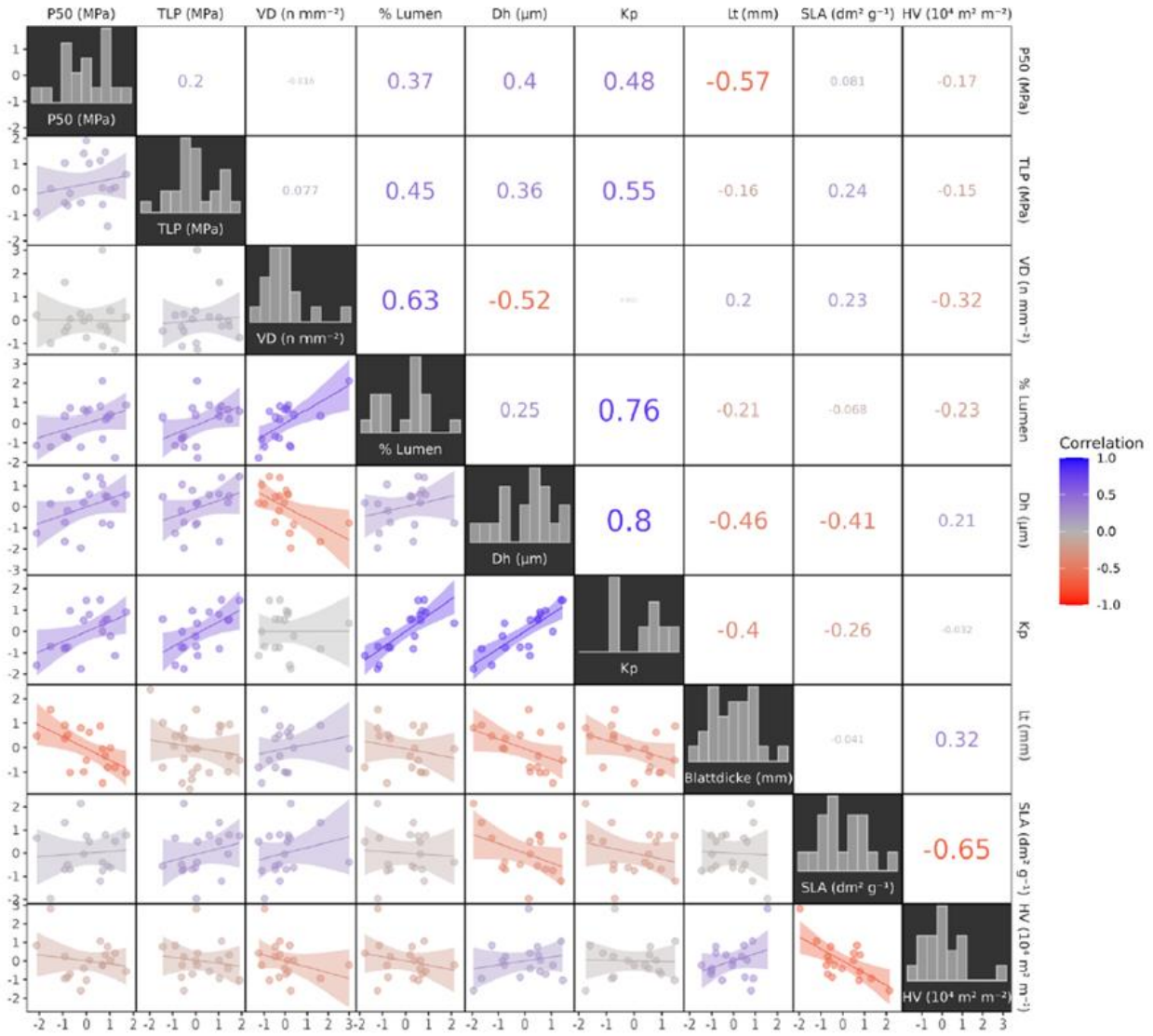

Figure 5.5: Correlation matrix of the species level averages of the analysed variables. Shown are the water potential at 50% loss of conductance (P_{50}, MPa), leaf turgor loss point (TLP, MPa), vessel density (V_D, n mm²), the lumen to sapwood area ratio ($\%_{Lumen}$), the hydraulically-weighted vessel diameter (D_h, µm), the conductivity (K_p, kg m^{-1} MPa^{-1} s^{-1}), leaf thickness (L_t, mm), leaf specific area (*SLA*, dm^2 g^{-1}) and the Huber-Value (i.e., the investment of stem tissue per unit leaf area fed, *HV*).The upper panel shows the Pearson correlations, the lower panel observed values overlaid with linear regression fits with 95% confidence intervals and the plot diagonal histograms for the corresponding variables. Figure created with R package corrmorant v. 0.0.0.9007 (https://github.com/r-link/corrmorant). (Edited from Isasa et al. Unpublished)

According to our preliminary phylogenetic analysis (Fig. 5.6), the species can be divided into different groups according to the degree of relatedness.

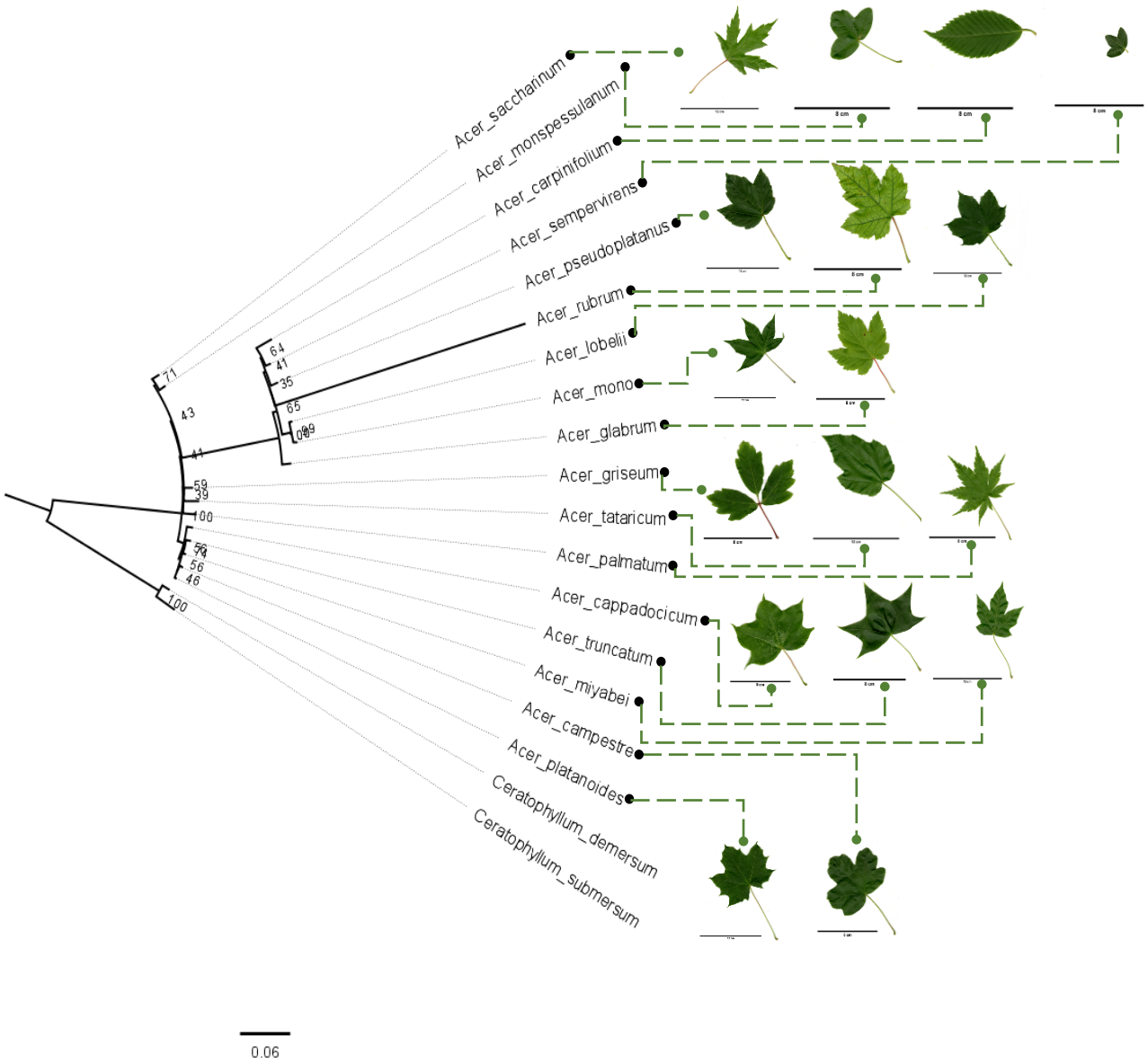

Figure 5.6: Maximum likelihood phylogenetic tree based on *mat*K–*trn*K, *atp*B-*rbc*L, *ycf*1 and ITS markers. Insets of the phylogenetic tree show leaf anatomy representative of all *Acer* species and the outgroup Ceratophyllum. Photos credits: A. Maxi Lea Wagner.

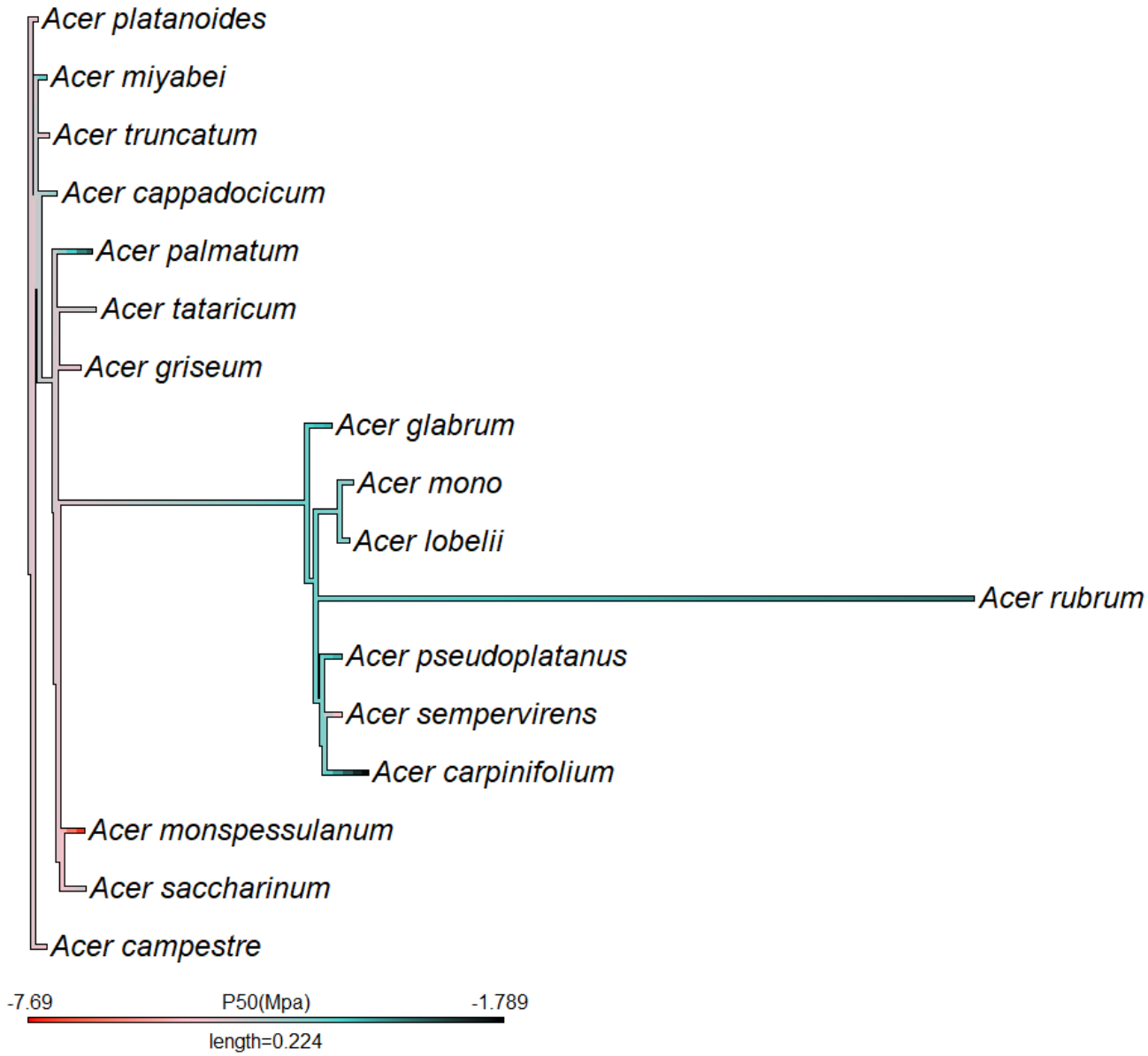

Figure 5.7: The spectrum of estimated trait evolution variation in 17 Sapindaceae species in 50% loss of conductivity (P_{50}) Branch colors reflect changes in trait value through time (reconstructed using maximum likelihood).

The measurement show (Fig. 5.7) that the genus Acer is diverse and variable, which is also proven by the literature (Gao et al. 2020). *Acer platanoides*, *Acer truncatum*, *Acer tataricum*, *Acer griseum*, *Acer sempervirens*, *Acer monspessulanum*, *Acer* saccharinum and *Acer campestre* are shown to be drought-resistant tree species. *Acer campestre* will play an important role in our forests as a mixed tree species, as it has proven to be a drought-tolerant species. While *Acer*

pseudoplatanus, currently of economic importance and thus widely planted in European forests, is considered as a drought-sensitive species. *Acer monspessulanum* is less suitable for our forests but better as a low-maintenance drought-resistant urban tree. Further aspects like identifying bioclimatic relations and drought-related traits in the *Acer* genus are necessary for a better understanding of their evolution and adaptation to a future climate.

Finally, I would like to highlight one of our main goals for this study, which is to understand how global change affects drought-related traits in the *Sapindaceae* family. The persistence of tree populations and diversity is determined by phenotypic plasticity, evolutionary changes in phenology (Alberto et al. 2013), the evolution of plastic responses in functional traits (Gienapp et al. 2008) or species distributions (Blackman et al. 2012, Larter et al. 2017, Skelton et al. 2020). We would identify the possibility of a link between the adaptation of the xylem hydraulic system, the drought-related traits and the native range's climate in the Sapindaceae family. Natural selection promotes range-wide adaptation to different environmental factors over generations.

A deeper understanding of the patterns and sources of intraspecific trait variation is needed. There has been extensive research on the inter-specific variation of traits related to water regulation and many of these traits vary systematically along an aridity gradient. The pattern of intraspecific trait variation, however, is less clear, with the environmental drivers not fully understood. Variation in hydraulic traits among species follows a similar pattern, with traits generally shifting toward drought tolerance as habitat water availability decreases. Despite variations in environmental dryness, hydraulic traits can be highly conservative in other species. The traits of a population may also change over time, but studies focusing on this issue are rare. According to Guo et al. 2020; Sorek et al. 2021 and Wu et al. 2021, certain hydraulic traits, such as vulnerability to embolism or hydraulic capacitance, may change seasonal or interannually, changing overall water regulation strategies at different times. Ontogenetic differences or shifts in environmental conditions over time can cause this type of variation. In order to uncover the source of variation within species, it is helpful to separate observed differences into genotype variation and phenotypic plasticity.

As a result, it is necessary to develop global databases to improve models in order to evaluate accurately whether natural selection and migration may again allow populations to adapt adequately to their new climates. If genetics determine trait expression, then we should expect small differences in targeted traits across populations and we should be able to apply a single trait value to models regardless of growth conditions. However, a controlled environment experiment or transect study in the field will be required to uncover the environmental driver and then calculate the trait value in models based on environmental variables.

5.4. Outlook

5.4.1. Implication on plant functional trait databases

Trees in general show a large variation in the anatomy, physiology and structural roles of xylem. This applies to intra-species relationships as well as between the different tree species. The importance of xylem research can be transferred to the terrestrial water balance, since 80% of the evapotranspiration is made by plants. (Hammond et al. 2021). The xylem plays an essential role in many complex processes, more precisely in the water and carbon cycle. Moreover, the xylem possible deficiency can provoke damages and devastating consequences for plants and life dependent on plants.

A great deal of research has never been possible due to the lengthy process of compiling functional trait data into global databases. A database not only keeps data current, but it also allows widespread access to information and helps us to avoid duplication. Indeed, for mapping and analysing spatial distributions, databases on occurrence are needed (e.g., the *Global Biodiversity Information Facility*, GBIF). With the help of statistical models of phylogenetic signal in traits, missing values of closely related species can often be predicted with high accuracy. Plant functional ecologists and ecosystem modelers must explore alternative methods to deal with a lack of information. Functional trait databases can be rapidly imputed using evolutionary comparative methods (Swenson 2013) because of the phylogenetic signal in traits (Chapter 3). Several recent improvements have made it possible to compile large trait databases (Kattge et al. 2011) and generate massive phylogenetic trees using this signal in many cases. At a continental scale, this facilitates the mapping of plant function.

As a result, it is crucial to continue compiling large trait databases, such as TRY (Kattge et al. 2011) and the xylem functional traits database (XFT), which is currently being built. The XFT contains more than 4,500 unique observations of xylem vulnerability on six continents (Hammond et al. 2021).

5.4.2. Model optimisation to predict drought induced embolism

Identifying drought-prone species and predicting embolism resistance remain a challenge (Li et al. 2022), which is why a collection of structural and physiological traits is crucial. Different species of plants exhibit many functional traits that are mathematically correlated. There can be positive correlations due to shared ancestry, functional convergence, or co-selection, while negative correlations can result from trade-offs in function or structure (Wright et al. 2007, Reich 2014; Bartlett et al. 2016). This approach allows us to gain an understanding of the principles, species coexistence, as well as traits variation across species.

Due to a lack of knowledge, we are unable to predict embolism resistance and when plants will die under extreme drought. A simple hydraulic branch-level trait model can be used to determine

how long it takes trees and other woody plants to desiccate to lethal water potentials after stomatal closure (Blackman et al. 2016).

In one hand we can find process-based vegetation models (VMs) that simulate plant physiological processes (e.g., photosynthesis and transpiration) and ecological interactions (e.g., competition for scarce resources, governing forest responses to climate) (Trugman et al 2021). In order to determine whether certain mechanisms are sufficient to produce patterns observed in nature, vegetation models are an important hypothesis testing tool. VMs that are hydraulically enabled could be used to predict embolism resistance, but they are still very simplistic. Moreover, VMs have not yet been able to predict mortality at broad spatial scales, which is a critical goal for predicting the terrestrial carbon cycle under climate change.

On the other hand, land surface models (LSMs) can also be useful tools to capture vegetation dynamics on spatiotemporal scales and simulate vegetation growth, mortality and reproduction, but they are rarely able to accurately predict vegetation responses to environmental perturbations, especially in drought conditions. Plant embolism has emerged as a key determinant of tree death in the past few years as significant progress has been made regarding the physiological mechanisms supporting drought response (Barros et al. 2022, Guan et al 2022, Shao et al 2022). Despite this, current LSMs are unable to predict drought-induced embolism and drought-related tree mortality.

Furthermore, dynamic forest models can be used to predict future forest changes and/or analyse their ecosystem functions. The level of detail, time resolution and spatial resolution of these models differ significantly. Additionally, it is necessary to describe the physiological processes and trade-offs that affect tree structure and development over time. As a result, a mechanistic approach examining these processes explicitly would allow us to assess the impact of environmental change across a large spatial area (Urban et al. 2016, Cabral et al. 2017). Although large-scale vegetation dynamics and carbon cycle predictions are made, forest structure is typically simplified (Cramer et al. 2001, Purves and Pacala 2008). In temperate forests, there are few well-studied tree species that allow models to be parameterized at the species level. For dynamic forest models, temperate trees present a particular challenge because of their high species numbers and diverse ecological strategies.

With functional-structural tree models (FSTMs), it is possible to simulate tree structure even more in detail. FSTMs depict trees as interconnected structural and functional units, such as branches, leaves, or reproductive organs, in 3D space (Godin and Sinoquet 2005, Sievänen et al. 2014). With these 'virtual tree' models, structural tree growth and the interaction between tree architecture and physiological processes can be modelled (Petter et al. 2021a, b).

In drought conditions, we are especially interested in species that can withstand negative xylem pressure. In models of global dynamic vegetation described before, static functions are used to simulate species distributions, but these fail to incorporate hydraulic characteristics that vary by species (Anderegg 2015). A trait-based approach to predicting drought impacts is therefore more relevant than a functional type-based approach.

Plant hydraulic traits would need to be available for a large number of species and biomes to be integrated into vegetation models. This is why databases are so useful.
Many leaf traits have been associated with xylem safety, both at the branch and foliar levels (Part II, Chapter 2 and Part III, Section 5.2), including wood density, conduit size, pit membrane properties, hydraulic safety margins, stomata control, sapwood-to-leaf area ratios and many others. There is, therefore, no way to predict how traits will change across species.
A recently developed tree and forest model that adequately describes the three-dimensional structure of trees based on physiological principles of photosynthesis, carbon allocation and structural growth can be used to develop mechanistic models for predicting xylem safety (Petter et al. 2021). Based on the pipe theory (Shinozaki et al. 1964), leaf and wood traits are combined to simulate tree performance and growth. Dynamic variables such as biomass, tree growth and forest structure dynamics should be added to emergent patterns in addition to structural details of trees. Petter et al. 2021 have successfully calibrated this model to fit Neotropical Forest data.
The model could be calibrated to temperate trees with standardized conditions (age and environment) and replicated across individual trees of the same species to conduct further simulation experiments.
Due to this, the model will serve as a starting point for calibrating hydraulic, wood and leaf traits. For instance, if the calibrated model underperforms when predicting structure, it may be possible to incorporate additional traits (such as hydraulic efficiency, embolism resistance, stomatal conductance, vessel size and density) to understand their impact on model performance when predicting tree growth and structure. The calibrated model will be used to forecast tree distributions under environmental change (e.g., as in Cabral et al. 2013). This will thus be able to predict tree survival based on physiological constraints.

5.5. Final conclusion

In the end, I expect that this thesis helps fill gaps in knowledge about plant drought-induced tree mortality trait relationships, evolution and adaptation of drought-related traits due to climate variation.
In the first chapter, I provide the information concerning the wood anatomical attributes which are easy measurable traits. Those traits were correlated with embolism resistance. Furthermore, it is shown that wood anatomical attributes, such as vessel dimensions and embolism resistance, are linked. However, these relationships cannot be explained by a common scaling of both traits, but rather by many structural parameters of the pits. This section also showed that differences in the studied ranges of variables, missing covariates and conflation of different scales of aggregation may reinforce existing controversies about diameter - embolism resistance relationships.
The second Chapter provides a methodological comparison of common embolism resistance measurements method. It explored the possibility of a new fast, precise and expansive method (the pneumatic method). These findings verified that the xylem embolism resistance measured by the

pneumatic method and the flow centrifuge method are comparable. Nevertheless, the method should be tested on long vessel species (i.e., tropical species). Furthermore, our study points out that there is an existing potential artefact associated with xylem water potential determination and species-specific drying behavior that requires further study.

In the third Chapter of this dissertation, I present how drought-related traits are phylogenetically controlled by their associations with ecological variables. In this regard, it is important to point out that wood traits and xylem embolism resistance have a strong relationship with both evolutionary histories and bioclimatic factors, depending on the studied families. In agreement with our knowledge, distinct families adopt different strategies. Contributing to the development of a shared database is useful for predicting xylem safety using mechanistic models because stem embolism resistance predicts species growth and survival ecological distribution and both macro- and micro-evolutionary patterns.

To conclude, drought-related tree embolism is a ramification of complex interactions, consisting of multiple physiological processes associated with carbon and hydraulic dynamics. In future research, generating trees and forests can be routinely modelled in a standardized way to mechanistically account for and calibrate species dynamics. A fundamental knowledge of drought-related traits values as well as their relationships with one another will help to calibrate and expand these models. Furthermore, high genetic variation may allow species to survive longer than expected in novel climates (i.e., evolutionary extinction debt). Nevertheless, eco-evolutionary dynamics are still rarely considered. A more ambitious, but perhaps even more motivating inclusion of such a platform in Earth Science modelling would allow for the interaction between biodiversity and other components of the Earth system, such as the atmosphere, the hydrological cycle and land use, as well as initiatives for a common biodiversity modeling platform in addition to such earth system dynamics.

References

Alberto, F.J., Aitken, S.N., Alía, R., González-Martínez, S.C., Hänninen, H., Kremer, A., Lefèvre, F., Lenormand, T., Yeaman, S., Whetten, R., Savolainen, O., 2013. Potential for evolutionary responses to climate change – evidence from tree populations. Glob Change Biol 19, 1645–1661. https://doi.org/10.1111/gcb.12181

Anderegg, W.R.L., 2015. Spatial and temporal variation in plant hydraulic traits and their relevance for climate change impacts on vegetation. New Phytol 205, 1008–1014. https://doi.org/10.1111/nph.12907

Anderegg, W.R.L., Klein, T., Bartlett, M., Sack, L., Pellegrini, A.F.A., Choat, B., Jansen, S., 2016. Meta-analysis reveals that hydraulic traits explain cross-species patterns of drought-induced tree mortality across the globe. Proc. Natl. Acad. Sci. U.S.A. 113, 5024–5029. https://doi.org/10.1073/pnas.1525678113

Arseniou, G., MacFarlane, D.W., 2021. Fractal dimension of tree crowns explains species functional-trait responses to urban environments at different scales. Ecol Appl 31. https://doi.org/10.1002/eap.2297

Barros, F. de V., Bittencourt, P.L., Eller, C.B., Signori-Müller, C., Meireles, L.D., Oliveira, R.S., 2022. Phytogeographical origin determines Tropical Montane Cloud Forest hydraulic trait composition. Functional Ecology 36, 607–621. https://doi.org/10.1111/1365-2435.14008

Bartlett, M.K., Scoffoni, C., Sack, L., 2012. The determinants of leaf turgor loss point and prediction of drought tolerance of species and biomes: a global meta-analysis: Drivers of plant drought tolerance. Ecology Letters 15, 393–405. https://doi.org/10.1111/j.1461-0248.2012.01751.x

Bartlett, M.K., Klein, T., Jansen, S., Choat, B., Sack, L., 2016. The correlations and sequence of plant stomatal, hydraulic and wilting responses to drought. Proc. Natl. Acad. Sci. U.S.A. 113, 13098–13103. https://doi.org/10.1073/pnas.1604088113

Bentley, L.P., Stegen, J.C., Savage, V.M., Smith, D.D., von Allmen, E.I., Sperry, J.S., Reich, P.B., Enquist, B.J., 2013. An empirical assessment of tree branching networks and implications for plant allometric scaling models. Ecol Lett 16, 1069–1078. https://doi.org/10.1111/ele.12127

Blackmann, C.J., Brodribb, T.J., Jordan, G.J., 2012. Leaf hydraulic vulnerability influences species' bioclimatic limits in a diverse group of woody angiosperme 11.

Blackman, C.J., Pfautsch, S., Choat, B., Delzon, S., Gleason, S.M., Duursma, R.A., 2016. Toward an index of desiccation time to tree mortality under drought: Desiccation time to tree mortality. Plant, Cell & Environment 39, 2342–2345. https://doi.org/10.1111/pce.12758

Brodribb, T.J., 2009. Xylem hydraulic physiology: The functional backbone of terrestrial plant productivity. Plant Science 177, 245–251. https://doi.org/10.1016/j.plantsci.2009.06.001

Brodribb, T.J., Cochard, H., 2009. Hydraulic Failure Defines the Recovery and Point of Death in Water-Stressed Conifers. Plant Physiology 149, 575–584. https://doi.org/10.1104/pp.108.129783

Busov, V.B., Brunner, A.M., Strauss, S.H., 2008. Genes for control of plant stature and form. New Phytologist 177, 589–607. https://doi.org/10.1111/j.1469-8137.2007.02324.x

Cabral, J.S., Valente, L., Hartig, F., 2017. Mechanistic simulation models in macroecology and biogeography: state-of-art and prospects. Ecography 40, 267–280. https://doi.org/10.1111/ecog.02480

Caudullo, G. and de Rigo, D., 2016. Acer platanoides in Europe: distribution, habitat, usage and threats. European Atlas of Forest Tree Species. Luxembourg: Publ. Off. EU, p.e019159

Chave, J., Andalo, C., Brown, S., Cairns, M.A., Chambers, J.Q., Eamus, D., Fölster, H., Fromard, F., Higuchi, N., Kira, T., Lescure, J.-P., Nelson, B.W., Ogawa, H., Puig, H., Riéra, B., Yamakura, T., 2005. Tree allometry and improved estimation of carbon stocks and balance in tropical forests. Oecologia 145, 87–99. https://doi.org/10.1007/s00442-005-0100-x

Cramer, W., Bondeau, A., Woodward, F.I., Prentice, I.C., Betts, R.A., Brovkin, V., Cox, P.M., Fisher, V., Foley, J.A., Friend, A.D., Kucharik, C., Lomas, M.R., Ramankutty, N., Sitch, S., Smith, B., White, A., Young-Molling, C., 2001. Global response of terrestrial ecosystem structure and function to CO_2 and climate change: results from six dynamic global vegetation models: ECOSYSTEM DYNAMICS, CO_2 and CLIMATE CHANGE. Global Change Biology 7, 357–373. https://doi.org/10.1046/j.1365-2486.2001.00383.x

Delzon, S., Cochard, H., 2014. Recent advances in tree hydraulics highlight the ecological significance of the hydraulic safety margin. New Phytol 203, 355–358. https://doi.org/10.1111/nph.12798

Dorji, Y., Schuldt, B., Neudam, L., Dorji, R., Middleby, K., Isasa, E., Körber, K., Ammer, C., Annighöfer, P., Seidel, D., 2021. Three-dimensional quantification of tree architecture from mobile laser scanning and geometry analysis. Trees 35, 1385–1398. https://doi.org/10.1007/s00468-021-02124-9

Duursma, R.A., Blackman, C.J., Lopéz, R., Martin-StPaul, N.K., Cochard, H., Medlyn, B.E., 2019. On the minimum leaf conductance: its role in models of plant water use and ecological and environmental controls. New Phytol 221, 693–705. https://doi.org/10.1111/nph.15395

Gao, J., Liao, P.-C., Huang, B.-H., Yu, T., Zhang, Y.-Y., Li, J.-Q., 2020. Historical biogeography of Acer L. (Sapindaceae): genetic evidence for Out-of-Asia hypothesis with multiple dispersals to North America and Europe. Sci Rep 10, 21178. https://doi.org/10.1038/s41598-020-78145-0

Guan, X., Wen, Y., Zhang, Y., Chen, Z., Cao, K.-F., 2022. Stem hydraulic conductivity and embolism resistance of Quercus species are associated with their climatic niche. Tree Physiology tpac119. https://doi.org/10.1093/treephys/tpac119

Guo, J.S., Hultine, K.R., Koch, G.W., Kropp, H., Ogle, K., 2020. Temporal shifts in iso/anisohydry revealed from daily observations of plant water potential in a dominant desert shrub. New Phytol 225, 713–726. https://doi.org/10.1111/nph.16196

Godin, C., Sinoquet, H., 2005. Functional–structural plant modelling. New Phytologist 166, 705–708. https://doi.org/10.1111/j.1469-8137.2005.01445.x

Grimm, G.W., Denk, T., Hemleben, V., 2007. Evolutionary history and systematics of Acer section Acer – a case study of low-level phylogenetics. Plant Syst. Evol. 267, 215–253. https://doi.org/10.1007/s00606-007-0572-8

Grossman, J.J., 2021. Evidence of Constrained Divergence and Conservatism in Climatic Niches of the Temperate Maples (Acer L.). Forests 12, 535. https://doi.org/10.3390/f12050535

Halley, J.M., Hartley, S., Kallimanis, A.S., Kunin, W.E., Lennon, J.J., Sgardelis, S.P., 2004. Uses and abuses of fractal methodology in ecology: Fractal methodology in ecology. Ecology Letters 7, 254–271. https://doi.org/10.1111/j.1461-0248.2004.00568.x

Hammond, W., Choat, B., Johnson, D., Ali Ahmed, M., Anderegg, L., Barigah, T.S., Barros, F., Bartlett, M., Bauerle, T., Beikircher, B. and Bittencourt, P., 2021, December. The global vulnerability of plant xylem. In AGU Fall Meeting Abstracts (Vol. 2021, pp. B31F-07).

Hochberg, U., Rockwell, F.E., Holbrook, N.M., Cochard, H., 2018. Iso/Anisohydry: A Plant–Environment Interaction Rather Than a Simple Hydraulic Trait. Trends in Plant Science 23, 112–120. https://doi.org/10.1016/j.tplants.2017.11.002

Hollender, C.A., Dardick, C., 2015. Molecular basis of angiosperm tree architecture. New Phytol 206, 541–556. https://doi.org/10.1111/nph.13204

Horn, H.S., 1976. The adaptive geometry of trees, 2., paperback print. ed, Monographs in population biology. Princeton Univ. Pr, Princeton, N.J.

Johnson, D.M., McCulloh, K.A., Woodruff, D.R., Meinzer, F.C., 2012. Hydraulic safety margins and embolism reversal in stems and leaves: Why are conifers and angiosperms so different? Plant Science 195, 48–53. https://doi.org/10.1016/j.plantsci.2012.06.010

Jones, H.G., Sutherland, R.A., 1991. Stomatal control of xylem embolism. Plant Cell Environ 14, 607–612. https://doi.org/10.1111/j.1365-3040.1991.tb01532.x

Kattge, J., Díaz, S., Lavorel, S., Prentice, I.C., Leadley, P., Bönisch, G., Garnier, E., Westoby, M., Reich, P.B., Wright, I.J., Cornelissen, J.H.C., Violle, C., Harrison, S.P., Van BODEGOM, P.M., Reichstein, M., Enquist, B.J., Soudzilovskaia, N.A., Ackerly, D.D., Anand, M., Atkin, O., Bahn, M., Baker, T.R., Baldocchi, D., Bekker, R., Blanco, C.C., Blonder, B., Bond, W.J., Bradstock, R., Bunker, D.E., Casanoves, F., Cavender-Bares, J., Chambers, J.Q., Chapin Iii, F.S., Chave, J., Coomes, D., Cornwell, W.K., Craine, J.M., Dobrin, B.H., Duarte, L., Durka, W., Elser, J., Esser, G., Estiarte, M., Fagan, W.F., Fang, J., Fernández-Méndez, F., Fidelis, A., Finegan, B.,

Flores, O., Ford, H., Frank, D., Freschet, G.T., Fyllas, N.M., Gallagher, R.V., Green, W.A., Gutierrez, A.G., Hickler, T., Higgins, S.I., Hodgson, J.G., Jalili, A., Jansen, S., Joly, C.A., Kerkhoff, A.J., Kirkup, D., Kitajima, K., Kleyer, M., Klotz, S., Knops, J.M.H., Kramer, K., Kühn, I., Kurokawa, H., Laughlin, D., Lee, T.D., Leishman, M., Lens, F., Lenz, T., Lewis, S.L., Lloyd, J., Llusià, J., Louault, F., Ma, S., Mahecha, M.D., Manning, P., Massad, T., Medlyn, B.E., Messier, J., Moles, A.T., Müller, S.C., Nadrowski, K., Naeem, S., Niinemets, Ü., Nöllert, S., Nüske, A., Ogaya, R., Oleksyn, J., Onipchenko, V.G., Onoda, Y., Ordoñez, J., Overbeck, G., Ozinga, W.A., Patiño, S., Paula, S., Pausas, J.G., Peñuelas, J., Phillips, O.L., Pillar, V., Poorter, H., Poorter, L., Poschlod, P., Prinzing, A., Proulx, R., Rammig, A., Reinsch, S., Reu, B., Sack, L., Salgado-Negret, B., Sardans, J., Shiodera, S., Shipley, B., Siefert, A., Sosinski, E., Soussana, J.-F., Swaine, E., Swenson, N., Thompson, K., Thornton, P., Waldram, M., Weiher, E., White, M., White, S., Wright, S.J., Yguel, B., Zaehle, S., Zanne, A.E., Wirth, C., 2011. TRY - a global database of plant traits: TRY - A GLOBAL DATABASE OF PLANT TRAITS. Global Change Biology 17, 2905–2935. https://doi.org/10.1111/j.1365-2486.2011.02451.x

Kenis, K., Keulemans, J., 2007. Study of tree architecture of apple (Malus × domestica Borkh.) by QTL analysis of growth traits. Mol Breeding 19, 193–208. https://doi.org/10.1007/s11032-006-9022-5

Kramer, P.J., Boyer, J.S., 1995. Water relations of plants and soils. Academic Press, San Diego.

Kuuluvainen, T., 1992. Tree Architectures Adapted to Efficient Light Utilization: Is There a Basis for Latitudinal Gradients? Oikos 65, 275. https://doi.org/10.2307/3545019

Larter, M., Pfautsch, S., Domec, J., Trueba, S., Nagalingum, N., Delzon, S., 2017. Aridity drove the evolution of extreme embolism resistance and the radiation of conifer genus *Callitris*. New Phytol 215, 97–112. https://doi.org/10.1111/nph.14545

Li, X., Xi, B., Wu, X., Choat, B., Feng, J., Jiang, M., Tissue, D., 2022. Unlocking Drought-Induced Tree Mortality: Physiological Mechanisms to Modeling. Front. Plant Sci. 13, 835921. https://doi.org/10.3389/fpls.2022.835921

Lindh, M., Falster, D.S., Zhang, L., Dieckmann, U., Brännström, Å., 2018. Latitudinal effects on crown shape evolution. Ecol Evol 8, 8149–8158. https://doi.org/10.1002/ece3.4275

Malhi, Y., Jackson, T., Patrick Bentley, L., Lau, A., Shenkin, A., Herold, M., Calders, K., Bartholomeus, H., Disney, M.I., 2018. New perspectives on the ecology of tree structure and tree communities through terrestrial laser scanning. Interface Focus. 8, 20170052. https://doi.org/10.1098/rsfs.2017.0052

Martin-StPaul, N., Delzon, S., Cochard, H., 2017. Plant resistance to drought depends on timely stomatal closure. Ecol Lett 20, 1437–1447. https://doi.org/10.1111/ele.12851

McDowell, N.G., 2011. Mechanisms Linking Drought, Hydraulics, Carbon Metabolism and Vegetation Mortality. Plant Physiology 155, 1051–1059. https://doi.org/10.1104/pp.110.170704

Niinemets, U., Kull, O., 1995. Effects of light availability and tree size on the architecture of assimilative surface in the canopy of Picea abies: variation in needle morphology. Tree Physiology 15, 307–315. https://doi.org/10.1093/treephys/15.5.307

Petter, G., Zotz, G., Kreft, H., Cabral, J.S., 2021. Agent-based modeling of the effects of forest dynamics, selective logging and fragment size on epiphyte communities. Ecol. Evol. 11, 2937–2951. https://doi.org/10.1002/ece3.7255, a

Petter, G., Kreft, H., Ong, Y., Zotz, G., Cabral, J.S., 2021. Modelling the long-term dynamics of tropical forests: From leaf traits to whole-tree growth patterns. Ecological Modelling 460, 109735. https://doi.org/10.1016/j.ecolmodel.2021.109735, b

Poorter, L., Bongers, L., Bongers, F., 2006. Architecture of 54 MOIST-FOREST TREE SPECIES: TRAITS, TRADE-OFFS and FUNCTIONAL GROUPS. Ecology 87, 1289–1301. https://doi.org/10.1890/0012-9658(2006)87[1289:AOMTST]2.0.CO;2

Powell, T.L., Galbraith, D.R., Christoffersen, B.O., Harper, A., Imbuzeiro, H.M.A., Rowland, L., Almeida, S., Brando, P.M., Costa, A.C.L., Costa, M.H., Levine, N.M., Malhi, Y., Saleska, S.R., Sotta, E., Williams, M., Meir, P., Moorcroft, P.R., 2013. Confronting model predictions of carbon fluxes with measurements of Amazon forests subjected to experimental drought. New Phytol 200, 350–365. https://doi.org/10.1111/nph.12390

Purves, D., Pacala, S., 2008. Predictive Models of Forest Dynamics. Science 320, 1452–1453. https://doi.org/10.1126/science.1155359

Reich, P.B., Ellsworth, D.S., Walters, M.B., 1998. Leaf structure (specific leaf area) modulates photosynthesis-nitrogen relations: evidence from within and across species and functional groups: SLA regulates photosynthetic nitrogen use. Functional Ecology 12, 948–958. https://doi.org/10.1046/j.1365-2435.1998.00274.x

Rosas, T., Mencuccini, M., Batlles, C., Regalado, Í., Saura-Mas, S., Sterck, F., Martínez-Vilalta, J., 2021. Are leaf, stem and hydraulic traits good predictors of individual tree growth? Functional Ecology 35, 2435–2447. https://doi.org/10.1111/1365-2435.13906

Saarinen, N., Calders, K., Kankare, V., Yrttimaa, T., Junttila, S., Luoma, V., Huuskonen, S., Hynynen, J., Verbeeck, H., 2021. Understanding 3D structural complexity of individual Scots pine trees with different management history. Ecol. Evol. 11, 2561–2572. https://doi.org/10.1002/ece3.7216

Sack, L., Cowan, P.D., Jaikumar, N., Holbrook, N.M., 2003. The 'hydrology' of leaves: co-ordination of structure and function in temperate woody species: Leaf 'hydrology.' Plant, Cell & Environment 26, 1343–1356. https://doi.org/10.1046/j.0016-8025.2003.01058.x

Sack, L., Holbrook, N.M., 2006. LEAF HYDRAULICS. Annu. Rev. Plant Biol. 57, 361–381. https://doi.org/10.1146/annurev.arplant.56.032604.144141

Sack, L., Scoffoni, C., Johnson, D.M., Buckley, T.N., Brodribb, T.J., 2015. The Anatomical Determinants of Leaf Hydraulic Function, in: Hacke, U. (Ed.), Functional and Ecological Xylem Anatomy. Springer International Publishing, Cham, pp. 255–271. https://doi.org/10.1007/978-3-319-15783-2_10

Sarmento Cabral, J., Jeltsch, F., Thuiller, W., Higgins, S., Midgley, G.F., Rebelo, A.G., Rouget, M., Schurr, F.M., 2013. Impacts of past habitat loss and future climate change on the range dynamics of South African Proteaceae. Diversity Distrib. 19, 363–376. https://doi.org/10.1111/ddi.12011

Scotti-Saintagne, C., Mariette, S., Porth, I., Goicoechea, P.G., Barreneche, T., Bodénès, C., Burg, K., Kremer, A., 2004. Genome Scanning for Interspecific Differentiation Between Two Closely Related Oak Species [Quercus robur L. and Q. petraea (Matt.) Liebl.]. Genetics 168, 1615–1626. https://doi.org/10.1534/genetics.104.026849

Seidel, D., 2018. A holistic approach to determine tree structural complexity based on laser scanning data and fractal analysis. Ecol Evol 8, 128–134. https://doi.org/10.1002/ece3.3661

Seidel, D., Ehbrecht, M., Dorji, Y., Jambay, J., Ammer, C., Annighöfer, P., 2019. Identifying architectural characteristics that determine tree structural complexity. Trees 33, 911–919. https://doi.org/10.1007/s00468-019-01827-4

Shao, J., Zhou, X., Zhang, P., Zhai, D., Yuan, T., Li, Z., He, Y., McDowell, N.G., 2022. Embolism resistance explains mortality and recovery of five subtropical evergreen broadleaf trees to persistent drought. Ecology. https://doi.org/10.1002/ecy.3877

Shinozaki, K., Yoda, K., Hozumi, K., Kira, T., 1964. A Quantitative analysis of plant form – The pipe model theory : Basic analyses. https://doi.org/10.18960/seitai.14.3_97

Sievänen, R., Godin, C., DeJong, T.M., Nikinmaa, E., 2014. Functional–structural plant models: a growing paradigm for plant studies. Annals of Botany 114, 599–603. https://doi.org/10.1093/aob/mcu175

Skelton, R.P., Anderegg, L.D.L., Diaz, J., Kling, M.M., Papper, P., Lamarque, L.J., Delzon, S., Dawson, T.E., Ackerly, D.D., 2021. Evolutionary relationships between drought-related traits and climate shape large hydraulic safety margins in western North American oaks. Proc. Natl. Acad. Sci. U.S.A. 118, e2008987118. https://doi.org/10.1073/pnas.2008987118

Skelton, R.P., Brodribb, T.J., McAdam, S.A.M., Mitchell, P.J., 2017. Gas exchange recovery following natural drought is rapid unless limited by loss of leaf hydraulic conductance: evidence from an evergreen woodland. New Phytol 215, 1399–1412. https://doi.org/10.1111/nph.14652

Sorek, Y., Greenstein, S., Netzer, Y., Shtein, I., Jansen, S., Hochberg, U., 2021. An increase in xylem embolism resistance of grapevine leaves during the growing season is coordinated with stomatal regulation, turgor loss point and intervessel pit membranes. New Phytol 229, 1955–1969. https://doi.org/10.1111/nph.17025

Sparks, J.P., Black, R.A., 1999. Regulation of water loss in populations of Populus trichocarpa: the role of stomatal control in preventing xylem cavitation. Tree Physiology 19, 453–459. https://doi.org/10.1093/treephys/19.7.453

Sperry, J.S., Hacke, U.G., Oren, R., Comstock, J.P., 2002. Water deficits and hydraulic limits to leaf water supply: Water deficits and hydraulic limits to leaf water supply. Plant, Cell & Environment 25, 251–263. https://doi.org/10.1046/j.0016-8025.2001.00799.x

Sterck, F.J., Bongers, F., 2001. Crown development in tropical rain forest trees: patterns with tree height and light availability: *Crown development in tropical trees*. Journal of Ecology 89, 1–13. https://doi.org/10.1046/j.1365-2745.2001.00525.x

Swenson, N.G., 2013. The assembly of tropical tree communities - the advances and shortcomings of phylogenetic and functional trait analyses. Ecography 36, 264–276. https://doi.org/10.1111/j.1600-0587.2012.00121.x

Tiebel, K., Huth, F., Frischbier, N., Wagner, S., 2020. Restrictions on natural regeneration of storm-felled spruce sites by silver birch (Betula pendula Roth) through limitations in fructification and seed dispersal. Eur J Forest Res 139, 731–745. https://doi.org/10.1007/s10342-020-01281-9

Trugman, A.T., 2022. Integrating plant physiology and community ecology across scales through trait-based models to predict drought mortality. New Phytologist 234, 21–27. https://doi.org/10.1111/nph.1782

Tyree, M.T., Ewers, F.W., 1991. The hydraulic architecture of trees and other woody plants. New Phytologist 119, 345–360. https://doi.org/10.1111/j.1469-8137.1991.tb00035.x

Tyree, M.T., Sperry, J.S., 1989. Vulnerability of Xylem to Cavitation and Embolism. Annu. Rev. Plant. Physiol. Plant. Mol. Biol. 40, 19–36. https://doi.org/10.1146/annurev.pp.40.060189.000315

Urban, M.C., Bocedi, G., Hendry, A.P., Mihoub, J.-B., Pe'er, G., Singer, A., Bridle, J.R., Crozier, L.G., De Meester, L., Godsoe, W., Gonzalez, A., Hellmann, J.J., Holt, R.D., Huth, A., Johst, K., Krug, C.B., Leadley, P.W., Palmer, S.C.F., Pantel, J.H., Schmitz, A., Zollner, P.A., Travis, J.M.J., 2016. Improving the forecast for biodiversity under climate change. Science 353, aad8466. https://doi.org/10.1126/science.aad8466

Urban, M.C., Travis, J.M.J., Zurell, D., Thompson, P.L., Synes, N.W., Scarpa, A., Peres-Neto, P.R., Malchow, A.-K., James, P.M.A., Gravel, D., De Meester, L., Brown, C., Bocedi, G., Albert, C.H., Gonzalez, A., Hendry, A.P., 2022. Coding for Life: Designing a Platform for Projecting and Protecting Global Biodiversity. BioScience 72, 91–104. https://doi.org/10.1093/biosci/biab099

Valladares, F., Niinemets, Ü., 2007. The Architecture of Plant Crowns: From Design Rules to Light Capture and Performance, in: Pugnaire, F.I., Valladares, F. (Eds.), Functional Plant Ecology. CRC Press, pp. 101–150. https://doi.org/10.1201/9781420007626-4

Watt, M.S., Moore, J.R., McKinlay, B., 2005. The influence of wind on branch characteristics of Pinus radiata. Trees 19, 58–65. https://doi.org/10.1007/s00468-004-0363-6

West, G.B., Enquist, B.J., Brown, J.H., 2009. A general quantitative theory of forest structure and dynamics. Proc. Natl. Acad. Sci. U.S.A. 106, 7040–7045. https://doi.org/10.1073/pnas.0812294106

Wright, I.J., Ackerly, D.D., Bongers, F., Harms, K.E., Ibarra-Manriquez, G., Martinez-Ramos, M., Mazer, S.J., Muller-Landau, H.C., Paz, H., Pitman, N.C.A., Poorter, L., Silman, M.R., Vriesendorp, C.F., Webb, C.O., Westoby, M., Wright, S.J., 2007. Relationships Among Ecologically Important Dimensions of Plant Trait Variation in Seven Neotropical Forests. Annals of Botany 99, 1003–1015. https://doi.org/10.1093/aob/mcl066

Wu, G., Guan, K., Li, Y., Novick, K.A., Feng, X., McDowell, N.G., Konings, A.G., Thompson, S.E., Kimball, J.S., De Kauwe, M.G., Ainsworth, E.A., Jiang, C., 2021. Interannual variability of ecosystem iso/anisohydry is regulated by environmental dryness. New Phytologist 229, 2562–2575. https://doi.org/10.1111/nph.17040

Appendices

6. Appendices

6.1. Chapter 1

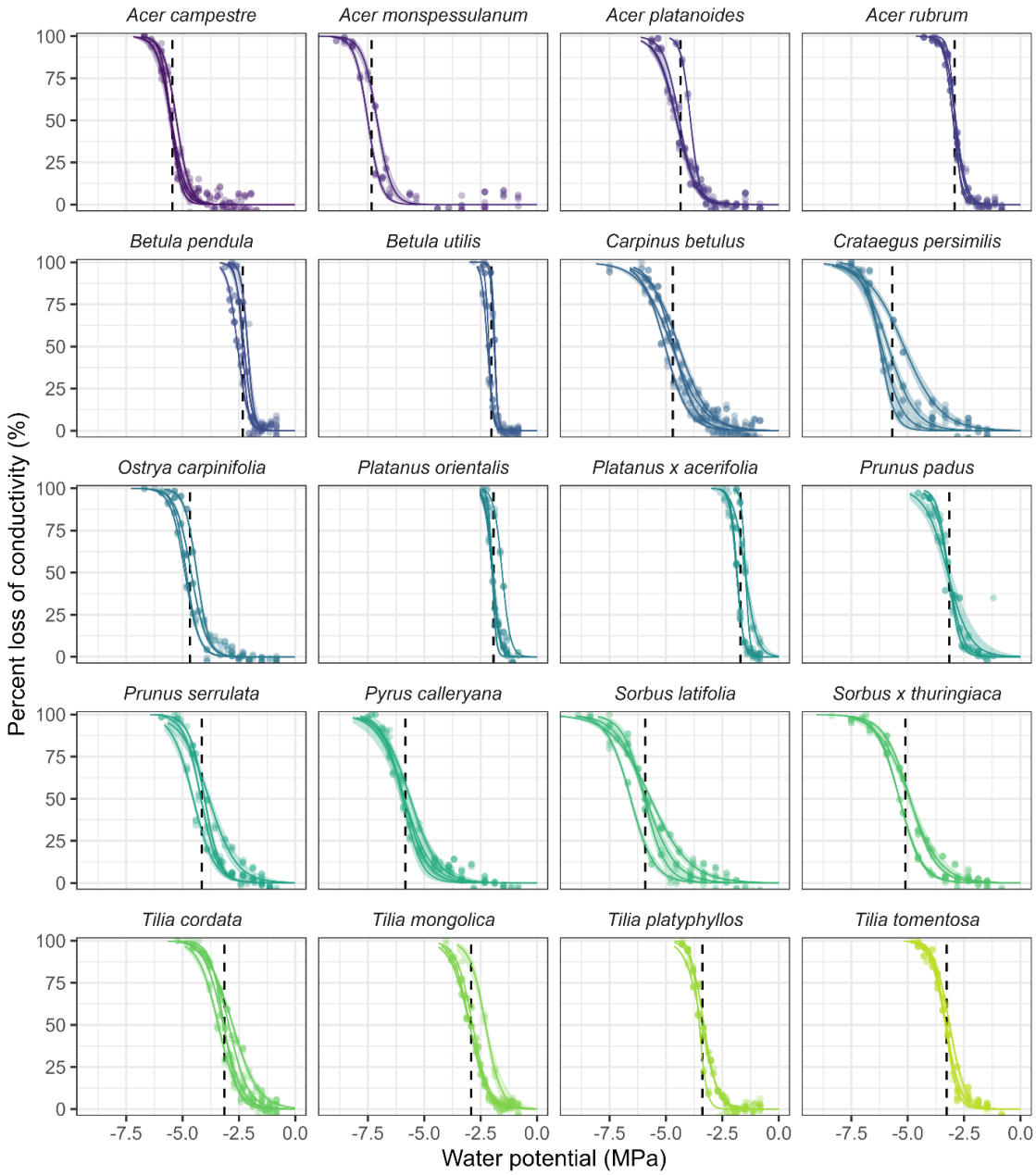

Appendix 1, Figure S1: Raw data for the Cavitron vulnerability curves measured on the samples from the Stutel dataset. Shown is the change of conductivity with decreasing water potential for each of the measured samples (rescaled to PLC based on the model estimate of K_{sat} according to Eqn. (3)). Given are the model estimates (colored lines) ± 95% confidence bounds (shaded areas) for each sample, as well as the species level average P_{50} (dashed vertical lines).

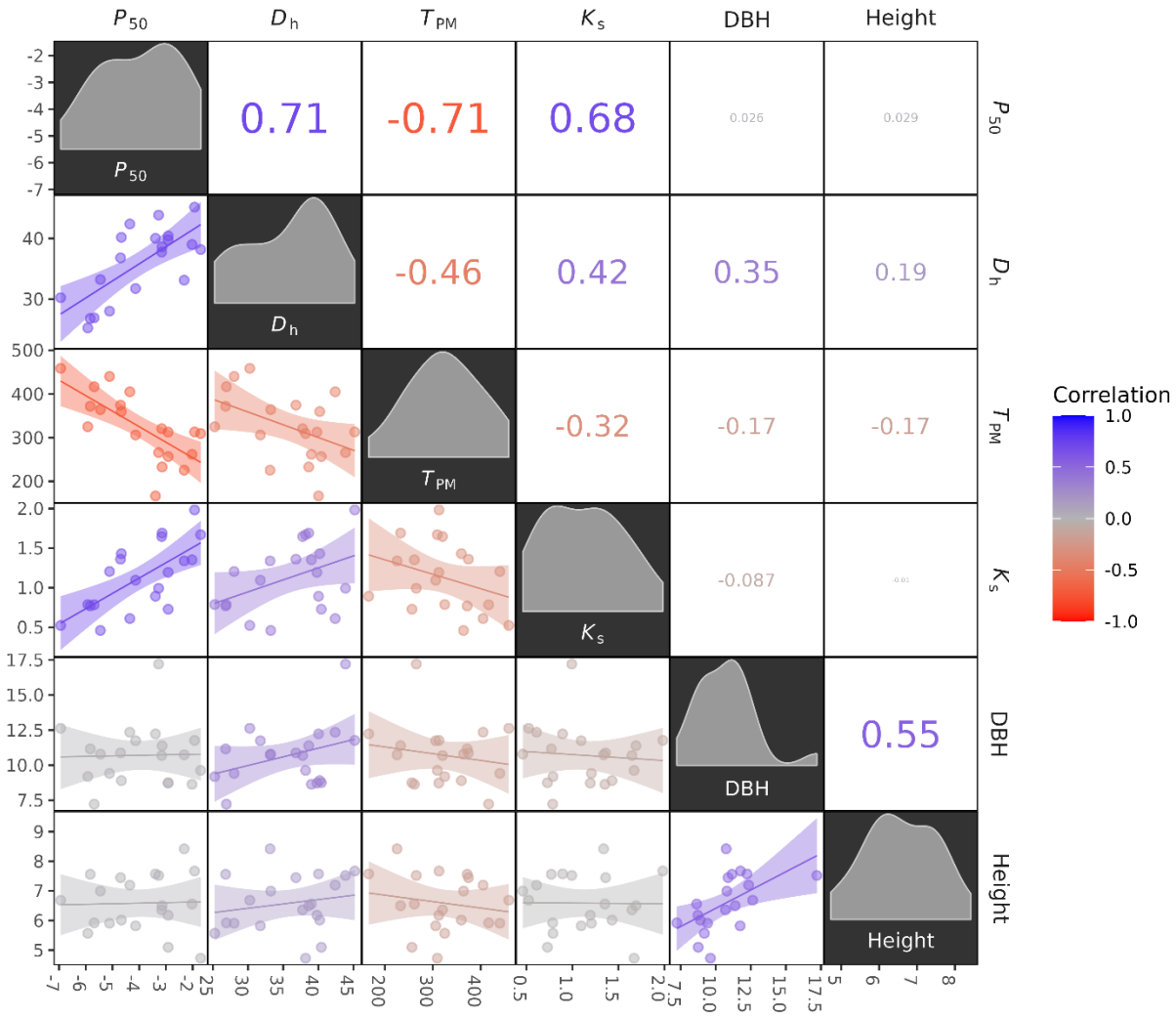

Appendix 1, Figure S2: Correlation matrix of the species level averages of the analyzed variables. Shown are the water potential at 50% loss of conductance (P_{50}, MPa), the hydraulically-weighted vessel diameter (D_h, µm), the pit membrane thickness (T_{PM}, nm), the specific conductivity (K_s, kg m^{-1} MPa^{-1} s^{-1}), the tree diameter at breast height (DBH, cm) and the tree height (Height, m). The upper panel shows the Pearson correlations, the lower panel observed values overlaid with linear regression fits with 95% confidence intervals and the plot diagonal histograms for the corresponding variables. Figure created with R package corrmorant v. 0.0.0.9007 (https://github.com/r-link/corrmorant).

Appendix 2, Table S1: Summary of the analyzed variables. Shown are the species (*A. monspessulanum* from the botanical garden Würzburg listed separately as BGWÜ), the number of trees for the wood anatomical and hydraulic measurements (n_{tree}, including the number of replicate samples in parenthesis for *A. monspessulanum*), the number of pit membranes analyzed for each pit membrane measurement (n_{pit}) and the mean ± standard deviation of the water potential at 50% loss of hydraulic conductivity (P_{50}), hydraulically-weighted vessel diameter (D_h), the central, edge and mean pit membrane thickness (T_{PM} center, edge and mean, respectively), specific conductivity (K_s), diameter at breast height (DBH) and tree height (Height).

Species	n_{tree}	n_{pit}	P_{50} (MPa)	D_h (µm)	T_{PM} center (nm)	T_{PM} edge (nm)	T_{PM} mean (nm)	K_S (kg m^{-1} MPa^{-1} s^{-1})	DBH (cm)	Height (m)
Acer campestre	4	27	-5.45 ± 0.12	33.2 ± 2.2	364.1 ± 40.3	262.7 ± 19.4	313.4 ± 24.7	0.46 ± 0.15	10.8 ± 0.6	7.0 ± 0.2
Acer monspessulanum	2	16	-7.33 ± 0.04	27.3 ± 1.2	458.6 ± 111.0	236.4 ± 38.8	347.5 ± 63.7	0.52 ± 0.01	12.6 ± 0.7	6.7 ± 0.1
Acer monspessulanum BGWÜ	22 (64)	16	-6.90 ± 0.31	30.5 ± 1.8						
Acer platanoides	4	15	-4.35 ± 0.29	42.4 ± 0.3	404.9 ± 42.1	249.7 ± 26.6	327.3 ± 31.9	0.61 ± 0.16	12.3 ± 0.7	7.2 ± 0.2
Acer rubrum	4	9	-2.92 ± 0.05	39.8 ± 3.0	312.6 ± 40.5	240.5 ± 56.6	276.6 ± 37.8	1.19 ± 0.30	8.7 ± 0.6	6.2 ± 0.2
Betula pendula	4	27	-2.32 ± 0.19	33.1 ± 2.3	225.5 ± 50.2	184.3 ± 33.1	204.9 ± 40.0	1.34 ± 0.11	10.7 ± 1.2	8.4 ± 0.8
Betula utilis	4	3	-2.02 ± 0.16	39.0 ± 1.5	261.7 ± 68.3	216.0 ± 68.6	238.8 ± 65.5	1.35 ± 0.13	8.6 ± 0.7	6.6 ± 0.3
Carpinus betulus	4	16	-4.70 ± 0.25	36.8 ± 1.7	374.4 ± 58.4	255.3 ± 27.1	314.8 ± 37.1	1.36 ± 0.11	10.9 ± 0.9	7.4 ± 0.3
Crataegus persimilis	4	16	-5.69 ± 0.82	26.9 ± 0.8	416.6 ± 112.1	253.8 ± 50.6	335.2 ± 70.0	0.79 ± 0.04	7.2 ± 0.4	5.9 ± 0.1
Ostrya carpinifolia	4	10	-4.67 ± 0.24	40.2 ± 1.7	359.6 ± 55.3	278.0 ± 47.7	318.8 ± 46.9	1.43 ± 0.21	8.9 ± 0.2	6.0 ± 0.2
Platanus orientalis	4	10	-1.93 ± 0.10	45.2 ± 3.2	313.0 ± 32.3	191.2 ± 35.2	252.1 ± 28.6	1.98 ± 0.13	11.8 ± 0.9	7.7 ± 0.1
Platanus x acerifolia	4	10	-1.70 ± 0.19	38.2 ± 3.1	309.4 ± 25.1	255.2 ± 29.5	282.3 ± 24.9	1.67 ± 0.23	9.6 ± 0.6	4.7 ± 0.4
Prunus padus	3	11	-3.16 ± 0.04	37.8 ± 1.2	320.3 ± 40.2	218.2 ± 42.7	269.3 ± 36.3	1.65 ± 0.28	10.7 ± 0.8	6.4 ± 0.1
Prunus serrulata	4	12	-4.14 ± 0.29	31.7 ± 1.2	306.1 ± 71.2	221.3 ± 36.2	263.7 ± 50.6	1.09 ± 0.46	11.7 ± 0.5	5.8 ± 0.4
Pyrus calleryana	4	9	-5.83 ± 0.16	26.8 ± 1.7	371.8 ± 96.2	234.2 ± 58.5	303.0 ± 73.7	0.77 ± 0.28	11.2 ± 1.0	7.6 ± 0.8
Sorbus latifolia	4	16	-5.92 ± 0.43	25.3 ± 2.7	324.9 ± 60.5	245.5 ± 44.2	285.2 ± 48.8	0.79 ± 0.07	9.2 ± 0.7	5.6 ± 0.3
Sorbus x thuringiaca	4	8	-5.11 ± 0.23	28.0 ± 1.4	440.0 ± 65.2	323.2 ± 52.9	381.6 ± 55.7	1.21 ± 0.05	9.4 ± 0.6	5.9 ± 0.3
Tilia cordata	4	6	-3.14 ± 0.24	38.6 ± 2.5	232.8 ± 32.5	193.0 ± 19.7	212.9 ± 23.9	1.69 ± 0.17	11.4 ± 0.8	6.5 ± 0.4
Tilia mongolica	4	13	-2.92 ± 0.08	40.4 ± 2.6	256.6 ± 43.8	187.2 ± 32.3	221.9 ± 36.6	0.73 ± 0.23	8.8 ± 0.3	5.1 ± 0.1
Tilia platyphyllos	4	13	-3.39 ± 0.11	40.0 ± 3.2	166.5 ± 25.1	164.4 ± 18.6	165.4 ± 18.4	0.89 ± 0.17	12.2 ± 0.3	7.6 ± 0.2
Tilia tomentosa	4	7	-3.28 ± 0.09	43.9 ± 3.3	265.7 ± 24.9	169.4 ± 9.9	217.6 ± 14.7	0.99 ± 0.10	17.2 ± 1.0	7.5 ± 0.5

Appendix 3, Table S2: Parameter estimates of the linear regression models of the water potential at 50% loss of hydraulic conductivity (P_{50}) against hydraulically-weighted vessel diameter (D_h), pit membrane thickness (T_{PM}) and specific conductivity (K_s) that are shown in Figure 2–4 in the main text. For each model term, given are the regression estimate with the corresponding standard error, t-value and the p-value for the null hypothesis that the parameter is equal to zero.

Model	Term	Estimate	Std. error	*t*-value	*p*-value	
$P_{50} \sim D_h$	(Int.)	-10.383	1.523	-6.819	< 0.001	***
	D_h	0.178	0.042	4.262	< 0.001	***
$P_{50} \sim T_{PM}$	(Int.)	0.632	1.102	0.574	0.573	
	T_{PM}	-0.014	0.003	-4.294	< 0.001	***
$P_{50} \sim K_s$	(Int.)	-6.687	0.730	-9.157	< 0.001	***
	K_s	2.404	0.608	3.958	< 0.001	***
$P_{50} \sim D_h$ (restr. range)	(Int.)	-0.593	6.260	-0.095	0.927	
	D_h	-0.068	0.157	-0.432	0.676	
$P_{50} \sim D_h$ (ACMO)	(Int.)	-6.896	0.627	-11.003	< 0.001	***
	D_h	-0.001	0.021	-0.048	0.961	
$P_{50} \sim D_h + T_{PM}$	(Int.)	-5.181	2.044	-2.534	0.021	*
	D_h	0.122	0.038	3.166	0.006	**
	T_{PM}	-0.010	0.003	-3.198	0.005	**

Appendix 4, Table S3: Parameter estimates of the mixed-effects models for the $P_{50} - D_h$ relationship (note that D_h was centered around 0 to obtain an interpretable intercept). Above: regular linear mixed-effects model (LME); below: LME with within-species centering. Shown are the parameter estimates with their MCMC standard error, 95% credible intervals, the $\widehat{R}$-statistic and bulk and tail effective sample sizes. 95% credible intervals excluding zero are displayed in bold. Note that the regular LME misses the strong cross-species relationship and that the within-species relationship is biased upwards compared to the alternative model formulation.

Model	Parameter	Estimate	SE	95% CI	Rhat	Bulk ESS	Tail ESS
Regular LME	Intercept	-3.992	0.349	**-4.690 –-3.295**	1.002	1303	2384
	Slope	0.019	0.018	-0.015 – 0.053	1.001	6539	6325
	SD(Intercept)	1.528	0.273	**1.094 – 2.175**	1.001	2027	3932
	SD(Slope)	0.031	0.018	**0.005 – 0.073**	1.000	4155	5161
	cor(Int., Slope)	-0.243	0.371	-0.844 – 0.576	1.001	9036	6887
	Residual SD	0.297	0.025	**0.254 – 0.350**	1.000	8706	7692
Within-species centering	Intercept	-4.195	0.268	**-4.710 –-3.663**	1.003	1829	3600
	Slope (between)	0.177	0.046	**0.085 – 0.267**	1.003	2166	3364
	Slope (within)	0.007	0.018	-0.029 – 0.042	1.000	13069	7134
	SD(Intercept)	1.186	0.221	**0.842 – 1.704**	1.001	2541	4411
	SD(Slope)	0.029	0.017	**0.005 – 0.071**	1.000	6680	6129
	cor(Int., Slope)	-0.005	0.406	-0.749 – 0.756	1.000	11011	7380
	Residual SD	0.297	0.025	**0.254 – 0.350**	1.000	11069	7853

6.2. Chapter 2

Appendix 5, Table S1: Comparison of the estimated xylem water potential at 12%, 50% and 88% loss of conductivity / percent air discharged (P_{12}, P_{50} and P_{88}, respectively) and slope of the vulnerability curve (S_{50}) for the 12 studied diffuse-porous tree species for the pneumatic (15 sec AD interval) and flow-centrifuge method. Given are the means and propagated standard errors including the inferential uncertainty of the PLC measurements. Asterisks (*) indicate xylem pressures measured with stem psychrometers; hashes (#) indicate individuals from the same species measured with the pressure bomb.

	P_{12} (MPa)		P_{50} (MPa)		P_{88} (MPa)		S_{50} (-% MPa^{-1})	
Species	**Cavitron**	**Pneu. (16 s)**	**Cavitron**	**Pneu. (16 s)**	**Cavitron**	**Pneu. (16 s)**	**Cavitron**	**Pneu. (16 s)**
Betula pendula	-2.07 ± 0.03	-1.36 ± 0.05	-2.38 ± 0.01	-1.85 ± 0.02	-2.69 ± 0.03	-2.49 ± 0.05	134.1 ± 10.5	77.4 ± 5.4
Betula utilis	-1.92 ± 0.01	-1.37 ± 0.05	-2.09 ± 0.00	-2.05 ± 0.02	-2.24 ± 0.01	-2.71 ± 0.05	267.0 ± 11.9	71.4 ± 4.5
Carpinus betulus	-3.74 ± 0.06	-2.65 ± 0.08	-4.75 ± 0.03	-4.06 ± 0.03	-5.76 ± 0.05	-5.47 ± 0.08	48.0 ± 2.1	34.4 ± 1.7
Crataegus persimilis	-4.96 ± 0.17	-3.36 ± 0.21	-6.02 ± 0.06	-5.63 ± 0.09	-7.05 ± 0.16	-7.56 ± 0.23	46.9 ± 5.4	17.0 ± 1.4
Ostrya carpinifolia	-4.09 ± 0.04	-3.53 ± 0.07	-4.72 ± 0.02	-4.98 ± 0.03	-5.32 ± 0.04	-6.44 ± 0.07	75.7 ± 4.0	33.5 ± 1.4
Platanus acerifolia	-1.55 ± 0.02	-1.00 ± 0.05	-1.85 ± 0.01	-1.42 ± 0.02	-2.14 ± 0.02	-1.97 ± 0.04	154.7 ± 8.1	94.7 ± 8.0
Platanus orientalis	-1.73 ± 0.04	-1.51 ± 0.04	-1.97 ± 0.02	-1.71 ± 0.02	-2.25 ± 0.04	-1.91 ± 0.04	135.9 ± 16.0	130.6 ± 17.9
Pyrus calleryana	-4.73 ± 0.10	-3.91 ± 0.30	-5.79 ± 0.04	-6.31 ± 0.13	-6.82 ± 0.09	-9.00 ± 0.43	45.9 ± 3.4	19.1 ± 2.2
Sorbus latifolia	-3.94 ± 0.18	-4.40 ± 0.15	-5.69 ± 0.07	-6.34 ± 0.06	-7.39 ± 0.14	-8.13 ± 0.13	28.1 ± 2.2	20.3 ± 1.3
*Tilia cordata**	-2.45 ± 0.02	-2.26 ± 0.00	-3.02 ± 0.01	-2.55 ± 0.00	-3.60 ± 0.02	-2.84 ± 0.00	84.4 ± 2.7	114.2 ± 1.0
Tilia cordata#	-2.45 ± 0.04	-1.46 ± 0.07	-3.15 ± 0.02	-2.21 ± 0.03	-3.85 ± 0.04	-3.03 ± 0.06	56.0 ± 2.8	61.0 ± 4.3
Tilia japonica	-2.35 ± 0.02	-1.35 ± 0.15	-3.00 ± 0.01	-2.92 ± 0.05	-3.64 ± 0.02	-4.49 ± 0.14	74.4 ± 1.7	31.0 ± 2.4
*Tilia platyphyllos**	-1.82 ± 0.03	-2.20 ± 0.01	-2.68 ± 0.01	-2.70 ± 0.00	-3.54 ± 0.02	-3.19 ± 0.01	55.5 ± 1.5	83.5 ± 0.9
Tilia platyphyllos#	-2.95 ± 0.02	-1.43 ± 0.05	-3.43 ± 0.01	-1.91 ± 0.02	-3.92 ± 0.02	-2.42 ± 0.05	82.5 ± 3.2	91.2 ± 8.2

Appendix 6, Table S2: Summary of a set of metrics describing the agreement between the two analyzed methods for the estimated parameters for the xylem water potential at 12%, 50% and 88% loss of conductivity (P_{12}, P_{50} and P_{88}, respectively) and the slope at 50% loss of conductivity (S_{50}). Given are the comparisons between the flow-centrifuge method and the pneumatic method at 15, 30, 60, 90 and 115 sec air discharge intervals. The values indicating the highest agreement are highlighted in bold.

Parameter	AD time	Pearson ρ	MSD	RMSD
P_{12}	16 sec	**0.834 (0.761−0.917)**	**0.517 (0.286− 0.733)**	**0.827 (0.658−0.992)**
	30 sec	0.834 (0.749−0.911)	0.574 (0.349− 0.774)	0.861 (0.713−1.012)
	60 sec	0.803 (0.696−0.902)	0.662 (0.429− 0.898)	0.957 (0.775−1.137)
	90 sec	0.770 (0.642−0.885)	0.720 (0.463− 0.972)	1.034 (0.812−1.280)
	115 sec	0.739 (0.579−0.879)	0.771 (0.498− 1.036)	1.102 (0.845−1.348)
P_{50}	16 sec	0.955 (0.932−0.978)	**0.129 (-0.048− 0.302)**	0.542 (0.412−0.651)
	30 sec	0.959 (0.937−0.978)	0.189 (0.014− 0.355)	0.521 (0.402−0.631)
	60 sec	0.961 (0.939−0.978)	0.269 (0.106− 0.425)	**0.519 (0.394−0.638)**
	90 sec	0.962 (0.940−0.979)	0.315 (0.170− 0.458)	0.529 (0.397−0.647)
	115 sec	**0.962 (0.939−0.980)**	0.343 (0.202− 0.493)	0.538 (0.400−0.671)
P_{88}	16 sec	0.937 (0.908−0.963)	-0.259 (-0.572− 0.068)	1.018 (0.706−1.301)
	30 sec	**0.939 (0.912−0.962)**	-0.196 (-0.529− 0.134)	0.971 (0.687−1.248)
	60 sec	0.938 (0.910−0.962)	-0.125 (-0.472− 0.175)	0.929 (0.651−1.178)
	90 sec	0.937 (0.909−0.961)	-0.090 (-0.398− 0.196)	0.905 (0.658−1.143)
	115 sec	0.937 (0.906−0.960)	**-0.085 (-0.409− 0.196)**	**0.896 (0.667−1.131)**
$\log(S_{50})$	16 sec	**0.555 (0.367−0.717)**	**-0.298 (-0.523−-0.053)**	**0.758 (0.636−0.883)**
	30 sec	0.549 (0.357−0.722)	-0.300 (-0.541−-0.063)	0.756 (0.631−0.871)
	60 sec	0.544 (0.374−0.722)	-0.306 (-0.539−-0.067)	0.758 (0.631−0.880)
	90 sec	0.544 (0.348−0.721)	-0.311 (-0.537−-0.070)	0.763 (0.631−0.884)
	115 sec	0.545 (0.342−0.722)	-0.330 (-0.554−-0.074)	0.771 (0.638−0.898)

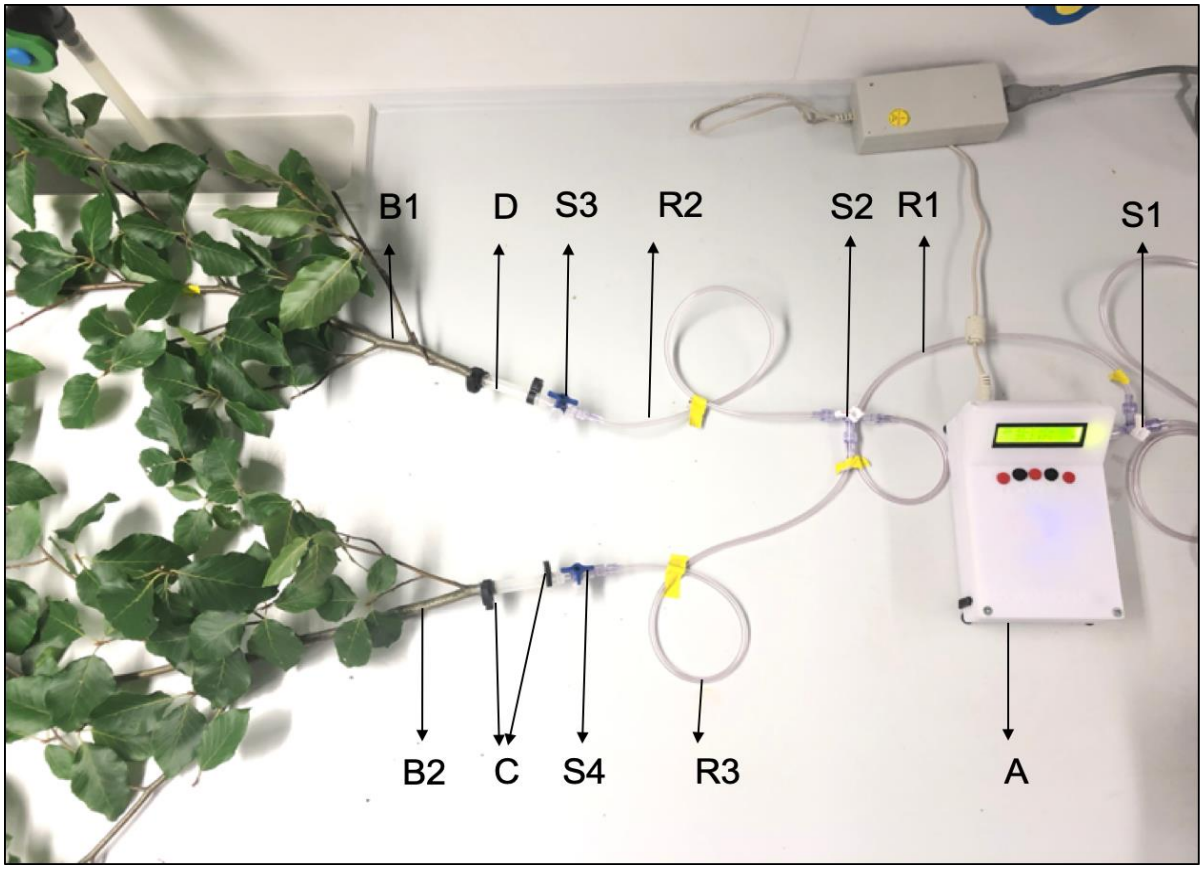

Appendix 6, Figure S1: Documentation of the applied set-up. A – Pneumatron: device for air discharge measurements; B1 and B2: – branch 1 and branch 2; C – Plastic clamps to tighten the connection of elastic tubing and branch to avoid leakage; D – Elastic tube to connect the branch to the vacuum reservoir; R1, R2, R3 – Vacuum reservoir; S1, S2, S3 and S4 – three-way stopcocks for switching the connection between the pneumatic apparatus and the two branches.

Appendix 7, Figure S2: Documentation of the stopcock, plastic clamps and elastic tubing used for connecting the pneumatic apparatus with rigid tubing to the branch. The red color marks the point to where the branch was inserted into the tubing. To calculate the volume of elastic tubing, the empty weight of stopcock, plastic clamps and elastic tubing was measured and filled up to the red mark with water after measurement and weighed again. The weight of the water was later converted into the corresponding volume at the temperature at the time of measurement.

Appendix 8, Figure S3: Storage of branch samples during the measurement. a) Samples being dried on the bench to induce embolism. Drying intervals between air discharge measurements varied from about 15 min at the initial stages to 6-8 h at higher desiccation levels. All of these branches were measured simultaneously, which highlights the advantage of the high sample throughput of the pneumatic method. b) Branch samples kept for equilibration by covering them in black plastic bags before measurement. Initially, the branches were kept for 30 min for equilibration before each measurement, which was increased to at least one hour at the later stages.

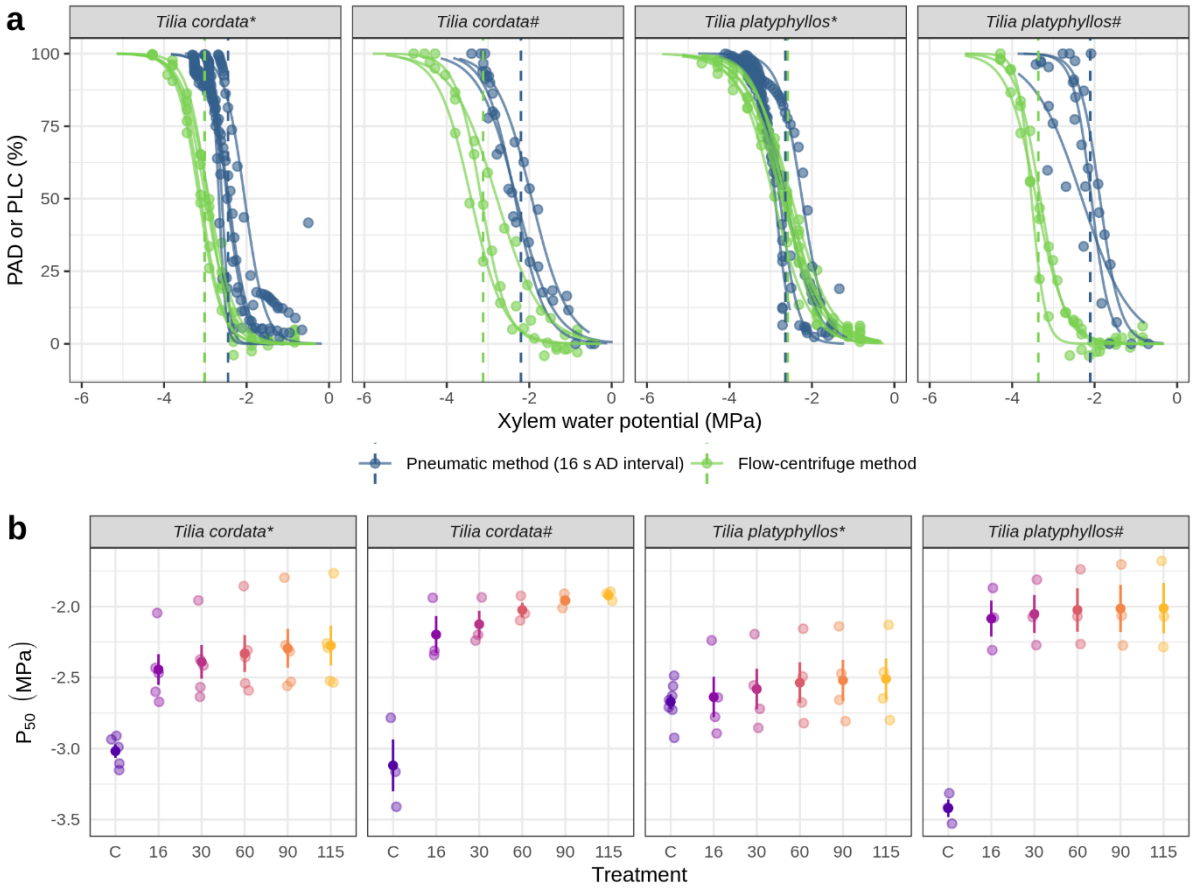

Appendix 9, Figure S4: Comparison of VC and P_{50} estimates measured using stem psychrometer and pressure chamber a) Xylem vulnerability curves obtained with the pneumatic method for 15 sec air discharge interval (green) and curves from the flow-centrifuge method (blue) for two *Tilia* species. Circles: observed values (for the centrifuge data, rescaled from conductance to PLC using the estimated k_{sat}); solid lines: predicted PLC/PAD; dashed lines: estimated P_{50}. b) Comparison of P_{50} values between the flow-centrifuge and different air discharge intervals for the pneumatic method (compared on the same branch). C indicates the P_{50} values from the flow-centrifuge method, 16, 30, 60, 90 and 115 indicate AD measurement intervals evaluated from the pneumatic method. Shown are the raw estimates overlaid with their mean ± SE. Asterisks (*) indicate xylem pressures measured with stem psychrometers; hashes (#) indicate individuals from the same species measured with the pressure bomb.

6.3. Chapter 3

Appendix 10, Table S1*:* GenBank accessions for DNA sequences used in the phylogenetic analyses.

Specie	Phylogeny			
	GenBank			
	chloroplast			nuclear
	atpB-rblc	ycf1	matK	ITS
Betulaceae (6 species)				
Betula alleghaniensis	x	MN531412.1	x	MN531354.1
Betula lenta	FJ423682.1	KP642954.1	NC_039992.1	MN531372.1
Betula maximowicziana	x	MN531416.1	x	MN531358.1
Betula pendula	LT996895.1	KX676526.1	LT996895.1	MN531378.1
Betula pubescens	NC_039996.1	MN531422.1	NC_039996.1	MH014809.1
Betula utilis	x	MH659707.1	x	MH808501.1
Malvaceae (6 species)				
Tilia americana	GU981686.1	MK520755.1	x	KF694729.1
Tilia cordata	x	MK608699.1	KP088239.1	KF897521.1
Tilia japonica	x	LT671650.1	x	KF694724.1
Tilia mongolica	MW386998.1	MW386998.1	MW386998.1	KF445430.1
Tilia platyphyllos	AJ233113.1	KP089346.1	KP088234.1	MT227678.1
Tilia tomentosa	x	MG221044.1	x	KF694727.1
Rosaceae (6 species)				
Prunus avium	EF513128.1	HQ235112.1	MK622380.1	KY749331.1
Prunus mahaleb	x	MW369056.1	x	JQ776828.1
Prunus padus	x	MW369034.1	x	MK180726.1
Prunus pensylvanica	MN427872.1	MN427872.1	MN427872.1	x
Prunus sargentii	MW392082.1	MW369042.1	KP088418.1	MN644321.1
Prunus serrulata	MN652612.1	MT220838.1	KP088397.1	MT227741.1
Sapindaceae (6 species)				
Acer campestre	MW067033.1	KX229835	MW067033.1	KY649427.1
Acer monspessulanum	MW067056.1	KU549987	MW067056.1	KT587665.1
Acer platanoides	MN315279.1	KX677002	MN315279.1	LK022679.1
Acer rubrum	MN864509.1	MG220697	MN864509.1	AJ634586.1
Acer tataricum	HQ266407.1	EU749289.1	NC_056228.1	AY605463.1
Acer saccharinum	MW067085.1	KP088939.1	KP088229.1	MH711104.1
Outgroup (2 species)				
Ceratophyllum submersum	AF293860.1	JN895363.1	x	GU206356.1
Ceratophyllum demersum	D89552.1	MG220983.1	AM712908.1	GU206359.1

Appendix 11, Table S2: Average values over the occurrence points for the six selected bioclimatic variables. For each variable (1) indicates the lowest average value and (2), the highest average value.

Specie	Six selected bioclimatic variables					
	Isothermality (%)	**Mean temperature of the warmest quarter (°C)**	**Mean temperature of the coldest quarter (°C)**	**Mean Annual Precipitation (mm)**	**Mean Precipitation of the driest quarter (mm)**	**Mean Precipitation warmest of the quarter (mm)**
Betulaceae (6 species)						
Betula alleghaniensis	28.14	18.18	-6.51	1037.51	204.59	285.33
Betula lenta	31.91	20.09	-2.25	1132.32	241.60	303.66
Betula maximowicziana	26.04	18.68	-3.17	1501.70	222.27	541.62
Betula pendula	29.16	16.36	-2.62	749.76	131.62	219.75
Betula pubescens	27.12	13.97	-4.79	794.52	136.16	225.36
Betula utilis	35.89	14.01	-1.89	743.35	82.78	300.40
Malvaceae (6 species)						
Tilia americana	31.90	20.56	-2.66	988.07	172.53	290.79
Tilia cordata	28.81	16.54	-1.94	764.16	137.96	220.52
Tilia japonica	25.80	20.06	-1.94	1624.43	233.40	583.33
Tilia mongolica	29.38	20.79	-3.07	788.71	101.13	336.33
Tilia platyphyllos	33.00	16.86	1.59	803.47	154.50	213.73
Tilia tomentosa	32.91	17.82	1.80	787.79	149.24	210.84
Rosaceae (6 species)						
Prunus avium	32.86	17.16	1.42	835.83	151.72	211.80
Prunus padus	27.92	15.64	-3.81	760.68	130.93	232.23
Prunus pensylvanica	26.79	17.03	-9.16	912.32	168.42	269.48
Prunus sargentii	26.67	21.23	-1.65	1397.88	160.22	605.38
Prunus serrulata	31.35	20.44	2.34	1261.60	171.50	455.86
Prunus mahaleb	33.41	17.98	1.69	765.68	144.57	195.65
Sapindaceae (6 species)						
Acer campestre	32.63	17.42	1.56	793.98	150.17	211.98
Acer monspessulanum	35.09	19.34	4.03	762.39	131.77	152.34
Acer platanoides	23.98	14.86	-5.35	702.91	112.62	212.65
Acer rubrum	27.03	17.29	-7.75	965.03	178.96	269.30
Acer saccharinum	30.85	16.72	-1.08	763.30	141.07	239.27
Acer tataricum	25.23	17.73	-5.79	657.33	108.91	217.45

Appendix 12, Table S3: Evolution model test. For each trait, three evolutionary models were tested, Brownian Motion (BM), Ornstein–Uhlenbeck (OU) and Early Burst (EB). The AICc value for each model is presented and the lowest value for each trait is presented in bold. Model parameters: "Pagel's Lambda"(for BM), "alpha" rate of adaptation (for OU), "a" rate change (for EB).

Specie	Trait	Model	AICc	Model parameters		
				Parameters	Rate of evolution (sigsq)	Root state (z0)
Betulaceae	P_{50}	BM	23.62819	lambda = 1.000000	sigsq = 4821.222890	z0 = -2.023688
		OU	33.613980	alpha = 2.718282	sigsq = 4821.250160	z0 = -2.023689
		EB	**17.673472**	a = -3476.757310	sigsq = 7594.751548	z0 = -2.023289
	D_h	BM	54.632769	lambda = 1.000000	sigsq = 159778.749879	z0 = 31.598189
		OU	54.618205	alpha = 2.718282	sigsq = 159770.342297	z0 = 31.598203
		EB	**44.63277**	a = -1533.057902	sigsq = 319519.493534	z0 = 31.607560
	WD	BM	9.171723	lambda = 1.000000	sigsq = 433.274274	z0 = 0.629423
		OU	19.157423	alpha = 2.718282	sigsq = 433.270560	z0 = 0.629424
		EB	**6.660122**	a = 3266.645588	sigsq = 1021.740135	z0 = 0.629238
Malvaceae	P_{50}	BM	**15.03465**	lambda = 0.000000	sigsq = 18.931543	z0 = -2.999104
		OU	25.015193	alpha = 2.718282	sigsq = 42.064378	z0 = -3.017887
		EB	25.034652	a = -0.000001	sigsq = 41.680568	z0 = -3.020223
	D_h	BM	**37.78767**	lambda = 0.000000	sigsq = 1158.703017	z0 = 39.541242
		OU	47.787672	alpha = 0.000000	sigsq = 1849.107590	z0 = 39.926160
		EB	47.787674	a = 0.000001	sigsq = 1848.639491	z0 = 39.926160
	WD	BM	-**7.9093**	lambda = 0.000000	sigsq = 0.399456	z0 = 0.405805
		OU	2.055673	alpha = 2.718282	sigsq = 0.916324	z0 = 0.406854
		EB	2.090700	a = -0.000001	sigsq = 0.910322	z0 = 0.407211
Rosaceae	P_{50}	BM	**24.60274**	lambda = 0.000000	sigsq = 52.308844	z0 = -3.672455
		OU	34.557207	alpha = 2.718282	sigsq = 267.198987	z0 = -3.603989
		EB	34.602741	a = -0.000001	sigsq = 266.335307	z0 = -3.604188
	D_h	BM	**45.47143**	lambda = 0.000000	sigsq = 3616.537761	z0 = 34.019171
		OU	55.435657	alpha = 2.718282	sigsq = 8670.966572	z0 = 35.711552
		EB	55.471430	a = -0.000001	sigsq = 8628.887367	z0 = 35.684419
	WD	BM	-**8.073958**	lambda = 0.000000	sigsq = 0.461390	z0 = 0.661102
		OU	1.908763	alpha = 2.718282	sigsq = 1.157875	z0 = 0.640242
		EB	1.926042	a = -0.000001	sigsq = 1.148704	z0 = 0.639732
Sapindaceae	P_{50}	BM	30.37812	lambda = 1.00000	sigsq = 211.787446	z0 = -4.352846
		OU	**30.36996**	alpha = 2.718282	sigsq = 216.837958	z0 = -4.352854
		EB	30.3781	a = -0.000001	sigsq = 211.787467	z0 = -4.352846
	D_h	BM	**44.26077**	lambda = 0.763637	sigsq = 4789.010335	z0 = 42.390216
		OU	54.211884	alpha = 2.718282	sigsq = 11531.111164	z0 = 42.390382
		EB	54.260751	a = - 0.000001	sigsq = 11339.140987	z0 = 42.390531
	WD	BM	-**5.256082**	lambda = 0.422736	sigsq = 0.931946	z0 = 0.501249
		OU	4.645487	alpha = 2.718282	sigsq = 2.979447	z0 = 0.501241
		EB	4.743891	a = - 0.000001	sigsq = 2.954201	z0 = 0.501241
All Species	P_{50}	BM	**109.2783**	lambda = 0.997803	sigsq = 283.249468	z0 = -3.377076
		OU	111.029831	alpha = 2.718282	sigsq = 3149.859398	z0 = -3.325041
		EB	111.906679	a = -0.000002	sigsq = 3147.896196	z0 = -3.381656
	D_h	BM	**224.4076**	lambda = 0.007178	sigsq = 376.645768	z0 = 36.163733
		OU	226.145660	alpha = 2.718282	sigsq = 381400.780588	z0 = 36.202135
		EB	227.035946	a = -0.000001	sigsq = 381833.435878	z0 = 37.590520
	WD	BM	**54.06307**	lambda = 0.618337	sigsq = 0.182901	z0 = 0.572138
		OU	55.799779	alpha = 2.718282	sigsq = 315.406069	z0 = 0.566535
		EB	56.691527	a = -0.000001	sigsq = 315.338447	z0 = 0.573086

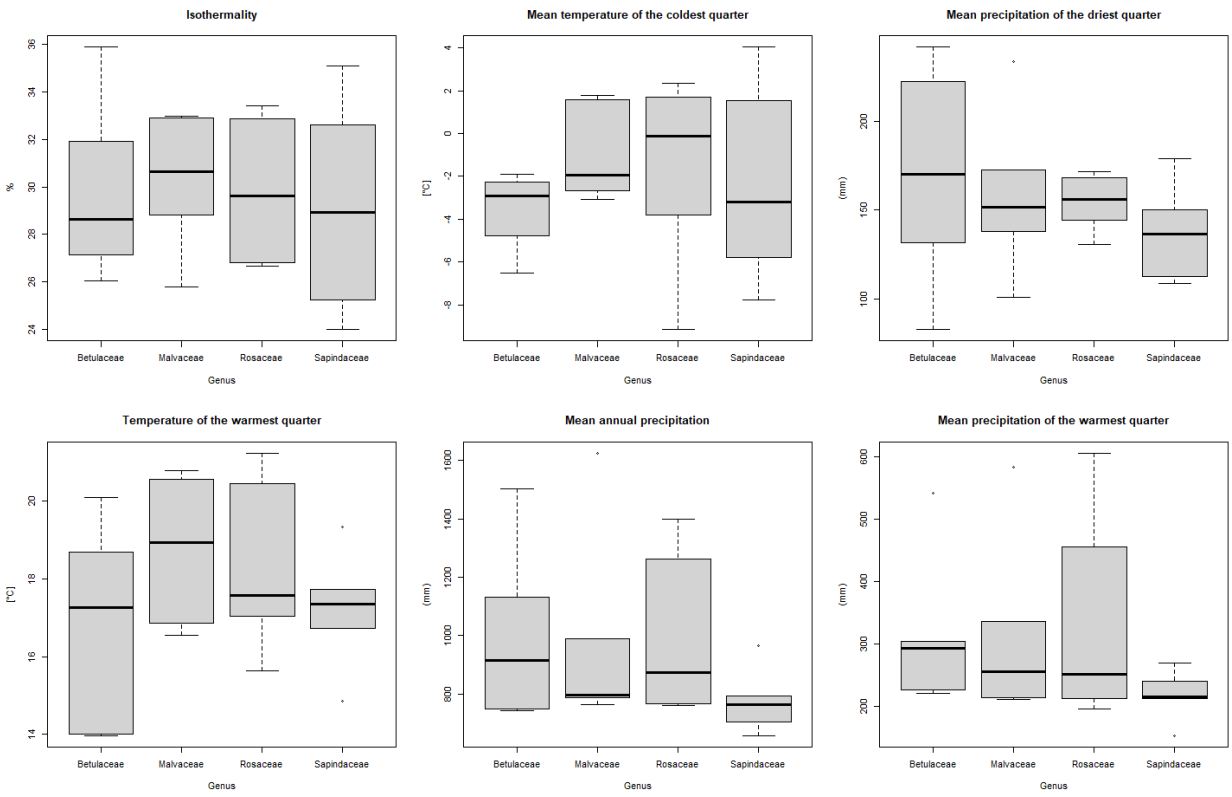

Appendix 13, Figure S1: Distribution of the six genera for six bioclimatic variables of A) isothermality, B) mean temperature of the coldest quarter, C) mean precipitation of the driest quarter, D) mean temperature of the warmest quarter, E) mean precipitation of the warmest quarter. Shown are raw data from genus overlaid with mean ± standard errors. Significant differences among groups were determined using a modified one-way analysis of variance (ANOVA) accounting for heteroscedasticity (Herberich et al. 2010)

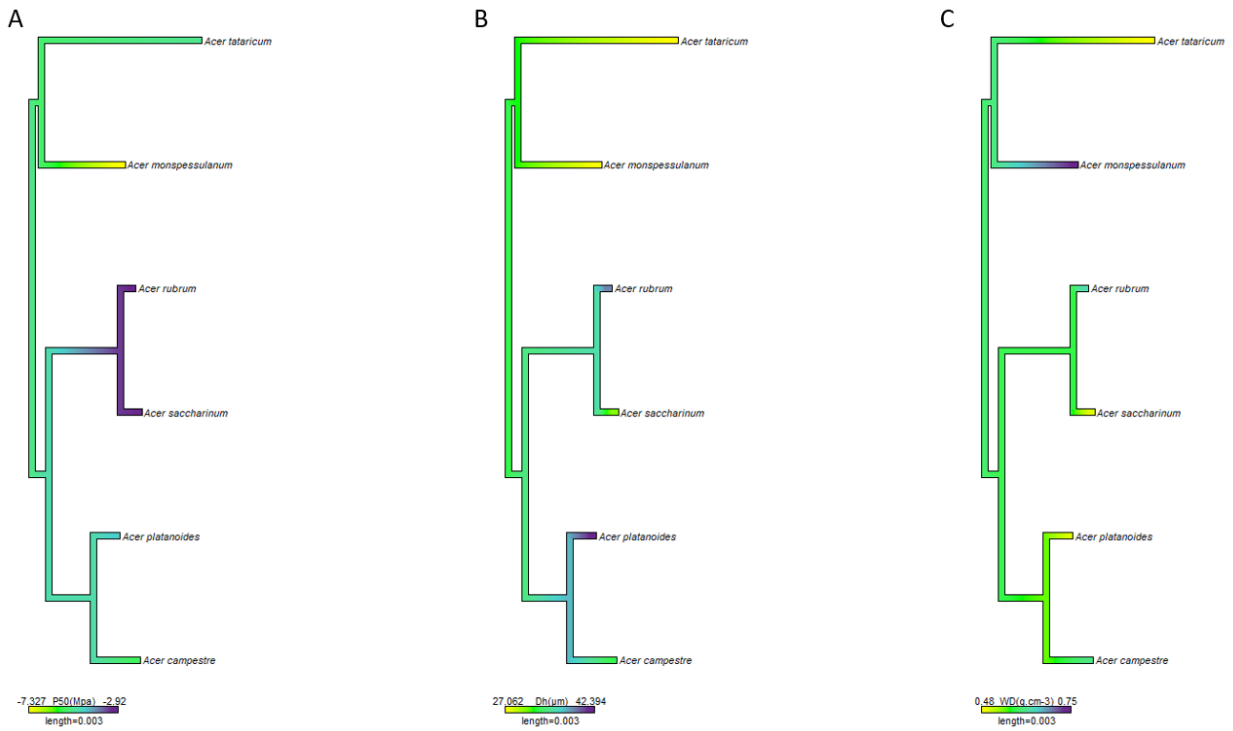

Appendix 14, Figure S2: The spectrum of traits evolution variation in six *Acer* species. A) 50% loss of conductivity (P_{50}), B) hydraulically-weighted vessel diameter (D_h), C) wood density (*WD*). Branch colors reflect changes in traits evolution through time (reconstructed using maximum likelihood).

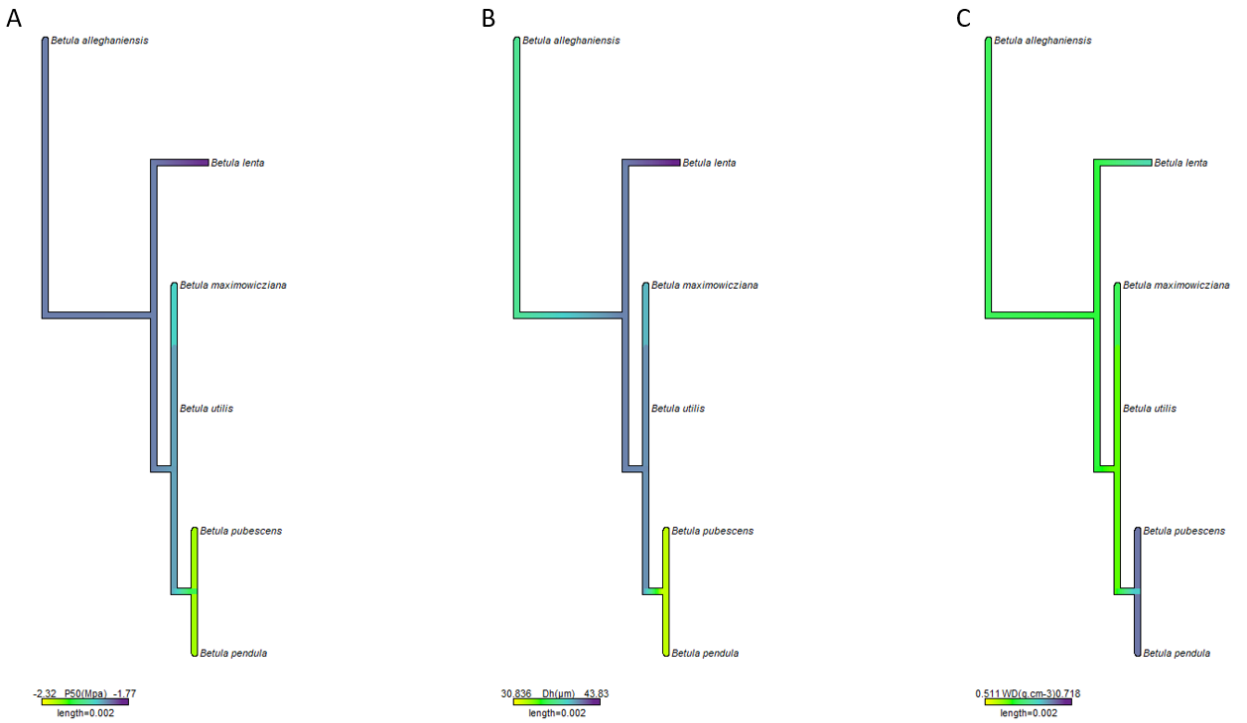

Appendix 15, Figure S3: The spectrum of traits evolution variation in six *Betula* species. A) 50% loss of conductivity (P_{50}), B) hydraulically-weighted vessel diameter (D_h), C) wood density (*WD*). Branch colors reflect changes in traits evolution through time (reconstructed using maximum likelihood).

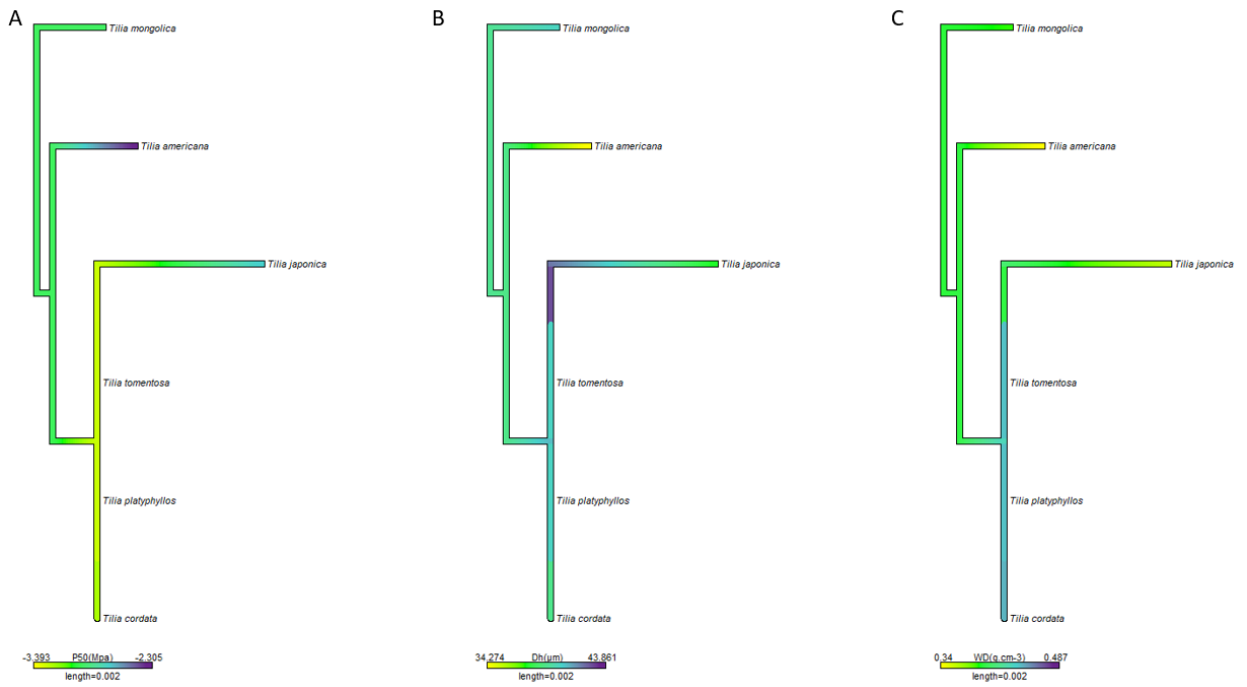

Appendix 16, Figure S4: The spectrum of traits evolution variation in six sample *Tilia* species. A) 50% loss of conductivity (P_{50}), B) hydraulically-weighted vessel diameter (D_h), C) wood density (*WD*). Branch colors reflect changes in traits evolution through time (reconstructed using maximum likelihood).

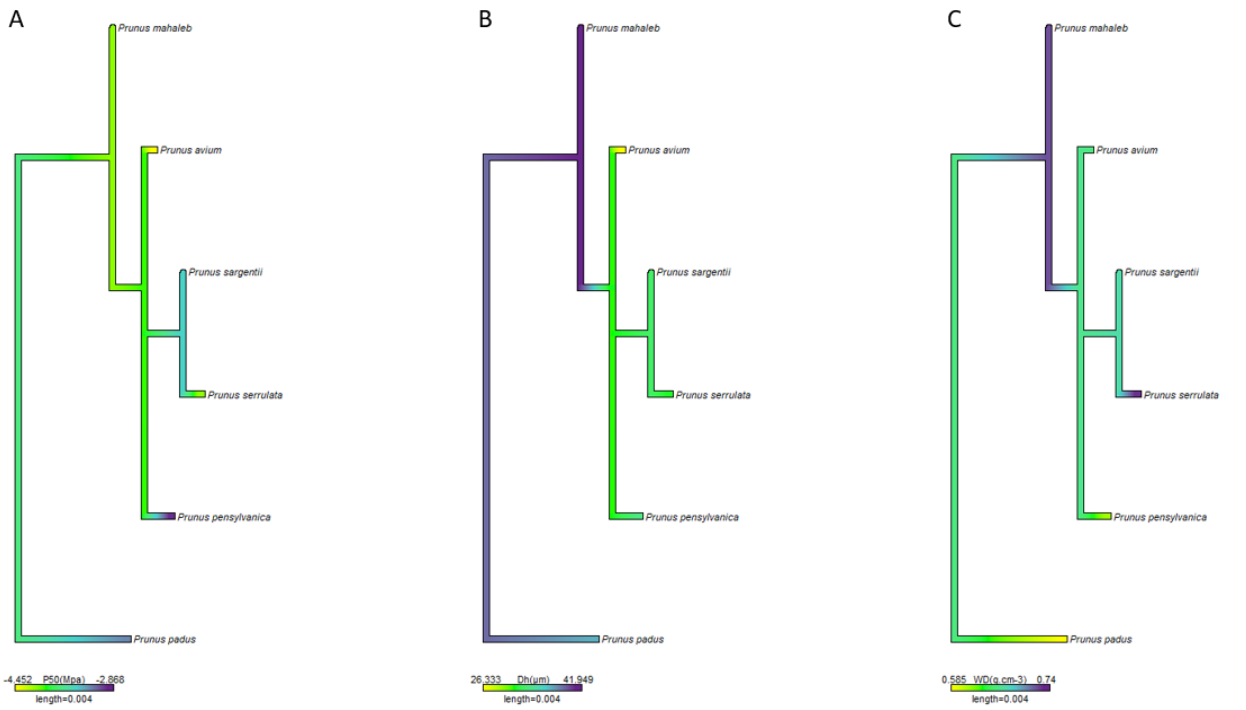

Appendix 17, Figure S4: The spectrum of traits evolution variation in six sample Prunus species. A) 50% loss of conductivity (P_{50}), B) hydraulically-weighted vessel diameter (D_h), C) wood density (*WD*). Branch colors reflect changes in traits evolution through time (reconstructed using maximum likelihood).

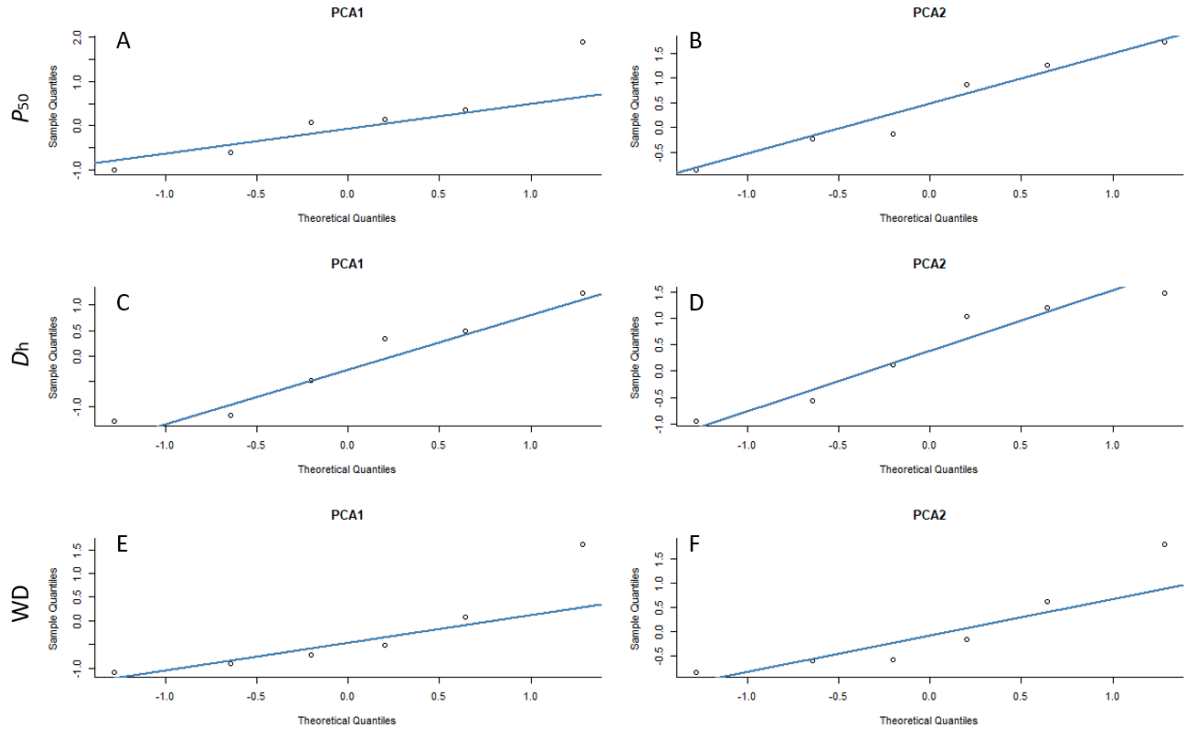

Appendix 18, Figure S6: Quantile-quantile plot of drought-related traits, in Sapindaceae family, showing the relationship of the observed sample quantiles (black dots, n=6) and the theoretical quantiles from the standard normal distribution (mean of zero and standard deviation of 1). Blue solid line indicates the mean of the data. Panels in the left column present QQ plots for the residuals under the PCA1 loadings of the averaged environmental variables and panels in the right column present the QQ plots for the residuals PCA2 loadings of the averaged environmental

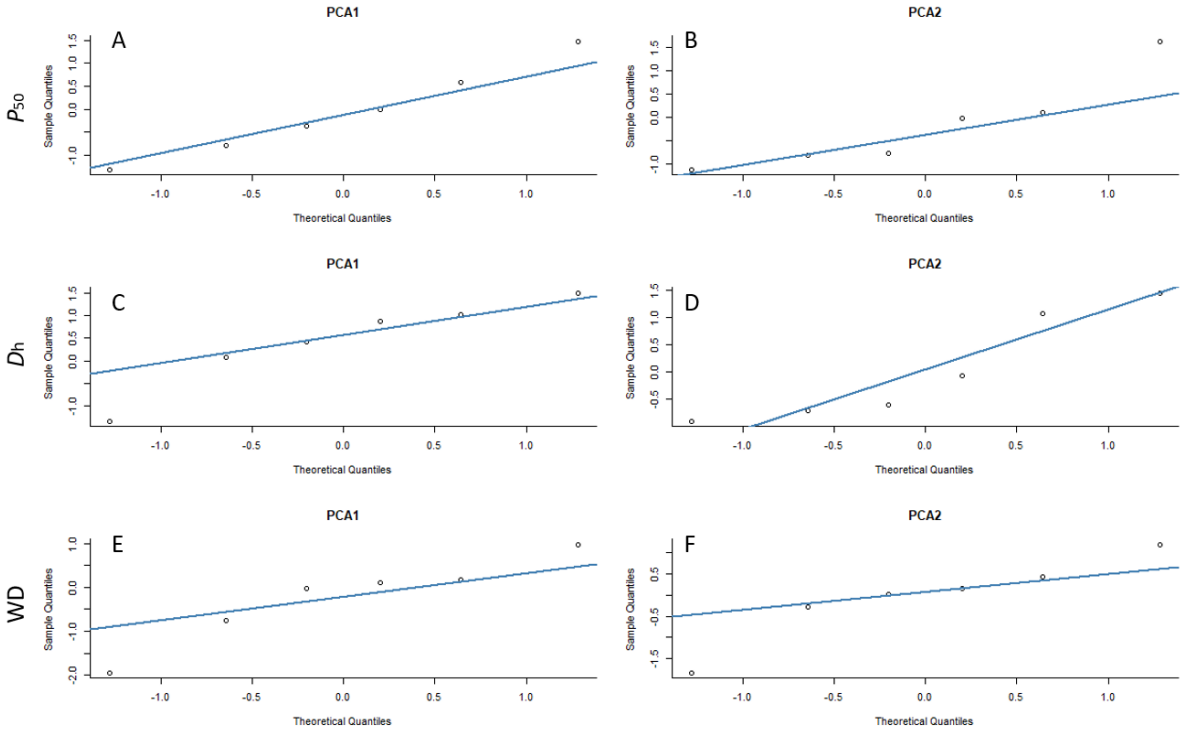

Appendix 19, Figure S7: Quantile-quantile plot of drought-related trait, in Betulaceae family, showing the relationship of the observed sample quantiles (black dots, n=6) and the theoretical quantiles from the standard normal distribution (mean of zero and standard deviation of 1). Blue solid line indicates the mean of the data. Panels in the left column present QQ plots for the residuals under the PCA2.1 loadings of the averaged environmental variables and panels in the right column present the QQ plots for the residuals under PCA2.2 loadings of the averaged environmental variables.

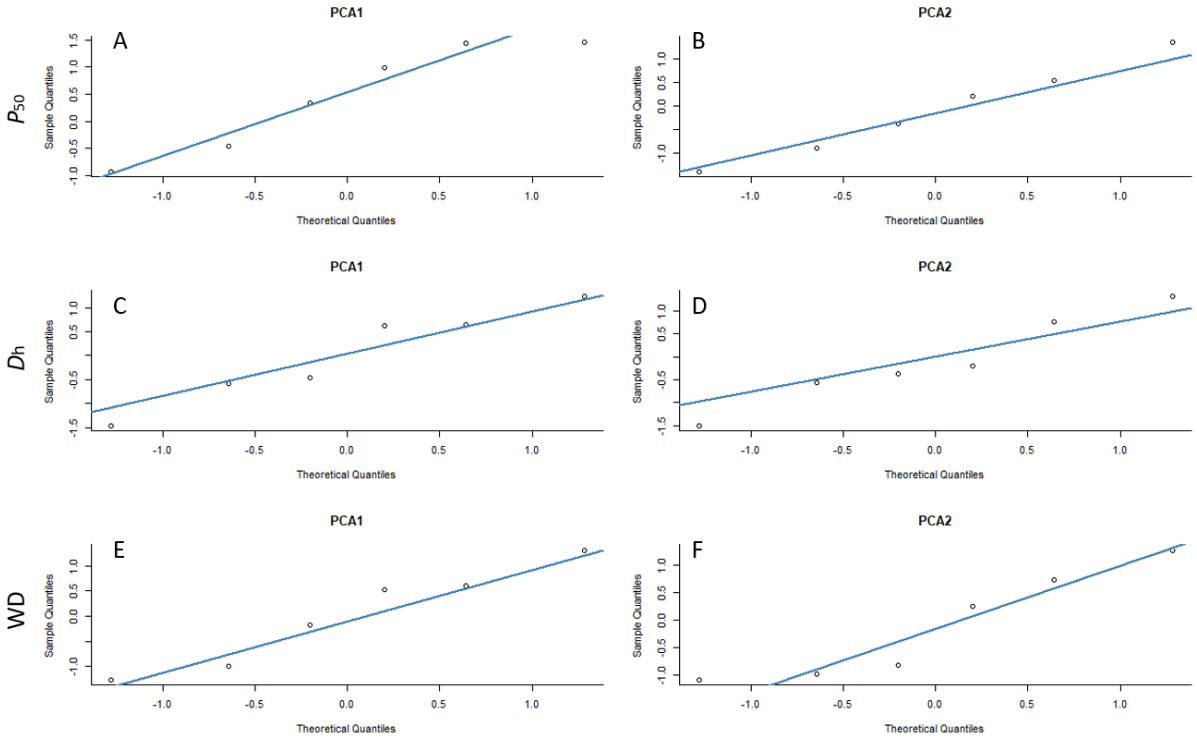

Appendix 20, Figure S8: Quantile-quantile plot of drought-related trait, in Rosaceae family, showing the relationship of the observed sample quantiles (black dots, n=6) and the theoretical quantiles from the standard normal distribution (mean of zero and standard deviation of 1). Blue solid line indicates the mean of the data. Panels in the left column present QQ plots for the residuals under the PCA2.1 loadings of the averaged environmental variables and panels in the right column present the QQ plots for the residuals under PCA2.2 loadings of the averaged environmental variables.

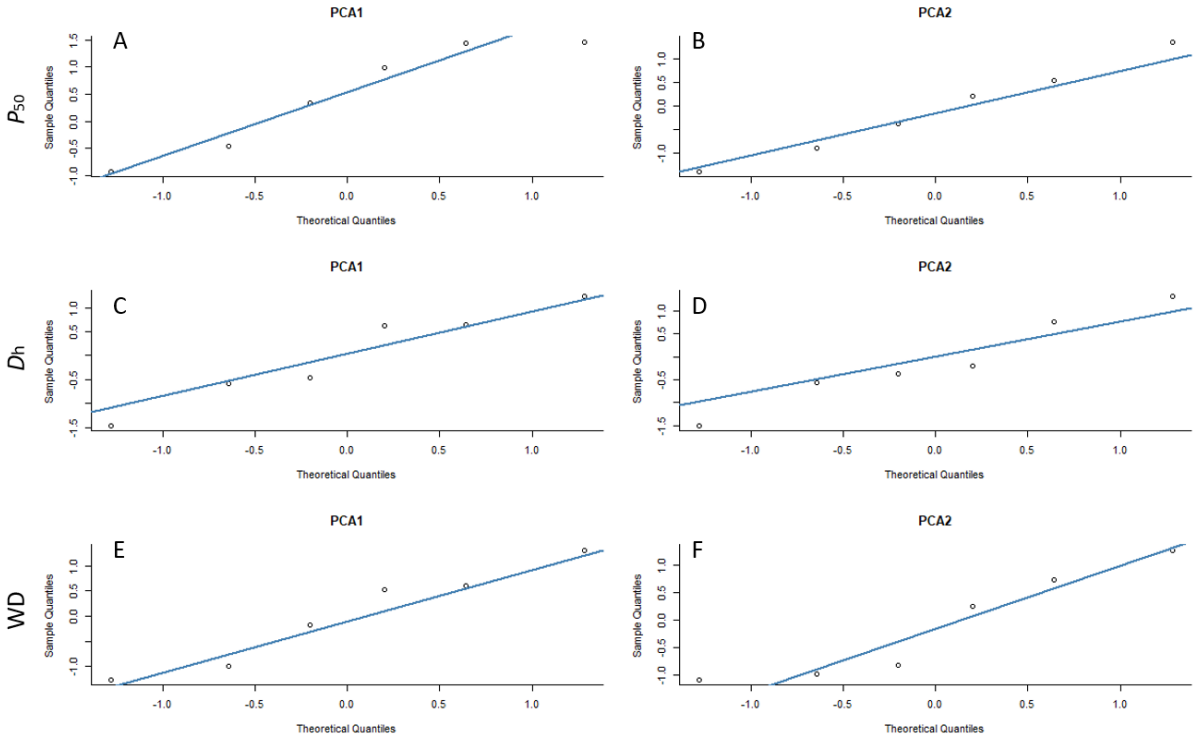

Appendix 21, Figure S9: Quantile-quantile plot of drought- related trait, in Malvaceae family, showing the relationship of the observed sample quantiles (black dots, n=6) and the theoretical quantiles from the standard normal distribution (mean of zero and standard deviation of 1). Blue solid line indicates the mean of the data. Panels in the left column present QQ plots for the residuals under the PCA2.1 loadings of the averaged environmental variables and panels in the right column present the QQ plots for the residuals under PCA2.2 loadings of the averaged environmental variables.

Acknowledgments

Publication list

First-author ship

Emilie Isasa, Roman Link, Steven Jansen, Fon Tezeh, Lucian Kaack, Juliano Sarmento Cabral, Bernhard, Schuldt. (2022, Submitted – Major revisions). Addressing controversies in the xylem embolism resistance – vessel diameter relationship. *New Phytologist*.

Emilie Isasa, Ana Paula Moraes, Bernhard Schuldt, Juliano Sarmento Cabral (2023, In preparation). Relationships between drought induced traits and environmental preferences across four genera of temperate trees. *New Phytologist*.

Emilie Isasa, Alina Maxi lea, Ana Paula Moraes, Bernhard Schuldt, Juliano Sarmento Cabral (2023, In preparation). Relationships between hydraulic traits and habitat preference across 20 worldwide *Acer* species. *New Phytologist.*

Co-author ship

Lucian Kaack, Matthias Weber, **Emilie Isasa**, Zohreh Karimi, Shan Li, Luciano Pereira, Christophe L. Trabi, Ya Zhang, H.Jochen Schen, Bernhard Schuldt, Volker Schmidt, Steven Jansen (2021). Pore constrictions in intervessel pit membranes provide a mechanistic explanation for xylem embolism resistance in angiosperms. (doi: 10.1111/nph.17282).

Sharath S. Paligi, Roman M. Link, **Emilie Isasa**, Paulo Bittencourt, Juliano Sarmento Cabral, Steven Jansen,Rafael S. Oliveira, Luciano Pereira, Bernhard Schuldt (2021). Accuracy of the pneumatic method for estimating xylem vulnerability to embolism in temperate diffuse-porous tree species. (doi: 10.1101/2021.02.15.431295v1).

Yonten Dorji, Bernhard Schuldt, Liane Neudam, Rinzin Dorji, Kali Middleby, **Emilie Isasa**, Klaus Körber, Christian Ammer, Peter Annighöfer, Dominik Seidel (2021). Three-dimensional quantification of tree architecture from mobile laser scanning and geometry analysis. (doi: 10.1007/s00468-021-02124-9).

Yonten Dorji, **Emilie Isasa**, Juliano Sarmento Cabral, Bernhard Schuldt, Peter Annighöfer, Dominik Seidel (2023, In preparation). Insights into the relationship between xylem safety and tree structural complexity from Terrestrial Laser Scanning and fractal analysis. *Trees*.

Curriculum Vitae

Affidavit

I hereby confirm that my thesis entitled “Relationship between wood properties, drought-induced embolism and environmental preferences across temperate diffuse-porous broadleaved trees” is the result of my own work. I did not receive any help or support from commercial consultants. All sources and / or materials applied are listed and specified in the thesis.

Furthermore, I confirm that this thesis has not yet been submitted as part of another examination process neither in identical nor in similar form.

Würzburg,
Place, Date Signature

Eidesstattliche Erklärung

Hiermit erkläre ich an Eides statt, die “Dissertation Beziehung zwischen Holzeigenschaften, trockenheitsbedingter Embolie und Umweltpräferenzen bei zerstreutporigen Laubbäumen der gemäßigten Breiten” eigenständig, d.h. insbesondere selbständig und ohne Hilfe eines kommerziellen Promotionsberaters, angefertigt und keine anderen als die von mir angegebenen Quellen und Hilfsmittel verwendet zu haben.

Ich erkläre außerdem, dass die Dissertation weder in gleicher noch in ähnlicher Form bereits in einem anderen Prüfungsverfahren vorgelegen hat.

Würzburg,
Ort, Datum Unterschrift